

Polish Academy of Sciences

Nałęcz Institute of Biocybernetics and Biomedical Engineering

Doctoral Thesis

**The influence of noise characteristics on the relative stability of attractors in bistable biochemical systems**

Joanna Jaruszewicz

Advisor: Prof. Tomasz Lipniacki, IPPT PAN

February 6, 2014

The study was performed within the TEAM Project “Mechanistic aspects and spatial effects in cell signalling” funded by the Foundation for Polish Science (TEAM/2009-3/6) in the years 2009-2013.



# Contents

<b>1</b>	<b>List of articles included in this thesis</b>	<b>1</b>
<b>2</b>	<b>Summary</b>	<b>2</b>
<b>3</b>	<b>Summary (in Polish)</b>	<b>4</b>
<b>4</b>	<b>Introduction</b>	<b>6</b>
4.1	Molecular noise – the origins and consequences for living cells . . . . .	6
4.2	Bi- and multistability in regulatory networks . . . . .	12
4.3	Modeling noisy cellular networks . . . . .	14
4.4	Experimental and theoretical studies on dividing bacteria . . . . .	17
<b>5</b>	<b>Objectives and hypotheses</b>	<b>19</b>
5.1	Hypothesis A: The noise characteristics determines the most probable state of a cell. . . . .	19
5.2	Hypothesis B: Decrease in cell growth rate stabilizes the epigenetic state of a bacteria. . . . .	21
5.3	Hypothesis C: Behavior of a spatially extended stochastic bistable system depends on the substrate diffusivity and size of the reactor. . . . .	22
<b>6</b>	<b>Conclusions</b>	<b>24</b>
	<b>Appendices</b>	<b>37</b>

# 1. List of articles included in this thesis

This Doctoral Dissertation is a composition of articles published in journals indexed in the Institute of Scientific Information Master Journal List. The articles included in this thesis:

- I. Jaruszewicz J, Zuk PJ, Lipniacki T, *Type of noise defines global attractors in bistable molecular regulatory systems*, Journal of Theoretical Biology, (Elsevier), 317: 140–151, 2013.
- II. Jaruszewicz J, Lipniacki T, *Toggle switch: noise determines the winning gene*, Physical Biology, (IOP Press, Great Britain), 10(3), 2013.
- III. Jaruszewicz J, Kimmel M, Lipniacki T, *Stability of bacterial toggle switches is enhanced by cell cycle lengthening by several orders of magnitude*, accepted for publication in the Physical Review E, (American Physical Society), 2014.
- IV. Zuk PJ, Kočańczyk M, Jaruszewicz J, Bednorz W, Lipniacki T, *Dynamics of a stochastic spatially extended system predicted by comparing deterministic and stochastic attractors of the corresponding birth-death process*, Physical Biology, (IOP Press, Great Britain), 9(5): 055002, 2012.
- V. Kočańczyk M, Jaruszewicz J, Lipniacki T, *Stochastic transitions in a bistable reaction system on the membrane*, Journal of the Royal Society Interface, (Royal Society Publishing), 10(84): 20130151, 2013.

## 2. Summary

Stochasticity is an inherent property of regulatory networks in living cells. Random fluctuations of molecules levels arise from small numbers of interacting molecules. Such molecular noise can be attenuated to assert precise response for a signal. However cells often exploit stochasticity, as it introduces heterogeneity, which can be beneficial in fluctuating environments, increasing chances for survival. Understanding the influence of different types of noise on the state of the system can be especially interesting for synthetic biology, providing additional tool for controlling the systems behavior.

In my research I analyzed the influence of different types of noise, originating from distinct molecular processes like gene switching, transcription, translation, diffusion of molecules and cell division, on the choice of the preferred state in bistable biochemical systems. I applied mathematical description of Markov processes to analyze stochastic models of a single self-regulating gene, auto-activating kinases and a pair of mutually repressing genes in growing and dividing cells. The model of auto-activating kinases was analyzed both in a well-mixed reactor and in a spatially heterogeneous compartment. All other systems were analyzed assuming perfect mixing, which is a good approximation for bacterial cells and small compartments in eukaryotic cells.

I showed that the type of noise determines the most stable stationary state. In a self-regulating gene model I found a subdomain in the parameter space, in which the system is preferably in the active state (high gene expression) for dominating gene switching noise, while for dominating transcriptional noise, the system is preferably inactive (low gene expression). In the toggle switch model I showed that increasing gene switching noise for one gene, significantly increases its chances of “winning” over the second gene, while decreasing dimerization noise for one gene has the opposite effect, i.e., significantly decreases its chances of “winning” over the second gene.

Another important source of noise is cell growth and division. I showed that the epigenetic states of a bistable system are stabilized, when the cell growth rate decreases. In the toggle switch model the non-growing and non-dividing cells switch six orders of magnitude slower than cells dividing every one hour. The observed effect is caused mainly by decreasing protein and mRNA burst sizes with an increasing cycle length, as magnitude of protein level fluctuations is highly influenced by the protein burst size, and to a lesser degree by the mRNA burst size.

State-to-state switching in spatially extended bistable systems was analyzed in a model of auto-activating kinases. First, a simple birth-death process was analyzed in a well-mixed

reactor with addition of flux into and out of the reactor (additive noise). Results of this preliminary analysis suggested that in the spatially extended system (not perfectly mixed), the level of diffusion and the size of the reactor can determine the state of a bistable system. This hypothesis was confirmed in the analysis of the model of auto-activating kinases on a two-dimensional triangular lattice. The same system can be preferably inactive in a small compartment, while in a larger compartment it will activate due to traveling wave propagation, which can arise due to an external stimulation or even spontaneously due to a localized stochastic activation.

### 3. Summary (in Polish)

#### Wpływ charakterystyki szumu na względną stabilność atraktorów w bistabilnych układach biochemicznych

Bistabilność i multistabilność obecne w układach regulatorowych w szczególności w procesie ekspresji genów pełnią ważne funkcje zarówno w komórkach bakteryjnych jak i eukariotycznych definiując optymalne stany epigenetyczne komórki. Bistabilność populacji bakterii umożliwia komórkom o tym samym genotypie przejawianie odmiennych cech fenotypowych, co zwiększa szansę na przetrwanie populacji w zmiennym środowisku. Losowość (stochastyczność) z kolei umożliwia przeskoki między wyróżnionymi stanami.

Jednym ze sposobów uwzględnienia losowości w procesie regulacji ekspresji genów jest dodanie do równań deterministycznych parametru szumu (dyfuzji). Otrzymuje się w ten sposób tzw. przybliżenie Langevina. W pracy pokazano, że opis ten nie stanowi satysfakcjonującego przybliżenia. Dokładniejszy opis stochastyczny uzyskuje się traktując poszczególne reakcje, np. utworzenie lub degradację molekuly, jako zdarzenia losowe, które zachodzą zgodnie z zadanym (wyznaczonym przez parametry modelu) rozkładem prawdopodobieństwa. Opisany w ten sposób proces ma charakter procesu Markowa z czasem ciągłym. Proces ten zadaje nieskończony układ równań  $M$  (chemical master equations), którego stacjonarne rozwiązanie określa rozkład prawdopodobieństwa liczby molekuł i pozwala wnioskować na temat względnej stabilności atraktorów (stabilnych stanów stacjonarnych), gdy ten rozkład jest bimodalny. Jednakże, poza szczególnymi przypadkami, analityczne rozwiązanie równań  $M$  jest niemożliwe, a numeryczne niezwykle trudne. Motywuje to metody przybliżone (np. opis Langevina) i symulacyjne (z wykorzystaniem algorytmu Gillespiego).

Celem pracy jest wykazanie wpływu charakterystyki szumu na względną stabilność atraktorów układu biochemicznego. Rozpatrywane są podstawowe modele regulacji ekspresji genów - podstawowego procesu biologii komórki, oraz model autoaktywujących się kinaz. Badane modele w deterministycznym opisie (przy pomocy równań różniczkowych) wykazują bistabilność, t. j. posiadają dwa stabilne rozwiązania stacjonarne. W stochastycznych opisie modeli, wyodrębnione zostały poszczególne grupy reakcji, które są traktowane jako źródła różnych typów szumu. W szczególności rozpatrywane są następujące komponenty szumu: szum przełączania genu, transkrypcyjny, translacyjny, dimeryzacji, szum związany ze wzrostem i podziałami komórki oraz szum związany z dyfuzją molekuł. Celem jest zbadanie wpływu wielkości poszczególnych typów szumu na wybór globalnego atraktora, t. j. stanu stacjonarnego, w otoczeniu którego koncentruje się większość masy prawdopodobieństwa,

oraz wyznaczenie czasów przeskoków pomiędzy stanami stacjonarnymi.

W pracy rozpatrywane są dwa podstawowe bistabilne układy ekspresji genów: układ pojedynczego genu z nieliniowym dodatnim sprzężeniem zwrotnym oraz układ wzajemnie wyciszających się genów, tzw. "toggle switch". W modelu pojedynczego genu uwzględnione zostały procesy przełączania genu pomiędzy stanami aktywnym i nieaktywnym, produkcja i degradacja molekuł mRNA i białka. Nieliniowość sprzężenia jest konsekwencją aktywacji genu na skutek przyłączenia dimeru białka lub niezależnie dwóch molekuł białka. W obu przypadkach tempo aktywacji genu zależy od kwadratu liczby molekuł białka. W modelu zostało pokazane, że dla fizjologicznego zakresu parametrów od tego, który rodzaj szumu jest dominujący, zależy, który z dwóch stanów układu jest preferowany. Pokazano i wyjaśniono przeciwstawny efekt zmniejszania szumu transkrypcyjnego i szumu przełączania genu oraz znikomy wpływ zmiany szumu translacyjnego na określenie preferowanego stanu stacjonarnego (bardziej stabilnego atraktora). W modelu "toggle switch" pokazano, że zwiększenie szumu przełączania jednego z genów sprzyja wyborowi stanu, w którym drugi z genów jest bardziej aktywny. Natomiast zwiększenie szumu dimeryzacji białka będącego wynikiem ekspresji jednego z genów sprzyja aktywacji tego samego genu.

W modelu bakteryjnego układu "toggle switch" w dzielących się komórkach został zbadany wpływ podziałów komórkowych na wybór preferowanego stanu oraz na średni czas przebywania w poszczególnych stanach. Problem analizowano w zależności od długości cyklu komórkowego określonego z kolei dostępnością substancji odżywczych. Pokazano istotne zwiększenie tempa przełączeń w komórkach o krótszym cyklu komórkowym.

Dynamika przełączeń pomiędzy epigenetycznymi stanami komórki była rozpatrywana również w przestrzennym modelu autoaktywujących się kinaz. Model przeanalizowano najpierw przy założeniu, że komórka stanowi dobrze wymieszany reaktor (czyli dyfuzja jest duża w stosunku do rozmiaru komórki). W tak uproszczonym modelu uwzględniono przepływ kinaz pomiędzy reaktorem a jego otoczeniem. Uzyskane wyniki pozwoliły postawić następującą hipotezę: w bistabilnych układach przestrzennych szybkość dyfuzji oraz rozmiar reaktora mogą decydować o wyborze preferowanego stanu układu. Analiza modelu autoaktywujących się kinaz na dwuwymiarowej trójkątnej siatce potwierdziła słuszność postawionej hipotezy. Pokazano, że ten sam układ może być nieaktywny w małym reaktorze, podczas gdy w większym reaktorze zostanie zaaktywowany przez propagację fali aktywacji, która może powstać dzięki spontanicznej lokalnej aktywacji.

Wyniki opisane w pracy doktorskiej mogą znaleźć zastosowanie w biologii syntetycznej do projektowania układów regulatorowych umożliwiającich reprogramowanie komórek. Szczególnie cennym byłoby selektywne reprogramowanie komórek, np. rakowych lub zainfekowanych wirusem.

Badania były prowadzone w ramach projektu TEAM: "Efekty molekularne i przestrzenne w sygnalizacji komórkowej" finansowanego przez Fundację na rzecz Nauki Polskiej (TEAM/2009-3/6) w latach 2009-2013.

# 4. Introduction

## 4.1 Molecular noise – the origins and consequences for living cells

### Origins of noise

Chemical reactions are probabilistic by nature [1, 2]. Molecular noise in cells arises from small numbers of interacting molecules and from fluctuations in extra- and intra-cellular conditions. The level of gene expression varying from cell to cell was experimentally observed for the first time in production of beta-galactosidase in individual cells of *Escherichia coli*, reported in 1957 [3]. Thirty years later appeared first studies using an expression reporter in single cells, which confirmed the large cell-to-cell variability in the expression of beta-galactosidase [4]. An increase of the inducer dose was found not to cause the uniform increase of expression in every cell, as it was expected, but it increased the probability that the gene is expressed at high level. Individuality of bacterial cells was first explained by Poissonian fluctuations of small numbers in 1976 [5]. The first theoretical models of stochastic gene expression appeared over twenty years later [6, 7]. Gene expression was modelled using a stochastic formulation of chemical kinetics derived by Gillespie [8]. It was proposed that proteins are produced in short bursts of a variable number of molecules, when a small number of mRNA appears due to promoter activation. It was also shown that stochastic effects in gene expression can explain why some *E. coli* cells infected by a  $\lambda$  phage followed the lytic pathway, leading to the host cell death and release of new phages, while others chose the lysogenic pathway, in which the nucleic acid of the phage integrates into the bacterial chromosome and is transmitted to daughter-cells until the lytic cycle is triggered by an environmental change, like UV radiation, or by a stochastic switch.

Noise affecting all biochemical systems present in living cells can be classified as intrinsic or extrinsic. Intrinsic noise is inherent to the analyzed system. It originates from small numbers of interacting molecules present in this system. Extrinsic component of noise originates from random fluctuations of other cellular components, such as concentrations of regulatory proteins, polymerases, ribosomes, which vary between cells. In the model of gene expression presented in Fig. 4.1, the intrinsic noise originates from random events of reactions: gene activation and inactivation, mRNA transcription and degradation, and protein translation and degradation. Each reaction occurs with a given propensity, i.e., a probability that the

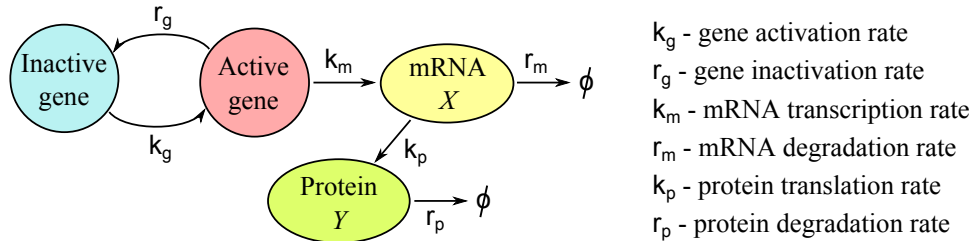


Figure 4.1: Schematic of gene expression.

reaction occurs in time  $t$  divided by  $t$  in the limit of  $t$  converging to 0. Physiological ranges of gene expression kinetic parameters are listed in the Table 4.1. These parameters are also subject to extrinsic noise, which causes them to fluctuate in time and vary between cells. Below, the origins and properties of the intrinsic noise in regulatory networks are described.

Two basic measures are used to quantify noise in the protein level: the coefficient of variation and Fano factor. The coefficient of variation (CV) defined as the standard deviation divided by mean is a dimensionless measure. The Fano factor (FF, index of dispersion) is defined as a variance divided by mean.  $FF = 1$  for the Poisson distribution. When the  $FF < 1$ , like in the binomial distribution, a dataset contains patterns of occurrence that are more regular than the randomness associated with a Poisson process. For clumped, concentrated data  $FF > 1$ , like in the negative binomial distribution and geometric distribution. For a stochastic model described by the schematic in Fig. 4.1, the mean protein number  $E(Y)$  equals  $k_m k_p / r_m r_p$  and the Fano factor of the protein number is given by the formula [9]:

$$FF = \frac{r_m r_p r_g (r_m + r_p + r_g + k_g)}{k_g (r_m + r_p) (r_m + k_g + r_g) (r_p + k_g + r_g)} E(Y) + \frac{k_p}{r_m + r_p} + 1. \quad (4.1)$$

The first term in this formula can be used to quantify the contribution of random gene switching to protein level fluctuations. This term converges to zero for  $k_g$  and  $r_g$  much higher than the other rate constants. For  $k_g$  and  $r_g$  much smaller than the other rate constants it converges to  $E(Y) r_g / k_g$ . The second term is approximately equal to the mean protein burst size  $b$  (defined as  $k_p / r_m$ ), when  $r_p \ll r_m$ . This condition ( $r_p \ll r_m$ ) is usually satisfied in both prokaryotes and eukaryotes, see Table 4.1 with annotations.

Random switching of the gene state was first proposed in the model in [10]. It was shown that the operator state switching can significantly affect the protein distribution, not only quantitatively but also qualitatively. Noisy genetic switches can have bifurcations driven solely by the rate of operator switching even when the underlying deterministic system remains unchanged. Operator switching results in emergence of mRNA bursts, which were observed experimentally, first in eukaryotes (*Saccharomyces cerevisiae*) [11, 12], then also in *E. coli* cells [13]. However, bursts observed in eukaryotes, are longer and less frequent [14, 15]. It was proposed that chromatin remodeling may play role in stochastic switching in eukaryotes [12, 16], while transcription factors binding and unbinding to the DNA result in noisy transcription in both prokaryotes and eukaryotes.

One of the main sources of randomness in protein levels in bacterial [6], as well as in eukaryotic cells [4, 17–20] are protein bursts. Theoretical analysis of protein bursting in bacteria [21, 22] revealed that the FF of the protein number distribution approximately equals  $(b + 1)$ . It was shown that the production of proteins in a two-step process enables an independent control of the mean and variance of the molecule distribution. However, reduction of noise by increasing the number of transcripts is costly. That means that living organisms during evolutionary adaptation have made trade-offs between energy efficiency and attenuation of fluctuations by a decrease of the protein burst size.

Theoretical models were verified in experiments [23–25], which confirmed the existence of random, sharp bursts of proteins in *E. coli* cells. Additionally, contributions of frequencies of transcription and translation to fluctuations in the protein level were computed [23] basing on measurements of expression of a green fluorescent reporter gene in the chromosome of *Bacillus subtilis*. The experiments confirmed earlier theoretical predictions [22] that the CV depends inversely on the rate of transcription and does not depend on the translation rate. Recent experiments providing a quantitative analysis of *E. coli* transcriptome and proteome [26] show a very small (below 1) mean number of mRNA for most of the genes. When translation occurs in large bursts, these rare events of transcription result in high fluctuations of the protein number.

The two mechanisms by which noise is generated - extrinsic and intrinsic - were experimentally discriminated and their relative contribution to the level of fluctuations was measured in *E. coli* [27]. These relative contributions were calculated on the basis of the degree of correlation between two distinguishable fluorescent protein markers expressed from two copies of the same promoter. The extrinsic noise affects both promoters in one cell in the same way, while intrinsic noise introduces differences in the expression of these genes. Thus the intrinsic noise  $\eta_{int}$  can be defined as the mean relative difference in fluorescence intensity of the two promoters:

$$\eta_{int}^2 = \frac{\langle (c - y)^2 \rangle}{2\langle c \rangle \langle y \rangle}. \quad (4.2)$$

$c$  and  $y$  denote vectors of average fluorescence intensities from the two promoters. Extrinsic noise  $\eta_{ext}$  is defined as normalized covariance of fluorescence intensity of the two promoters:

$$\eta_{ext}^2 = \frac{\langle cy \rangle - \langle c \rangle \langle y \rangle}{\langle c \rangle \langle y \rangle}. \quad (4.3)$$

The examination revealed that at low levels of expression both forms of noise are present. At intermediate expression levels extrinsic noise dominates. At high expression levels both forms of noise have comparable and small magnitudes. It was also confirmed that noise has a genetic component. Analytical expressions for extrinsic and intrinsic noise levels were derived in [28]. Later, time-lapse measurements showed that in *E. coli* the time scale for intrinsic and extrinsic fluctuations are different: for intrinsic noise it is less than 9 minutes, while for extrinsic noise it is approximately the length of the cell cycle [29]. Taniguchi et al. [26] measured the intrinsic and extrinsic noise limits. The squared CV of the protein number has an intrinsic component equal at least  $1/\mu_p$  and extrinsic component equal at least 0.1.

In yeasts noise is mostly influenced by extrinsic sources [12, 16], such as a cell size, variation in common upstream factors, and chromosomal location of the gene. In bacteria extrinsic noise arises mostly due to variation in common upstream factors [27].

Table 4.1: Physiological kinetic parameters ranges.

Reaction	Symbol	Prokaryotes ( <i>E. coli</i> , volume $1\mu m^3$ )	Eukaryotes (mammalian cell, vol. $2 \times 10^3 \mu m^3$ )
gene switching	$k_g, r_g$	(1)	(1)
mRNA transcription	$k_m$	$\leq 0.84[1/s]$ <sup>(2)</sup>	$\leq 0.84[1/s]$ <sup>(3)</sup>
protein translation	$k_p$	$\sim 10^{-2} \div \sim 10[1/s]$ <sup>(4)</sup>	$0.018 \div 1.8[1/s]$ <sup>(5)</sup>
mRNA degradation	$r_m$	$6 \times 10^{-4} \div 10^{-2}[1/s]$ <sup>(6)</sup>	$1.7 \times 10^{-5}[1/s] \div 1.7 \times 10^{-3}[1/s]$ <sup>(7)</sup>
protein degradation	$r_p$	$\sim 1.4 \times 10^{-5} \div \sim 10^{-2}[1/s]$ <sup>(8)</sup>	$1.7 \times 10^{-6}[1/s] \div 1.7 \times 10^{-3}[1/s]$ <sup>(9)</sup>
mRNA number	$X$	$10^{-4} \div 5$ <sup>(10)</sup>	$0.5 \div 5 \times 10^4$ <sup>(11)</sup>
protein number	$Y$	$10^{-1} \div 10^4$ <sup>(12)</sup>	$\sim 50 \div 10^8$ <sup>(13)</sup>

*Gene switching:*

<sup>(1)</sup> For prokaryotes gene switching is faster than for eukaryotes [11]. Slow gene switching in eukaryotes is causing large mRNA bursts [15]. The transcriptional bursting was also observed at an *E. coli* promoter [13].

*mRNA transcription:*

<sup>(2)</sup> For *E. coli* maximal transcription rate:  $0.16 \div 0.84/s$  [30].

<sup>(3)</sup> For eukaryotes maximal transcription rate:  $0.16 \div 0.84/s$  [31].

*Protein translation:*

<sup>(4)</sup> Translation initiation intervals are of the order of seconds, although they are specific for each mRNA [32]. *E. coli*: translation initiation rate may vary at least 1000-fold [33]; examples of translation initiation frequencies:  $\beta$ -galactosidase –  $0.31/s$  (spacing between ribosomes: 110 nucleotides), galactoside acetyltransferase –  $0.06/s$  (spacing between ribosomes: 580 nucleotides) [30]; maximal peptide chain elongation rate:  $20aa/s$  [34, 35]; average peptide chain elongation rate:  $12aa/s$  [30].

<sup>(5)</sup> Translation rate for eukaryotes:  $0.018 \div 1.8/s$  [36].

*mRNA degradation:*

<sup>(6)</sup> The vast majority of mRNAs in a bacterial cell are very unstable, having a half-life of about 3 minutes (decay rate  $3 \times 10^{-3}/s$ ) – bacterial mRNAs are both rapidly synthesized and rapidly degraded [37]. *E. coli*: mRNA half-lives span between 1 and 18 minutes (decay rates  $10^{-2}/s \div 6 \times 10^{-4}/s$ ) [38].

<sup>(7)</sup> The eukaryotic mRNAs are more stable than prokaryotic with half-lives exceeding 10 hours (decay rate  $2 \times 10^{-5}/s$ ). However many eukaryotic mRNA half-lives are of order of 30 minutes (decay rate  $3 \times 10^{-4}/s$ ) or less [37]. Mammalian mRNA degradation rates:  $1.7 \times 10^{-5}/s \div 1.7 \times 10^{-3}/s$  [39].

*Protein degradation:*

<sup>(8)</sup> Most of bacterial proteins are very stable, with degradation rates:  $1.4 \times 10^{-5} \div 5.6 \times 10^{-5}/s$  [40]. Some proteins have much higher degradation rates. *E. coli* RNase R has

degradation rate of  $10^{-3}/s$  (in exponential phase) [41], factor  $\sigma^{32}$  has degradation rate of  $10^{-2}/s$  (in steady-state growth phase) [42].

<sup>(9)</sup> Yeast: protein degradation rates:  $2 \times 10^{-5}/s \div 8 \times 10^{-3}/s$  [43]; Mammals: protein degradation rates:  $1.7 \times 10^{-6}/s \div 1.7 \times 10^{-3}/s$  [39].

*mRNA number:*

<sup>(10)</sup> *E. coli*: average mRNA copy number  $10^{-4} \div 5$  molecules/cell [26].

<sup>(11)</sup> Mammals (Mice): average mRNA copy number observed in natural transcriptomes:  $0.5 \div 5 \times 10^4$  molecules/cell [44], [45]. Yeast: typically  $0.3 \div 200$  molecules of mRNA/cell [46], most genes has  $0.1 \div 2$  mRNA/cell [47];

*Protein number:*

<sup>(12)</sup> *E. coli*: average protein copy number  $10^{-1} \div 10^4$  molecules/cell [26].

<sup>(13)</sup> Mammals: maximal protein copy number  $10^8$  molecules/cell [48]. Yeast:  $50 \div 10^6$  protein molecules/cell [49]; most yeast genes:  $10^3 \div 5 \times 10^4$  protein molecules/cell [50].

## Noise control mechanisms

In spite of the stochasticity in regulatory mechanisms, many regulatory pathways have highly predictable outcomes. To decrease influence of noise cells use redundancy in genes (duplicates or paralogues) [51–53] and in regulatory pathways [54, 55], (multiple) feedback loops [56] and checkpoints to assure the proper order and synchronized development of events, like in the cell cycle control [57–59].

Sensitivity to noise is attenuated in developmental pathways of metazoans. For example *Caenorhabditis elegans* developed regulation mechanism (basing on interlocking feedback loops) to avoid stochastic outcome in differentiation of gonadal precursor cells. An anchor cell (cell A) and a ventral uterus cell (cell U) are derived from Z1 and Z4 gonadal precursor cells. First, cell A arises (as a result of differentiation) randomly from either cell Z1 or cell Z4. Then, due to the regulatory feedback via intercellular signaling, the second of the two gonadal cells (Z1 or Z4) becomes a cell U. In this way, the final regulatory outcome is not affected.

Another example of mechanism decreasing sensitivity to noise in the input is hysteresis. Due to hysteresis, induced by noise rapid stochastic switching on and off (chatter), appearing in ultrasensitive systems, can be avoided. Such mechanism is very commonly exploited by cells. It is present, for example, in the bacterial chemotaxis in flagellar motor response [60, 61].

## Noise exploitation

It was commonly assumed that noise is undesirable for cells as it reduces precision of control. However, it turned out that cells not always tend to eliminate or attenuate noise. In many cases noise is beneficial. It can introduce heterogeneity, which increases chances for survival in varying environment [5, 7, 62–67]. Intrinsic stochasticity enables coexistence of two developmental pathways in population of phage  $\lambda$ -infected *E. coli* cells: lytic and lysogenic [7].

Extracellular noise, present in cell-to-cell signaling systems due to environment perturbations, if common to all cells, can also enhance synchronous oscillations [68] or even induce such oscillations in deterministically monostable systems [69, 70].

Noise can help to achieve reliable cellular decisions under fluctuating extracellular conditions. Such mechanism is exploited in the soil bacterium *Bacillus subtilis* during reversible progression toward commitment (spore formation) [71]. In stressful environment the majority of *B. subtilis* cells form spores, which are extremely resistant. It was observed that sporulation proceeds through noisy and reversible steps toward an irreversible, switch-like dynamics of the commitment to spore formation. Analysis of a mathematical model of this process showed that reversible progression allows cells to remain responsive to long-term environmental fluctuations, while the existence of the irreversible commitment point enables reliable execution of cell fate choice, which is robust against short-term reductions in stress. This combination of gradual and all-or-none dynamics during cell fate choice allows *B. subtilis* colonies to survive in changing environment. Similar strategy is exploited in mammalian cells in decisions concerning apoptosis [72].

Signal fluctuations, instead of reducing precision of control, can sharpen the response of the regulated process [73–75]. It was shown that internal noise in cellular control systems can be used to increase sensitivity by stochastic focusing [74]. The stochastic focusing is present in the system of gene expression with repression, where number of repressor molecules exponentially decreases. The signal is defined as a repressor number. The answer of the system is defined as a waiting time for the first transcribed mRNA. It was shown that in this system random signal fluctuations reduce fluctuations in the controlled process. This effect (the stochastic focusing) can be observed in all systems where reaction rates depend nonlinearly on randomly fluctuating concentrations.

Another noise-driven mechanism present in cells is a stochastic resonance, emerging in nonlinear systems, when noise enhances detection of weak signals [76, 77]. This effect was first observed in bistable stochastic systems under periodic external force. It was shown that in such system the average time of state-to-state transitions is correlated with the periodicity of the external forcing. Without noise or with very small magnitude of noise the system oscillates near one of the stationary points, see Fig. 4.2 (A). When noise is present but the periodic force is absent, the process is a diffusion process in a bistable potential (with two local minima). In such case mean transition times  $T_{transition}$  between steady states, i.e., between minima of the potential, are determined by the diffusion coefficient and the potential. When both noise and a periodic force are present, the response of the system is negligible unless the period of the forcing is close to  $T_{transition}$ , see Fig. 4.2 (B) compared to Fig. 4.2 (A). The amplitude of the response has a sharp maximum for an intermediate (finite) level of noise, Fig. 4.3. This sharp maximum is one of the principal signatures of the stochastic resonance, as it significantly enhances sensitivity to a weak periodic signal. The stochastic resonance can be observed also in systems with coexisting attractors other than fixed points. Stochastic resonance has been reported and quantified in many diverse systems, among them in neural models [78, 79], physiological neural populations [80–82] and networks [83], chemical reactions [84] and ion channels [85].

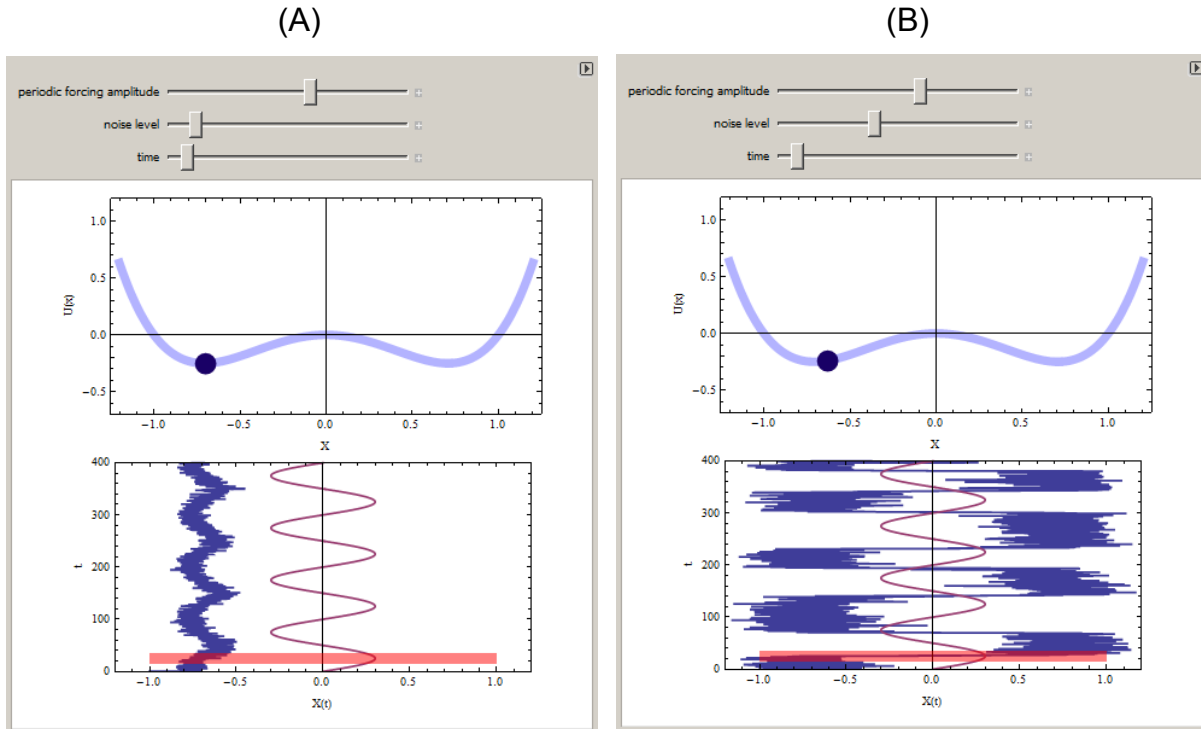


Figure 4.2: Response of the bistable stochastic systems under a periodic external force for small noise magnitude (A) and medium noise magnitude (B). The upper panels show the bistable potential. The lower panels show the response (blue) and the periodic force (red). Images from the website of the Wolfram Demonstration Project (<http://demonstrations.wolfram.com/StochasticResonance>)

Recent experiments confirm that intracellular molecular noise can reduce uncertainty. Noise in *hoxb1a/krox20* expression during development of rhombomeres in the zebrafish hindbrain promotes sharpening of boundaries between adjacent segments [86]. The morphogen retinoic acid induces expression of *hoxb1a* and *krox20* genes in different neighboring domains. Experimental analysis revealed that edges around these gene expression domains are at first rough and then sharpen within a few hours. Computational analysis of a spatial stochastic model showed that fluctuations in the morphogen initially induce a rough boundary, which requires noise in *hoxb1a/krox20* expression to sharpen.

## 4.2 Bi- and multistability in regulatory networks

The bistable regulatory elements play an important role in living organisms as they enhance heterogeneity and may allow cells in multicellular organism to specialize and specify their fate. Decisions between cell death, survival, proliferation and senescence are associated with bistability and stochasticity, magnitude of which controls transition rates between the

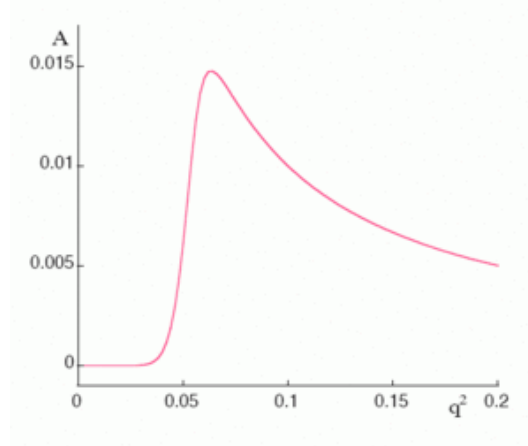


Figure 4.3: The dependence of an amplitude ( $A$ ) of the periodic component of the response of a bistable stochastic systems under a periodic external force on the noise magnitude (i.e., variance in the signal  $q^2$ ). The system is described by a symmetric quartic potential  $U(x) = x^4/4 - x^2/2$ . The periodic force has an amplitude equal  $2\pi/10^5$  and frequency equal 0.001. Image from the Scholarpedia article on the stochastic resonance.

particular attractors [87–89]. In prokaryotes the bistability is regarded as an optimal strategy for coping with infrequent changes in the environment [66].

The simplest regulatory element exhibiting bistability is the self-regulating gene controlled by a nonlinear positive feedback [90–94]. While not often found as an isolated entity, the self-regulating gene is a common element of biological networks; for example, 40% of *E. coli* transcription factors negatively regulate their own transcription [95]. Sinderen et al. demonstrated that transcription factor comK acts as an autoregulatory switch in *Bacillus subtilis* [96]. The synthetic auto-regulatory eukaryotic gene switch was studied in *Saccharomyces cerevisiae* [97]. The other intensively studied regulatory elements exhibiting bistability are the auto-activating kinases system in mammalian cells [98–100], lactose utilization network [101] in *E. coli*, the genetic toggle switch - a pair of mutual repressors [102, 103]. A classical example of the toggle switch is the regulatory circuit governing alternative lysogenic and lytic states of phage lambda [104].

Necessary conditions for bistability are the positive feedback loop and ultrasensitivity. The latter requires that two mechanisms are present: a mechanism filtering out small stimuli thus enabling a stable "off" state, and a mechanism stabilizing high state [105]. In systems with underlying bistability, even for low noise, the stochastic trajectories exhibit stochastic jumps between basins of attraction and thus diverge qualitatively from the deterministic solutions. The relative stability of steady states depends on the system volume (or noise strength) [106]. Despite the low copy number of proteins and mRNAs, genetic switches may exhibit very low transition rates, resulting in stable epigenetic properties that persist in simplest organisms for many generations [104, 107]. The attractors of genetic networks can be associated with distinct cell types achieved during cell differentiation [107, 108]. In

a single cell in the long time scale the relative occupancy of steady states is determined by their relative stability. The same, however, may not be true for cell population when the two steady states are associated with different growth rates. As demonstrated by Nevozhay et al. the fraction of cells in the most strongly attracting steady state may be low, if these cells have lower growth rate than cells in the less stable steady state [109]. Thus, in the context of cell population the relative occupancy of a given state is defined by the rates of state-to-state transitions (or memory) and fitness associated with particular steady states.

### 4.3 Modeling noisy cellular networks

#### Master equations and the Gillespie algorithm

Due to noise present in living cells, modeling cellular dynamics using ordinary differential equations (ODEs) leads to imprecise or sometimes even qualitatively wrong results.

In a more accurate approach, all variables represent discrete numbers of molecules, instead of continuous concentrations, as in previously described approaches. Reaction rates are replaced with propensities, i.e., probabilities for each reaction to happen in an infinitesimal period of time. Such description represents a continuous time Markov process. In Markov processes the probabilities of state transitions satisfy the Chapman-Kolmogorov equation:

$$P(X_3, t_3 | X_1, t_1) = \sum_{X_2} \{P(X_3, t_3 | X_2, t_2)P(X_2, t_2 | X_1, t_1)\}, \quad (4.4)$$

for  $t_1 < t_2 < t_3$  denoting time, and  $X_1, X_2, X_3$ , denoting states of the system. The master equation:

$$\frac{dp_X(t)}{dt} = \sum_{X'} \{W_{XX'}p_{X'}(t) - W_{X'X}p_X(t)\}, \quad (4.5)$$

where  $W_{XX'}$  denotes the propensity of transition from state  $X$  to  $X'$ , can be derived from the equation (4.4) in the limit of  $t_3 \rightarrow t_1$ , see [2].

In this approach, like in the ODE description, it is assumed that the system is well mixed. This assumption is satisfied, when the size of the reactor is smaller than a ball of radius  $\sqrt{D/k}$ , where  $k$  ( $\sim 1/s$ ) is a rate of the fastest reaction. In *E. coli* (size  $\sim 4 \mu m^3$ ) diffusion coefficient  $D$  of proteins (monomers or complexes) of size 20-130 kDa ranges between 5 and  $10 \mu m^2/s$  [110, 111]. Which means that a well-mixed approximation is reasonable for bacteria.

Master equations theoretically provide an analytical description for the probability distribution of all variables present in the system. However, this equations can be solved only in the simplest cases [90, 112–114]. In some cases approximated methods can be applied [2, 115–117].

Approximation of the solution to master equations can be obtained by Monte Carlo simulations performed using the Gillespie algorithm [8]. In the algorithm, the time for the next reaction event is calculated from the exponential distribution and the system is updated accordingly in an iterative manner.

## Langevin equations

A master equation describing a birth–death process with  $N$  species and  $M$  reactions can be approximated by the Langevin equations [118]:

$$\frac{dx_i(t)}{dt} = \sum_{j=1}^M v_{ij}r_j(x) + \sum_{j=1}^M v_{ij}r_j(x)^{1/2}\eta_j(t), \quad (4.6)$$

( $i=1,\dots,N$ ), where  $x$  is a vector of concentrations,  $v$  is a stoichiometric matrix,  $r$  is a vector of propensities and  $\eta_j(t)$  are temporally uncorrelated, statistically independent Gaussian white noises.

Solution can be obtained by solving a corresponding Fokker–Planck (or Kolmogorov forward) equation:

$$\begin{aligned} \frac{\partial P(x,t)}{\partial t} = & - \sum_{i=1}^N \frac{\partial}{\partial x_i} \left[ \left( \sum_{j=1}^M v_{ji}r_j(x) \right) P(x,t) \right] + \\ & + \frac{1}{2} \sum_{i,i'=1}^N \frac{\partial^2}{\partial x_i \partial x_{i'}} \left[ \left( \sum_{j=1}^M v_{ji}v_{ji'}r_j(x) \right) P(x,t) \right]. \end{aligned} \quad (4.7)$$

These equations were at first obtained by a truncation of the Taylor series expansion of the master equations (Kramers, Moyal). Then, they were derived from master equations with additional assumptions, which are satisfied for large number of molecules [118]. However, for systems involving more than a few species, it is impossible to solve the Fokker–Planck equation, even numerically. In such case, solutions can be approximated by Monte Carlo simulations of the Langevin equations.

One can obtain Langevin equations by incorporating noise (diffusion) term to ODEs. The noise term is defined basing on the observed properties (characteristics) of noise in the system. In this approach various noise sources present in the system are replaced by white noise, which magnitude is either constant (additive noise) or is a function of the solution (multiplicative noise), in the simplest case is proportional to the solution (as in geometric Brownian motion equation). The equivalent Fokker-Planck equation describes the evolution of the probability density function. This approach in multistable systems can lead to qualitatively wrong results, because type of noise alone can determine which state is predominant. This effect was shown in one of the articles included in this thesis (article I). This work, together with article (II), addresses the question of influence of dominating type of noise on the relative stability of the steady states in bistable systems. A description of these results can be found in the chapters 5 and 6.

For one-dimensional bistable system the Fokker-Planck equation can be applied to calculate the mean first passage time from one stable state (a) to the other (c) through an unstable point (b). The Fokker-Planck equation takes the form:

$$\frac{\partial P(x,t)}{\partial t} = - \frac{\partial}{\partial x_i} A(x)P(x,t) + \frac{1}{2} \frac{\partial^2}{\partial x^2} B(x)P(x,t), \quad (4.8)$$

where  $A(x) = \sum_{j=1}^M v_j r_j(x)$  and  $B(x) = \sum_{j=1}^M v_j^2 r_j(x)$ . The mean first passage time  $T(x)$  satisfies [119]:

$$A(x) \frac{\partial T(x)}{\partial x} + \frac{1}{2} B(x) \frac{\partial^2 T(x)}{\partial x^2} = -1, \quad (4.9)$$

with boundary conditions:  $T(c) = 0$  and  $\frac{\partial T(0)}{\partial x} = 0$  for a switch from  $a$  to  $c$  and  $T(a) = 0$  and  $\frac{\partial T(\infty)}{\partial x} = 0$  for a switch from  $c$  to  $a$ . This equation solves to:

$$T_{a \rightarrow c} = 2 \int_a^c \frac{dy}{\Psi(y)} \int_0^y \frac{\Psi(z)}{B(z)} dz, \quad (4.10)$$

$$T_{c \rightarrow a} = 2 \int_a^c \frac{dy}{\Psi(y)} \int_y^\infty \frac{\Psi(z)}{B(z)} dz, \quad (4.11)$$

where

$$\Psi(x) = \exp \int_{x_0}^x \frac{2A(y)}{B(y)} dy, \quad (4.12)$$

with  $x_0 = 0$  for  $a \rightarrow c$  transition and  $x_0 = a$  for  $c \rightarrow a$  transition.

## Spatially extended systems

Cells are a very crowded environment. Their interiors are 20-30% volume-occupied by macromolecules [120–123]. Diffusion in cytoplasm is reduced from three- to tenfold compared to water [124, 125]. While a well-mixed approximation is reasonable for bacteria, in eukaryotic cells, which have more complex cellular architecture and larger size, spatial heterogeneity plays an important role and therefore cannot be neglected [126]. Diffusion on the cellular membrane, which contains lipid rafts and large proteins, is approximately ten times smaller than in cytoplasm.

Spatial organization can be taken into account by introducing different cellular compartments into an ODE model. More accurate approach is to model systems using reaction-diffusion equations, i.e., partial differential equations (PDEs).

Another idea is to divide the cell volume into well-mixed compartments and perform stochastic simulations within these compartments taking into account transport between compartments. The Gillespie algorithm with compartments was implemented, e.g., in Dizzy - a software tool for stochastically and deterministically modeling the spatially homogeneous kinetics [127] or in compartmental BNGL [128]. The more accurate approach is to perform stochastic Monte Carlo simulations on the lattice with compartment size of one molecule size, see articles (IV) and (V) included in this thesis. However, such simulations are very slow for large number of molecules or in 3-D. Switching between steady states and correspondence between stochastic and deterministic attractors in the bistable spatially extended systems remain unresolved issues, which were approached in this thesis (articles IV and V).

## 4.4 Experimental and theoretical studies on dividing bacteria

Recent development of experimental techniques enabled observation of single molecules in living cells. As a result, the cell growth and divisions can be described more precisely than before. Observations of fast growing *Escherichia coli* cells, which are able to divide even every 20 minutes, show extreme level of cellular activity including continuous reproduction of genome [129], increased number of mRNAs, ribosomal RNAs and proteins necessary to perform gene expression [130, 131]. Replication elongation rate also increases with increasing nutrient availability [132, 133]. However, for rapid growth (more than one doubling/hour) this rate is relatively constant and replication lasts approximately 40 minutes [133]. Partitioning of molecules between daughter-cells in *E. coli* is binomial [13]. *E. coli* and *B. subtilis* cells growing fast and dividing more frequently than every hour are larger than slower growing cells and can have up to 8 origins of replication per cell. However when the doubling time increases beyond a certain threshold ( $\sim 60$  minutes for *B. subtilis*) cell size becomes essentially constant [134]. Not all bacteria are able to process more than one replication at a time. Mycobacteria have always at most one genome replication proceeding [135].

The average protein lifetime in fast growing bacteria is much longer than the cell cycle length. In result, protein levels are much lower than in the stationary state which would be reached by the system in the absence of divisions. When nutrients level increases, the number of polymerases and ribosomes increases [130] and a cell grows faster. This is accomplished by an increase of the translation and transcription rates. When the translation rate increases, protein burst size increases, implicating an increase of the Fano factor of the protein level distribution.

Until now, most of the regulatory network models did not include effects of the cell growth (with different rates) and divisions. However, the latest experimental results suggest that the cell cycle length highly affects the dynamics of regulatory networks. Studying the deterministic model of the repressilator, i.e., the system of three mutually repressing genes  $A \rightarrow B \rightarrow C \rightarrow A$ , Osella et al. demonstrated that the cell growth and division may qualitatively change the network dynamics [136]. A few studies were also performed on stochastic models of gene expression including cell growth and division [21, 28, 137]. These studies are summarized below.

The first stochastic model of gene expression in growing and dividing bacteria appeared in 1978 [137]. The protein number distribution was analytically calculated under assumption that there are  $N$  gene copies which can produce one mRNA each with probability  $\gamma$  in one time point during the cycle, i.e., there is only one mRNA burst per cell cycle of size binomially distributed with parameters  $N, \gamma$ . It was also assumed that the protein number decreases only due to dilution (i.e., there is no protein degradation) and that the probability that a cell of age  $t$  has a given number of molecules is independent of generation.

Cell division (every 35 minutes) was considered also in the analysis of random fluctuations in the number of protein molecules during LacZ gene expression [21]. Gene multiplication was neglected in the model and linear volume change of the growing cell has been assumed.

Molecules were partitioned equally between daughter-cells. The model includes also randomly changing pools of free RNA polymerases and ribosomes, thus taking into account extrinsic fluctuations of transcription and translation rates. The performed analysis showed that protein number fluctuations are influenced mostly by the protein burst size.

The mathematical analysis of protein number fluctuations in dividing cells was presented in [28]. In the model the gene copy number doubles at a certain time  $\tau$  during each cell cycle and after division all molecule numbers are divided by 2. mRNA level was approximated by the steady state level, which is justified since mRNA lifetime in bacteria is much shorter than the cell cycle length. Then, the average protein number was derived (as a function of time from division). The Fano factor (variance/mean) of protein level distribution (as a function of time in the cell cycle) was calculated under assumption that the protein degradation rate is much smaller than the mRNA degradation rate. This assumption is justified for bacteria, as their protein lifetime is usually two orders of magnitude longer than mRNA lifetime.

Although the cell growth and division significantly influence gene expression dynamics and molecule levels, this influence was not taken into account in earlier studies of bistable systems. This issue is addressed in this thesis (article III). Switching in non-equilibrium stochastic systems is analyzed and the dependence of the switching rate on the cell cycle length is shown.

## 5. Objectives and hypotheses

In my research I analyzed the following open problems: (1) the influence of the type of noise on the relative stability of the steady states, (2) switching in non-equilibrium systems and (3) correspondence between deterministic and stochastic attractors in spatially extended systems.

The hypotheses investigated in this thesis are as follows:

- A. The noise characteristics determines the global attractor in biochemical systems, i.e., the most probable state of a cell.
- B. Decrease in cell growth rate stabilizes the epigenetic state of a bacteria.
- C. Behavior of a spatially extended stochastic bistable system depends on the substrate diffusivity and size of the reactor.

### 5.1 Hypothesis A: The noise characteristics determines the most probable state of a cell.

This hypothesis was demonstrated based on the analysis of two bistable models:

- model of a single gene with a nonlinear positive feedback (article I),
- model of a toggle switch – a pair of mutually repressing genes (article II).

As stated in the Introduction, noise in gene expression network can originate from various sources. In this analysis I took into account only intrinsic noise, neglecting extrinsic noise. Intrinsic noise sources can be further classified on the basis of the process from which they originate. Therefore noise types such as transcriptional, translational, dimerization and gene switching noise can be distinguished. In the articles (I) and (II) I showed that a dominating type of noise in the bistable system can determine which of the two steady states is preferred.

In the model of a self-regulating gene three types of noise are present: gene switching noise, transcriptional and translational noise. The model is described by a continuous time Markov process. Gene activation and inactivation, mRNA transcription, protein translation and degradation of molecules are explicitly included in the model. Each of these reactions changes the state of the system, defined by the three variables: the state of the gene (active

or inactive), the mRNA number and the protein number. Each reaction can occur at a random exponentially distributed time with expected value equal to the inverse of the assumed propensity of the reaction. In this analysis I focused on the parameter domain (lying within physiological range) for which the system is bistable. The two preferred states of the system are referred to as: inactive, with low protein number, and active, with high protein number.

As a first step, I examined a simplified version of the model: a two-step model, in which the processes of transcription and translation are combined into one process of protein production. This simplification enabled analytical treatment of the problem. Two further approximations of the model were considered: the *continuous* approximation, in which the protein production and degradation noise was neglected, and the *adiabatic* approximation, in which the gene switching noise was neglected. In the *continuous* approximation (with gene switching noise only) I calculated analytically the stationary probability distribution of the protein number. Then, I found the separatrix dividing the parameter domain into two subdomains: one in which the probability that the system is in the active state converges to 1 for decreasing noise magnitude, and the second subdomain in which the probability that the system is in the active state converges to 0 for decreasing noise magnitude. Similarly, the analogous separatrix was calculated for the *adiabatic* approximation. I showed that this second separatrix is different than the separatrix obtained for the *continuous* approximation. In this way, I found a subdomain between these two separatrices, in which the type of noise present in the system determines the preferred state. In this subdomain the preferred state of the system with two types of noise is determined by the relative magnitude of this two types of noise. Specifically, when the gene switching noise is dominating, the system is preferably active, while when the protein production and degradation noise is dominating, the system is preferably inactive. This effect was analyzed numerically with application of the Gillespie algorithm.

Next, the effect was observed and analyzed numerically in the exact three-step model. Similarly to the case of the two-step model, when the gene switching noise is dominating, the system is preferably active, while when the transcriptional noise is dominating, the system is preferably inactive. Changes in the magnitude of the translational noise did not affect significantly the protein number probability distribution.

The hypothesis (A) was also verified in a different bistable model: a pair of mutually repressing genes (toggle switch) (article II). The model is described by a continuous time Markov process. The state of the system is defined by eight random variables: states (active or repressed by a dimer of the opposite gene) of gene 1 and gene 2, mRNA 1 and mRNA 2 numbers, protein monomer 1 and protein monomer 2 numbers and protein dimer 1 and protein dimer 2 numbers. The state of the system can be changed by one of the sixteen reactions (eight for each gene): gene activation and inactivation, mRNA transcription and degradation, protein monomer translation and degradation, and protein dimer formation and dissociation to monomers. A gene becomes repressed when the protein dimer of the second gene binds to its promoter. The system is preferably in one of the two states: state 1, in which the level of protein 1 is high, while the level of protein 2 is low, and state 2, in which the level of protein 2 is high, while protein 1 level is low. For simplicity, I assumed that the

system is symmetric, i.e., the default values of all reaction rate constants for both genes are equal.

In this model I investigated the influence of gene switching noise, transcriptional, translational and dimerization noise on the choice of the preferred state of the system and calculated mean first passage times (MFPTs) between the two states, depending on the noise magnitude. The analysis revealed that, as in the case of the self-regulating gene model, the type of dominating noise determines which state is preferred. Increasing the gene switching noise for one gene, significantly increases its chances of “winning” over the second gene, while decreasing dimerization noise for one gene has the opposite effect, i.e., it decreases its chances of “winning” over the second gene. Next, I performed the Latin hypercube sampling to examine the robustness of the effect. Performed sensitivity analysis shows that the effect is present for a relatively wide range of parameters.

## 5.2 Hypothesis B: Decrease in cell growth rate stabilizes the epigenetic state of a bacteria.

This hypothesis was verified in the article (III) included in this thesis. I built a model of a genetic toggle switch in growing and dividing bacteria. In this model I assumed that the cell size is proportional to the level of the “house-keeping” protein. This “house-keeping” protein represents all proteins with constitutive expression and its level is high enough to be described by a continuous concentration instead of a discrete molecule number. Thus, the dynamics of cell growth can be described by a deterministic model. A cell divides, when the “house-keeping” protein level reaches a certain level. Decreased nutrient level results in slower rates of transcription translation, and in a longer time in which cells reach the division size. It is assumed that the transcription and translation rates change in the same way for the “house-keeping” gene and the toggle genes, reflecting changes in the levels of ribosomes and polymerases. Three types of cell division were considered: equal division with molecules equally distributed between daughter-cells, division with molecules binomially distributed (with  $p = 0.5$ ) between daughter-cells and unequal cell division with molecules binomially distributed (with  $p$  being a random variable with the mean value equal to 0.5) between daughter-cells.

I considered cell cycle lengths of at least one hour. For faster growth rates, not considered in this model, cell size just before cell division is larger and there is more than one genome replication simultaneously proceeding. When cells divide at least as frequent as every hour, cell size just before cell division for different growth rates is approximately constant and there is at most one genome replication proceeding [129, 134]. I considered two cases of replication of the genes included in the model: occurring just before cell division or in the middle of the cell cycle. The replication time influences the stationary states of the system, as an earlier replication leads to higher protein level, which results in the lower noise level. However, this effect does not change the main result.

The model was analyzed with application of Gillespie algorithm simulations. The analy-

sis revealed that the state-to-state switching rate significantly decreases with increasing cell cycle length. This effect is caused by multiple factors. The biggest impact has a decrease of the protein burst size, when the translation rate decreases. A decrease in the transcriptional bursts size (ratio of the transcription rate to gene inactivation rate) has a smaller effect. When the cell cycle length is shorter than the average protein lifetime (approximately 9 hours), the protein level decreases mostly due to dilution. Then, the probability distribution of waiting times for a switch is equal to the probability distribution of waiting times for occurrence of approximately four subsequent cell cycles during which no protein is produced [138]. Approximately four divisions are needed to decrease protein number from the high to the low state. The probability that no protein is produced during a given number of subsequent cell cycles is exponentially decreasing with increasing cycle length  $T$  [138]. This decrease is largest for translation rate varying with the cycle length and constant transcription rate.

The analysis of the toggle switch model was supplemented with an analysis of the model of a single gene expression without auto-regulation in dividing cells. In this model the protein distribution is unimodal. I showed that the standard deviation of the protein number decreases with increasing cycle length, due to a decrease in the protein burst size and/or an increase in the transcriptional bursts size.

As a next step, I plan to take into account cell cycle lengths shorter than one hour with multiple gene copies and the cell size depending on the growth rate.

### **5.3 Hypothesis C: Behavior of a spatially extended stochastic bistable system depends on the substrate diffusivity and size of the reactor.**

This hypothesis was verified in the articles (IV) and (V) included in this thesis. First, a simple one-dimensional birth-death process - a bistable model of kinase activation - was analyzed (article IV) in (1) a well-mixed compartment (Markov process with continuous time), (2) in the deterministic approximation in a spatially heterogeneous compartment (reaction-diffusion equation).

For the stochastic process Paweł Zuk calculated (analytically) the stationary probability distribution of the active kinases number. I calculated the solution for the reaction-diffusion equation. Then, we found a separatrix in the parameter space, dividing it into two subdomains: in the first subdomain the active state is preferred for noise decreasing to 0 (i.e., increasing reactor size), in the second subdomain the inactive state is preferred for noise decreasing to 0. We calculated the analogous separatrix for the deterministic approximation, in which the system activates or inactivates due to traveling wave propagation. This second separatrix, was found to be different, than the separatrix for the stochastic process. When we added a flux, with in-flux equal to out-flux, the deterministic description remained unchanged, while the stochastic description changed. We showed that for increasing flux the separatrix for the stochastic model converges to the separatrix for the deterministic approx-

imation. Fig. 5.1 shows a schematic for a birth-death model in 1-D reactor with well-mixed compartments with flux  $f_i$ .

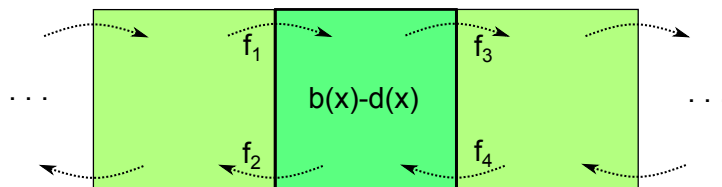


Figure 5.1: Schematic of a one-dimensional reactor with compartments. Molecule number in one compartment changes due to birth and death events, in-flux ( $f_1 + f_4$ ) and out-flux ( $f_2 + f_3$ ) from and to neighboring compartments.

This result can be explained as follows. In the stochastic model, described by birth and death rates  $b(x)$  and  $d(x)$ , the noise intensity depends on the number of active kinases  $x$  present in the system (multiplicative noise). Flux  $f$  added to the model introduces additive noise, i.e., noise which magnitude does not depend on the active kinase number  $x$  present in the system. Adding such flux is a way of introducing diffusion. Therefore, increase of the reactor size, which decreases multiplicative (non-uniform) noise, together with increasing additive (uniform) diffusion-like noise renders the systems behavior similar to that of the deterministic spatially extended model.

On the basis of these observations we proposed a hypothesis that in the spatially extended stochastic system the size of the compartment and substrate diffusivity can determine the preferred state of the system and a mode of activation: due to a traveling wave of activation or through a spontaneous stochastic activation. This hypothesis was confirmed in the analysis of a stochastic kinase auto-activation reaction-diffusion model on a two-dimensional lattice (article IV and V). Kinases can be in one of the three states: unphosphorylated (of very low activity), singly phosphorylated (moderately active), doubly phosphorylated (fully active). Kinases are dephosphorylated by phosphatases present explicitly in the model. The model was analyzed by means of kinetic Monte Carlo simulations implemented by Marek Kočańczyk. The preferred state of the system is determined by diffusion and size of the reactor. We showed that for the same reaction rates, a small perfectly mixed reactor is preferably inactive, while a larger, spatially heterogeneous reactor activates, when a wave of activation propagates as in the deterministic approximation. I added to the model a numerical analysis of the deterministic approximation by a reaction-diffusion system. I showed that the profile and velocity of a traveling front obtained in continuous reaction-diffusion system agrees with that estimated in kinetic Monte Carlo simulations. The deterministic traveling waves were calculated with use of the finite-element method implemented in Comsol Multiphysics (Comsol Inc., Sweden).

## 6. Conclusions

Bistable elements are important as they introduce epigenetic differences between cells, allowing genetically identical cells to behave differently and to pass this behavior to the daughter cells. Transitions between the two states can be a result of changing environment or of stochasticity present in cells (spontaneous transitions). Nowadays, experimental techniques enable observations of single cells, or even single molecules. These observations revealed that noise is present in cellular regulatory networks and plays important role in adaptation to changing environment. Noise can enhance sensitivity to signals, introduce new type of response like oscillations and increase chances for survival. Biological experiments are accompanied by modeling, which helps to unravel the dynamics of biochemical networks. Even simple circuits including few types of molecules can have a complex and unintuitive dynamics. Modeling helps to increase understanding of complex interactions between proteins, RNAs and genes. It allows for manipulating aspects of the process that are difficult to access experimentally and even to predict existence of unknown elements of the process. Such predictions can be then verified in experiments. Therefore modeling serves as both a hypothesis-testing and a hypothesis-generating tool.

I analyzed the influence of different sources of stochasticity, i.e., molecule number fluctuations originating from distinct processes like gene switching, transcription, translation, diffusion of molecules and cell division, on the choice of the preferred state in bistable biochemical systems. I analyzed stochastic models, described by Markov processes, of the following circuits: a single self-regulating gene, auto-activating kinases, a genetic toggle switch (a pair of mutually repressing genes) in non-growing and non-dividing cells, and in growing and dividing bacteria. The models were analyzed analytically or numerically with application of the Gillespie algorithm, or kinetic Monte Carlo methods.

Results of the analysis of a single self-regulating gene and a genetic toggle switch models in a well-mixed compartment are described in the articles (I) and (II). They confirm the hypothesis (A), as they show that the type of noise can determine the most stable stationary state. In particular, for a self-regulating gene model I demonstrated that there exists a subdomain in the parameter space, in which the system is preferably in the active state (high gene expression) for dominating gene switching noise, while for dominating transcriptional noise, the system is preferably inactive (low gene expression). In the toggle switch model I showed that increasing the gene switching noise for one gene, significantly increases its chances of “winning” over the second gene, while decreasing dimerization noise for the same gene has the opposite effect, i.e., significantly decreases its chances of “winning” over the

second gene. I showed that the Langevin equations can lead to qualitatively wrong results, when different noise sources are replaced by an arbitrary additive or multiplicative white noise (article I).

Another important source of noise in cells are growth and division. In the article (III) I showed that the epigenetic state of a bistable system is stabilized, when the cell growth rate decreases. In the toggle switch model the non-growing and non-dividing cells can switch (spontaneously) six orders of magnitude slower than cells dividing every one hour. This result confirms the hypothesis (B). The observed effect is caused mainly by a decreasing protein burst size with increasing cycle length, as magnitude of protein level fluctuations is highly influenced by the protein burst size, and to a lesser degree by the mRNA burst size.

State-to-state switching in spatially extended bistable systems was analyzed in the articles (IV) and (V). The preliminary results of the analysis of a simple birth-death process in a well-mixed reactor suggested that in a spatially extended systems the level of diffusion and the size of reactor can determine the state of a bistable system. This hypothesis was confirmed in the analysis of the model of auto-activating kinases on a two-dimensional triangular lattice. The same system in a small compartment can be preferably inactive, while in a larger compartment it will activate due to the traveling wave propagation. The results confirm the hypothesis (C).

This findings can be applied in synthetic biology to construct regulatory networks enabling reprogramming of cells, by means of manipulating the magnitude of noise of an appropriate type. Especially, control of the state of growing bacteria by modulating type and level of nutrients, can be very useful. Eukaryotic cells compared to bacteria have a larger size and more complex structure resulting in spatial heterogeneity. Control of the state in eukaryotic cells can be achieved by plasma membrane deformation or formation of lipid rafts, which modify the effective size of the compartment, or with addition of buffers or extracellular ligands, which control the diffusivity.

Type of noise is specific to a given organism. In bacteria transcriptional noise is dominating, due to a small number of mRNA, which is on average less than 1. In eukaryotes mRNA and proteins are more abundant, resulting in small transcriptional and translational noise. Simultaneously, the gene activation and inactivation is a more complex and time-consuming process than in bacteria, resulting in higher gene switching noise.

Relative magnitudes of different noise types change also during cell cycle and development. The growth of the cell volume decreases translational and transcriptional noise, while genome replication decreases gene switching noise. During embryogenesis of fruit fly noise is decreased, when just after fertilization cell replicates its genome thirteen times before the 5000 nuclei and the cytoplasm are partitioned into separate cells [139].

The mechanism of stabilization of the epigenetic state can be exploited by persister cells. Persister cells form a sub-colony of non-growing and non-dividing cells which are more resistant to stress. An inhibition of cell growth alone can stabilize the state of persistence, while rare switching to the normal growth state can result in replenishing of a colony of fast growing and dividing cells.

# Bibliography

- [1] D. A. McQuarrie, C. J. Jachimowski, and M. E. Russell, “Kinetics of small systems. II”, *Journal of Chemical Physics*, vol. 40, no. 10, pp. 2914–2921, 1964.
- [2] N. G. van Kampen, *Stochastic Processes in Physics and Chemistry*. Amsterdam: Elsevier, 1992.
- [3] A. Novick and M. Weiner, “Enzyme induction as an all-or-none phenomenon”, *Proceedings of the National Academy of Sciences of the United States of America*, vol. 43, no. 7, p. 553, 1957.
- [4] M. Ko, H. Nakauchi, and N. Takahashi, “The dose dependence of glucocorticoid-inducible gene expression results from changes in the number of transcriptionally active templates”, *The EMBO journal*, vol. 9, no. 9, p. 2835, 1990.
- [5] J. L. Spudich, D. Koshland Jr, *et al.*, “Non-genetic individuality: chance in the single cell”, *Nature*, vol. 262, no. 5568, pp. 467–471, 1976.
- [6] H. McAdams and A. Arkin, “Stochastic mechanisms in gene expression”, *Proceedings of the National Academy of Sciences of the United States of America*, vol. 94, no. 3, pp. 814–819, 1997.
- [7] A. Arkin, J. Ross, and H. H. McAdams, “Stochastic kinetic analysis of developmental pathway bifurcation in phage  $\lambda$ -infected *Escherichia coli* cells”, *Genetics*, vol. 149, no. 4, pp. 1633–1648, 1998.
- [8] D. T. Gillespie, “Exact stochastic simulation of coupled chemical reactions”, *The Journal Physical Chemistry*, vol. 81, no. 25, pp. 2340–2361, 1977.
- [9] P. Paszek, *Modeling stochasticity in gene regulation*. PhD thesis, Rice University, 2006.
- [10] T. B. Kepler and T. C. Elston, “Stochasticity in transcriptional regulation: origins, consequences, and mathematical representations”, *Biophysical Journal*, vol. 81, no. 6, pp. 3116–3136, 2001.
- [11] W. J. Blake, M. Kærn, C. R. Cantor, and J. J. Collins, “Noise in eukaryotic gene expression”, *Nature*, vol. 422, no. 6932, pp. 633–637, 2003.

- [12] J. M. Raser and E. K. O’Shea, “Control of stochasticity in eukaryotic gene expression”, *Science*, vol. 304, no. 5678, pp. 1811–1814, 2004.
- [13] I. Golding, J. Paulsson, S. M. Zawilski, and E. C. Cox, “Real-time kinetics of gene activity in individual bacteria”, *Cell*, vol. 123, no. 6, pp. 1025–1036, 2005.
- [14] J. R. Chubb, T. Treck, S. M. Shenoy, and R. H. Singer, “Transcriptional pulsing of a developmental gene”, *Current Biology*, vol. 16, no. 10, pp. 1018–1025, 2006.
- [15] A. Raj, C. S. Peskin, D. Tranchina, D. Y. Vargas, and S. Tyagi, “Stochastic mRNA synthesis in mammalian cells”, *PLoS Biology*, vol. 4, no. 10, p. e309, 2006.
- [16] A. Becskei, B. B. Kaufmann, and A. van Oudenaarden, “Contributions of low molecule number and chromosomal positioning to stochastic gene expression”, *Nature Genetics*, vol. 37, no. 9, pp. 937–944, 2005.
- [17] I. L. Ross, C. M. Browne, D. A. Hume, *et al.*, “Transcription of individual genes in eukaryotic cells occurs randomly and infrequently”, *Immunology and Cell Biology*, vol. 72, no. 2, pp. 177–185, 1994.
- [18] J. Elliott, R. Festenstein, M. Tolaini, and D. Kioussis, “Random activation of a transgene under the control of a hybrid hCD2 locus control region/Ig enhancer regulatory element”, *The EMBO journal*, vol. 14, no. 3, p. 575, 1995.
- [19] G. Zlokarnik, P. A. Negulescu, T. E. Knapp, L. Mere, N. Burren, L. Feng, M. Whitney, K. Roemer, and R. Y. Tsien, “Quantitation of transcription and clonal selection of single living cells with  $\beta$ -lactamase as reporter”, *Science*, vol. 279, no. 5347, pp. 84–88, 1998.
- [20] J. Chelly, J.-P. Concordet, J.-C. Kaplan, and A. Kahn, “Illegitimate transcription: transcription of any gene in any cell type”, *Proceedings of the National Academy of Sciences*, vol. 86, no. 8, pp. 2617–2621, 1989.
- [21] A. M. Kierzek, J. Zaim, and P. Zielenkiewicz, “The effect of transcription and translation initiation frequencies on the stochastic fluctuations in prokaryotic gene expression”, *Journal of Biological Chemistry*, vol. 276, no. 11, pp. 8165–8172, 2001.
- [22] M. Thattai and A. van Oudenaarden, “Intrinsic noise in gene regulatory networks”, *Proceedings of the National Academy of Sciences*, vol. 98, no. 15, pp. 8614–8619, 2001.
- [23] E. M. Ozbudak, M. Thattai, I. Kurtser, A. D. Grossman, and A. van Oudenaarden, “Regulation of noise in the expression of a single gene”, *Nature genetics*, vol. 31, no. 1, pp. 69–73, 2002.
- [24] J. Yu, J. Xiao, X. Ren, K. Lao, and X. S. Xie, “Probing gene expression in live cells, one protein molecule at a time”, *Science*, vol. 311, no. 5767, pp. 1600–1603, 2006.

- [25] L. Cai, N. Friedman, and X. S. Xie, “Stochastic protein expression in individual cells at the single molecule level”, *Nature*, vol. 440, no. 7082, pp. 358–362, 2006.
- [26] Y. Taniguchi, P. J. Choi, G.-W. Li, H. Chen, M. Babu, J. Hearn, A. Emili, and X. S. Xie, “Quantifying E. coli proteome and transcriptome with single-molecule sensitivity in single cells”, *Science*, vol. 329, no. 5991, pp. 533–538, 2010.
- [27] M. B. Elowitz, A. J. Levine, E. D. Siggia, and P. S. Swain, “Stochastic gene expression in a single cell”, *Science*, vol. 297, no. 5584, pp. 1183–1186, 2002.
- [28] P. S. Swain, M. B. Elowitz, and E. D. Siggia, “Intrinsic and extrinsic contributions to stochasticity in gene expression”, *Proceedings of the National Academy of Sciences*, vol. 99, no. 20, pp. 12795–12800, 2002.
- [29] N. Rosenfeld, J. W. Young, U. Alon, P. S. Swain, and M. B. Elowitz, “Gene regulation at the single-cell level”, *Science*, vol. 307, no. 5717, pp. 1962–1965, 2005.
- [30] D. Kennell and H. Riezman, “Transcription and translation initiation frequencies of the Escherichia coli lac operon”, *Journal of Molecular Biology*, vol. 114, no. 1, pp. 1–21, 1977.
- [31] F. C. Kafatos, “The cocoonase zymogen cells of silk moths: a model of terminal cell differentiation for specific protein synthesis”, *Current Topics in Developmental Biology*, vol. 7, pp. 125–191, 1972.
- [32] B. S. Laursen, H. P. Sørensen, K. K. Mortensen, and H. U. Sperling-Petersen, “Initiation of protein synthesis in bacteria”, *Microbiology and Molecular Biology Reviews*, vol. 69, no. 1, pp. 101–123, 2005.
- [33] L. L. Sampson, R. W. Hendrix, W. M. Huang, and S. R. Casjens, “Translation initiation controls the relative rates of expression of the bacteriophage lambda late genes.”, *Proceedings of the National Academy of Sciences of the United States of America*, vol. 85, no. 15, pp. 5439–5443, 1988.
- [34] R. Young and H. Bremer, “Polypeptide-chain-elongation rate in Escherichia coli B/r as a function of growth rate”, *Biochemical Journal*, vol. 160, no. 2, pp. 185–194, 1976.
- [35] H. Bremer, J. Hymes, and P. P. Dennis, “Ribosomal RNA chain growth rate and RNA labeling patterns in Escherichia coli B-r”, *Journal of Theoretical Biology*, vol. 45, no. 2, pp. 379–403, 1974.
- [36] A. A. Cohen, T. Kalisky, A. Mayo, N. Geva-Zatorsky, T. Danon, I. Issaeva, R. B. Kopito, N. Perzov, R. Milo, A. Sigal, and U. Alon, “Protein dynamics in individual human cells: experiment and theory”, *PLoS One*, vol. 4, no. 4, p. e4901, 2009.
- [37] B. Alberts, A. Johnson, J. Lewis, K. R. Raff, M., and P. Walter, *Molecular Biology of the Cell*. New York: Garland Science, 2002.

- [38] J. A. Bernstein, A. B. Khodursky, P.-H. Lin, S. Lin-Chao, and S. N. Cohen, “Global analysis of mRNA decay and abundance in *Escherichia coli* at single-gene resolution using two-color fluorescent DNA microarrays”, *Proceedings of the National Academy of Sciences of the United States of America*, vol. 99, no. 15, pp. 9697–9702, 2002.
- [39] J. L. Hargrove, “Microcomputer-assisted kinetic modeling of mammalian gene expression”, *FASEB Journal*, vol. 7, no. 12, pp. 1163–1170, 1993.
- [40] K. P. Jayapal, S. Sui, R. J. Philp, Y.-J. Kok, M. G. S. Yap, T. J. Griffin, and W.-S. Hu, “Multitagging proteomic strategy to estimate protein turnover rates in dynamic systems”, *Journal of Proteome Research*, vol. 9, no. 5, pp. 2087–2097, 2010.
- [41] C. Chen and M. P. Deutscher, “RNase R is a highly unstable protein regulated by growth phase and stress”, *RNA*, vol. 16, no. 4, pp. 667–672, 2010.
- [42] H. El-Samad, H. Kurata, J. C. Doyle, C. A. Gross, and M. Khammash, “Surviving heat shock: control strategies for robustness and performance”, *Proceedings of the National Academy of Sciences of the United States of America*, vol. 102, no. 8, pp. 2736–2741, 2005.
- [43] A. Belle, A. Tanay, L. Bitincka, R. Shamir, and E. K. O’Shea, “Quantification of protein half-lives in the budding yeast proteome.”, *Proceedings of the National Academy of Sciences of the United States of America*, vol. 103, no. 35, pp. 13004–13009, 2006.
- [44] A. Mortazavi, B. A. Williams, K. McCue, L. Schaeffer, and B. Wold, “Mapping and quantifying mammalian transcriptomes by RNA-Seq.”, *Nature Methods*, vol. 5, no. 7, pp. 621–628, 2008.
- [45] G. A. Galau, W. H. Klein, R. J. Britten, and E. H. Davidson, “Significance of rare mRNA sequences in liver”, *Archives of Biochemistry and Biophysics*, vol. 179, no. 2, pp. 584–599, 1977.
- [46] V. E. Velculescu, L. Zhang, W. Zhou, J. Vogelstein, M. A. Basrai, D. Bassett, Jr, P. Hieter, B. Vogelstein, and K. W. Kinzler, “Characterization of the yeast transcriptome”, *Cell*, vol. 88, no. 2, pp. 243–251, 1997.
- [47] F. C. Holstege, E. G. Jennings, J. J. Wyrick, T. I. Lee, C. J. Hengartner, M. R. Green, T. R. Golub, E. S. Lander, and R. A. Young, “Dissecting the regulatory circuitry of a eukaryotic genome”, *Cell*, vol. 95, no. 5, pp. 717–728, 1998.
- [48] C. E. Sims and N. L. Allbritton, “Analysis of single mammalian cells on-chip”, *Lab Chip*, vol. 7, no. 4, pp. 423–440, 2007.
- [49] S. Ghaemmaghami, W.-K. Huh, K. Bower, R. W. Howson, A. Belle, N. Dephoure, E. K. O’Shea, and J. S. Weissman, “Global analysis of protein expression in yeast”, *Nature*, vol. 425, no. 6959, pp. 737–741, 2003.

- [50] S. P. Gygi, Y. Rochon, B. R. Franza, and R. Aebersold, “Correlation between protein and mRNA abundance in yeast”, *Molecular and Cellular Biology*, vol. 19, no. 3, pp. 1720–1730, 1999.
- [51] A. P. Bird, “Gene number, noise reduction and biological complexity”, *Trends in Genetics*, vol. 11, no. 3, pp. 94–100, 1995.
- [52] J. H. Thomas, “Thinking about genetic redundancy”, *Trends in Genetics*, vol. 9, no. 11, pp. 395–399, 1993.
- [53] M. A. Nowak, M. C. Boerlijst, J. Cooke, and J. M. Smith, “Evolution of genetic redundancy”, *Nature*, vol. 388, no. 6638, pp. 167–171, 1997.
- [54] H. Weintraub, “The MyoD family and myogenesis: redundancy, networks, and thresholds”, *Cell*, vol. 75, no. 7, pp. 1241–1244, 1993.
- [55] M. Kerszberg, “Accurate reading of morphogen concentrations by nuclear receptors: a formal model of complex transduction pathways”, *Journal of Theoretical Biology*, vol. 183, no. 1, pp. 95–104, 1996.
- [56] A. Becskei and L. Serrano, “Engineering stability in gene networks by autoregulation”, *Nature*, vol. 405, no. 6786, pp. 590–593, 2000.
- [57] L. H. Hartwell and T. A. Weinert, “Checkpoints: controls that ensure the order of cell cycle events”, *Science*, vol. 246, no. 4930, pp. 629–634, 1989.
- [58] W. K. Kaufmann and R. S. Paules, “DNA damage and cell cycle checkpoints”, *FASEB Journal*, vol. 10, no. 2, pp. 238–247, 1996.
- [59] W. A. Wells, “The spindle-assembly checkpoint: aiming for a perfect mitosis, every time”, *Trends in cell biology*, vol. 6, no. 6, pp. 228–234, 1996.
- [60] C. J. Morton-Firth and D. Bray, “Predicting temporal fluctuations in an intracellular signalling pathway”, *Journal of Theoretical Biology*, vol. 192, no. 1, pp. 117–128, 1998.
- [61] A. Bren and M. Eisenbach, “Changing the direction of flagellar rotation in bacteria by modulating the ratio between the rotational states of the switch protein FliM”, *Journal of Molecular Biology*, vol. 312, no. 4, pp. 699–709, 2001.
- [62] M. Thattai and A. Van Oudenaarden, “Stochastic gene expression in fluctuating environments”, *Genetics*, vol. 167, no. 1, pp. 523–530, 2004.
- [63] T. Çağatay, M. Turcotte, M. B. Elowitz, J. Garcia-Ojalvo, and G. M. Süel, “Architecture-dependent noise discriminates functionally analogous differentiation circuits”, *Cell*, vol. 139, no. 3, pp. 512–522, 2009.

- [64] D. M. Wolf, V. V. Vazirani, and A. P. Arkin, “A microbial modified prisoner’s dilemma game: How frequency-dependent selection can lead to random phase variation”, *Journal of Theoretical Biology*, vol. 234, no. 2, pp. 255–262, 2005.
- [65] D. M. Wolf, V. V. Vazirani, and A. P. Arkin, “Diversity in times of adversity: Probabilistic strategies in microbial survival games”, *Journal of Theoretical Biology*, vol. 234, no. 2, pp. 227–253, 2005.
- [66] E. Kussell and S. Leibler, “Ecology: Phenotypic diversity, population growth, and information in fluctuating environments”, *Science*, vol. 309, no. 5743, pp. 2075–2078, 2005.
- [67] W. J. Blake, G. Balázsi, M. A. Kohanski, F. J. Isaacs, K. F. Murphy, Y. Kuang, C. R. Cantor, D. R. Walt, and J. J. Collins, “Phenotypic consequences of promoter-mediated transcriptional noise”, *Molecular Cell*, vol. 24, no. 6, pp. 853–865, 2006.
- [68] J. M. G. Vilar, H. Y. Kueh, N. Barkai, and S. Leibler, “Mechanisms of noise-resistance in genetic oscillators”, *Proceedings of the National Academy of Sciences of the United States of America*, vol. 99, no. 9, pp. 5988–5992, 2002.
- [69] T. Zhou, L. Chen, and K. Aihara, “Molecular communication through stochastic synchronization induced by extracellular fluctuations”, *Physical Review Letters*, vol. 95, no. 17, p. 178103, 2005.
- [70] M. Springer and J. Paulsson, “Biological physics: Harmonies from noise”, *Nature*, vol. 439, no. 7072, pp. 27–28, 2006.
- [71] A. Kuchina, L. Espinar, J. Garcia-Ojalvo, and G. Suel, “Reversible and noisy progression towards a commitment point enables adaptable and reliable cellular decision-making”, *PLoS Computational Biology*, vol. 7, no. 11, 2011.
- [72] H.-S. Choi, S. Han, H. Yokota, and K.-H. Cho, “Coupled positive feedbacks provoke slow induction plus fast switching in apoptosis”, *FEBS Letters*, vol. 581, no. 14, pp. 2684–2690, 2007.
- [73] J. Paulsson, O. Berg, and M. Ehrenberg, “Stochastic focusing: Fluctuation-enhanced sensitivity of intracellular regulation”, *Proceedings of the National Academy of Sciences of the United States of America*, vol. 97, no. 13, pp. 7148–7153, 2000.
- [74] J. Paulsson and M. Ehrenberg, “Random signal fluctuations can reduce random fluctuations in regulated components of chemical regulatory networks”, *Physical Review Letters*, vol. 84, no. 23, pp. 5447–5450, 2000.
- [75] O. G. Berg, J. Paulsson, and M. Ehrenberg, “Fluctuations in repressor control: thermodynamic constraints on stochastic focusing”, *Biophysical Journal*, vol. 79, no. 6, pp. 2944–2953, 2000.

- [76] K. Wiesenfeld and F. Moss, “Stochastic resonance and the benefits of noise: From ice ages to crayfish and SQUIDS”, *Nature*, vol. 373, no. 6509, pp. 33–36, 1995.
- [77] M. D. McDonnell and D. Abbott, “What is stochastic resonance? Definitions, misconceptions, debates, and its relevance to biology”, *PLoS Computational Biology*, vol. 5, no. 5, 2009.
- [78] A. Bulsara, E. Jacobs, T. Zhou, F. Moss, and L. Kiss, “Stochastic resonance in a single neuron model: Theory and analog simulation”, *Journal of Theoretical Biology*, vol. 152, no. 4, pp. 531–555, 1991.
- [79] A. Longtin, A. Bulsara, and F. Moss, “Time-interval sequences in bistable systems and the noise-induced transmission of information by sensory neurons”, *Physical Review Letters*, vol. 67, no. 5, pp. 656–659, 1991.
- [80] J. Douglass, L. Wilkens, E. Pantazelou, and F. Moss, “Noise enhancement of information transfer in crayfish mechanoreceptors by stochastic resonance”, *Nature*, vol. 365, no. 6444, pp. 337–340, 1993.
- [81] J. Levin and J. Miller, “Broadband neural encoding in the cricket cercal sensory system enhanced by stochastic resonance”, *Nature*, vol. 380, no. 6570, pp. 165–168, 1996.
- [82] P. Cordo, J. Ingils, S. Verschueren, J. Collins, D. Merfeld, S. Rosenblum, S. Buckley, and F. Moss, “Noise in human muscle spindles”, *Nature*, vol. 383, no. 6603, pp. 769–770, 1996.
- [83] B. Gluckman, T. Netoff, E. Neel, W. Ditto, M. Spano, and S. Schiff, “Stochastic resonance in a neuronal network from mammalian brain”, *Physical Review Letters*, vol. 77, no. 19, pp. 4098–4101, 1996.
- [84] D. Leonard and L. Reichl, “Stochastic resonance in a chemical reaction”, *Physical Review E*, vol. 49, no. 2, pp. 1734–1737, 1994.
- [85] S. Bezrukov and I. Vodyanoy, “Noise-induced enhancement of signal transduction across voltage-dependent ion channels”, *Nature*, vol. 378, no. 6555, pp. 362–364, 1995.
- [86] L. Zhang, K. Radtke, L. Zheng, A. Q. Cai, T. F. Schilling, and Q. Nie, “Noise drives sharpening of gene expression boundaries in the zebrafish hindbrain”, *Molecular Systems Biology*, vol. 8, 2012.
- [87] J. Hasty, J. Pradines, M. Dolnik, and J. J. Collins, “Noise-based switches and amplifiers for gene expression”, *Proceedings of the National Academy of Sciences*, vol. 97, no. 5, pp. 2075–2080, 2000.
- [88] K. Puszyński, B. Hat, and T. Lipniacki, “Oscillations and bistability in the stochastic model of p53 regulation”, *Journal of Theoretical Biology*, vol. 254, no. 2, pp. 452–465, 2008.

- [89] T. Lipniacki, B. Hat, J. R. Faeder, and W. S. Hlavacek, “Stochastic effects and bistability in T cell receptor signaling”, *Journal of Theoretical Biology*, vol. 254, no. 1, pp. 110–122, 2008.
- [90] J. Hornos, D. Schultz, G. Innocentini, J. Wang, A. Walczak, J. Onuchic, and P. Wolynes, “Self-regulating gene: An exact solution”, *Physical Review E*, vol. 72, no. 5, p. 051907, 2005.
- [91] A. M. Walczak, J. N. Onuchic, and P. G. Wolynes, “Absolute rate theories of epigenetic stability”, *Proceedings of the National Academy of Sciences of the United States of America*, vol. 102, no. 52, pp. 18926–18931, 2005.
- [92] R. Karmakar and I. Bose, “Positive feedback, stochasticity and genetic competence”, *Physical Biology*, vol. 4, no. 01, pp. 29–37, 2007.
- [93] D. Schultz, J. N. Onuchic, and P. G. Wolynes, “Understanding stochastic simulations of the smallest genetic networks”, *Journal of Chemical Physics*, vol. 126, p. 245102, 2007.
- [94] D. Siegal-Gaskins, E. Grotewold, and G. D. Smith, “The capacity for multistability in small gene regulatory networks”, *BMC Systems Biology*, vol. 3, no. 1, p. 96, 2009.
- [95] N. Rosenfeld, M. B. Elowitz, and U. Alon, “Negative autoregulation speeds the response times of transcription networks”, *Journal of Molecular Biology*, vol. 323, no. 5, pp. 785–793, 2002.
- [96] D. Van Sinderen and G. Venema, “comK acts as an autoregulatory control switch in the signal transduction route to competence in *Bacillus subtilis*”, *Journal of Bacteriology*, vol. 176, no. 18, pp. 5762–5770, 1994.
- [97] A. Becskei, B. Séraphin, and L. Serrano, “Positive feedback in eukaryotic gene networks: cell differentiation by graded to binary response conversion”, *The EMBO journal*, vol. 20, no. 10, pp. 2528–2535, 2001.
- [98] H. Ogasawara and M. Kawato, “The protein kinase m $\zeta$  network as a bistable switch to store neuronal memory”, *BMC systems biology*, vol. 4, no. 1, p. 181, 2010.
- [99] R. Roskoski, “Src kinase regulation by phosphorylation and dephosphorylation”, *Biochemical and Biophysical Research Communications*, vol. 331, no. 1, pp. 1–14, 2005.
- [100] J. M. Bradshaw, “The Src, Syk, and Tec family kinases: distinct types of molecular switches”, *Cellular Signalling*, vol. 22, no. 8, pp. 1175–1184, 2010.
- [101] E. M. Ozbudak, M. Thattai, H. N. Lim, B. I. Shraiman, and A. Van Oudenaarden, “Multistability in the lactose utilization network of *Escherichia coli*”, *Nature*, vol. 427, no. 6976, pp. 737–740, 2004.

- [102] A. Lipshtat, A. Loinger, N. Q. Balaban, and O. Biham, “Genetic toggle switch without cooperative binding”, *Physical Review Letters*, vol. 96, p. 188101(4), 2006.
- [103] A. Chatterjee, Y. N. Kaznessis, and W.-S. Hu, “Tweaking biological switches through a better understanding of bistability behavior”, *Current Opinion in Biotechnology*, vol. 19, no. 5, pp. 475–481, 2008.
- [104] M. Ptashne, *A Genetic Switch–Phage Lambda Revisited*. Cold Spring Harbor, New York: Cold Spring Harbor Laboratory Press, 2004.
- [105] T. Wilhelm, “The smallest chemical reaction system with bistability”, *BMC systems biology*, vol. 3, no. 1, p. 90, 2009.
- [106] M. Vellela and H. Qian, “Stochastic dynamics and non-equilibrium thermodynamics of a bistable chemical system: the Schlögl model revisited”, *Journal of the Royal Society Interface*, vol. 6, no. 39, pp. 925–940, 2009.
- [107] M. Acar, A. Becskei, and A. van Oudenaarden, “Enhancement of cellular memory by reducing stochastic transitions”, *Nature*, vol. 435, no. 7039, pp. 228–232, 2005.
- [108] H. Chang, P. Oh, D. Ingber, and S. Huang, “Multistable and multistep dynamics in neutrophil differentiation”, *BMC Cell Biology*, vol. 7, no. 1, p. 11, 2006.
- [109] D. Nevozhay, R. M. Adams, E. Van Itallie, M. R. Bennett, and G. Balázsi, “Mapping the environmental fitness landscape of a synthetic gene circuit”, *PLoS Computational Biology*, vol. 8, no. 4, p. e1002480, 2012.
- [110] A. Nenninger, G. Mastroianni, and C. W. Mullineaux, “Size dependence of protein diffusion in the cytoplasm of *Escherichia coli*”, *Journal of Bacteriology*, vol. 192, no. 18, pp. 4535–4540, 2010.
- [111] M. B. Elowitz, M. G. Surette, P.-E. Wolf, J. B. Stock, and S. Leibler, “Protein mobility in the cytoplasm of *Escherichia coli*”, *Journal of Bacteriology*, vol. 181, no. 1, pp. 197–203, 1999.
- [112] T. J. N. Grima R., D. R. Schmidt, “Steady-state fluctuations of a genetic feedback loop: An exact solution”, *Journal of Chemical Physics*, vol. 137, p. 035104, 2012.
- [113] P. Bokes, J. R. King, A. T. Wood, and M. Loose, “Exact and approximate distributions of protein and mRNA levels in the low-copy regime of gene expression”, *Journal of Mathematical Biology*, vol. 64, no. 5, pp. 829–854, 2012.
- [114] H. Pendar, T. Platini, and R. V. Kulkarni, “Exact protein distributions for stochastic models of gene expression using partitioning of Poisson processes”, *Physical Review E*, vol. 87, no. 4, p. 042720, 2013.

- [115] R. Kubo, K. Matsuo, and K. Kitahara, “Fluctuation and relaxation of macrovariables”, *Journal of Statistical Physics*, vol. 9, no. 1, pp. 51–96, 1973.
- [116] G. Haag, W. Weidlich, and P. Alber, “Approximation methods for stationary solutions of discrete master equations”, *Zeitschrift für Physik B Condensed Matter*, vol. 26, no. 2, pp. 207–215, 1977.
- [117] G. Jenkinson and J. Goutsias, “Numerical integration of the master equation in some models of stochastic epidemiology”, *PLoS one*, vol. 7, no. 5, p. e36160, 2012.
- [118] D. T. Gillespie, “The chemical Langevin equation”, *The Journal of Chemical Physics*, vol. 113, p. 297, 2000.
- [119] C. W. Gardiner *et al.*, *Handbook of stochastic methods*, vol. 3. Springer Berlin, 1985.
- [120] S. B. Zimmerman and S. O. Trach, “Estimation of macromolecule concentrations and excluded volume effects for the cytoplasm of *Escherichia coli*”, *Journal of Molecular Biology*, vol. 222, no. 3, pp. 599–620, 1991.
- [121] S. B. Zimmerman and A. P. Minton, “Macromolecular crowding: biochemical, biophysical, and physiological consequences”, *Annual Review of Biophysics and Biomolecular Structure*, vol. 22, no. 1, pp. 27–65, 1993.
- [122] A. P. Minton, “Molecular crowding: Analysis of effects of high concentrations of inert cosolutes on biochemical equilibria and rates in terms of volume exclusion”, *Methods in Enzymology*, vol. 295, pp. 127–149, 1998.
- [123] A. P. Minton, “The effect of volume occupancy upon the thermodynamic activity of proteins: some biochemical consequences”, *Molecular and Cellular Biochemistry*, vol. 55, no. 2, pp. 119–140, 1983.
- [124] R. J. Ellis, “Macromolecular crowding: an important but neglected aspect of the intracellular environment”, *Current Opinion in Structural Biology*, vol. 11, no. 1, pp. 114–119, 2001.
- [125] K. Luby-Phelps, “Cytoarchitecture and physical properties of cytoplasm: volume, viscosity, diffusion, intracellular surface area”, *International Review of Cytology*, vol. 192, pp. 189–221, 1999.
- [126] B. N. Kholodenko, “Spatially distributed cell signalling”, *FEBS Letters*, vol. 583, no. 24, pp. 4006–4012, 2009.
- [127] S. Ramsey, D. Orrell, and H. Bolouri, “Dizzy: stochastic simulation of large-scale genetic regulatory networks”, *Journal of Bioinformatics and Computational Biology*, vol. 3, no. 02, pp. 415–436, 2005.

- [128] L. A. Harris, J. S. Hogg, and J. R. Faeder, “Compartmental rule-based modeling of biochemical systems”, in *Winter Simulation Conference*, pp. 908–919, Winter Simulation Conference, 2009.
- [129] S. Cooper and C. E. Helmstetter, “Chromosome replication and the division cycle of *Escherichia coli* Br”, *Journal of Molecular Biology*, vol. 31, no. 3, pp. 519–540, 1968.
- [130] M. Scott, C. W. Gunderson, E. M. Mateescu, Z. Zhang, and T. Hwa, “Interdependence of cell growth and gene expression: origins and consequences”, *Science*, vol. 330, no. 6007, pp. 1099–1102, 2010.
- [131] K. Valgepea, K. Adamberg, A. Seiman, and R. Vilu, “*Escherichia coli* achieves faster growth by increasing catalytic and translation rates of proteins”, *Molecular Biosystems*, vol. 9, pp. 2344–2358, 2013.
- [132] M. Bipatnath, P. P. Dennis, and H. Bremer, “Initiation and velocity of chromosome replication in *Escherichia coli* B/r and K-12”, *Journal of Bacteriology*, vol. 180, no. 2, pp. 265–273, 1998.
- [133] O. Michelsen, M. J. T. de Mattos, P. R. Jensen, and F. G. Hansen, “Precise determinations of C and D periods by flow cytometry in *Escherichia coli* K-12 and B/r”, *Microbiology*, vol. 149, no. 4, pp. 1001–1010, 2003.
- [134] M. G. Sargent, “Control of cell length in *Bacillus subtilis*”, *Journal of Bacteriology*, vol. 123, no. 1, pp. 7–19, 1975.
- [135] I. Santi, N. Dhar, D. Bousbaine, Y. Wakamoto, and J. D. McKinney, “Single-cell dynamics of the chromosome replication and cell division cycles in mycobacteria”, *Nature Communications*, vol. 4, 2013.
- [136] M. Osella and M. C. Lagomarsino, “Growth-rate-dependent dynamics of a bacterial genetic oscillator”, *Physical Review E*, vol. 87, no. 1, p. 012726, 2013.
- [137] O. G. Berg, “A model for the statistical fluctuations of protein numbers in a microbial population”, *Journal of Theoretical Biology*, vol. 71, no. 4, pp. 587–603, 1978.
- [138] C. Zong, L.-h. So, L. A. Sepúlveda, S. O. Skinner, and I. Golding, “Lysogen stability is determined by the frequency of activity bursts from the fate-determining gene”, *Molecular Systems Biology*, vol. 6, p. 440, 2010.
- [139] J. A. Campos-Ortega, *The embryonic development of *Drosophila melanogaster**. Springer, 1997.

# Appendices

## Declaration

I declare that Joanna Jaruszewicz, M. Sc., contributed to the research published in:

**Jaruszewicz J, Zuk PJ, Lipniacki T, *Type of noise defines global attractors in bistable molecular regulatory systems*, Journal of Theoretical Biology, (Elsevier), 317: 140–151, 2013,**

completing the following research tasks:

- performed calculations of probability distributions of the protein number in Matlab and Mathematica,
- performed numerical simulations using the Gillespie algorithm,
- analyzed the results,
- contributed in the manuscript preparation.

.....

M. Sc. Joanna Jaruszewicz

.....

Prof. Tomasz Lipniacki

## Declaration

I declare that Joanna Jaruszewicz, M. Sc., contributed to the research published in:

**Jaruszewicz J, Lipniacki T, *Toggle switch: noise determines the winning gene*, Physical Biology, (IOP Press, Great Britain), 10(3), 2013,**

completing the following research tasks:

- calculated deterministic approximations of the models in Matlab and Mathematica,
- performed numerical simulations using the Gillespie algorithm,
- analyzed the results,
- contributed in the manuscript preparation.

.....

M. Sc. Joanna Jaruszewicz

.....

Prof. Tomasz Lipniacki

## Declaration

I declare that Joanna Jaruszewicz, M. Sc., contributed to the research published in:

**Jaruszewicz J, Kimmel M, Lipniacki T, *Stability of bacterial toggle switches is enhanced by cell cycle lengthening by several orders of magnitude*, accepted for publication in the Physical Review E, (American Physical Society), 2014,**

completing the following research tasks:

- building the models of the toggle switch and single gene in dividing cells
- calculated deterministic approximations of the models in Matlab and Mathematica,
- implemented the Gillespie algorithm in dividing cells in C++ and performed numerical simulations,
- analyzed the results,
- prepared the manuscript.

.....

M. Sc. Joanna Jaruszewicz

.....

Prof. Tomasz Lipniacki

## Declaration

I declare that Joanna Jaruszewicz, M. Sc., contributed to the research published in:

**Zuk PJ, Kočańczyk M, Jaruszewicz J, Bednorz W, Lipniacki T, *Dynamics of a stochastic spatially extended system predicted by comparing deterministic and stochastic attractors of the corresponding birth-death process*, Physical Biology, (IOP Press, Great Britain), 9(5): 055002, 2012,**

completing the following research tasks:

- performed calculations for reaction-diffusion model in Comsol,
- contributed in performing numerical simulations of the stochastic spatially extended model,
- contributed in the manuscript preparation.

.....

M. Sc. Pawel Jan Zuk

.....

Prof. Tomasz Lipniacki

## Declaration

I declare that Joanna Jaruszewicz, M. Sc., contributed to the research published in:

**Kochańczyk M, Jaruszewicz J, Lipniacki T, *Stochastic transitions in a bistable reaction system on the membrane*, Journal of the Royal Society Interface, (Royal Society Publishing), 10(84): 20130151, 2013,**

completing the following research tasks:

- performed calculations for reaction-diffusion model in Comsol,
- contributed in performing numerical simulations of the stochastic spatially extended model.

.....

M. Sc. Marek Kochończyk

.....

Prof. Tomasz Lipniacki

I) Jaruszewicz J, Zuk PJ, Lipniacki T, *Type of noise defines global attractors in bistable molecular regulatory systems*, Journal of Theoretical Biology, (Elsevier), 317: 140–151, 2013.



## Type of noise defines global attractors in bistable molecular regulatory systems

Joanna Jaruszewicz<sup>a</sup>, Pawel J. Zuk<sup>a,b</sup>, Tomasz Lipniacki<sup>a,c,\*</sup>

<sup>a</sup> Institute of Fundamental Technological Research, Polish Academy of Sciences, 02-106 Warsaw, Poland

<sup>b</sup> Institute of Theoretical Physics, Faculty of Physics, University of Warsaw, 00-681 Warsaw, Poland

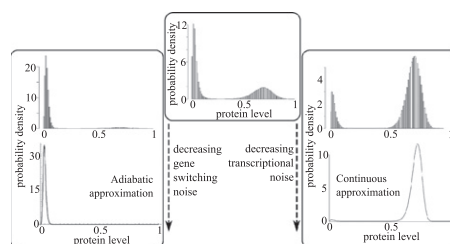
<sup>c</sup> Department of Statistics, Rice University, Houston, TX 77005, USA

### HIGHLIGHTS

- ▶ We analyze stochastic bistable model of single autoregulatory gene.
- ▶ Gene switching, transcriptional and translational noises are considered.
- ▶ We show that the most stable attractor is determined by the type of noise.
- ▶ The noise characteristics changes during cell cycle and development.
- ▶ Noise type changes modify the relative occupancy of epigenetic attractors.

### GRAPHICAL ABSTRACT

Influence of noise on the stationary probability distribution for a single autoregulatory gene with bistability. For low gene switching noise (fast gene switching) the system settles in the inactive steady state (low protein level). For low transcriptional noise (high transcription rate) the system settles in the active steady state (high protein level).



### ARTICLE INFO

#### Article history:

Received 4 June 2012

Received in revised form

24 September 2012

Accepted 2 October 2012

Available online 11 October 2012

#### Keywords:

Gene expression

Bistability

Stochastic processes

Epigenetic attractors

### ABSTRACT

The aim of this study is to demonstrate that in molecular dynamical systems with the underlying bi- or multistability, the type of noise determines the most strongly attracting steady state or stochastic attractor. As an example we consider a simple stochastic model of autoregulatory gene with a nonlinear positive feedback, which in the deterministic approximation has two stable steady state solutions. Three types of noise are considered: transcriptional and translational – due to the small number of gene product molecules and the gene switching noise – due to gene activation and inactivation transitions. We demonstrate that the type of noise in addition to the noise magnitude dictates the allocation of probability mass between the two stable steady states. In particular, we found that when the gene switching noise dominates over the transcriptional and translational noise (which is characteristic of eukaryotes), the gene preferentially activates, while in the opposite case, when the transcriptional noise dominates (which is characteristic of prokaryotes) the gene preferentially remains inactive. Moreover, even in the zero-noise limit, when the probability mass generically concentrates in the vicinity of one of two steady states, the choice of the most strongly attracting steady state is noise type-dependent. Although the epigenetic attractors are defined with the aid of the deterministic approximation of the stochastic regulatory process, their relative attractivity is controlled by the type of noise, in addition to noise magnitude. Since noise characteristics vary during the cell cycle and development, such mode of regulation can be potentially employed by cells to switch between alternative epigenetic attractors.

© 2012 Elsevier Ltd. All rights reserved.

\* Corresponding author at: Department of Statistics, Rice University, Houston, TX 77005, USA.

E-mail addresses: [jjarusz@ippt.gov.pl](mailto:jjarusz@ippt.gov.pl) (J. Jaruszewicz), [pzuk@ippt.gov.pl](mailto:pzuk@ippt.gov.pl) (P.J. Zuk), [tomek@rice.edu](mailto:tomek@rice.edu), [tlipnia@ippt.gov.pl](mailto:tlipnia@ippt.gov.pl) (T. Lipniacki).

### 1. Introduction

From the mathematical perspective intracellular regulatory processes can be considered as stochastic dynamical systems.

Stochasticity arises due to the limited number of reacting molecules such as gene copies, mRNA or proteins. In systems with underlying bistability, even for low noise, the stochastic trajectories exhibit stochastic jumps between basins of attraction and thus diverge qualitatively from the deterministic solutions. The relative stability of steady states depends on the system volume (or noise strength) (Vellela and Qian, 2009). In this study, we analyze the bistable stochastic system with three different types of noise and demonstrate that the dominating type of noise determines the most strongly attracting steady state (global stochastic attractor). That is, two systems with the same deterministic approximation may have qualitatively different stationary probability distributions (SPD) depending on the noise characteristic, even in the zero noise limit.

We consider two models of gene expression with autoregulation. We will assume that the gene is positively regulated by its own product in a cooperative manner, which leads to the nonlinear positive feedback and bistability. Single-cell experiments suggest that gene expression can be described by a three-stage model (Blake et al., 2003; Raser and O’Shea, 2004). The gene promoter can switch between two states (Ko, 1991; Raj et al., 2006; Chubb et al., 2006), one active and one inactive. Such transitions could be associated with binding and unbinding of repressors or transcription factors or with changes in chromatin structure. Transcription can only occur if the promoter is active. The next two stages are mRNA transcription and protein translation. In certain cases when mRNA is very unstable and quickly translated, transcription and translation processes can be lumped together (Kepler and Elston, 2001; Hornos et al., 2005). The resulting model has thus two stages: gene regulation and protein synthesis. Such simplification allows for analytical treatment of the problem, however, lumping of transcription and translation processes may influence the impact of feedback on noise strength (Marquez-Lago and Stelling, 2010). Therefore, in addition to the simplified two-stage model we analyze numerically a more detailed three-stage model in which processes of gene regulation, mRNA transcription and protein translation are explicitly included. The considered models have three types of noise: *transcriptional and translational* – due to the limited number of product molecules, and *gene switching* noise – due to gene state transitions.

*Transcriptional and translational noises* are characteristic for prokaryotes in which the mRNA and protein numbers are very small (McAdams and Arkin, 1997; Kierzek et al., 2001; Ozbudak et al., 2002). Recently, Taniguchi et al. (2010) quantified the mean expression of more than 1000 *Escherichia coli* genes and found that the most frequent average protein number is of order of 10, while the most frequent average mRNA number is smaller than one. The gene switching in prokaryotes is thought to be very fast and thus gene regulation is frequently considered in the so called adiabatic approximation (Hornos et al., 2005), as a process that includes only mRNA transcription and protein translation (Thattai and Oudenaarden, 2001; Swain et al., 2002; Shahrezaei and Swain, 2008).

*Gene switching noise* is important in eukaryotes (Blake et al., 2003; Ko, 1991; Chubb et al., 2006; Raj and Oudenaarden, 2009) in which the transitions between the *on* and *off* states are much less frequent. Analysis of gene expression in mammalian cells showed that mRNA is synthesized in bursts, during periods of time when the gene is transcriptionally active (Raj et al., 2006). Slow gene switching can result in bimodal mRNA and protein probability distributions even in systems without underlying bistability (Hornos et al., 2005; Shahrezaei and Swain, 2008). Bimodality may arise also without bistability in two-stage cascades in which the regulatory gene produces transcription factors that have a nonlinear effect on the activity of the target gene

(Ochab-Marcinek and Tabaka, 2010). In contrast to prokaryotes, in eukaryotes the characteristic mRNA and protein numbers are much larger. Therefore the transcriptional and translational noises in many cases may be neglected (Lipniacki et al., 2006, 2007; Bobrowski et al., 2007) or considered in the diffusion approximation (van Kampen, 2007; Kepler and Elston, 2001). Cell cycle transcriptional regulator gene SWI6 in yeast is an example of a gene with expression noise originating almost only from gene switching noise, while transcriptional noise is negligible (Becksei et al., 2005).

The bistable regulatory elements received a lot of attention in the last decade as they enhance heterogeneity and may allow cells in multicellular organism to specialize and specify their fate. Decisions between cell death, survival, proliferation and senescence are associated with bistability and stochasticity, magnitude of which controls transition rates between the particular attractors (Hasty et al., 2000; Puszyński et al., 2008; Lipniacki et al., 2008). In prokaryotes the bistability is regarded as an optimal strategy for coping with infrequent changes in the environment (Kussell and Leibler, 2005).

The simplest regulatory element exhibiting bistability is the self-regulating gene controlled by a nonlinear positive feedback (Hornos et al., 2005; Walczak et al., 2005; Karmakar and Bose, 2007; Hat et al., 2007; Schultz et al., 2007; Siegal-Gaskins et al., 2009). While not often found as an isolated entity, the self-regulating gene is a common element of biological networks; for example, 40% of *E. coli* transcription factors negatively regulate their own transcription (Rosenfeld et al., 2002). van Sinderen and Vemnema (1994) demonstrated that transcription factor comK acts as an autoregulatory switch in *Bacillus subtilis*. The synthetic auto-regulatory eukaryotic gene switch was studied in *Saccharomyces cerevisiae* (Becksei et al., 2001). The other intensively studied regulatory element exhibiting bistability is the toggle switch – a pair of mutual repressors (Lipshtat et al., 2006; Chatterjee et al., 2008). A classical example is the double-negative regulatory circuit governing alternative lysogenic and lytic states of phage lambda (Ptashne, 2004), lactose utilization network (Ozbudak et al., 2004) or Delta–Notch regulation (Sprinzak et al., 2010).

Despite the low copy number of proteins and mRNAs genetic switches may exhibit very low transition rates, resulting in stable epigenetic properties that persist in simplest organisms for many generations (Ptashne, 2004; Acar et al., 2005), reviewed by Chatterjee et al. (2008). The attractors of genetic networks can be associated with distinct cell types achieved during cell differentiation (Acar et al., 2005; Chang et al., 2006). In a single cell, in the long time scale the relative occupancy of steady states is determined by their relative stability. The same, however, may not be true for cell population when the two steady states are associated with different growth rates. As demonstrated, by Nevozhay et al. (2012) using synthetic bistable gene circuit, the fraction of cells in the most strongly attracting steady state may be low, if these cells have lower growth rate than cells in the less stable steady state. Thus, in the context of cell population the relative occupancy of a given state is defined by rates of state to state transitions (or memory) and fitness associated with particular steady states.

The paper is organized as follows: in the following section we consider the two-stage gene autoregulation model and its three approximations:

- the deterministic approximation,
- the continuous approximation with the gene switching noise only,
- and the adiabatic approximation with the transcriptional and translational noise only.

Based on two last approximations, we demonstrate that the type of noise determines the global attractor. Then, we numerically calculate the SPD in the case when two types of noise are present and show that the most strongly attracting steady state is determined by the prevalent type of noise. For a relatively large subdomain in the parameter space, the SPD is concentrated either in one or the other stable steady state depending on the dominating type of noise. We supplement our consideration of the two-stage model by the analysis of the SPD following from Langevin equations in which the white noise term is added to the equation obtained in the deterministic approximation.

Finally, to confirm our findings, we consider a more detailed, three-stage model in which processes of gene regulation, mRNA transcription and protein translation are explicitly included, which enables distinguishing of transcriptional and translational noises. Within the latter model we demonstrate that the global attractor is determined by relative magnitudes of the transcriptional and gene switching noises, while the translational noise is the least important. We conclude discussing these two types of noise in the context of gene expression in bacteria and eukaryotes.

## 2. Results

### 2.1. Two-stage model and its approximations

We assume that the gene may be in one of the two states – active or inactive, Fig. 1A. In this model we assume that the protein is synthesized directly from the gene, with the rate constant  $Q$  only when the gene is active and is degraded with the rate constant  $r$ . We chose time units in which  $r=1$ . The rate constant  $Q$  is proportional to the product of transcription and translation rate constants  $Q_1$  and  $Q_2$ . The autoregulation arises when gene activation and/or inactivation rates  $c(Y)$  and  $b(Y)$  depend on the level of synthesized protein  $Y$ . The model defines a time continuous Markov process described by two random variables: the gene state  $G(t) \in \{0,1\}$  and number of protein molecules  $Y(t) \in \mathbb{N}$ . The resulting transition propensities are

$$\begin{cases} G=0 \rightarrow G=1, & c(Y), \\ G=1 \rightarrow G=0, & b(Y), \\ Y=n \rightarrow Y=n+1, & QG, \\ Y=n \rightarrow Y=n-1, & n. \end{cases} \quad (1)$$

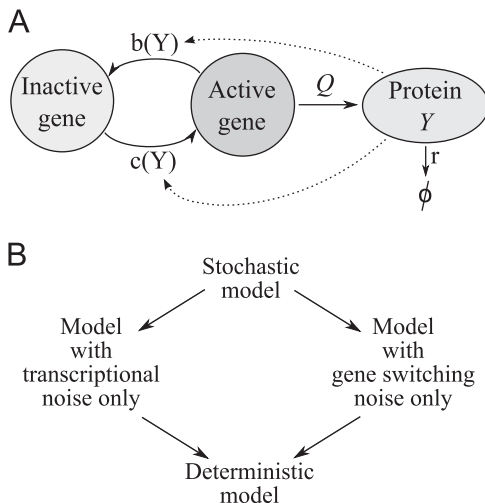


Fig. 1. Two-stage gene expression model. (A) Schematic of the model (B) Stochastic model and its three approximations.

Let  $g_n$  denote the probability that  $\{G, Y\} = \{1, n\}$  and  $h_n$  denote the probability that  $\{G, Y\} = \{0, n\}$ . Probabilities  $g_n$  and  $h_n$  follow a countable set of chemical master equations:

$$\begin{cases} \frac{dg_n}{dt} = Q(g_{n-1} - g_n) + (n+1)g_{n+1} - ng_n + c(n)h_n - b(n)g_n, \\ \frac{dh_n}{dt} = (n+1)h_{n+1} - nh_n - c(n)h_n + b(n)g_n, \end{cases} \quad (2)$$

where we set  $g_{-1} = 0$  to close the first of Eqs. (2).

Here, we focus on such  $c(n)$  and  $b(n)$  that define the positive nonlinear autoregulation leading to bistability. Thus, we assume

$$c(n) = c_0 + (c_2/Q^2)n^2, \quad b(n) = b_0 \quad \text{with } c_0, c_2, b_0 > 0. \quad (3)$$

Such type of regulation arises in the case when the gene is switched on by its own product in a cooperative manner or by the other transcription factor present at some constant level. In order to analyze systems with various average numbers of proteins, but having the same deterministic limit, the nonlinear term  $(c_2/Q^2)n^2$  is scaled by  $Q$ , which is equivalent to the assumption that the gene switching rates are proportional to the protein concentration rather than to the protein number.

Even in the stationary case, the system (2) can be solved analytically using a moment generating function only in the case when  $c(n)$  and  $b(n)$  are both constant, or one of them is constant and the other is linear in  $n$  (Hornos et al., 2005). In our case (3), due to the second order nonlinearity in  $c(n)$ , the method proposed by Hornos et al. (2005) leads to the third order ordinary differential equation, we failed to solve. We will thus estimate the marginal SPD  $f_n = g_n + h_n$  corresponding to the exact model by Monte Carlo simulations of the system (1). Analytically, we will study three approximations to the exact model: the continuous approximation with the gene switching noise only, the adiabatic approximation with the transcriptional noise only, and the deterministic approximation, Fig. 1B.

#### 2.1.1. Deterministic approximation

This classical approximation (Ackers et al., 1982) is justified when the transition rates  $c(n)$  and  $b(n)$  are much greater than one, and simultaneously the characteristic number of protein molecules is very large. In such a case one may consider  $y=Y/Q$  as a continuous variable. The scaled protein level  $y(t)$  is given by a single ordinary differential equation:

$$\frac{dy}{dt} = G(y) - y \quad \text{where } G(y) = \frac{c(y)}{c(y) + b(y)}. \quad (4)$$

In our specific case,  $c(y) = c_0 + c_2y^2$  and  $b(y) = b_0$ , thus the stationary solutions of Eq. (4) are the real roots of the third order polynomial:

$$W = -c_2y^3 + c_2y^2 - (c_0 + b_0)y + c_0 = 0. \quad (5)$$

We will focus on the bistable case when  $W$  has three real roots such that  $0 < y_1 < y_2 < y_3 < 1$ . Steady states  $y_1$  and  $y_3$  are stable, while  $y_2$  is unstable. Due to the fact that  $W$  has the same coefficient at the third and the second power, its roots satisfy  $y_1 + y_2 + y_3 = 1$ . The original coefficients  $b_0, c_0, c_2$  may be recovered from the roots by the following relations:

$$c_0 = \frac{b_0y_1y_2y_3}{y_1(y_2+y_3)+y_2y_3(1-y_1)}, \quad c_2 = \frac{b_0}{y_1(y_2+y_3)+y_2y_3(1-y_1)}. \quad (6)$$

Due to relation  $y_3 = 1 - y_1 - y_2$ , the  $(y_1, y_2, y_3)$  parameter space may be reduced to the domain  $D \ni \{y_1, y_2\}$  such that  $y_1 < y_2$  and  $1 - y_1 - y_2 = y_3 > y_2$ .

#### 2.1.2. Continuous approximation

The model with noise resulting only from gene switching was analyzed previously in Karmakar and Bose (2007). When the

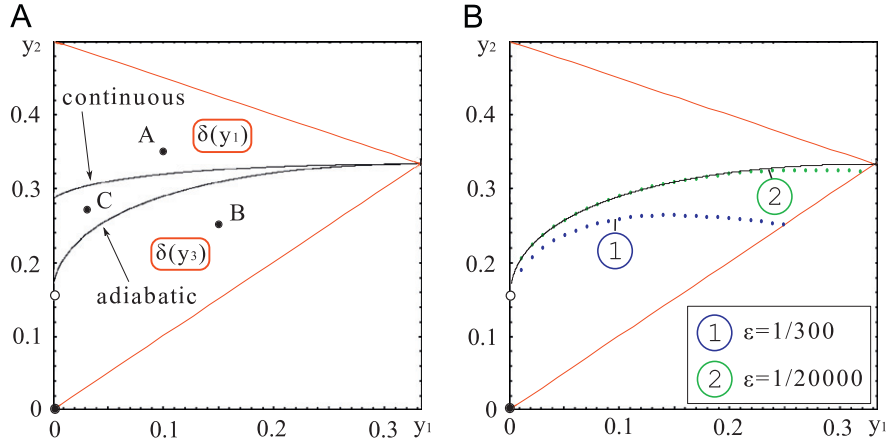


**Fig. 2.** Bistability domain in  $\{y_1, y_2\}$  space. Panel (A): the two black curves divide the domain into three subdomains: in the subdomain  $\mathcal{A}$  (containing point  $A$ ), the SPDs of adiabatic and continuous approximations concentrate in  $y_1$ ; in the subdomain  $\mathcal{B}$  (containing point  $B$ ), the SPDs of the two approximations concentrate in  $y_3$ . In the subdomain  $\mathcal{C}$  (bounded by separatrices  $S_{\text{adiabatic}}$  and  $S_{\text{continuous}}$ ), the SPD for the continuous approximation ( $\varepsilon=0$ ) is concentrated in  $y_3$  while the SPD for the adiabatic approximation ( $\sigma=0$ ) is concentrated in  $y_1$ . Panel (B): continuous line – analytically calculated division curve  $y_2(y_1)$  for the adiabatic approximation ( $\sigma=0$ ) in the  $\varepsilon \rightarrow 0$  limit; dotted lines are the separation lines for a finite noise parameter  $\varepsilon=1/300$  and  $\varepsilon=1/20,000$ .

characteristic number of protein molecules is very large, as in the deterministic case,  $y=Y/Q$  may be considered a continuous variable which follows:

$$\frac{dy}{dt} = G - y, \quad (7)$$

where  $G$ , as in the exact model, is given by the process (1). These assumptions define a time continuous piece-wise deterministic Markov process. Probabilities  $g_n(t)$  and  $h_n(t)$  are now replaced by the continuous functions  $g(y,t)$ ,  $h(y,t)$  that satisfy (Lipniacki et al., 2006; Bobrowski et al., 2007)

$$\frac{\partial h}{\partial t} - \frac{\partial}{\partial y}(yh) = b(y)g - c(y)h, \quad (8)$$

$$\frac{\partial g}{\partial t} + \frac{\partial}{\partial y}((1-y)g) = -b(y)g + c(y)h. \quad (9)$$

The above system has the following stationary solution (Hat et al., 2007)

$$h(y) = \exp\left[\int \left(\frac{-b(y)}{(1-y)} + \frac{c(y)-1}{y}\right) dy\right], \quad g(y) = \frac{yh(y)}{(1-y)}. \quad (10)$$

In our specific case, when  $c(y) = c_0 + c_2 y^2$  and  $b(y) = b_0$ , the marginal SPD  $f(y) = g(y) + h(y)$  may be expressed analytically:

$$f(y; c_2, c_0, b_0) = C e^{(1/2)c_2 y^2} y^{c_0-1} (1-y)^{b_0-1}, \quad (11)$$

where  $C$  is such that  $\int_0^1 f(y) dy = 1$ .

Now, we will replace original coefficients  $b_0, c_0, c_2$  by  $y_1, y_2$  (see Eq. (6)) and introduce  $\sigma \equiv 1/b_0$ . Let us notice that for such defined  $\sigma$  all gene switching noise rates  $b_0, c_0, c_2$  are inversely proportional to  $\sigma$ . The coefficient  $\sigma$  is an inverse of the adiabaticity coefficient, introduced in Hornos et al. (2005), and will be referred to as a measure of gene switching noise. Specifically, we will consider the SPD in the limit  $\sigma \rightarrow 0$ . In this limit the SPD given by Eq. (11) converges either to the Dirac delta in  $y_1$  or in  $y_3$ , i.e. to  $\delta(y_1)$ , or to  $\delta(y_3)$  for all  $\{y_1, y_2\} \in D$ , except  $\{y_1, y_2\}$  such that

$$\lim_{\sigma \rightarrow 0} \frac{f(y_1; y_1, y_2, \sigma)}{\sigma^{-1} f(y_3; y_1, y_2, \sigma)} = C_1 \quad \text{where } 0 < C_1 < \infty. \quad (12)$$

Eqs. (6), (11) and (12) define (in the implicit form) the separatrix  $S_{\text{continuous}}$

$$\left(\frac{1-y_1}{y_1+y_2}\right) \left(\frac{y_1}{1-y_1-y_2}\right)^{p_1} e^{p_2} = 1, \quad (13)$$

where

$$p_1 = \frac{y_1 y_2 (1-y_1-y_2)}{(1-y_1)(1-y_2)(y_1+y_2)}, \quad p_2 = \frac{2y_1+y_2-1}{2(1-y_1)(y_1+y_2)}. \quad (14)$$

That is, in the continuous approximation, the bistability domain  $D$  is split by the separatrix  $S_{\text{continuous}}$  (on which  $0 < C_1 < \infty$ ) into two subdomains. For  $\{y_1, y_2\}$  above the separatrix  $S_{\text{continuous}}$   $C_1 = \infty$  and the SPD converges to  $\delta(y_1)$  as  $\sigma \rightarrow 0$ , while for  $\{y_1, y_2\}$  below the separatrix  $S_{\text{continuous}}$   $C_1 = 0$  and the SPD converges to  $\delta(y_3)$ , see Fig. 2A.

Simulations of the stochastic process in the continuous approximation, i.e. simulation of a piece-wise continuous process given by Eqs. (1) and (7), were performed using the Haseltine and Rawlings (2002) algorithm (Lipniacki et al., 2007). These simulations show significantly different behavior of the protein level  $y(t)$  near each of the two stable stationary points (see Fig. 3C and D). When the trajectory is in the vicinity of  $y_1$  (Fig. 3D) the characteristic time for which the gene is switched off  $\sim 1/c(y_1)$  is much longer than the characteristic time for which the gene is switched on  $\sim 1/b_0$ . When the trajectory is in the vicinity of  $y_3$  (Fig. 3C) these two times are similar. The characteristic departures from both states  $y_1$  and  $y_3$  are larger towards  $y_2$  than in the opposite direction. For low noise there are relatively few transitions through the unstable state  $y_2$ . The frequency of these transitions decreases to zero with decreasing noise.

### 2.1.3. Adiabatic approximation

This approximation is justified when transition rates  $c(n)$  and  $b(n)$  are much larger than the protein degradation rate constant. In such a case,  $G$  may be replaced (Hornos et al., 2005; Bobrowski, 2006) by its expected value  $G = G(n) = c(n)/(c(n) + b(n))$ . This approximation leads to a birth–death process with birth and death propensities:

$$\begin{aligned} B(n) &= G(n)Q, \\ D(n) &= n. \end{aligned} \quad (15)$$

As in the case of the continuous approximation, the simulations show that trajectories near each stable stationary point differ significantly, Fig. 4. The birth and death events are less frequent near  $y_1$  than near  $y_3$ .

Let  $F_n$  denote the stationary probability that the number of protein molecules is equal to  $n$ . In the steady state the net probability current between neighboring states  $N$  and  $N+1$  is

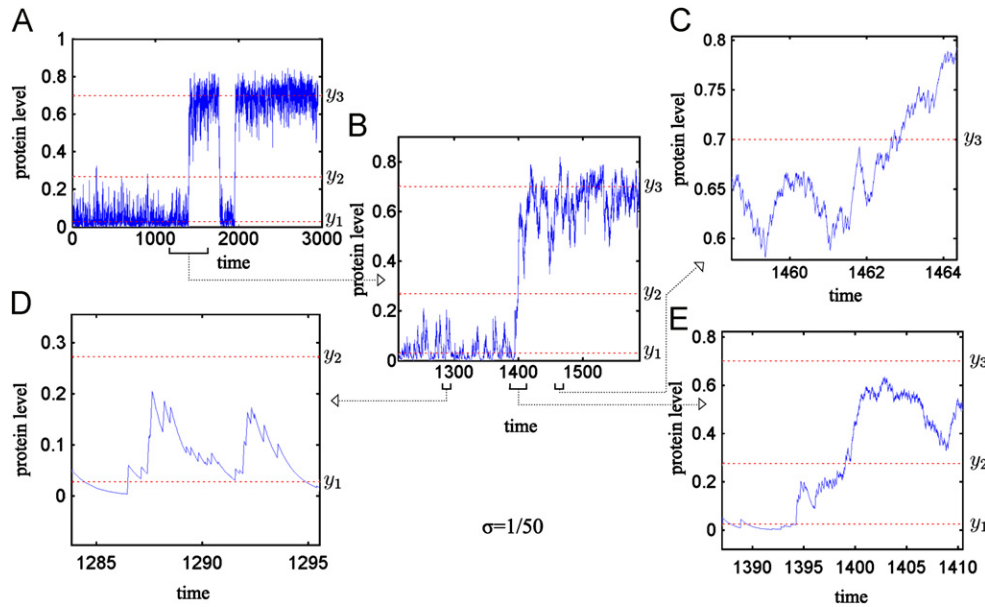


**Fig. 3.** Two-stage model: Stochastic simulation trajectory for the continuous approximation,  $\varepsilon = 0$ . Protein level obtained in the numerical simulation for  $\sigma = 1/50$ . The three steady states  $y_1 = 0.03$  (stable),  $y_2 = 0.27$  (unstable) and  $y_3 = 0.7$  (stable) of the deterministic approximation are shown by the dashed lines. For such  $y_1, y_2, y_3$  (corresponding to point C in Fig. 2A) the SPD of the continuous approximation converges to  $\delta(y_3)$  as  $\sigma \rightarrow 0$ , see Fig. 5C. Time is given in units in which the protein degradation rate constant is equal to 1. Panel (B) shows the zoomed region from Panel (A) around transition from the low to the high protein level, the further detail of this transition is shown in Panel (E); Panel (D) shows trajectory in the vicinity of the steady state  $y_1$ ; Panel (C) shows trajectory in the vicinity of the steady state  $y_3$ .

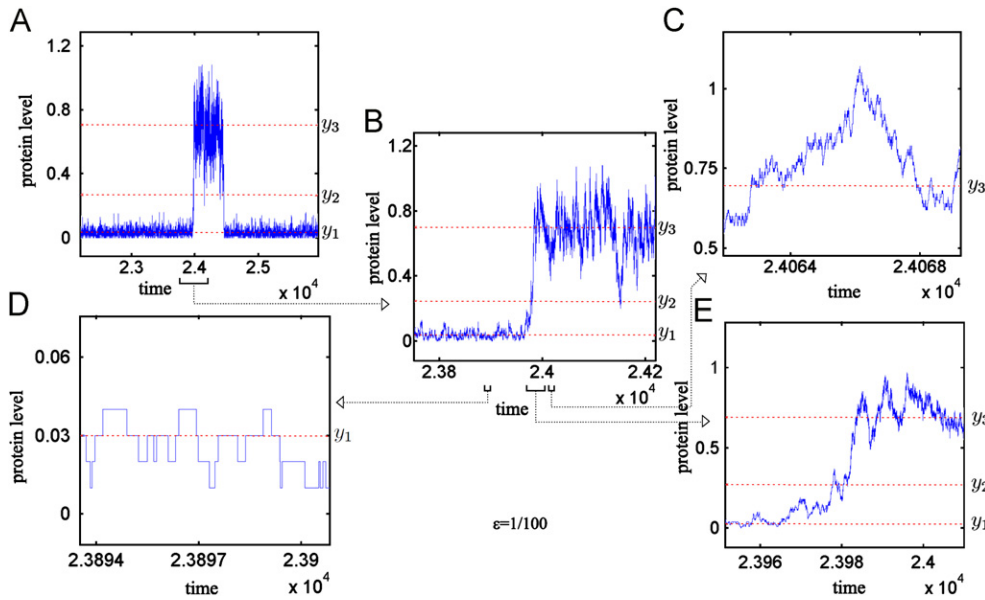


**Fig. 4.** Two-stage model: Stochastic simulation trajectory for adiabatic approximation,  $\sigma = 0$ . Protein level obtained in the numerical simulation for  $\varepsilon = 1/100$ . The three steady states  $y_1 = 0.03$  (stable),  $y_2 = 0.27$  (unstable) and  $y_3 = 0.7$  (stable) of the deterministic approximation are shown by the dashed lines. For such  $y_1, y_2, y_3$  (corresponding to point C in Fig. 2A) the SPD of the adiabatic approximation converges to  $\delta(y_1)$  as  $\varepsilon \rightarrow 0$ , see Fig. 5C. Panel (B) shows the zoomed region from Panel (A) around transition from the low to high protein level, the detail of this transition is shown in Panel (E); Panel (D) shows trajectory in the vicinity of steady state  $y_1$ ; Panel (C) shows trajectory in the vicinity of steady state  $y_3$ .

equal to zero, i.e.

$$F_n B(n) - F_{n+1} D(n+1) = 0, \tag{16}$$

which gives  $F_n$  in the form:

$$F_n = F_0 \prod_{i=0}^{n-1} \frac{B(i)}{D(i+1)}. \tag{17}$$

Eq. (17) defines the discrete probability density function  $F_n$  when

$\sum_{n=1}^{\infty} (\prod_{i=0}^{n-1} B(i)/D(i+1)) < \infty$ , which is satisfied provided that for sufficiently large  $j$ ,  $B(i)/D(i+1) < a < 1$  for all  $i > j$ . Since  $B(i)/D(i+1) < Q/n$ , the last condition holds. Now, we may choose  $F_0$  such that  $\sum_{n=0}^{\infty} F_n = 1$ . We analyze the discrete probability density  $F_n$  for small  $\varepsilon = 1/Q$ . In the limit of  $\varepsilon \rightarrow 0$ , the adiabatic approximation converges to the deterministic approximation, and so the coefficient  $\varepsilon$  will be considered as a measure of transcriptional and translational noise. Let  $F^Q(y) := QF_n$ , where  $y := n/Q$ , i.e.  $F^Q(y) = QF^Q(0) \prod_{i=1}^{yQ-1} \mathbf{b}(i/Q)/\mathbf{d}(i/Q + 1/Q)$ , where  $\mathbf{b}(i/Q) := B(i)$ ,

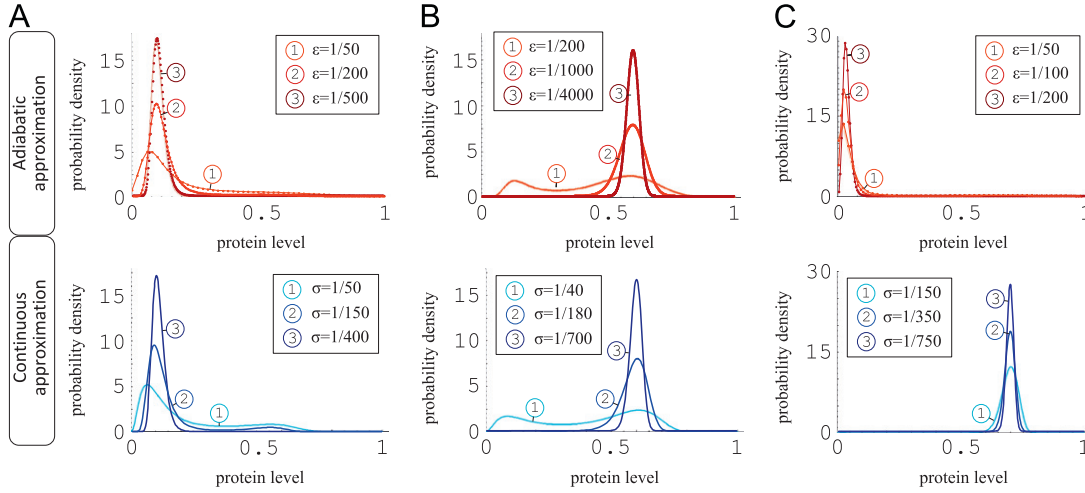


**Fig. 5.** The SPDs for the adiabatic and continuous approximations. Columns A, B and C correspond to points A, B and C in Fig. 2A. Upper row panels – the adiabatic approximation, lower row panels – the continuous approximation. For  $y_1 = 0.03, y_2 = 0.27$ , in the zero noise limit (column C), the SPDs of the adiabatic and the continuous approximations converge, respectively, to  $\delta(y_1)$ , and  $\delta(y_3)$ .

$\mathbf{d}(i/Q) := D(i)$ . Now,

$$\log F^Q(y) = \log Q + \log F^Q(0) + \sum_{i=1}^{yQ-1} \log \frac{\mathbf{b}(i/Q)}{\mathbf{d}(i/Q + 1/Q)}. \quad (18)$$

In the limit of  $\varepsilon \rightarrow 0$ ,  $\mathbf{d}(i/Q + 1/Q) \rightarrow \mathbf{d}(i/Q)$ . Next, replacing the sum by the integral, we obtain

$$\log F^Q(y) = \log Q + \log F^Q(0) + Q \int_0^y \log \frac{\mathbf{b}(z)}{\mathbf{d}(z)} dz, \quad (19)$$

thus

$$F^Q(y) = Q F^Q(0) \exp\left(Q \int_0^y \log \frac{\mathbf{b}(z)}{\mathbf{d}(z)} dz\right). \quad (20)$$

Since  $\int_0^\infty F^Q(z) dz = 1$  we get

$$F^Q(y) = \frac{\exp(Q\phi(y))}{\int_0^\infty \exp(Q\phi(z)) dz}, \quad (21)$$

where

$$\phi(y) = \int_0^y \log \frac{\mathbf{b}(z)}{\mathbf{d}(z)} dz. \quad (22)$$

The Laplace's method implies that in the limit of  $Q \rightarrow \infty$ , the function  $F^Q(y)$  converges to the Dirac delta distribution  $\delta(y_m)$  in the unique global maximum  $y_m$  of  $\phi(y)$ , provided that such global maximum exists. In our case  $\mathbf{b}(y) = Q(c_0 + c_2 y^2)/(c_0 + c_2 y^2 + b_0)$  and  $\mathbf{d}(y) = Qy$ . Using Eqs. (6) and (22) we obtain

$$\begin{aligned} \phi(y) = & 2\sqrt{y_1 y_2 y_3} \arctan\left[\frac{y}{\sqrt{y_1 y_2 y_3}}\right] \\ & - 2\sqrt{y_2 y_3 + y_1(y_3 + y_2)} \arctan\left[\frac{y}{\sqrt{y_2 y_3 + y_1(y_3 + y_2)}}\right] \\ & + y \left(1 + \log\left[\frac{y_1 y_2 y_3 + y^2}{y(y_2 y_3 + y_1(y_3 + y_2) + y^2)}\right]\right). \end{aligned} \quad (23)$$

Since the extrema of  $F^Q(y)$  coincide with the extrema of  $\phi(y)$ , the global maximum of  $\phi(y)$  is either in  $y_1$  or  $y_3$ , thus the SPD converges either to  $\delta(y_1)$  or to  $\delta(y_3)$  as  $Q \rightarrow \infty$ . Only in the non-generic case, in which  $\phi(y)$  has no global maximum, i.e. when

$$\phi(y_1) = \phi(y_3) \quad (24)$$

the SPD converges to the sum of two Dirac delta functions  $A_1 \delta(y_1) + A_3 \delta(y_3)$ . Eqs. (23) and (24) define the separatrix  $S_{\text{adiabatic}}$ . For  $\{y_1, y_2\}$  above the separatrix  $S_{\text{adiabatic}}$  the SPD converges to  $\delta(y_1)$ , while for  $\{y_1, y_2\}$  below the separatrix  $S_{\text{adiabatic}}$  the SPD converges to  $\delta(y_3)$  as  $\varepsilon \rightarrow 0$ , Fig. 2A. The allocation of probability mass depends

also on the magnitude of noise. In Fig. 2B we show the separatrices, (defined as lines  $y_2(y_1)$  on which the SPD is equally distributed between the two basins of attraction) obtained from Eq. (17) for two values of  $\varepsilon$ . The separatrices converge to  $S_{\text{adiabatic}}$  as  $\varepsilon \rightarrow 0$ .

### 2.2. SPD dependence on the transcriptional and gene switching noise magnitudes

Simulations in the continuous and adiabatic models (see Figs. 3 and 4) were both performed for point  $C = \{y_1 = 0.03, y_2 = 0.27\}$  in the parameter space shown in Fig. 2A. For the continuous approximation the characteristic departures from the stable steady states  $y_1$  and  $y_3$  are of similar magnitude. The case of the adiabatic approximation is different. Here, the fluctuations around point  $y_3$  are much larger than around point  $y_1$ . This suggests that the average time spent in the vicinity of point  $y_1$  before the transition to point  $y_3$  will be longer than the average time spent in the vicinity of point  $y_3$  before the reverse transition. As a result the SPD for the adiabatic approximation will concentrate around point  $y_1$ , while for the continuous approximation the SPD will concentrate around  $y_3$ . This effect should be even more pronounced in the low noise limit when the transitions between the two attractors are less frequent. Accordingly, as shown in Fig. 2A the separatrices  $S_{\text{adiabatic}}$  and  $S_{\text{continuous}}$  are different, and together they bound domain  $\mathcal{C}$ , such that in the zero noise limit for  $\{y_1, y_2\} \in \mathcal{C}$ , the SPD of the continuous model converges to  $\delta(y_1)$ , while the SPD of the adiabatic model converges to  $\delta(y_3)$ . In the further analysis we consider the three sets of roots shown in Fig. 2A, i.e.

$$\begin{aligned} A &= \{0.1, 0.35\} \in \mathcal{A}, \\ B &= \{0.15, 0.25\} \in \mathcal{B}, \\ C &= \{0.03, 0.27\} \in \mathcal{C}. \end{aligned}$$

In Fig. 5, we compare the SPD of the adiabatic and of the continuous approximations. For  $\{y_1, y_2\} = A$  and  $\{y_1, y_2\} = B$  the SPDs obtained in both approximations are concentrated (in the low noise limit) in the vicinity of the same steady state,  $y_1$  and  $y_3$ , respectively, for A and B. However, for  $\{y_1, y_2\} = C$ , the SPD of the adiabatic approximation is concentrated in the vicinity of  $y_1$ , while the SPD of the continuous approximation is concentrated in the vicinity of  $y_3$ . Let us also note that in case B the magnitude of noise controls the relative allocation of probability mass between basins of attraction of steady states  $y_1$  and  $y_3$ .

In the adiabatic approximation the gene switching noise  $\sigma$  is, by definition, identically 0. Similarly, in the continuous approximation

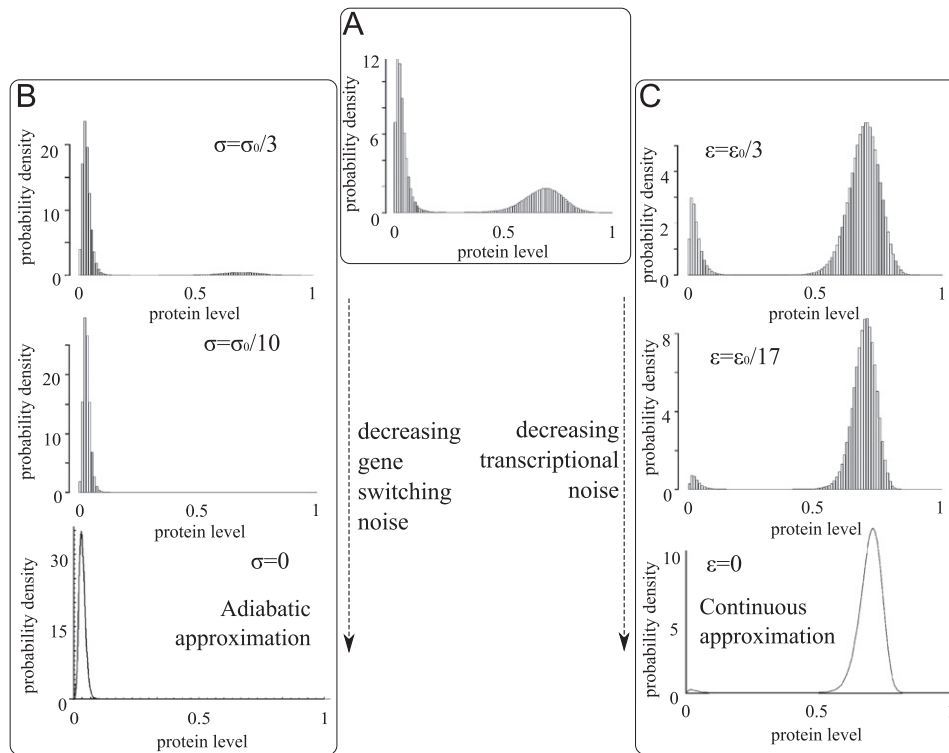


**Fig. 6.** The SPD of the two-stage model obtained in Monte Carlo simulations for  $y_1 = 0.03$ ,  $y_2 = 0.27$  (point C in Fig. 2A). Panel (A) shows the bimodal SPD in the case when the magnitudes of two types of noise are comparable:  $\varepsilon_0 = 1/300$ ,  $\sigma_0 = 1/100$ . Panel (B) consisting of three subpanels shows the SPD for the constant transcriptional noise  $\varepsilon_0$  and decreasing gene switching noise  $\sigma$ . Panel (C) also consisting of three subpanels, shows the SPD for the constant gene switching noise  $\sigma_0$  and decreasing transcriptional noise  $\varepsilon$ . The lowest subpanels show the analytically calculated SPDs for the adiabatic and continuous approximations.

the transcriptional and translational noise  $\varepsilon$  is identically 0. We thus showed that in the parameter subdomain  $\mathcal{C}$  the system settles in the inactive state for  $\varepsilon/\sigma = \infty$  (adiabatic approximation) and settles in the active state for  $\varepsilon/\sigma = 0$  (continuous approximation). This suggests that there exist a range of parameters for which noise ratio  $\varepsilon/\sigma$  determines which of the two steady states is the most strongly attracting. We now verify this conjecture considering the exact model with different  $\varepsilon$  and  $\sigma$  values, see Fig. 6. To estimate the SPD we performed long-run Monte Carlo simulations of the system (1) using the Gillespie (1977) algorithm. For the analysis shown in Fig. 6, we chose  $C = \{0.03, 0.27\} \in \mathcal{C}$ . Such a choice of  $\{y_1, y_2\}$  produces the equimodal SPD in the case when magnitudes of transcriptional and gene switching noises are comparable (and sufficiently large), i.e.  $\varepsilon = 1/300$  and  $\sigma = 1/100$ . We observe that when magnitude of the transcriptional or gene-switching noise decreases to zero the SPD becomes unimodal. As expected from the analysis shown in Fig. 5, the SPD is concentrated in  $y_1$  as  $\sigma \rightarrow 0$  (adiabatic approximation limit), and in  $y_3$  as  $\varepsilon \rightarrow 0$  (continuous approximation limit). Therefore, we demonstrated that when two types of noise are present, their relative magnitudes determine the global attractor. This effect has an analog in equilibrium selection in evolutionary games (Miekiusz, 2005).

### 2.3. Langevin approach

The classical approach to complex stochastic systems involves Langevin equation in which various noise sources are replaced by white noise, which magnitude is either constant (additive noise) or is a function of the solution (multiplicative noise), in the simplest case is proportional to the solution (as in geometric Brownian motion equation). Here, we follow this procedure starting from the deterministic approximation of our model.

Langevin–Ito equation extending deterministic equation (4) is

$$\frac{dy}{dt} = A(y) + \xi(t)\sqrt{B(y)/V} \quad \text{where } A(y) := G(y) - y \quad (25)$$

and  $\xi(t)$  is a Gaussian white noise, with

$$\langle \xi(t) \rangle = 0, \quad \langle \xi(t)\xi(t') \rangle = \delta(t-t'). \quad (26)$$

In this description  $\sqrt{B(y)/V}$  is identified as noise intensity, where  $V$  is the volume of the reactor. In the case of additive noise  $B(y) = \text{const} = B_0$ . We consider also the case of multiplicative noise, assuming that its magnitude is proportional to  $y(t)$  and set  $B(y) = y$ . The other choice of multiplicative noise was made by Frigola et al. (2012), who assumed that magnitude of noise is proportional to the sum of birth and death rates (in our case it would be  $G(y) + y$ ). One should notice that such a choice is in a sense arbitrary since adding any function  $f(y)$  to birth and death rates, leaves deterministic equation unchanged but changes its stochastic counterpart.

The Fokker–Planck equation corresponding to the above Langevin–Ito equation reads (van Kampen, 2007)

$$\frac{\partial F(y,t)}{\partial t} = -\frac{\partial}{\partial y}((A(y))F(y,t)) + \frac{1}{2V} \frac{\partial^2}{\partial y^2}(B(y)F(y,t)). \quad (27)$$

In the stationary case ( $\partial F(y,t)/\partial t = 0$ ) this equation solves explicitly to

$$F(y) = \frac{CV}{B(y)} \exp(-2V\phi(y)), \quad (28)$$

where  $\phi(y)$

$$\phi(y) = -\int_0^y \frac{A(z)}{B(z)} dz \quad (29)$$

has the meaning of a potential. In the case of additive noise,  $B(y) = B_0$ ,  $\phi(y)$  is proportional to the deterministic potential  $\phi(y) = -\int_0^y A(z) dz$ .

Analogously to the previous section the separatrices  $S_{\text{additive}}$  and  $S_{\text{multiplicative}}$  are given in implicit form by  $\phi(y_1) = \phi(y_3)$ . In Fig. 7 we show them together with previously determined separatrices  $S_{\text{adiabatic}}$  and  $S_{\text{continuous}}$  in  $y_1, y_2$  plane. In order to calculate these two new separatrices, we make use of Eqs. (6) giving  $c_0$  and  $c_2$  as functions of  $y_1, y_2$  and  $y_3$ .

The alternative way of calculating separatrices  $S_{\text{additive}}$  and  $S_{\text{multiplicative}}$  involves the, so called, Dynkin equation (dual to Fokker–Plank equation) for the first mean passage time (MFPT)  $T_{\theta, \gamma}(y)$  from  $y$  to the absorbing boundary at  $y = \theta$ , with the reflective boundary at  $y = \gamma$  (see the book of Gardiner et al., 2004 for the MFPT introduction, and Nevozhay et al., 2012; Frigola et al., 2012 for the recent relevant application of this method):

$$-1 = A(y) \frac{\partial T_{\theta, \gamma}(y)}{\partial y} + \frac{1}{2V} B(y) \frac{\partial^2 T_{\theta, \gamma}(y)}{\partial y^2}. \quad (30)$$

The boundary conditions are  $T_{\theta, \gamma}(\theta) = 0$ , and  $dT_{\theta, \gamma}/dy = 0$  at  $y = \gamma$ . In the low noise limit, the probability mass fraction concentrated in the vicinity of the steady state  $y_1$  is  $(T_{3 \rightarrow 1}) / (T_{3 \rightarrow 1} + T_{1 \rightarrow 3})$ , where  $T_{1 \rightarrow 3}$  is the MFPT from  $y_1$  to  $y_3$  and  $T_{3 \rightarrow 1}$  is the MFPT from  $y_3$  to  $y_1$ . To calculate  $T_{1 \rightarrow 3}$  we set  $\theta = y_3$  and  $\gamma = 0$ , while to calculate  $T_{3 \rightarrow 1}$  we set  $\theta = y_1$  and  $\gamma = \infty$ . Our separatrices are given by equality  $T_{3 \rightarrow 1} = T_{1 \rightarrow 3}$  in  $V \rightarrow \infty$  limit. Obviously, MFPTs give more information than just the probability mass allocation as they account for cell memory (Nevozhay et al., 2012). Times  $T_{1 \rightarrow 3}$  and  $T_{3 \rightarrow 1}$  may be obtained in explicit integral forms from Eq. (30) (Gardiner, 2004).

In summary, using the classical Langevin approach we confirmed that a prediction of the most strongly attracting steady state, strongly depends on assumed noise, here, either additive or multiplicative. As one could expect, the additive noise separatrix closely matches with that of continuous approximation in which noise results solely from gene switching, while the multiplicative noise separatrix closely matches with that of the adiabatic approximation for which the magnitude of noise grows with the number of molecules. As already said, in the original stochastic model the most strongly attracting steady state is determined by the relative magnitude of gene switching, transcriptional and translational noises, and thus in general it may not be predicted basing on the Langevin equation in which all noise sources are lumped together and replaced by white noise. By considering arbitrary noise functions we showed recently, that any steady state can become a global stochastic attractor for particular choice of noise (Zuk et al., 2012).

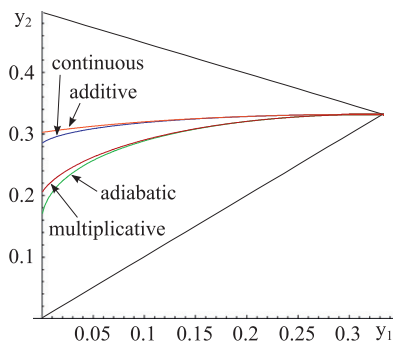


Fig. 7. Separatrices the calculated for the continuous and adiabatic approximations (as in Fig. 2A) compared with those resulting from the Fokker–Plank equation with assumed either additive or multiplicative noise. For each of approximations for  $y_1, y_2$  above the separatrix, the global attractor is in  $y_1$ , while for  $y_1, y_2$  below the separatrix the global attractor is in  $y_3$ .

### 2.4. Three-stage model

In this section we consider a more detailed model of an autoregulatory gene and demonstrate that the choice of the most strongly attracting steady state is governed by the relative magnitudes of gene switching, transcriptional and translational noises. The following three processes are included in the model: the gene activation/inactivation, mRNA transcription and protein translation, Fig. 8. The mRNA is synthesized with the rate constant  $Q_1$  and is degraded with the rate constant  $r_1$ . The protein is translated on the mRNA template with the rate constant  $Q_2$  and is degraded with the rate constant  $r_2$ . The transcriptional and translational noises are characterized, respectively, by parameters  $\varepsilon_1 = r_1/Q_1$  and  $\varepsilon_2 = r_2/Q_2$ . Thus the characteristic number of proteins (achieved when the gene is turned on for infinitely long time) is equal to  $N = 1/(\varepsilon_1 \varepsilon_2)$ . As in the previous model we assume that the gene may be in one of two states: inactive  $G=0$  (no mRNA synthesis) or  $G=1$ , active due to binding of its own protein or some transcription factor implicitly present in the model at constant concentration. The transition from state  $G=0$  to  $G=1$  proceeds with rate  $c_0 + (c_2/N^2)Y^2$  (where  $Y$  is the number of proteins), while the transition from  $G=1$  to  $G=0$  proceeds with constant rate  $b_0$ . The coefficient  $c_2$  describing cooperative auto-activation scales with  $N^2$ , which is equivalent to the assumption that protein binding rate is proportional to the concentration rather than to the number of molecules. It is assumed that the cell size is proportional to the characteristic protein number  $N$ . As in the previous model the gene switching noise is characterized by the parameter  $\sigma = 1/b_0$ . The model defines a time continuous Markov process described by three random variables: the gene state  $G(t) \in \{0, 1\}$ , number of mRNA molecules  $X(t) \in \mathbb{N}$  and number of proteins  $Y(t) \in \mathbb{N}$ .

The assumed reaction rate constants are listed in Table 1. For a non-dimensional analysis we chose time units in which  $r_2 = 1$  (third column). Parameter values for prokaryotes and eukaryotes are calculated by assuming  $r_2 = 10^{-4}/s$ . As discussed in the Introduction, prokaryotes are characterized by large transcriptional and translational noise, while eukaryotes have larger gene switching noise. Therefore, in the example shown in Fig. 9, we assume for bacteria  $\varepsilon_1 = \varepsilon_{01}$ ,  $\varepsilon_2 = \varepsilon_{02}$ ,  $\sigma = \sigma_0/100$  and for eukaryotes  $\varepsilon_1 = \varepsilon_{01}/5$ ,  $\varepsilon_2 = \varepsilon_{02}/25$ ,  $\sigma = \sigma_0$ , where  $\varepsilon_{01} = 1/15$ ,  $\varepsilon_{02} = 1/75$  and  $\sigma_0 = 1/50$ . Parameters  $\varepsilon_{01}$ ,  $\varepsilon_{02}$  and  $\sigma_0$ , will be referred to as default parameters. They are so chosen that the SPD corresponding to the Markov process is bimodal, and the probability mass is equally distributed between two basins of attraction, Fig. 9A. Fig. 10 shows stochastic simulation trajectory corresponding to the SPD shown in Fig. 9A.

In the  $\sigma \rightarrow 0$ ,  $\varepsilon_1 \rightarrow 0$  and  $\varepsilon_2 \rightarrow 0$  limit, the considered Markov process for  $X(t), Y(t)$  can be approximated by the system of two ordinary differential equations for scaled variables  $x(t) = \varepsilon_1 X(t)$ ,  $y(t) = \varepsilon_1 \varepsilon_2 Y(t)$ :

$$\frac{dx}{dt} = r_1(\bar{G}(y) - x) \quad \text{where } \bar{G}(y) = \frac{c_0 + c_2 y^2}{c_0 + c_2 y^2 + b_0}, \quad (31)$$

$$\frac{dy}{dt} = r_2(x - y). \quad (32)$$

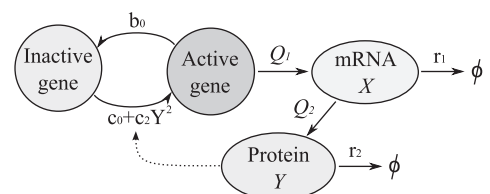


Fig. 8. Schematic of the three-stage model.

**Table 1**  
Model parameters.

Name	Symbol	Non-dimensional value	Value for bacteria	Value for eukaryotes
Transcriptional noise default value	$\varepsilon_{01}$	1/15		
Translational noise default value	$\varepsilon_{02}$	1/75		
Gene switching noise default value	$\sigma_0$	1/50		
Transcriptional noise	$\varepsilon_1$		$\varepsilon_{01}$	$\varepsilon_{01}/5$
Translational noise	$\varepsilon_2$		$\varepsilon_{02}$	$\varepsilon_{02}/25$
Gene switching noise	$\sigma$		$\sigma_0/100$	$\sigma_0$
Protein degradation	$r_2$	1	$10^{-4}/s^a$	$10^{-4}/s^b$
mRNA degradation	$r_1$		$10^{-3}/s^c$	$10^{-3}/s^d$
Inducible gene activation	$c_2$	$4.8r_2(\varepsilon_1\varepsilon_2)^2/\sigma$	$1.9 \times 10^{-6}/s^e$	$1.2 \times 10^{-12}/s^f$
Basal gene activation	$c_0$	$0.027r_2/\sigma$	$0.0135/s^e$	$0.000135/s^g$
Gene inactivation	$b_0$	$r_2/\sigma$	$0.5/s^e$	$0.005/s^g$
mRNA transcription	$Q_1$	$r_1/\varepsilon_1$	$0.015/s^h$	$0.075/s^i$
Protein translation	$Q_2$	$r_2/\varepsilon_2$	$0.0075/s^j$	$0.1875/s^k$
mRNA number in inactive (active) state		$0.03/\varepsilon_1$	0.5	2.28
Protein number in inactive (active) state		$(0.64/\varepsilon_1)$	$(10.6)^l$	$(53.2)^m$
		$0.03/\varepsilon_1\varepsilon_2$	34.3	4290.1
		$(0.64/\varepsilon_1\varepsilon_2)$	$(798.4)^n$	$(99799.4)^o$

<sup>a</sup> Most of bacterial proteins are very stable, with degradation rate constants:  $1.4 \times 10^{-5}$ – $5.6 \times 10^{-5}/s$  (Jayapal et al., 2010). Some proteins have much higher degradation rates. *E. coli* RNase R has degradation rate constant of  $10^{-3}/s$  (in exponential phase) (Chen and Deutscher, 2010), factor  $\sigma^{32}$  has degradation rate constant of  $10^{-2}/s$  (in steady-state growth phase) (El-Samad et al., 2005).

<sup>b</sup> Mammals: protein degradation rate constants:  $1.7 \times 10^{-6}$ – $1.7 \times 10^{-3}/s$  (Hargrove, 1993).

<sup>c</sup> The vast majority of mRNAs in a bacterial cell are very unstable, having a half-life of about 3 min (decay rate constant  $3 \times 10^{-3}/s$ ) (Alberts et al., 2002). *E. coli*: mRNA half-lives span between 1 and 18 min (decay rate constants  $10^{-2}$ – $6 \times 10^{-4}/s$ ) (Bernstein et al., 2002).

<sup>d</sup> The eukaryotic mRNAs are more stable than prokaryotic with half-lives exceeding 10 h (decay rate constant  $2 \times 10^{-5}/s$ ). However, many have half-lives are of order of 30 min (decay rate constant  $3 \times 10^{-4}/s$ ) or less (Alberts et al., 2002). Mammalian mRNA degradation rate constants:  $1.7 \times 10^{-5}$ – $1.7 \times 10^{-3}/s$  (Hargrove, 1993).

<sup>e</sup> For  $1 \mu\text{m}^3$  cell volume (bacterial cell)  $c_2 = 6.9/(\mu\text{M}^2 \times s)$ .

<sup>f</sup> For  $2 \times 10^3 \mu\text{m}^3$  cell volume (mammalian cell)  $c_2 = 1.7/(\mu\text{M}^2 \times s)$ .

<sup>g</sup> For prokaryotes gene switching is faster than for eukaryotes (Blake et al., 2003). Slow gene switching in eukaryotes is causing large mRNA bursts (Raj et al., 2006). However, the transcriptional bursting was also observed in *E. coli* promoter (Golding et al., 2005).

<sup>h</sup> For *E. coli* the maximal transcription rate constant:  $0.84/s$  (Kennel and Riezman, 1977).

<sup>i</sup> For eukaryotes the maximal transcription rate constant:  $0.84/s$  (Kafatos, 1972).

<sup>j</sup> Translation initiation intervals are specific for each mRNA (Laursen et al., 2005). *E. coli*: translation initiation rate constant may vary at least 1000-fold (Sampson et al., 1988); examples of translation initiation frequencies;  $\beta$ -galactosidase:  $0.31/s$  (spacing between ribosomes: 110 nucleotides), galactoside acetyltransferase:  $0.06/s$  (spacing between ribosomes: 580 nucleotides) (Kennel and Riezman, 1977); maximal peptide chain elongation rate:  $20\text{aa}/s$  (Young and Bremer, 1976; Bremer et al., 1974); average peptide chain elongation rate:  $12\text{aa}/s$  (Kennel and Riezman, 1977).

<sup>k</sup> Translation rate constant for eukaryotes:  $0.018$ – $1.8/s$  (Cohen et al., 2009).

<sup>l</sup> *E. coli*: average mRNA copy number:  $10^{-4}$ – $5$  molecules/cell (Taniguchi et al., 2010).

<sup>m</sup> Mammals (mice): average mRNA copy number observed in natural transcriptomes:  $0.5$ – $5 \times 10^4$  molecules/cell (Mortazavi et al., 2008; Galau et al., 1977).

<sup>n</sup> *E. coli*: average protein copy number:  $10^{-1}$ – $10^4$  molecules/cell (Taniguchi et al., 2010).

<sup>o</sup> Mammals: the maximal protein copy number:  $10^8$  molecules/cell (Sims and Allbritton, 2007). Most of yeast genes:  $10^3$ – $5 \times 10^4$  molecules/cell (Gygi et al., 1999).

In a relatively broad range of parameters the above system exhibits bistability. The stable steady states with high and low protein concentration will be referred to as active and inactive, respectively. For assumed parameters (Table 1) the three steady states are

Inactive:  $x_1 = 0.03$ ,  $y_1 = 0.03$ ;  
Unstable:  $x_2 = 0.26$ ,  $y_2 = 0.26$ ;  
Active:  $x_3 = 0.71$ ,  $y_3 = 0.71$ .

Let us note that stationary solutions of the system (31) and (32) depend only on  $c_0/b_0$  and  $c_2/b_0$ , i.e. are independent to noise parameters  $\sigma$ ,  $\varepsilon_1$ ,  $\varepsilon_2$ . Noise parameters, however, influence the SPD. As shown in Fig. 9, the SPD for default noise parameters (Table 1) is bimodal with the probability mass equally distributed between two basins of attraction, Fig. 9A. Decrease of the gene switching noise  $\sigma$  (with the transcriptional and translational noises kept constant) causes that the probability mass concentrates in the inactive state, Fig. 9B. In contrast, decrease of the transcriptional noise  $\varepsilon_1$  (with the gene switching and translational noises kept constant) causes that the probability mass concentrates in the active state, Fig. 9C. Decrease of the translational noise (simultaneously with transcriptional noise) does not significantly influence the SPD, Fig. 9D. Considering this observation, we focus on the normalized transcriptional to gene switching noise ratio, defined as  $R = (\varepsilon_1/\varepsilon_{01})/(\sigma/\sigma_0)$ . In Fig. 11 we

analyze the mass fraction of the SPD in the basin of attraction of the inactive state,  $S_1$ , as a function of  $R$ . Fraction  $S_1$  approaches unity as  $R^{-1} \rightarrow 0$  (for fixed  $\varepsilon_1$  and  $\varepsilon_2$ ) and approaches zero as  $R \rightarrow 0$  (for fixed  $\sigma$ ). The results presented in Figs. 9 and 11 demonstrate that the type of dominating noise determines the most strongly attracting steady state. The small  $R$  (transcriptional to gene switching noise ratio), characteristic for eukaryotes, promotes gene activation. In turn, large  $R$ , characteristic for bacteria, promotes gene inactivation.

### 3. Conclusions

We considered two models of a self-regulating gene with underlying bistability. In the simplified two-stage model, the transcription and translation processes were lumped together, which allowed for the analytical approach. Next, we considered the three-stage model with three types of noise; transcriptional and translational – due to the limited number of mRNA and protein molecules, and the gene-switching noise – due to gene activation and inactivation. Analysis of both models demonstrated that the relative magnitudes of transcriptional and translational, and gene switching noise determine how the SPD is allocated between the two basins of attraction. We found that the low ratio of transcription to gene switching noise ( $R$ ) promotes gene activation, while large  $R$  promotes gene inactivation.

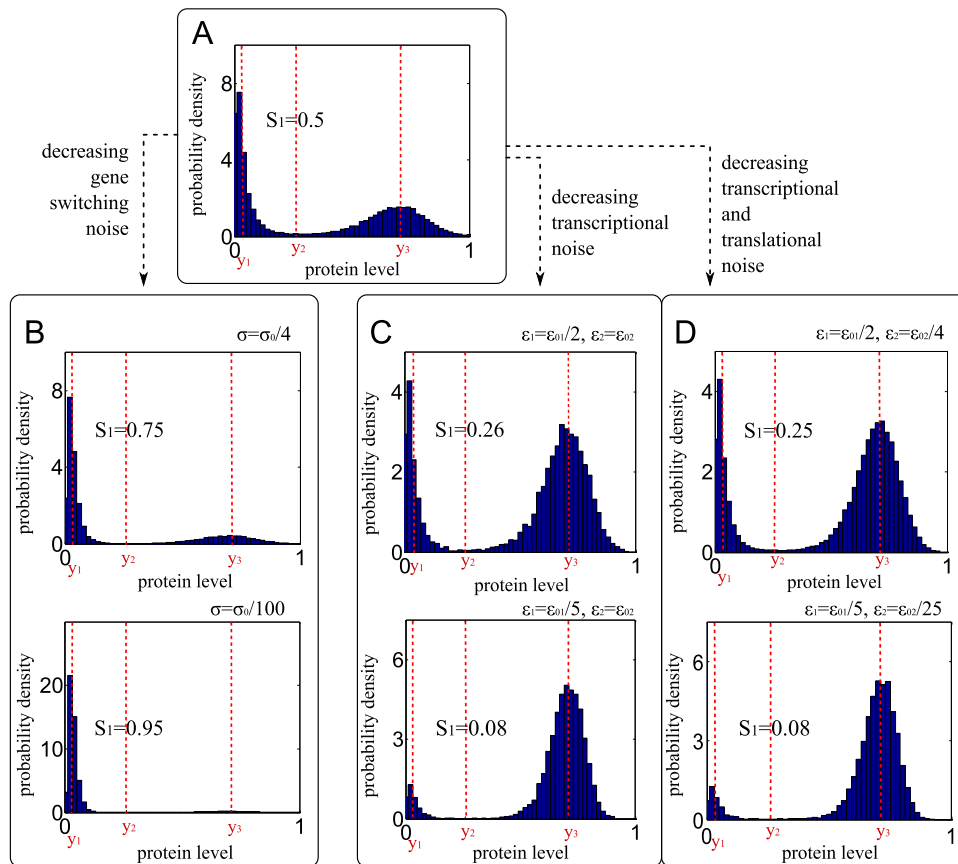


**Fig. 9.** The marginal SPD of the three-stage model for parameters from Table 1.  $S_1$  – mass fraction in the inactive state basin of attraction. Panel (A) shows almost “equimodal” SPD obtained in the case when  $\epsilon_{01} = 1/150$ ,  $\epsilon_{02} = 1/75$  and  $\sigma_0 = 1/50$ . Panel (B) shows the SPD of the constant transcriptional and translational noise  $\epsilon_1 = \epsilon_{01}$ , and  $\epsilon_2 = \epsilon_{02}$  and decreasing gene switching noise  $\sigma$ . Panel (C) shows the SPD for the constant gene switching noise  $\sigma = \sigma_0$ , constant translational noise  $\epsilon_2 = \epsilon_{02}$  and decreasing transcriptional noise  $\epsilon_1$ . Panel (D) shows the SPD for the constant gene switching noise  $\sigma = \sigma_0$  and decreasing transcriptional and translational noise parameters  $\epsilon_1$  and  $\epsilon_2$ .

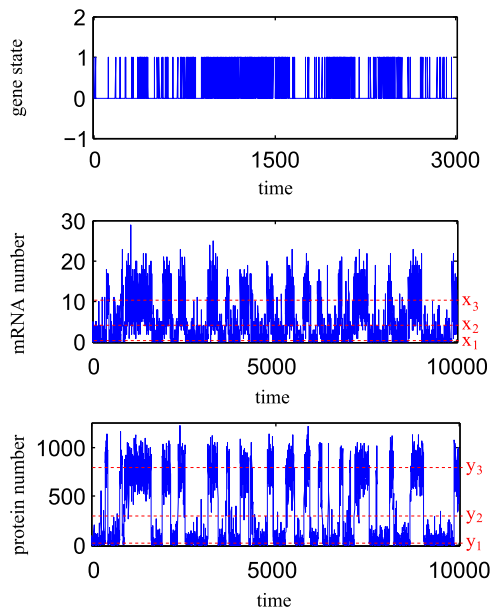


**Fig. 10.** Three-stage model: Stochastic simulation trajectory for default noise parameters  $\epsilon_1 = \epsilon_{01} = 1/150$ ,  $\epsilon_2 = \epsilon_{02} = 1/75$  and  $\sigma = \sigma_0 = 1/50$ . The corresponding SPD is shown in Fig. 9A. Time is given in units equal to the mean protein lifetime.

Behavior of living cells is inherently associated with noise, which can be either perceived as an obstacle to accurate signal processing, or as a necessary factor introducing heterogeneity in

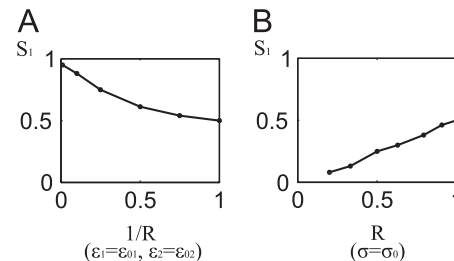


**Fig. 11.** Mass fraction in the vicinity of the inactive state,  $S_1$ , as a function of noise parameters ratio  $R = (\epsilon_1/\epsilon_{01})/(\sigma/\sigma_0)$ . Panel (A)  $S_1$  plotted as a function of  $R^{-1}$  for constant  $\epsilon_1 = \epsilon_{01}$  (and  $\epsilon_2 = \epsilon_{02}$ ). Panel (B)  $S_1$  as a function of  $R$  for constant  $\sigma = \sigma_0$ .

cell populations. Noise enables cells to explore the state space, and allocates the cell population between the local optima – the epigenetic attractors. In this study we demonstrated that in the given epigenetic landscape, defined by the deterministic approximation, the relative occupancy of the attractors is controlled by the type of noise, even in the limit in which noise amplitude converges to zero. The theoretical consequence of our finding is that the prediction of the most strongly attracting steady state or global attractor in the classical Langevin approach, in which all noise sources are replaced by white noise, may not, in general, be correct. Observation that the most strongly attracting steady state, is controlled by relative contributions of the gene switching and transcriptional noise may be exploited in synthetic biology, which enables controlling the magnitudes of different noise sources in designed systems; see eg. Kierzek et al. (2001) and Ozbudak et al. (2002) where

transcription and translation rates were independently modulated.

As already said the dominant noise is cell type-specific. The process of gene expression, analyzed in this study, involves at least three types of noise: gene-switching, transcriptional and translational. Eukaryotic and prokaryotic cells differ significantly in their gene expression noise characteristics. In eukaryotes, the most important source of noise are infrequent transitions between the *on* and *off* states (Raj et al., 2006; Becksei et al., 2005). In turn due to a large volume and correspondingly a large number of mRNA and proteins, the transcriptional and translational noises are relatively low. In the model the larger number of mRNA and protein was achieved by the increase of mRNA transcription and protein translational rate constants, which reflects the higher number of mRNA polymerases and ribosomes in eukaryotic cells. In prokaryotic cells gene activation and deactivation are thought to be very fast due to small volume, which implies easier contact and more frequent binding of transcription factors to the gene promoters. Thus, the gene switching noise in prokaryotes is typically low. Due to the small number of mRNA molecules and proteins, the gene expression noise in prokaryotic cells originates mostly from the transcription and translation events (Taniguchi et al., 2010). As a result eukaryotes, compared with prokaryotes, have a lower ratio of transcriptional to gene switching noise, which as demonstrated in this study promotes activation of autoregulatory genes.

In our study we concentrate on the gene expression noise, which is the most ubiquitous, but not always dominant source of noise in cell signaling. Earlier, we theoretically then experimentally demonstrated that at low dose TNF  $\alpha$  stimulation, noise associated with stochastic receptor activation dominates over gene expression noise in NF- $\kappa$ B system (Lipniacki et al., 2007; Tay et al., 2010). As a result, at low dose stimulation, individual cell responses became highly asynchronous, with fraction of responding cells decreasing with the stimulation dose (Tay et al., 2010; Turner et al., 2010).

Noise characteristics are not only cell type-specific, but may also change during the cell cycle and development. This opens the possibility that relative occupancy of steady states may be actively controlled by noise. For example cell volume growth in G<sub>1</sub> phase and DNA replication in S phase asynchronously modify the relative contributions of gene switching, transcriptional and translational noises. Much larger changes in noise magnitude and its characteristics accompany embryogenesis in fruit fly or frog. In the first case nuclear divisions (mitoses) begin following fertilization, but are not accompanied by division of cytoplasm (cytokinesis). Only after thirteen mitotic divisions, the approximately 5000 nuclei are partitioned into separate cells (Campos-Ortega, 1997). In the case of frog embryogenesis the huge egg is converted into a tadpole consisting of millions of much smaller cells containing the same amount of organic matter (Nieuwkoop and Faber, 1994). One might speculate that changes in noise magnitude and characteristics add to the formation of morphogen gradients (changing relative stability of predefined steady states) initiating body segmentation and cell differentiation. Such mode of control, would require a more precise tuning of parameters than the simple tilting of the epigenetic landscape. However, it would have the advantage of keeping the epigenetic attractors (potentially the most plausible states) unchanged, with simultaneous modification of their relative occupancy.

## Acknowledgements

We thank Dr Marek Kimmel for helpful comments. This study was supported by the Foundation for Polish Science grant TEAM/

2009–3/6, Polish Ministry of Science and Higher Education grant N N501 132936 and NSF/NIH grant No. R01-GM086885.

## References

- Acar, M., Becskei, A., van Oudenaarden, A., 2005. Enhancement of cellular memory by reducing stochastic transitions. *Nature* 435, 228–232.
- Ackers, G.K., Johnson, A.D., Shea, M.A., 1982. Quantitative model for gene regulation by lambda phage repressor. *Proc. Natl. Acad. Sci. U.S.A.* 79, 1129–1133.
- Alberts, B., Johnson, A., Lewis, J., Raff, M., Roberts, K., Walter, P., 2002. *Molecular Biology of the Cell*, fourth ed. Garland Science, New York.
- Becksei, A., Kaufmann, B.B., van Oudenaarden, A., 2005. Contributions of low molecule number and chromosomal positioning to stochastic gene expression. *Nat. Genet.* 37, 937–944.
- Becskei, A., Seraphin, B., Serrano, L., 2001. Positive feedback in eucaryotic gene networks: cell differentiation by graded to binary response conversion. *EMBO J.* 20, 2528–2535.
- Bernstein, J.A., Khodursky, A.B., Lin, P.-H., Lin-Chao, S., Cohen, S.N., 2002. Global analysis of mRNA decay and abundance in *Escherichia coli* single-gene resolution using two-color fluorescent DNA microarrays. *Proc. Natl. Acad. Sci. U.S.A.* 99, 9697–9702.
- Blake, W.J., Kaern, M., Cantor, C.R., Collins, J.J., 2003. Noise in eukaryotic gene expression. *Nature* 422, 633–637.
- Bobrowski, A., 2006. Degenerate convergence of semigroups related to a model of stochastic gene expression. *Semigroup Forum* 73, 345–366.
- Bobrowski, A., Lipniacki, T., Pichór, K., Rudnicki, R., 2007. Asymptotic behavior of distributions of mRNA and protein levels in a model of stochastic gene expression. *J. Math. Anal. Appl.* 333, 753–769.
- Bremer, H., Hymes, J., Dennis, P.P., 1974. Ribosomal RNA chain growth rate and RNA labelling patterns in *Escherichia Coli*. *J. Theor. Biol.* 45, 379–403.
- Campos-Ortega, J.A., 1997. *The Embryonic Development of Drosophila Melanogaster*, second ed. Springer.
- Chang, H.H., Oh, P.Y., Ingber, D.E., Huang, S., 2006. Multistable and multistep dynamics in neutrophil differentiation. *BMC Cell Biol.* 7, 11.
- Chatterjee, A., Kaznessis, Y.N., Hu, W.-S., 2008. Tweaking biological switches through a better understanding of bistability behavior. *Curr. Opin. Biotechnol.* 19, 475–481.
- Chen, C., Deutscher, M.P., 2010. RNase R is a highly unstable protein regulated by growth phase and stress. *RNA* 16, 667–672.
- Chubb, J.R., Trcek, T., Shenoy, S.M., Singer, R.H., 2006. Transcriptional pulsing of a developmental gene. *Curr. Biol.* 16, 1018–1025.
- Cohen, A.A., Kalisky, T., Mayo, A., Geva-Zatorsky, N., Danon, T., Issaeva, I., Kopito, R.B., Perzov, N., Milo, R., Sigal, A., Alon, U., 2009. Protein dynamics in individual human cells: experiment and theory. *PLoS One* 4, e4901.
- El-Samad, H., Kurata, H., Doyle, J.C., Gross, C.A., Khammash, M., 2005. Surviving heat shock: control strategies for robustness and performance. *Proc. Natl. Acad. Sci. U.S.A.* 102, 2736–2741.
- Frigola, D., Casanellas, L., Sancho, J.M., Ibanes, M., 2012. Asymmetric stochastic switching driven by intrinsic molecular noise. *PLoS One* 7, e31407.
- Galau, G.A., Klein, W.H., Britten, R.J., Davidson, E., 1977. Significance of rare mRNA sequences in liver. *Arch. Biochem. Biophys.* 179, 584–599.
- Gardiner, C.W., 2004. *Handbook of Stochastic Methods for Physics, Chemistry and the Natural Sciences*. Springer-Verlag, Berlin.
- Gillespie, D.T., 1977. Exact stochastic simulation of coupled chemical reactions. *J. Phys. Chem.* 81, 2340–2361.
- Golding, I., Paulsson, J., Zawilski, S.M., Cox, E.C., 2005. Real-time kinetics of gene activity in individual bacteria. *Cell* 123, 1025–1036.
- Gygi, S.P., Rochon, Y., Franza, B.R., Aebersold, R., 1999. Correlation between protein and mRNA abundance in yeast. *Mol. Cell Biol.* 19, 1720–1730.
- Hargrove, J.L., 1993. Microcomputer-assisted kinetic modeling of mammalian gene expression. *FASEB J.* 7, 1163–1170.
- Haseltine, E.L., Rawlings, J.B., 2002. Approximate simulation of coupled fast and slow reactions for stochastic chemical kinetics. *J. Chem. Phys.* 117, 6959–6969.
- Hasty, J., Pradines, J., Dolnik, M., Collins, J.J., 2000. Noise-based switches and amplifiers for gene expression. *Proc. Natl. Acad. Sci. U.S.A.* 97, 2075–2080.
- Hat, B., Paszek, P., Kimmel, M., Piechor, K., Lipniacki, T., 2007. How the number of alleles influences gene expression. *J. Statist. Phys.* 128, 511–533.
- Hornos, J.E.M., Schultz, D., Innocentini, G.C.P., Wang, J., Walczak, A.M., Onuchic, J.N., Wolynes, P.G., 2005. Self-regulating gene: an exact solution. *Phys. Rev. E* 72, 051907.
- Jayapal, K.P., Sui, S., Philp, R.J., Kok, Y.-J., Yap, M.G.S., Griffin, T.J., Hu, W.-S., 2010. Multitagging proteomic strategy to estimate protein turnover rates in dynamic Systems. *J. Proteome Res.* 9, 2087–2097.
- Kafatos, F.C., 1972. The cocoonase zymogen cells of silk moths: model of terminal cell differentiation for specific protein synthesis. *Curr. Topics Dev. Biol.* 7, 125–191.
- Karmakar, R., Bose, I., 2007. Positive feedback, stochasticity and genetic competence. *Phys. Biol.* 4, 29–37.
- Kennell, D., Riezman, H., 1977. Transcription and translation initiation frequencies of the *Escherichia coli* lac operon. *J. Mol. Biol.* 114, 1–21.
- Kepler, T.B., Elston, T.C., 2001. Stochasticity in transcriptional regulation: origins, consequences, and mathematical representations. *Biophys. J.* 81, 3116–3136.

- Kierzek, A.M., Zaim, J., Zielenkiewicz, P., 2001. The effect of transcription and translation initiation frequencies on the stochastic fluctuations in prokaryotic gene expression. *J. Biol. Chem.* 276, 8165–8172.
- Ko, M.S.H., 1991. Stochastic model for gene induction. *J. Theor. Biol.* 153, 181–194.
- Kussell, E., Leibler, S., 2005. Phenotypic diversity, and information in fluctuating environments. *Science* 309, 2075–2078.
- Laurson, B.S., Soerensen, H.P., Mortensen, K.K., Sperling-Petersen, H.U., 2005. Initiation of protein synthesis in bacteria. *Microbiol. Mol. Biol. Rev.* 69, 101–123.
- Lipniacki, T., Paszek, P., Marciniak-Czochra, A., Brasier, A.R., Kimmel, M., 2006. Transcriptional stochasticity in gene expression. *J. Theor. Biol.* 238, 348–367.
- Lipniacki, T., Puszyński, K., Paszek, P., Brasier, A.R., Kimmel, M., 2007. Single TNF $\alpha$  trimers mediating NF- $\kappa$ B activation: stochastic robustness of NF- $\kappa$ B signaling. *BMC Bioinformatics* 8, 376.
- Lipniacki, T., Hat, B., Faeder, J.R., Hlavacek, W.S., 2008. Stochastic effects and bistability in T cell receptor signaling. *J. Theor. Biol.* 254, 110–122.
- Lipshtat, A., Loinger, A., Balaban, N.Q., Biham, O., 2006. Genetic toggle switch without cooperative binding. *Phys. Rev. Lett.* 96, 188101.
- Marquez-Lago, T.T., Stelling, J., 2010. Counter-intuitive stochastic behavior of simple gene circuits with negative feedback. *Biophys. J.* 98, 1742–1750.
- McAdams, H.H., Arkin, A., 1997. Stochastic mechanisms in gene expression. *Proc. Natl. Acad. Sci. U.S.A.* 94, 814–819.
- Miekisz, J., 2005. Equilibrium selection in evolutionary? games with random matching of players. *J. Theor. Biol.* 232, 47–53.
- Mortazavi, A., Williams, B.A., McCue, K., Schaeffer, L., Wold, B., 2008. Mapping and quantifying mammalian transcriptomes by RNA-Seq. *Nat. Methods* 5, 621–628.
- Nevozhay, D., Adams, R.M., Van Itallie, E., Bennett, M.R., Balazsi, G., 2012. Mapping the environmental fitness landscape of a synthetic gene circuit. *PLoS Comput. Biol.* 8, e1002480.
- Nieuwkoop, P.D., Faber, J., 1994. *Normal Table of Xenopus laevis* (Daudin). Garland Publishing Inc, New York, London.
- Ochab-Marcinek, A., Tabaka, M., 2010. Bimodal gene expression in noncooperative regulatory systems. *Proc. Natl. Acad. Sci. U.S.A.* 107, 22096–22101.
- Ozbudak, E.M., Thattai, M., Kurtser, I., Grossman, A.D., Oudenaarden, A., 2002. Regulation of noise in the expression of a single gene. *Nat. Genet.* 31, 69–73.
- Ozbudak, E.M., Thattai, M., Lim, H.N., Shraiman, B.I., Oudenaarden, A., 2004. Multistability in the lactose utilization network of *Escherichia coli*. *Nature* 427, 737–740.
- Ptashne, M., 2004. *A Genetic Switch: Phage Lambda Revisited*, 3rd ed. Cold Harbor Spring Laboratory Press.
- Puszyński, K., Hat, B., Lipniacki, T., 2008. Oscillations and bistability in the stochastic model of p53 regulation. *J. Theor. Biol.* 254, 452–465.
- Raj, A., Oudenaarden, A., 2009. Single-molecule approaches to stochastic gene expression. *Annu. Rev. Biophys.* 38, 255–270.
- Raj, A., Peskin, C.S., Tranchina, D., Vargas, D.Y., Tyagi, S., 2006. Stochastic mRNA synthesis in mammalian cells. *PLoS Biol.* 4, 1707–1719.
- Raser, J.M., O'Shea, E.K., 2004. Control of stochasticity in eukaryotic gene expression. *Science* 304, 1811–1814.
- Rosenfeld, N., Elowitz, M., Alon, U., 2002. Negative autoregulation speeds the response times of transcription networks. *J. Mol. Biol.* 323, 785–793.
- Sampson, L.L., Hendrix, R.W., Huang, W.M., Casjens, S.R., 1988. Translation initiation controls the relative rates of expression of the bacteriophage  $\lambda$  late genes. *Proc. Natl. Acad. Sci. U.S.A.* 85, 5439–5443.
- Schultz, D., Onuchic, J.N., Wolynes, P.G., 2007. Understanding stochastic simulations of the smallest genetic networks. *J. Chem. Phys.* 126, 245102.
- Shahrezaei, V., Swain, P.S., 2008. Analytical distributions for stochastic gene expression. *Proc. Natl. Acad. Sci. U.S.A.* 105, 17256–17261.
- Siegal-Gaskins, D., Grotewold, E., Smith, G.D., 2009. The capacity for multistability in small gene regulatory networks. *BMC Syst. Biol.* 3, 96.
- Sims, C.E., Allbritton, N.L., 2007. Analysis of single mammalian cells on-chip. *Lab Chip* 7, 423–440.
- Sprinzak, D., Lakhanpal, A., Lebon, L., Santat, L.A., Fontes, M.E., Anderson, G.A., Garcia-Ojalvo, J., Elowitz, M.B., 2010. Cis-interactions between Notch and Delta generate mutually exclusive signalling states. *Nature* 465, 86–90.
- Swain, P.S., Elowitz, M.B., Siggia, E.D., 2002. Intrinsic and extrinsic contributions to stochasticity in gene expression. *Proc. Natl. Acad. Sci. U.S.A.* 99, 12795–12800.
- Taniguchi, Y., Choi, P.J., Li, G.W., Chen, H., Babu, M., Hearn, J., Emili, A., Xie, X.S., 2010. Quantifying *E. coli* proteome and transcriptome with single-molecule sensitivity in single cells. *Science* 329, 533–538.
- Tay, S., Hughey, J., Lee, T., Lipniacki, T., Quake, S.R., Covert, M.W., 2010. Single-cell NF- $\kappa$ B dynamics reveal digital activation and analogue information processing. *Nature* 466, 267–271.
- Thattai, M., Oudenaarden, A., 2001. Intrinsic noise in gene regulatory networks. *Proc. Natl. Acad. Sci. U.S.A.* 98, 8614–8619.
- Turner, D.A., Paszek, P., Woodcock, D.J., Nelson, D.E., Horton, C.A., Wang, Y., Spiller, D.G., Rand, D.A., White, M.R.H., Harper, C.V., 2010. Physiological levels of TNF  $\alpha$  stimulation induce stochastic dynamics of NF- $\kappa$ B responses in single living cells. *J. Cell Sci.* 123, 2834–2843.
- van Kampen, N.G., 2007. *Stochastic Processes in Physics and Chemistry*, 3rd ed. Elsevier Science & Technology Books.
- van Sinderen, D., Vemnema, G., 1994. comK acts as an autoregulatory control switch in the signal transduction route to competence in *Bacillus subtilis*. *J. Bacteriol.* 176, 5762–5770.
- Vellela, M., Qian, H., 2009. Stochastic dynamics and non-equilibrium thermodynamics of a bistable chemical system: the Schloegl model revisited. *J. R. Soc. Interface* 6, 925–940.
- Walczak, A.M., Onuchic, J.N., Wolynes, P.G., 2005. Absolute rate theories of epigenetic stability. *Proc. Natl. Acad. Sci. U.S.A.* 102, 18926–18931.
- Young, R., Bremer, H., 1976. Polypeptide-chain-elongation rate in *Escherichia coli* B/r as a function of growth rate. *Biochem. J.* 160, 185–194.
- Zuk, P.J., Kochanzyk, M., Jaruszewicz, J., Bednorz, W., Lipniacki, T., 2012. Dynamics of a stochastic spatially extended system predicted by comparing deterministic and stochastic attractors of the corresponding birth death process. *Phys. Biol.* 9, 055002.

II) Jaruszewicz J, Lipniacki T, *Toggle switch: noise determines the winning gene*, Physical Biology, (IOP Press, Great Britain), 10(3), 2013.

# Toggle switch: noise determines the winning gene

Joanna Jaruszewicz<sup>1</sup> and Tomasz Lipniacki<sup>1,2</sup>

<sup>1</sup> Institute of Fundamental Technological Research, Polish Academy of Sciences, 02-106 Warsaw, Poland

<sup>2</sup> Department of Statistics, Rice University, Houston, TX 77025, USA

E-mail: [tomek@rice.edu](mailto:tomek@rice.edu)

Received 15 October 2012

Accepted for publication 7 February 2013

Published 4 June 2013

Online at [stacks.iop.org/PhysBio/10/035007](http://stacks.iop.org/PhysBio/10/035007)

## Abstract

Bistable regulatory elements enhance heterogeneity in cell populations and, in multicellular organisms, allow cells to specialize and specify their fate. Our study demonstrates that in a system of bistable genetic switch, the noise characteristics control in which of the two epigenetic attractors the cell population will settle. We focus on two types of noise: the gene switching noise and protein dimerization noise. We found that the change of magnitudes of these noise components for one of the two competing genes introduces a large asymmetry of the protein stationary probability distribution and changes the relative probability of individual gene activation. Interestingly, an increase of noise associated with a given gene can either promote or suppress the activation of the gene, depending on the type of noise. Namely, each gene is repressed by an increase of its gene switching noise and activated by an increase of its protein-product dimerization noise. The observed effect was found robust to the large, up to fivefold deviations of the model parameters. In summary, we demonstrated that noise itself may determine the relative strength of the epigenetic attractors, which may provide a unique mode of control of cell fate decisions.

## 1. Introduction

Bi- and multi-stable regulatory elements play an important role in cell signaling by introducing heterogeneity in cell populations and allowing cells in a multicellular organism to specialize and specify their fate. Attractors of genetic networks can be associated with distinct cell types achieved during cell differentiation [1, 2]. Although multistationarity is not required for the emergence of co-existing phenotypes [3], decisions between cell death and survival, proliferation or senescence are likely associated with bistability. In prokaryotes, multistability is regarded as an optimal strategy for coping with varying environmental conditions [4].

In a single cell, the relative occupancy of steady states is determined by their relative stability, while at the population level it is additionally governed by growth rates associated with particular steady states [5]. Intuitively, the relative strength of the macroscopic steady states should be controlled by the ‘shape’ of the epigenetic landscape. Considering the epigenetic landscape as a potential energy landscape, one could expect that the stability of a steady state increases with the depth

of the associated potential well. The external stimulation that leads to the modification of the potential influences the relative stability of the steady states and may promote state-to-state transitions. Interestingly, noise itself was also found to be an important determinant of the relative occupancy of the macroscopic steady states [6–9]. As shown by Vellela and Qian [6], in a bistable system the noise magnitude controls the probability mass fraction in each of the two attraction basins. In the limit of zero noise, generically, all probability mass concentrates in the vicinity of the most stable steady state [7]. Surprisingly, also the noise type (in addition to the noise magnitude) influences the relative stability of the macroscopic steady states. Analyzing a single autoregulatory gene by means of the chemical Langevin equation, Frigola *et al* demonstrated that additive and multiplicative noise assumptions lead to different effective potentials [8]. Recently, by considering arbitrary noise functions, we showed that any steady state can become a global stochastic attractor for a particular choice of noise [7]. In the case of a single autoregulatory gene, we found that when the gene switching noise dominates the transcriptional/translational noise, the gene preferentially

activates, while in the opposite case the gene preferentially remains inactive [9].

In this study, we will focus on the role of noise in the toggle switch regulation. A toggle switch—a pair of mutual repressors—is considered as one of the most important regulatory elements exhibiting bistability [10–13]. Using a toggle switch, a single cell converts graded external stimuli into a binary answer expressing almost exclusively one of the two competing repressors. At the population level, the graded stimuli are encoded by the fraction of cells expressing instantaneously the particular gene. Classical examples of toggle switches include the lysis/lysogeny switch in  $\lambda$  phage [14–16], several mitogen-activated protein kinase cascades in animal cells [17–19], and cell cycle regulatory CI circuits in *Xenopus laevis* and *Saccharomyces cerevisiae* [20, 21]. Another example of a toggle switch in bacteria is a tetracycline resistance circuit in *Escherichia coli*.

A synthetic toggle switch in *E. coli* was constructed by Gardner *et al* [22]. It was forced to flip between the steady states using a transient chemical or thermal induction. The toggle was constructed using the Lac repressor (*lacI*) in conjunction with P<sub>trc</sub>-2 promoter and either a P<sub>L</sub>s1con promoter in conjunction with a temperature-sensitive  $\lambda$  repressor (*cts*) or a P<sub>L</sub>tetO-1 promoter in conjunction with a Tet repressor (*tetR*). The work of Gardner *et al* also provides a theoretical prediction of the conditions sufficient for bistability. Bistability arises when at least one of the inhibitors represses the expression of the competing gene with cooperativity greater than 1. Later, Lipshtat *et al* showed that exclusive toggle switches may exhibit bistability even without a cooperative binding [12]. In the exclusive switch, the two promoter sites overlap and thus two repressors cannot be bound simultaneously. In the simplest of the three considered models, despite the fact that the deterministic approximation predicts a single steady state, the stationary probability distribution (SPD) was found bimodal. The additional assumptions that either bound repressors may degrade, or that free repressor proteins may form inactive heterodimers led to bistable models with two macroscopic stable steady states [12].

Cells have evolved to survive in fluctuating environments taking advantage of the stochasticity present in the process of gene regulation. State-to-state transitions in a toggle switch are enabled by noise, whose magnitude controls switching rates [23, 24]. In a rapidly changing epigenetic landscape high noise is favorable as it allows for fast adaptation. It was shown theoretically that in a varied environment bacteria maximize fitness by tuning noise with the frequency of the environment fluctuations [25]. In the system of mutual repressors, the overall states stability can be controlled by noise associated with a mode of repression. As shown by Komorowski *et al*, translational repression contributes greater noise to gene expression than transcriptional repression [26]. Warren *et al* demonstrated that overlapping upstream gene regulatory domains increases toggle stability, i.e. decreases state-to-state transition rates [27]. In general, the transition times increase exponentially with the characteristic number of repressor molecules, and are reduced when proteins are synthesized in large bursts [28]. It is also known that the noise

magnitude affects the dynamical characteristics of the toggle switch. As shown by Dai *et al*, a deterministically bistable toggle switch has two stochastic (or noise) attractors only for a limited noise amplitude [29]. An excess of noise makes the toggle switch first tristable (with a new third state characterized by high expression of both genes), then monostable, with both genes expressing simultaneously. The model considered by Dai *et al* involves delays accounting for time duration of various gene expression processes. The considered delays are due to the formation of an open promoter complex, ribosome clearance, transcriptional and translational elongation and post-translational processing, see [30] for review.

In the current study, we answer the question whether noise itself can control relative stability of the two toggle macroscopic steady states. Such mode of control would enable activation or repression of a particular toggle gene without any modification of the associated epigenetic landscape. In the studied toggle switch model, we consider explicitly processes of mRNA transcription, protein translation, protein dimer formation and gene repression. Each of these processes introduces a different type of noise to the system. We will show that the change of the magnitudes of noise components for either of the two competing genes alters the protein SPD and changes the probability mass fraction in each of the two basins of attraction. Interestingly, a decrease of noise associated with a given gene can promote the activation of that gene or the other, depending on the type of noise.

## 2. Model

The toggle switch model consists of two competing genes: gene 1 and gene 2, figure 1. Each gene can be repressed by the competing gene protein dimer. Processes of gene repression, mRNA transcription, protein translation, dimer formation and dissociation are explicitly included in the model, table 1. Each of these processes is considered stochastic and contributes to noise in levels of molecules.

The model defines a time-continuous Markov process involving eight random variables: the gene 1 and gene 2 states,  $G_1(t), G_2(t) \in \{0 \text{ (repressed)}, 1 \text{ (active)}\}$ , numbers of molecules of mRNA 1 and mRNA 2,  $M_1(t), M_2(t) \in \mathbb{N}$ , numbers of molecules of the protein monomer 1 and protein monomer 2,  $P_1(t), P_2(t) \in \mathbb{N}$ , numbers of molecules of the protein dimer 1 and protein dimer 2,  $D_1(t), D_2(t) \in \mathbb{N}$ . The default transition propensities  $k_i$ , ( $i = 1, \dots, 9$ ) for each of the nine considered reactions (see figure 1) are assumed equal for both genes, table 1. These rates are chosen so that the system in the deterministic approximation is bistable, i.e. it has two stable steady-state solutions, each corresponding to a high expression of one gene and a low expression of the another, and the unstable steady state for which both genes have the same relatively low expression. The stochastic trajectories switch between the basins of attraction of these two stable steady states, figure 2. The full symmetry between the two genes (for the default parameters) is manifested by the symmetric SPD. The stochastic trajectories and the SPDs of the system were obtained in the Gillespie algorithm simulations [31].

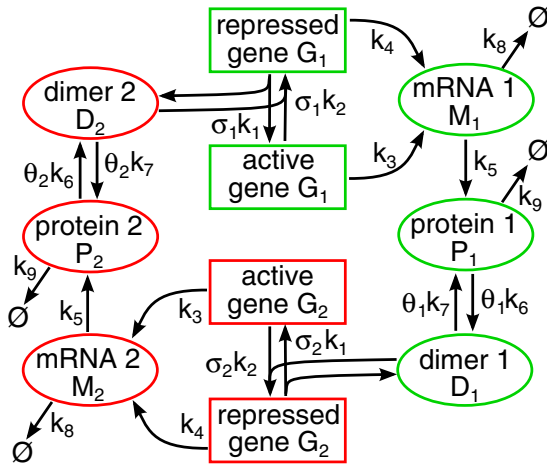


**Figure 1.** Schematic of the stochastic toggle switch model. Each of two genes can be repressed by the binding of the protein dimer molecule, the product of the competing gene. The repressed gene is activated by the dissociation of the dimer molecule (which returns to the pool of free dimers) from its promoter. We assume small, but non-zero mRNA transcription from the repressed genes. Other stochastic reactions explicitly included in the model are protein translation, dimer formation and its dissociation, and degradation of mRNA and protein monomer molecules. We assume that dimers are much more stable than monomers and thus we neglect their degradation. Coefficients  $\sigma_i$  and  $\theta_i$  control individual gene switching and dimerization noise components. For  $\sigma_1 = \sigma_2$  and  $\theta_1 = \theta_2$ , all reaction corresponding propensities are equal for both genes (symmetric case).

In the following section, we will analyze the dynamics of the model with respect to the magnitudes of individual noise components. In particular, we will focus on the gene switching and protein dimerization noises. The gene switching noise is controlled independently for each of the two genes by parameters  $\sigma_i$  ( $i = 1, 2$ ), which multiply simultaneously rate constants of gene activation and gene repression,  $k_1$  and  $k_2$ , respectively (see figure 1). The noise introduced by the gene switching decreases with the switching rates, and becomes zero in the adiabatic limit when these rates are infinite. We will thus consider  $1/\sigma_i$  as the gene switching noise parameter. The parameter  $\sigma_i$  controls noise in the system, but, as we will see in the following section, its value does not influence steady states of the deterministic approximation of the system. The dimerization noise is controlled by parameters  $\theta_i$  ( $i = 1, 2$ ), which multiply simultaneously dimer association and dimer dissociation rate constants, respectively  $k_6$  and  $k_7$ , see figure 1. Thus, the dimerization noise of the gene  $i$  product decreases with increasing  $\theta_i$ , but again the value of  $\theta_i$  does not influence the steady state of the deterministic approximation of the system.

The control of the toggle switch coefficients by dimerization and gene switching noise parameters was chosen because it allows us to separate noise effects from the effects resulting from the modification of macroscopic steady states of the system. Such an approach allows us to compare different stochastic systems having the same deterministic approximation.

**Table 1.** Reaction rate constants.

Reaction	Symbol	Default value $\sigma_i = 1, \theta_i = 1$	Physiological range for bacteria (volume $1 \mu\text{m}^3$ )
Gene activation by protein dimer dissociation	$\sigma_i k_1$	0.003 (1/s)	Unknown <sup>a</sup>
Gene repression by protein dimer binding	$\sigma_i k_2$	0.015 (1/(mlcl × s))	Unknown <sup>b</sup>
mRNA transcription from the active gene	$k_3$	0.02 (1/s)	$\leq 0.84$ (1/s) <sup>c</sup>
mRNA transcription from the repressed gene	$k_4$	0.0006 (1/s)	<sup>d</sup>
Protein translation	$k_5$	0.01 (1/(mlcl × s))	$\sim 10^{-2} \sim 10$ (1/s) <sup>e</sup>
Dimer formation	$\theta_i k_6$	0.0001 (1/(mlcl × s))	$1.63 \times 10^{-6} \sim 9.47$ (1/(mlcl × s)) <sup>f</sup>
Dimer dissociation to monomers	$\theta_i k_7$	0.01 (1/s)	$5 \times 10^{-8} \sim 1.9 \times 10^3$ (1/s) <sup>g</sup>
mRNA degradation	$k_8$	0.005 (1/s)	$10^{-2} \sim 6 \times 10^{-4}$ (1/s) <sup>h</sup>
Protein monomer degradation	$k_9$	0.0005 (1/s)	$\sim 1.4 \times 10^{-5} \sim 10^{-2}$ (1/s) <sup>i</sup>

mlcl=molecule

<sup>a,b</sup> For prokaryotes, gene switching is faster than for eukaryotes [37].

<sup>c,d</sup> For *E. coli*, maximal transcription rate:  $0.16 \sim 0.84 \text{ s}^{-1}$  [38].

<sup>e</sup> Translation initiation intervals are of the order of seconds, although they are specific for each mRNA [39]. *E. coli*: translation initiation rate may vary at least 1000-fold [40]; examples of translation initiation frequencies:  $\beta$ -galactosidase— $0.31 \text{ s}^{-1}$  (spacing between ribosomes: 110 nucleotides), galactoside acetyltransferase— $0.06 \text{ s}^{-1}$  (spacing between ribosomes: 580 nucleotides) [38]; maximal peptide chain elongation rate:  $20 \text{ aa s}^{-1}$  [41, 42]; average peptide chain elongation rate:  $12 \text{ aa s}^{-1}$  [38].

<sup>f</sup> All cell types:  $9.8 \times 10^2 / (M \times s) \sim 5.7 \times 10^9 / (M \times s)$  [43]; for  $1 \mu\text{m}^3$  volume (bacterial) cell:  $1.63 \times 10^{-6} / \text{mlcl} \times s \sim 9.47 / \text{mlcl} \times s$ .

<sup>g</sup> All cell types:  $5 \times 10^{-8} / s \sim 1.9 \times 10^3 / s$  [43]. Dissociation constant range:  $7.2 \times 10^{-17} M \sim 2.2 \times 10^{-6} M$  [43]; for  $1 \mu\text{m}^3$  volume (bacteria)  $4.34 \times 10^{-8} / \text{mlcl} \times s \sim 1.32 \times 10^3 / \text{mlcl} \times s$ .

<sup>h</sup> The vast majority of mRNAs in a bacterial cell are very unstable, having a half-life of about 3 min. Bacterial mRNAs are both rapidly synthesized and rapidly degraded [44]. The average mRNA copy number in *E. coli* is  $10^{-4} \sim 5$  mlcls/cell [45].

<sup>i</sup> Most bacterial proteins are very stable, with degradation rates:  $1.4 \times 10^{-5} \sim 5.6 \times 10^{-5} \text{ s}^{-1}$  [46]. Some proteins have much higher degradation rates. *E. coli* RNase R has a degradation rate of  $10^{-3} \text{ s}^{-1}$  (in exponential phase) [47], factor  $\sigma^{32}$  has a degradation rate of  $10^{-2} \text{ s}^{-1}$  (in steady-state growth phase) [48]. The average protein copy number in *E. coli* is  $10^{-1} \sim 10^4$  mlcls/cell [45].

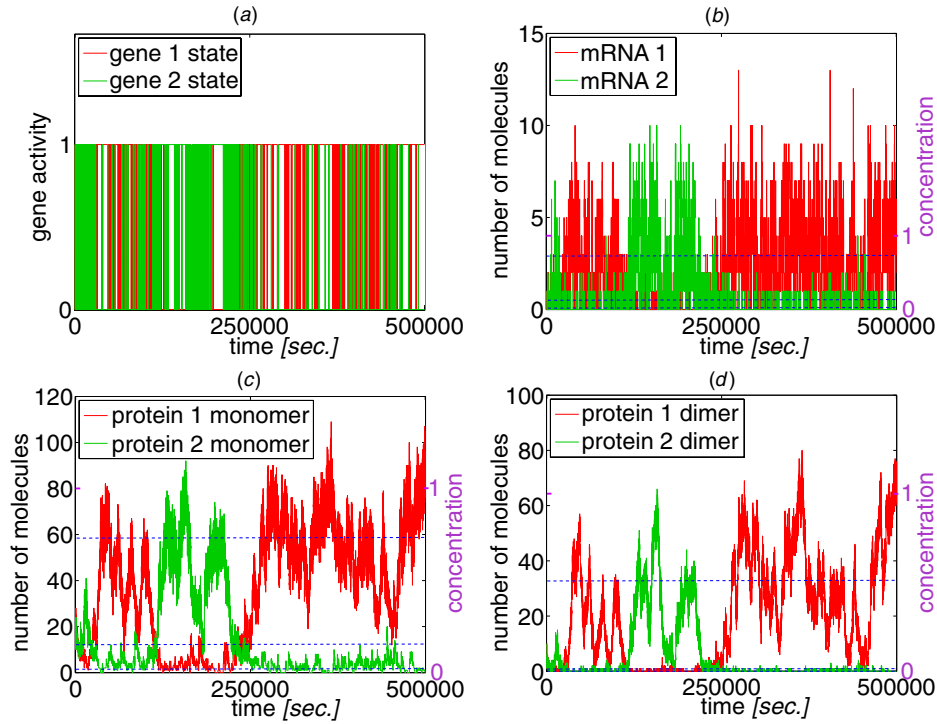


**Figure 2.** The stochastic simulation trajectories for  $\sigma_i = \theta_i = 1$ ,  $i = 1, 2$ . Dashed lines denote steady states of the deterministic approximation. On the left vertical axis numbers of molecules are given and on the right vertical axis we show the scaled ‘concentrations’ (see the text). The corresponding protein monomer SPD is shown in figure 4(a).

### 3. Results

#### 3.1. Deterministic approximation

We start the analysis of the model dynamics with an examination of its deterministic approximation. In the deterministic approximation, the stochastic variables describing gene states  $G_i$  are replaced by continuous variables  $g_i$ . The remaining variables,  $M_i$ ,  $P_i$  and  $D_i$ , are considered continuous and are scaled by their maximal values, respectively,  $M_0$ ,  $P_0$  and  $D_0$ , reached under the condition that each gene is in the active state:

$$\begin{aligned} M_0 &= k_3/k_8; & P_0 &= (k_3k_5)/k_8k_9; \\ D_0 &= k_6(k_3k_5)^2/(k_7(k_8k_9)^2). \end{aligned} \quad (1)$$

The scaled variables

$$m_i = M_i/M_0, \quad p_i = P_i/P_0, \quad d_i = D_i/D_0 \quad (2)$$

will be referred to as scaled ‘concentrations’. Now, the considered Markov process can be approximated by the system of eight ordinary differential equations:

$$\frac{dg_i}{dt} = \sigma_i(k_1(1 - g_i) - k_2D_0d_jg_i), \quad (3)$$

$$\frac{dm_i}{dt} = k_8g_i + \frac{k_4}{M_0}(1 - g_i) - k_8m_i, \quad (4)$$

$$\frac{dp_i}{dt} = 2\theta_i k_6 P_0 (d_i - p_i^2) + k_9(m_i - p_i), \quad (5)$$

$$\frac{dd_i}{dt} = \theta_i k_7 (p_i^2 - d_i), \quad (6)$$

where  $i = 1, 2$  and  $j = 3 - i$ . The deterministic approximation is accurate only when the characteristic numbers of molecules are large (enough to be replaced by the continuous concentrations). For bacteria this condition is seldom satisfied, and thus mass rate equations may serve only as a reference for the stochastic analysis. In particular, in equation (6), the loss of a (single) dimer molecule that binds DNA is neglected, although this loss is accounted for in stochastic simulations.

The steady-state values of  $p_i$  are given by the real roots of the fifth-order polynomial,

$$\begin{aligned} W(p_1) &= - (k_1^2 k_2 k_3 k_4 k_5^2 k_6 k_7^2 k_8^4 k_9^4 + k_1^3 k_7^3 k_8^6 k_9^6) \\ &+ (k_1^2 k_2 k_3^2 k_5^2 k_6 k_7^2 k_8^4 k_9^4 + k_1^3 k_7^3 k_8^6 k_9^6) p_1 \\ &- (2k_1 k_2^2 k_3^2 k_4^2 k_5^2 k_6^2 k_7^2 k_8^2 k_9^2 + 2k_1^2 k_2 k_3^2 k_5^2 k_6 k_7^2 k_8^4 k_9^4) p_1^2 \\ &+ (2k_1 k_2^2 k_3^3 k_4 k_5^2 k_6^2 k_7 k_8^2 k_9^2 + 2k_1^2 k_2 k_3^2 k_5^2 k_6 k_7^2 k_8^4 k_9^4) p_1^3 \\ &- (k_2^3 k_3^3 k_4^3 k_5^3 k_6^3 + k_1 k_2^2 k_3^2 k_4^2 k_5^2 k_6^2 k_7^2 k_8^2 k_9^2) p_1^4 \\ &+ (k_2^3 k_3^4 k_4^2 k_5^6 k_6^3 + k_1 k_2^2 k_3^2 k_4^2 k_5^2 k_6^2 k_7^2 k_8^2 k_9^2) p_1^5. \end{aligned} \quad (7)$$

The steady-state values of the remaining variables are given by the following relations:

$$p_2 = (k_1 k_7 k_8^2 k_9^2 + k_2 k_3^2 k_4 k_5^2 k_6 p_1^2) (k_1 k_7 k_8^2 k_9^2 + k_2 k_3^2 k_5^2 k_6 p_1^2)^{-1}, \quad (8)$$

$$m_1 = p_1, \quad d_1 = p_1^2, \quad (9)$$

$$m_2 = p_2, \quad d_2 = p_2^2, \quad (10)$$

$$g_1 = (k_1 k_7 k_8^2 k_9^2) (k_1 k_7 k_8^2 k_9^2 + k_2 k_3^2 k_5^2 k_6 d_2)^{-1}, \quad (11)$$

$$g_2 = (k_1 k_7 k_8^2 k_9^2) (k_1 k_7 k_8^2 k_9^2 + k_2 k_3^2 k_5^2 k_6 d_1)^{-1}. \quad (12)$$

For the assumed parameters (table 1), the polynomial  $W(p_1)$  has three real roots, and correspondingly the system has three steady states (figures 2 and 4(a)):

- the unstable state  $S_0$ :  $g_1 = g_2 \approx 0.12$ ,  $m_1 = p_1 = m_2 = p_2 \approx 0.15$ ,  $d_1 = d_2 \approx 0.022$ ,
- the stable state  $S_1$ :  
 $g_1 \approx 0.006$ ,  $g_2 \approx 0.71$ ,  $m_1 = p_1 \approx 0.72$ ,  $d_1 \approx 0.51$ ,  
 $m_2 = p_2 \approx 0.036$ ,  $d_2 \approx 0.0013$ ,
- the stable state  $S_2$ :  
 $g_1 \approx 0.71$ ,  $g_2 \approx 0.006$ ,  $m_1 = p_1 \approx 0.036$ ,  $d_1 \approx 0.0013$ ,  
 $m_2 = p_2 \approx 0.72$ ,  $d_2 \approx 0.51$ .

In the steady state  $S_1$ , gene 1 is mostly active while gene 2 is repressed. In the steady state  $S_2$ , gene 2 is mostly active and gene 1 is repressed. In the deterministic approximation, the choice of the stationary state is determined by the initial conditions, i.e. trajectories remain in the same basin of attraction. In figure 2, we show the correspondence between deterministic steady states  $S_0$ ,  $S_1$  and  $S_2$  and trajectories of the stochastic system. The scaled concentrations (given on the right-hand side of each panel) can be converted to the numbers of molecules (given on the left-hand side) by relations (2).

### 3.2. Stochastic model analysis

In the stochastic model, trajectories switch between the two basins of attraction, figure 2. Since the system is multidimensional, the exact determination of attraction basins is difficult. For practical purposes, in order to determine mean residence times  $T_1$  and  $T_2$  in the basins of states  $S_1$  and  $S_2$  (or shortly in states  $S_1$  and  $S_2$ ), we assume the following definitions of state-to-state transitions: the  $S_1$  to  $S_2$  transition occurs when  $P_2 - P_1 > P_0(p_1(S_1) - p_1(S_2))/3$  and in addition when  $D_2 - D_1 > D_0(d_1(S_1) - d_1(S_2))/3$ , and analogously for the reverse transition. Accordingly, the events in which only  $P_2 - P_1$  becomes greater than  $P_0(p_1(S_1) - p_1(S_2))/3$  are not counted as state-to-state transitions. When performing sensitivity analysis (section 3.3), we observe that for some sets of parameters (for which dimers have much higher stability than monomers) such pseudo-transitions are quite frequent but are not followed by a trajectory jump to the vicinity of the other steady state. For similar reasons, it is not enough to require that  $P_2$  and  $D_2$  simply exceed  $P_1$  and  $D_1$ , respectively. Such a definition would lead to multiple pseudo-transitions accompanying almost every single real transition.

Stationary probability mass fractions in the vicinities of stable steady states  $S_1$  to  $S_2$  can be estimated from the mean residence times as  $\pi^*(S_1) := T_1/(T_1 + T_2)$  and  $\pi^*(S_2) := T_2/(T_1 + T_2)$ . However, because the definition of

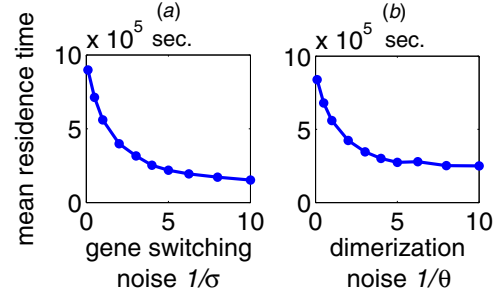


**Figure 3.** The mean residence time in states  $S_1$  and  $S_2$  calculated in the symmetric case as a function of the gene switching noise  $1/\sigma$  or dimerization noise  $1/\theta$ , where  $\sigma = \sigma_1 = \sigma_2$  and  $\theta = \theta_1 = \theta_2$ .

state-to-state transitions is arbitrary, we will also estimate probability mass fractions independently of the mean residence times for a cross validation. We make use of the fact that in the deterministic approximation the system is symmetric with respect to both genes. This allows us to define  $\pi(S_1) := \langle G_1 \rangle / (\langle G_1 \rangle + \langle G_2 \rangle)$  and  $\pi(S_2) := \langle G_2 \rangle / (\langle G_1 \rangle + \langle G_2 \rangle)$ , where  $\langle G_1 \rangle$  denotes the average state of gene 1, equal to the probability that the gene is active. The stationary probability mass fractions  $\pi(S_1)$  and  $\pi(S_2)$  will be estimated based on the long-run Gillespie algorithm simulations, having 1000 (for figures 3 and 5) or 100 (for figures 6 and 7)  $S_1$  to  $S_2$  (and reverse) transitions. Based on the same simulations we will also estimate the mean residence times  $T_1$  and  $T_2$ .

As one could expect, in the symmetric case, i.e. when  $\sigma_1 = \sigma_2 = \sigma$  and  $\theta_1 = \theta_2 = \theta$ , the mean residence times  $T_1$  and  $T_2$  are equal and decrease with increasing magnitude of noise in the system. As shown in figure 3, an increase of either of the two considered noise components (i.e.  $1/\sigma$  or  $1/\theta$ ) leads to a shortening of the mean residence times in states  $S_1$  and  $S_2$ . This allows for the interpretation of  $1/\sigma$  and  $1/\theta$  as, respectively, the gene switching and dimerization noise parameters. As analyzed earlier by Warren and ten Wolde [28], the mean residence time decreases with increasing transcriptional noise (inversely proportional to the number of product molecules). We also observe this effect within the considered toggle switch model, see appendix.

Responses of the system to a non-symmetric change of noise parameters are less intuitive. In figure 4, we analyze the changes of the SPD in response to the non-symmetric (only for gene 2) fivefold change of the gene switching or dimerization noise. As shown (figure 4(c)), the increase of the gene 2 switching noise induces a break of symmetry of the SPD, such that the probability mass fraction concentrates in the vicinity of state  $S_1$  (i.e. the state in which gene 1 is predominantly active) with  $\pi(S_1) = 0.84$ . In turn, the decrease of the gene 2 switching noise makes gene 2 dominant, with  $\pi(S_1) = 0.36$  (figure 4(e)). Surprisingly, the increase of the dimerization noise for the gene 2 protein causes the gene 2 activation (with  $\pi(S_1) = 0.19$ , figure 4(d)), while the decrease of the gene 2 protein dimerization noise causes the gene 1 activation (with  $\pi(S_1) = 0.64$ , figure 4(f)).

In short, an increase of noise associated with a given gene may either promote or suppress its activation depending on the

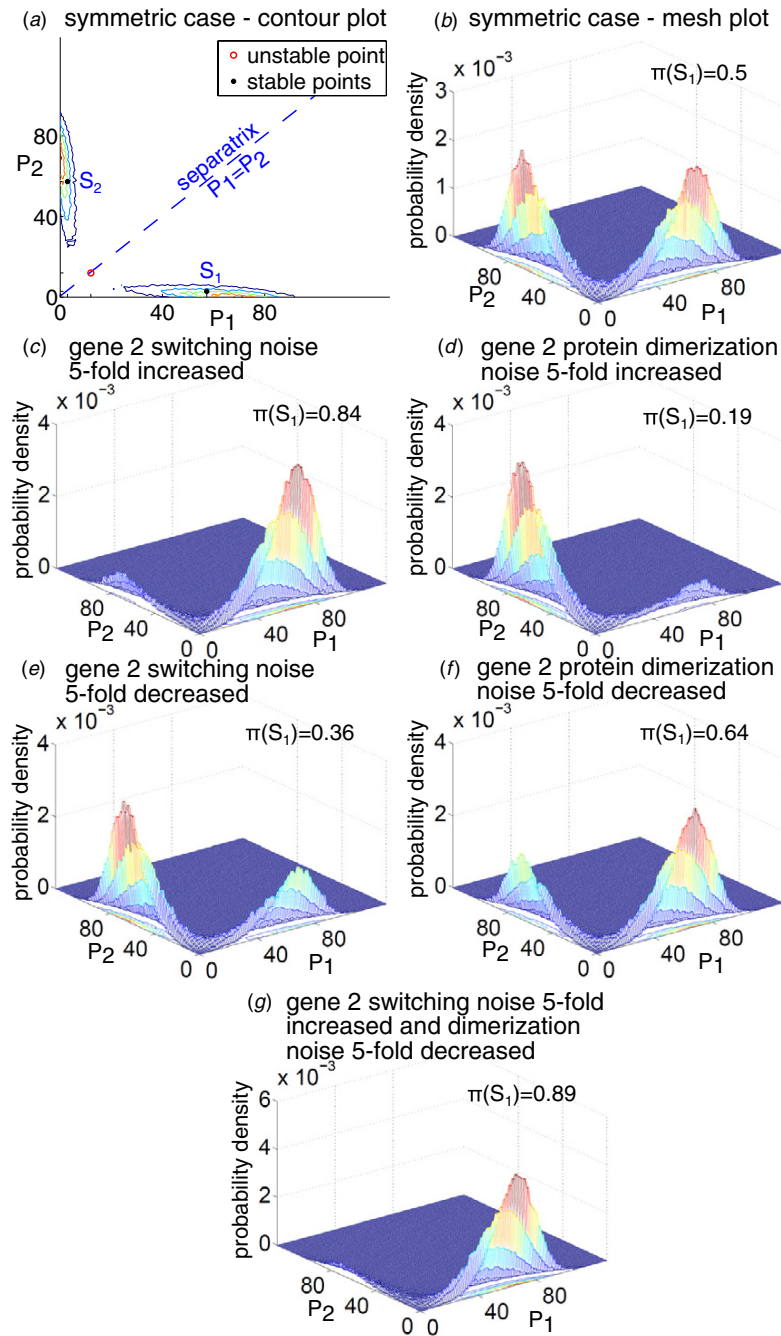


**Figure 4.** The SPDs of the stochastic model obtained in Monte Carlo simulations. Panels (a) and (b) show the contour and mesh plots in the symmetric case ( $\sigma_i = \theta_i = 1$ ,  $i = 1, 2$ ). Panel (a): the stable steady states of the corresponding deterministic model are marked with dots and the unstable steady state is marked with a circle. An increase or decrease of noise associated with the gene 2 expression causes the SPD to become asymmetric. Panels (c), (d), (e) and (f): increase of the gene switching noise causes the probability mass to concentrate in the vicinity of state  $S_1$ , while an increase of dimerization noise causes most of the probability mass to concentrate in the vicinity of state  $S_2$ . A decrease of the gene switching noise causes the probability mass to concentrate in state  $S_2$ , while a decrease of the dimerization noise causes most of the probability mass to concentrate in the vicinity of state  $S_1$ . Panel (g): a simultaneous fivefold increase of the gene 2 switching noise and a decrease of the gene 2 dimerization noise results in the largest asymmetry of the SPD, 89% of the probability mass concentrated in state  $S_1$ .

increased noise component. An increase of the gene switching noise promotes the activity of the competing gene, while an increase of the dimerization noise suppresses the competing gene activation. These two opposing effects can be combined

by the simultaneous fivefold increase of the gene 2 switching noise, and fivefold decrease of its product dimerization noise, which leads to an almost full suppression of the gene 2 activity, with  $\pi(S_1) = 0.89$ , figure 4(g).

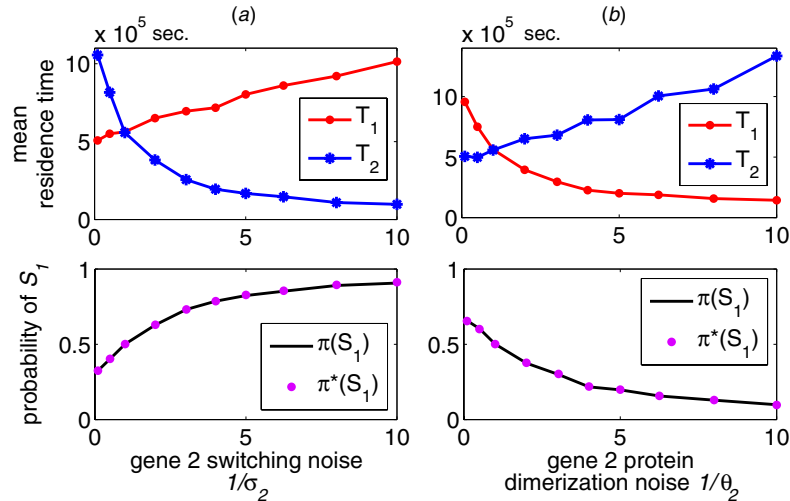


**Figure 5.** The mean residence times  $T_1$  and  $T_2$  in states  $S_1$  and  $S_2$  are plotted as a function of the gene 2 noise parameters  $1/\sigma_2$  and  $1/\theta_2$  (with the remaining noise parameters equal to 1). A decrease of  $1/\sigma_2$  increases the stability of state  $S_2$  and simultaneously decreases the stability of state  $S_1$  (panel (a)). In contrast, a decrease of  $1/\theta_2$  increases the stability of state  $S_1$  and decreases the stability of state  $S_2$  (panel (b)). The two bottom subpanels show the probability of state  $S_1$ , as a function of the gene 2 noise parameters estimated as  $\pi(S_1) = \langle G_1 \rangle / (\langle G_1 \rangle + \langle G_2 \rangle)$  (line) and  $\tilde{\pi}(S_1) = T_1 / (T_1 + T_2)$  dots.

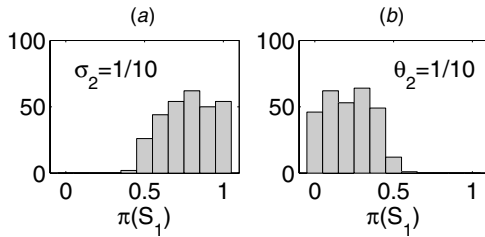


**Figure 6.** Histograms of probability  $\pi(S_1)$  for parameters tossed based on the Latin hypercube sampling. All nine tossed parameters may vary fivefold from their default values (except  $k_3$ , see the text for details). Panel (a): increased gene 2 switching noise parameter,  $1/\sigma_2 = 10$  (with  $\sigma_1 = \theta_1 = \theta_2 = 1$ ). Panel (b): increased gene 2 dimerization noise parameter,  $1/\theta_2 = 10$  (with  $\theta_1 = \sigma_1 = \sigma_2 = 1$ ). For the default parameters (see figure 5),  $\pi(S_1) = 0.91$  for  $1/\sigma_2 = 10$  and  $\pi(S_1) = 0.10$  for  $1/\theta_2 = 10$ .

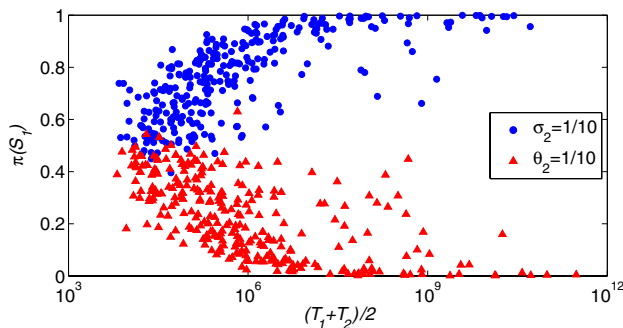


**Figure 7.** Scatter plots showing probability  $\pi(S_1)$  versus average mean residence time  $(T_1 + T_2)/2$ .

The results shown in figure 4 are supported by the analysis of the mean residence times  $T_1$  and  $T_2$ , figure 5. As shown in figure 5(a), an increase of the gene 2 switching noise induces

an increase of time  $T_1$  and a decrease of time  $T_2$ . In contrast, an increase of the gene 2 protein dimerization noise leads to an increase of time  $T_2$  and simultaneously leads to a decrease of time  $T_1$ . The above analysis implies that an increase of the gene switching noise stabilizes the gene in the inactive state, and destabilizes it in the active state. The increase of a given gene product dimerization noise stabilizes that gene in the active state and additionally eases inhibition of the competing gene.

As shown in figure 5, the probability mass fraction  $\pi(S_1)$  (defined, recall, as  $\pi(S_1) := \langle G_1 \rangle / (\langle G_1 \rangle + \langle G_2 \rangle)$ ) is almost equal to  $\pi^*(S_1) := T_1 / (T_1 + T_2)$ , showing the perfect consistency of these two measures. Accordingly,  $\pi(S_1)$  is a monotonically growing function of the gene 2 switching noise (with  $\pi(S_1) = 0.91$  for  $1/\sigma_2 = 10$ ) and a monotonically decreasing function of the gene 2 protein dimerization noise (with  $\pi(S_1) = 0.10$  for  $1/\theta_2 = 10$ ); see figure 5, two bottom subpanels.

The results presented in figures 3 and 5 can be explained as follows. As shown in figure 4, trajectories transit between states  $S_1$  and  $S_2$  through the vicinity of state  $S_0$  in which both genes are mainly repressed, and the levels of both proteins are low. Thus, the  $S_1$  to  $S_2$  transition requires the repression of the active gene ( $G_1$ ) by binding a protein dimer, product of the repressed gene ( $G_2$ ). These dimers arise infrequently due to the small mRNA synthesis from the repressed gene  $G_2$  (coefficient  $k_4$ , table 1). A detailed analysis of the trajectory whose short fragment is shown in figure 2 indicates that for the default parameters less than 1% of the active gene switching-off events leads to a state-to-state ( $S_1$  to  $S_2$  or reverse) transition, compare figures 2(a) and (c). When gene switching noise increases, say tenfold, the gene switching-off events are ten times less frequent, but the time for which the gene is switched off is ten times longer. We found that these longer switch-offs are much more effective, and almost all of

them lead to state-to-state transitions. As a result, the increase of the gene 2 switching noise shortens the mean residence time  $T_2$  (in  $S_2$ ), figure 5(a). A simultaneous increase of the gene switching noise for gene 1 and gene 2 shortens both  $T_1$  and  $T_2$ , respectively, as shown in figure 3(a).

As said, the active gene switching-offs follow synthesis of single dimers from the repressed gene. For the default parameters, a synthesis of a single dimer leads on average to  $k_2/k_7 = 1.5$  switching-off events (less when several dimers compete for the binding site). When the gene 2 dimerization noise increases, say tenfold, gene 2 dimers appear tenfold less frequently, but survive ten times longer. As a result appearance of a single dimer leads to  $k_2/(k_7/10) = 15$  switching-off events. Because these switch-offs arise in series, they have much higher chance to induce  $S_1$  to  $S_2$  transition. As a result when the gene 2 dimerization noise increases, the time  $T_1$  decreases, figure 5(b). Simultaneously, the time  $T_2$  increases, because an  $S_2$  to  $S_1$  transition requires longer repression of gene 2, necessary for protein dimers of gene 2 to dissociate to monomers, figure 5(b). The last effect, however, is weaker than the previous one, and therefore a simultaneous increase of protein 1 and protein 2 dimerization noises leads to the decrease of both  $T_1$  and  $T_2$ , respectively, as shown in figure 3(b).

### 3.3. Sensitivity analysis

In order to analyze the sensitivity of the presented results to a model parameters variation, we perform systematic robustness analysis based on the Latin hypercube parameter sampling. That is, we toss 600 points  $(X_i, i = 1, \dots, 9)$  from the nine-dimensional unit cube. Based on the tossed  $X_i$ , we calculated 600 sets of new coefficients  $K_i$  as

$$K_i = 5^{(1-2X_i)}k_i \quad \text{for } i \neq 3, \quad K_i = 2^{(1-2X_i)}k_i \quad \text{for } i = 3. \quad (13)$$

Thus, the new coefficients are allowed to vary fivefold above and fivefold below the default values, except for parameter  $k_3$  for which the variation was twofold. The fivefold variation of  $k_3$  led to very long mean residence times, increasing the numerical cost of simulations. From the obtained 600 sets of parameters, we left 322 sets for which the system in the deterministic approximation maintained bistability.

For these selected sets of parameters, we calculated the probability mass fraction  $\pi(S_1) := \langle G_1 \rangle / (\langle G_1 \rangle + \langle G_2 \rangle)$ , and the average mean transition time  $(T_1 + T_2)/2$  in the case when either gene switching or dimerization noise was increased tenfold for one of the genes. That is, we analyze two cases:

- (1) when the gene 2 switching noise parameter is  $1/\sigma_2 = 10$  (with  $\sigma_1 = \theta_1 = \theta_2 = 1$ ),
- (2) when the gene 2 dimerization noise parameter is  $1/\theta_2 = 10$  (with  $\theta_1 = \sigma_1 = \sigma_2 = 1$ ). Calculations were made using the same method as previously based on simulations with 100 transitions.

In the first (second) case, we managed to accomplish 292 (287) out of 322 simulations. In the remaining simulations, the  $S_1$  to  $S_2$  (or reverse) transitions rates were so small that we were not able to reach 100  $S_1$  to  $S_2$  transitions. In these cases, the relative state occupancies can be calculated using the forward flux sampling methods developed by the group of ten Wolde

[32, 33]. However, because these methods are challenging for multidimensional systems, we simply remove the unfinished simulations from the further analysis. As will be demonstrated later, since the studied effect of the SPD asymmetry increases with decreasing transition rates, we remain confident that the inclusion of these unfinished trajectories would only improve our results.

In figures 6(a) and (b), we show histograms of probability  $\pi(S_1)$  in the first and second cases, respectively. Let us recall that in simulations performed for the default parameters (figure 5), we obtained  $\pi(S_1) = 0.91$  for  $1/\sigma_2 = 10$  and  $\pi(S_1) = 0.1$  for  $1/\theta_2 = 10$ . Here, we found that for  $1/\sigma_2 = 10$ , the probability mass fraction  $\pi(S_1) > 0.5$  for 97% of tossed and computed sets of parameters, and that the average  $\langle \pi(S_1) \rangle = 0.77$ . For  $1/\theta_2 = 10$  case, the probability mass fraction  $\pi(S_1) < 0.5$  for 99% of tossed and computed sets of parameters, and the average  $\langle \pi(S_1) \rangle = 0.23$ .

In figure 7, we present the scatter plot showing the probability mass fraction  $\pi(S_1)$  versus average mean residence time  $(T_1 + T_2)/2$ . The dots and triangles correspond to  $1/\sigma_2 = 10$  and  $1/\theta_2 = 10$  cases, respectively. The presented data indicate that the asymmetry of the SPD increases with the mean residence time, i.e. the stability of the toggle switch. This finding is important, since bacterial toggle switches can be extremely stable with transition times exceeding millions of cell cycles [34].

## 4. Conclusions

In this study, we considered a bistable stochastic model of the genetic toggle switch. The reactions of mRNA transcription, protein translation, dimerization and gene repression by the binding of the competing protein dimers are explicitly included in the model. We focused on the two stochasticity sources present in the regulation: the gene switching and the protein dimerization noise. These two noise components were modified independently by changing simultaneously repressor binding and dissociation rate constants, or rate constants of a protein dimer formation and dissociation. This procedure enabled us to modify the noise characteristics of the system without influencing the deterministic limit of the process.

Our analysis demonstrated that an increase of noise associated with the expression of a particular gene introduces a large asymmetry in the SPD. Interestingly, we observe that each of the genes is repressed by increasing its gene switching noise (i.e. when its promoter repression and activation rates decrease). In contrast, the increased dimerization noise for a particular gene product leads to the preferential activation of the gene. We thus showed that various noise components associated with gene expression and protein processing antagonistically contribute to the strength of each of the two competing genes.

The sensitivity analysis based on the Latin hypercube parameters sampling demonstrated that the SPD asymmetry introduced by an increase of a particular noise component is statistically robust with respect to the large (up to fivefold) parameters deviations that change macroscopic steady states

as well as state-to-state transitions rate. The effect of the preferential gene inactivation due to gene switching noise increase, observed for the assumed default parameters, was conserved for 283 out of 292 tossed and computed parameter sets. Similarly, the effect of preferential gene activation due to its product protein dimerization noise increase was conserved for 283 out of 287 tossed and computed parameter sets. Importantly, we found that the scale of the noise introduced asymmetry positively correlates with the stability of the toggle switch. The asymmetry was statistically increasing with mean residence time, which calculated for the tossed parameters sets varied about eight orders of magnitude. This implies that the discovered effect can be important in bacterial toggle switches which may exhibit enormous stability, with one transition over millions of generation.

The observation that magnitudes of individual noise components determine the dominating gene opens the possibility of a new mode of toggle switch control. Such a control can be potentially exploited in synthetic biology, which offers tools for an independent modification of various noise sources [35, 36]. It remains an open question whether extracellular conditions can switch the toggle by modifications of noise components. Such regulation seems quite likely for bacteria. For example, the temperature can modify repressor binding and dissociation rate constants and level of nutrients may regulate the transcription and translation rates. The potential advantage of the noise driven control is such that it does not influence the macroscopic steady states of the system and thus ensures that the cell remains in one of the predefined local optima.

## Acknowledgments

We thank Marek Kochańczyk for help in numerical simulations. This study was supported by the FNP grant TEAM/2009-3/6 and NSF/NIH grant no. R01-GM086 885. Numerical simulations were carried out at the Zeus computer cluster at the ACK Cyfronet AGH in Kraków.

## Appendix. Decrease of the mean residence time with increasing transcriptional noise

Here, we analyze the effect of transcriptional noise introducing a new coefficient  $\xi$ . Multiplying the mRNA transcription rate coefficient  $k_3$  by  $\xi$ , and simultaneously dividing dimerization and DNA-dimer binding coefficients  $k_6$  and  $k_2$  by  $\xi$  we obtain systems characterized by  $\xi$ -fold larger (than default) number of mRNA, protein monomer and protein dimer molecules, but the same scaled concentrations. The inverse of coefficient  $\xi$  can be thus considered as a measure of transcriptional noise. In figure A1, we show that the mean residence time decreases with the magnitude of transcriptional noise  $1/\xi$ .

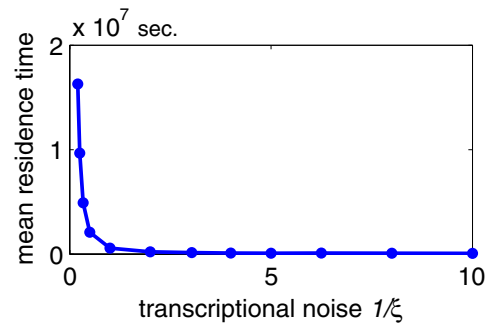


**Figure A1.** Mean residence time as a function of transcriptional noise  $1/\xi$ .

## References

- [1] Acar M, Becskei A and van Oudenaarden A 2005 Enhancement of cellular memory by reducing stochastic transitions *Nature* **435** 228–32
- [2] Chang H H, Oh P Y, Ingber D E and Huang S 2006 Multistable and multistep dynamics in neutrophil differentiation *BMC Cell. Biol.* **7** 11
- [3] Hoyle R B, Avitabile D and Kierzek A M 2012 Equation-free analysis of two-component system signalling model reveals the emergence of co-existing phenotypes in the absence of multistationarity *PLoS Comput. Biol.* **8** e1002396
- [4] Kussell E and Leibler S 2005 Phenotypic diversity, population growth, and information in fluctuating environments *Science* **309** 2075–8
- [5] Nevozhay D, Adams R M, Van Itallie E, Bennett M R and Balazsi G 2012 Mapping the environmental fitness landscape of a synthetic gene circuit *PLoS Comput. Biol.* **8** e1002480
- [6] Vellela M and Qian H 2009 Stochastic dynamics and non-equilibrium thermodynamics of a bistable chemical system: the Schloegl model revisited *J. R. Soc. Interface* **6** 925–40
- [7] Zuk P J, Kochańczyk M, Jaruszewicz J, Bednorz W and Lipniacki T 2012 Dynamics of a stochastic spatially extended system predicted by comparing deterministic and stochastic attractors of the corresponding birth–death process *Phys. Biol.* **9** 055002
- [8] Frigola D, Casanellas L, Sancho J M and Ibanes M 2012 Asymmetric stochastic switching driven by intrinsic molecular noise *PLoS One* **7** e31407
- [9] Jaruszewicz J, Zuk P J and Lipniacki T 2013 Type of noise defines global attractors in bistable molecular regulatory systems *J. Theor. Biol.* **317** 140–51
- [10] Ferrell J E Jr 2002 Self-perpetuating states in signal transduction: positive feedback, double-negative feedback and bistability *Curr. Opin. Cell. Biol.* **14** 140–8
- [11] Tian T and Burrage K 2006 Stochastic models for regulatory networks of the genetic toggle switch *Proc. Natl Acad. Sci. USA* **103** 8372–7
- [12] Lipshtat A, Loinger A, Balaban N Q and Biham O 2006 Genetic toggle switch without cooperative binding *Phys. Rev. Lett.* **96** 188101
- [13] Chatterjee A, Kaznessis Y N and Hu W-S 2008 Tweaking biological switches through a better understanding of bistability behavior *Curr. Opin. Biotechnol.* **19** 475–81
- [14] Ptashne M 1992 *A Genetic Switch: Phage and Higher Organisms* (Cambridge, MA: Cell Press and Blackwell Scientific Publications)
- [15] Arkin A, Ross J and McAdams H H 1998 Stochastic kinetic analysis of developmental pathway bifurcation in phage

- lambda-infected *Escherichia coli* cells *Genetics* **149** 1633–48
- [16] Tian T and Burrage K 2004 Bistability and switching in the lysis/lysogeny genetic regulatory network of bacteriophage  $\lambda$  *J. Theor. Biol.* **227** 229–37
- [17] Ferrell J E and Machleder E M 1998 The biochemical basis of an all-or-none cell fate switch in *Xenopus* oocytes *Science* **280** 895–8
- [18] Bhalla U S 2002 MAP kinase phosphatase as a locus of flexibility in a mitogen-activated protein kinase signaling network *Science* **297** 1018–23
- [19] Bagowski C P and Ferrell J E 2001 Bistability in the JNK cascade *Curr. Biol.* **11** 1176–82
- [20] Pomerening J R, Sontag E D and Ferrell J J 2003 Building a cell cycle oscillator: hysteresis and bistability in the activation of Cdc2 *Nature Cell. Biol.* **5** 346–51
- [21] Cross F R, Archambault V, Miller M and Klavstad M 2002 Testing a mathematical model of the yeast cell cycle *Mol. Biol. Cell.* **13** 52–70
- [22] Gardner T S, Cantor C R and Collins J J 2000 Construction of a genetic toggle switch in *Escherichia coli* *Nature* **403** 339–42
- [23] Puszynski K, Hat B and Lipniacki T 2008 Oscillations and bistability in the stochastic model of p53 regulation *J. Theor. Biol.* **254** 452–65
- [24] Lipniacki T, Hat B, Faeder J R and Hlavacek W S 2008 Stochastic effects and bistability in T cell receptor signaling *J. Theor. Biol.* **254** 110–22
- [25] Ribeiro A S 2008 Dynamics and evolution of stochastic bistable gene networks with sensing in fluctuating environments *Phys. Rev. E* **78** 061902
- [26] Komorowski M, Miekisz J and Kierzek A M 2009 Translational repression contributes greater noise to gene expression than transcriptional repression *Biophys. J.* **96** 372–84
- [27] Warren P B and ten Wolde P R 2004 Enhancement of the stability of genetic switches by overlapping upstream regulatory domains *Phys. Rev. Lett.* **92** 128101
- [28] Warren P B and ten Wolde P R 2005 Chemical models of genetic toggle switches *J. Phys. Chem. B* **109** 6812–23
- [29] Dai X, Yli-Harja O and Ribeiro A S 2009 Determining noisy attractors of delayed stochastic gene regulatory networks from multiple data sources *Bioinformatics* **25** 2362–8
- [30] Ribeiro A S 2010 Stochastic and delayed stochastic models of gene expression and regulation *Math. Biosci.* **223** 1–11
- [31] Gillespie D T 1977 Exact stochastic simulation of coupled chemical reactions *J. Phys. Chem.* **81** 2340–61
- [32] Allen R J, Warren P B and ten Wolde P R 2005 Sampling rare switching events in biochemical networks *Phys. Rev. Lett.* **94** 018104
- [33] Becker N B, Allen R J and ten Wolde P R 2012 Non-stationary forward flux sampling *J. Chem. Phys.* **136** 174118
- [34] Aurell E, Brown S, Johanson J and Sneppen K 2002 Stability puzzles in phage  $\lambda$  *Phys. Rev. E* **65** 051914
- [35] Kierzek A M, Zaim J and Zielenkiewicz P 2001 The effect of transcription and translation initiation frequencies on the stochastic fluctuations in prokaryotic gene expression *J. Biol. Chem.* **276** 8165–72
- [36] Ozbudak E M, Thattai M, Kurtser I, Grossman A D and Oudenaarden A 2002 Regulation of noise in the expression of a single gene *Nature Genet.* **31** 69–73
- [37] Blake W J, Kaern M, Cantor C R and Collins J J 2003 Noise in eukaryotic gene expression *Nature* **422** 633–7
- [38] Kennell D and Riezman H 1977 Transcription and translation initiation frequencies of the *Escherichia coli* lac operon *J. Mol. Biol.* **114** 1–21
- [39] Laursen B S, Soerensen H P, Mortensen K K and Sperling-Petersen H U 2005 Initiation of protein synthesis in bacteria *Microbiol. Mol. Biol. Rev.* **69** 101–23
- [40] Sampson L L, Hendrix R W, Huang W M and Casjens S R 1988 Translation initiation controls the relative rates of expression of the bacteriophage  $\lambda$  late genes *Proc. Natl Acad. Sci. USA* **85** 5439–43
- [41] Young R and Bremer H 1976 Polypeptide-chain-elongation rate in *Escherichia coli* B/r as a function of growth rate *Biochem. J.* **160** 185–94
- [42] Bremer H, Hymes J and Dennis P P 1974 Ribosomal RNA chain growth rate and RNA labelling patterns in *Escherichia coli* *J. Theor. Biol.* **45** 379–403
- [43] Bai H, Yang K, Yu D, Zhang C, Chen F and Lai L 2011 Predicting kinetic constants of protein–protein interactions based on structural properties *Proteins* **79** 720–34
- [44] Alberts B, Johnson A, Lewis J, Raff M, Roberts K and Walter P 2002 *Molecular Biology of the Cell* 4th edn (New York: Garland Science)
- [45] Taniguchi Y, Choi P J, Li G W, Chen H, Babu M, Hearn J, Emili A and Xie X S 2010 Quantifying *E. coli* proteome and transcriptome with single-molecule sensitivity in single cells *Science* **329** 533–8
- [46] Jayapal K P, Sui S, Philp R J, Kok Y-J, Yap M G S, Griffin T J and Hu W-S 2010 Multitagging proteomic strategy to estimate protein turnover rates in dynamic systems *J. Proteome Res.* **9** 2087–97
- [47] Chen C and Deutscher M P 2010 RNase R is a highly unstable protein regulated by growth phase and stress *RNA* **16** 667–72
- [48] El-Samad H, Kurata H, Doyle J C, Gross C A and Khammash M 2005 Surviving heat shock: control strategies for robustness and performance *Proc. Natl Acad. Sci. USA* **102** 2736–41

III) Jaruszewicz J, Kimmel M, Lipniacki T, *Stability of bacterial toggle switches is enhanced by cell cycle lengthening by several orders of magnitude*, accepted for publication in the Physical Review E, (American Physical Society), 2014.

# Stability of bacterial toggle switches is enhanced by cell-cycle lengthening by several orders of magnitude

Joanna Jaruszewicz,<sup>1</sup> Marek Kimmel,<sup>2,3</sup> and Tomasz Lipniacki<sup>1,4,\*</sup>

<sup>1</sup>*Institute of Fundamental Technological Research, Polish Academy of Sciences, 02-106 Warsaw, Poland*

<sup>2</sup>*Departments of Statistics and Bioengineering, Rice University, Houston, Texas 77005, USA*

<sup>3</sup>*Systems Engineering Group, Silesian University of Technology, 44-100 Gliwice, Poland*

<sup>4</sup>*Department of Statistics, Rice University, Houston, Texas 77005, USA*

(Received 27 October 2013; revised manuscript received 14 January 2014; published xxxxxx)

Bistable regulatory elements are important for nongenetic inheritance, increase of cell-to-cell heterogeneity allowing adaptation, and robust responses at the population level. Here, we study computationally the bistable genetic toggle switch—a small regulatory network consisting of a pair of mutual repressors—in growing and dividing bacteria. We show that as cells with an inhibited growth exhibit high stability of toggle states, cell growth and divisions lead to a dramatic increase of toggling rates. The toggling rates were found to increase with rate of cell growth, and can be up to six orders of magnitude larger for fast growing cells than for cells with the inhibited growth. The effect is caused mainly by the increase of protein and mRNA burst sizes associated with the faster growth. The observation that fast growth dramatically destabilizes toggle states implies that rapidly growing cells may vigorously explore the epigenetic landscape enabling nongenetic evolution, while cells with inhibited growth adhere to the local optima. This can be a clever population strategy that allows the slow growing (but stress resistant) cells to survive long periods of unfavorable conditions. Simultaneously, at favorable conditions, this stress resistant (but slowly growing—or not growing) subpopulation may be replenished due to a high switching rate from the fast growing population.

DOI: [10.1103/PhysRevE.00.002700](https://doi.org/10.1103/PhysRevE.00.002700)

PACS number(s): 87.10.Mn, 87.15.A–, 87.16.Yc, 87.17.Ee

## I. INTRODUCTION

Epigenetic mechanisms of biological evolution constitute an expanding research area, with important consequences for organism development, proliferative diseases such as cancer, and synthetic biology [1]. A genetic toggle switch, a pair of mutual repressors, is one of the most important circuits introducing bistability to gene regulatory networks [2–5]. Bi- and multistable regulatory elements introduce heterogeneity in cell populations and allow cells in a multicellular organism to specialize and specify their fate. Although multistability is not required for the emergence of coexisting phenotypes [6], decisions between cell death, survival, proliferation, or senescence are likely associated with bistability. In prokaryotes multistability is regarded as an optimal strategy for adapting to varying environmental conditions [7]. Classical examples of toggle switches include the lysis-lysogeny switch in  $\lambda$  phage [8–10], a tetracycline resistance circuit in *Escherichia coli*, Laslo switch in human hematopoiesis [11], several mitogen-activated protein kinase cascades in animal cells [12–14], and cell-cycle regulatory CI circuits in *Xenopus laevis* and *Saccharomyces cerevisiae* [15,16]. Gardner *et al.* [17] constructed a synthetic toggle switch in *E. coli* and provided a theoretical prediction of the conditions sufficient for bistability. Bistability may arise when at least one of the repressors inhibits the competing gene with cooperativity greater than one or when the promoter sites overlap, so the repressors cannot be bound simultaneously [4].

Gene expression in bacterial cells is considered noisy. Stochasticity originating from small numbers of mRNA and

protein molecules enables transitions between distinct states. In changing epigenetic landscape noise is favorable as it allows for adaptation; bacteria maximize fitness by tuning noise magnitude with the frequency of the environment fluctuations [18]. The influence of noise on transition rates in a genetic switch has been extensively studied [19–23]. It was shown that the relative stability of the steady states of a toggle as well as of a single autoregulatory gene is controlled by the type of noise [23,24].

In bacteria the average protein lifetime is typically longer than the cell cycle [25], which causes the system to be far from equilibrium. Observations of fast growing *Escherichia coli* cells, which are able to divide as frequently as every 20 min, show an extreme level of cellular activity including continuous reproduction of genome [26], increased number of mRNAs, ribosomal RNAs, and proteins necessary to perform gene expression [27–30]. At high nutrient availability and rapid cell growth DNA elongation rate is roughly constant and DNA replication lasts approximately 40 min [31]; however, at low nutrient levels DNA replication slows down [31,32]. Partitioning of molecules between daughter cells in *E. coli* is binomial [33]. *E. coli* and *B. subtilis* rapidly growing cells are larger than slowly growing cells and can have up to eight origins of replication per cell. However, when the doubling time increases beyond a certain threshold (~60 min for *B. subtilis*) cell size becomes essentially constant, and cells have at most one replication proceeding [34].

In this article we analyze how the cell-cycle length influences switching rates between two attracting trajectories (epigenetic states) in a bacterial toggle switch. We will consider cell-cycle lengths  $T \geq 1$  h and assume simultaneous replication of two toggle genes either just before cell division or (in the Appendix A) in the middle of cell cycle. In fact,

\*[tlipnia@ippt.pan.pl](mailto:tlipnia@ippt.pan.pl)

86 since DNA replication takes at least about 40 min (in *E. coli*), 105  
 87 different genes are present in different copy numbers at a given 106  
 88 time of the cell cycle. This effect may have a significant impact  
 89 on the dynamics of regulatory systems, especially in the case  
 90 of rapid growth ( $T < 1$  h), when genes may have up to eight  
 91 copies [26,35]. However, in natural systems genes composing  
 92 a toggle switch (like other regulatory modules) are typically  
 93 localized in a vicinity of each other [36,37]; see also EcoCyc  
 94 database [38]. In the case of synthetic toggle switches opposing  
 95 genes are typically introduced in one plasmid, and therefore  
 96 replicate in approximately the same time.

## 97 II. MODEL

98 The rate of cell growth and division times are determined  
 99 by the “housekeeping protein” level, which is assumed  
 100 proportional to the cell volume  $V(t)$ . Since there are many  
 101 genes responsible for protein mass production we assume  
 102 that the dynamics of the housekeeping protein level is  
 103 deterministic. Expression of the housekeeping gene is defined  
 104 by transcription rate constant  $k_m$ , translation rate constant  $k_p$ ,

protein degradation rate constant  $r_p$ , and mRNA degradation  
 rate constant  $r_m$ . Constants  $k_m$  and  $k_p$  depend on  $T$ , while  
 degradation rates  $r_p$  and  $r_m$  are assumed to be independent  
 of  $T$  [28,30]. The cell divides when the housekeeping protein  
 level (or equivalently cell volume) doubles. For simplicity  
 we assume equal assignment of housekeeping protein and  
 its mRNA to progeny cells. Cell growth rate is therefore  
 governed by the housekeeping protein accumulation. Such  
 assumption implies that in the case when no switches occur  
 the concentration of toggle proteins remains roughly constant  
 during the cell cycle.

The housekeeping mRNA  $m(t)$  and protein  $p(t)$  levels  
 satisfy the following ODEs:

$$\frac{dm}{dt} = k_m - r_m m, \quad \frac{dp}{dt} = k_p m - r_p p, \quad (1)$$

with conditions

$$m(T) = 2m(0), \quad p(T) = 2p(0). \quad (2)$$

The above system has explicit solutions,

$$\begin{aligned} m(t) &= \frac{k_m}{r_m} \left( 1 - \frac{1}{e^{r_m t} (2 - e^{-r_m T})} \right), \\ p(t) &= \frac{k_m k_p}{r_m r_p} \left[ 1 - \frac{1}{r_m - r_p} \left( \frac{r_m}{e^{r_p t} (2 - e^{-r_p T})} - \frac{r_p}{e^{r_m t} (2 - e^{-r_m T})} \right) \right] \quad \text{when } r_m \neq r_p, \\ p(t) &= \frac{k_m k_p}{r_m^2} \left( 1 - \frac{1}{e^{r_m t} (2 - e^{-r_m T})} \right) \quad \text{when } r_m = r_p, \end{aligned} \quad (3)$$

where  $t$  is the time from the last cell division. The cell volume  $V(t) = V_0[p(t)/p(0)]$  [where  $V_0 = V(0)$ ] is therefore given by  
 the expressions

$$V(t) = V_0 + V_0 \frac{r_m(2 - e^{-r_m T})(1 - e^{-r_p t}) - r_p(2 - e^{-r_p T})(1 - e^{-r_m t})}{r_m(2 - e^{-r_m T})(1 - e^{-r_p T}) - r_p(2 - e^{-r_p T})(1 - e^{-r_m T})}, \quad \text{when } r_m \neq r_p, \quad (4)$$

122 and

$$V(t) = V_0 + V_0 \frac{1 - e^{-r_m t}}{1 - e^{-r_m T}}, \quad \text{when } r_m = r_p. \quad (5)$$

123 Expressions (4) and (5) imply that  $V(T) = 2V_0$ , i.e., that the  
 124 cell doubles its size during the cycle.

125 We consider a symmetric toggle switch, defined by  
 126 the continuous time Markov process involving eight ran-  
 127 dom variables: gene 1 and gene 2 states  $G_1(t)$ ,  $G_2(t) \in$   
 128  $\{0(\text{repressed}), 1(\text{active})\}$ , numbers of the mRNA 1 and mRNA 2  
 129 molecules  $M_1(t)$ ,  $M_2(t) \in \mathbb{N}$ , numbers of the protein monomer  
 130 1 and protein monomer 2 molecules  $P_1(t)$ ,  $P_2(t) \in \mathbb{N}$ , and  
 131 numbers of the protein dimer 1 and protein dimer 2 molecules  
 132  $D_1(t)$ ,  $D_2(t) \in \mathbb{N}$  (Fig. 1). Processes of gene activation,  
 133 repression, mRNA transcription, protein translation, dimer forma-  
 134 tion, and dissociation are explicitly included in the model.  
 135 Propensities of the second-order (bimolecular) reactions are  
 136 assumed inversely proportional to  $V(t)$ . We assume that the  
 137 nutrient level influences the synthesis of the two toggle proteins  
 138  $P_1$  and  $P_2$  in the same way as it affects the housekeeping protein  
 139 synthesis. We assume that the toggle mRNAs transcription

rate constants equal  $k_m$  and toggle proteins translation rate  
 constants equal  $k_p$ .

Here, we will assume that the gene replication takes  
 place just before division; the case in which gene replication  
 takes place in the middle of cell cycle is considered in the  
 Appendix A and leads to similar results. DNA replication

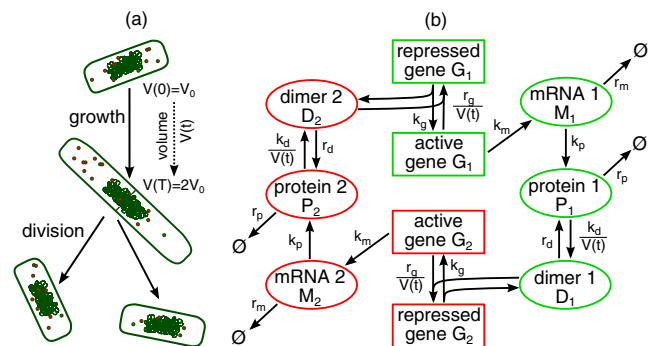


FIG. 1. (Color online) Schematic of the toggle switch model  
 in dividing cells. (a) Schematic of the cell growth and division.  
 (b) Schematic of the toggle switch system.

TABLE I. Reaction-rate constants.

Reaction	Symbol	Default value $V(t) = 1$ , $k_m = \bar{k}_m$ , $k_p = \bar{k}_p$	Parameter range for bacteria (vol. $1 \mu\text{m}^3$ )
Gene repression by protein dimer binding	$k_g/V(t)$	0.01	<sup>a</sup>
Gene activation by protein dimer unbinding	$r_g$	0.002	<sup>a</sup>
mRNA transcription from the active gene	$k_m$	0.005	$\leq 0.8[1/\text{s}]^{\text{b}}$
Protein translation	$k_p$	0.01	$\sim 10^{-2} \sim 10[1/\text{s}]^{\text{c}}$
Dimer formation	$k_d/V(t)$	0.0005	$1.6 \times 10^{-6} \sim 9.5 [1/\text{mlcl s}]^{\text{d}}$
Dimer dissociation to monomers	$r_d$	0.1	$5 \times 10^{-8} \sim 1.9 \times 10^3 [1/\text{s}]^{\text{e}}$
mRNA degradation	$r_m$	0.003	$10^{-2} \sim 6 \times 10^{-4} [1/\text{s}]^{\text{f}}$
Protein monomer degradation	$r_p$	0.00003	$\sim 1.4 \times 10^{-5} \sim 10^{-2} [1/\text{s}]^{\text{g}}$

<sup>a</sup>Gene switching is causing mRNA bursts observed at an *E. coli* promoter [33].

<sup>b</sup>For *E. coli* maximal transcription rate: 0.16–0.84/s [46].

<sup>c</sup>Translation initiation intervals are of the order of seconds, although they are specific for each mRNA [47]. *E. coli*: translation initiation rate may vary at least 1000-fold [48]; examples of translation initiation frequencies:  $\beta$ -galactosidase—0.31/s (spacing between ribosomes: 110 nucleotides), galactoside acetyltransferase—0.06/s (spacing between ribosomes: 580 nucleotides) [46]; maximal peptide chain elongation rate: 20 aa/s [49,50]; average peptide chain elongation rate: 12 aa/s [46].

<sup>d</sup>All cell types:  $9.8 \times 10^2/(\text{M s}) \sim 5.7 \times 10^9/(\text{M s})$  [51]; for  $1 \mu\text{m}^3$  volume (bacterial) cell:  $1.63 \times 10^{-6}/\text{mlcls} \sim 9.47/\text{mlcl s}$ .

<sup>e</sup>All cell types:  $5 \times 10^{-8}/\text{s} \sim 1.9 \times 10^3/\text{s}$  [51].

<sup>f</sup>The vast majority of mRNAs in a bacterial cell are very unstable, having a half-life of about 3 min (decay rate  $3 \times 10^{-3}/\text{s}$ )—bacterial mRNAs are both rapidly synthesized and rapidly degraded [52]. *E. coli*: mRNA half-lives span between 1 and 18 min (decay rates  $10^{-2}/\text{s} \sim 6 \times 10^{-4}/\text{s}$ ) [30].

<sup>g</sup>Most of the bacterial proteins are very stable, with degradation rates:  $1.4 \times 10^{-5} \sim 5.6 \times 10^{-5}/\text{s}$  [25]. Some proteins have much higher degradation rates. *E. coli* RNase R has a degradation rate of  $10^{-3}/\text{s}$  (in exponential phase) [53]; factor  $\sigma^{32}$  has a degradation rate of  $10^{-2}/\text{s}$  (in steady-state growth phase) [54].

146 requires that the two DNA strands separate and become acces-  
 147 sible to DNA polymerase, and therefore leads to dissociation of  
 148 DNA-bound proteins near the replication forks. Accordingly,  
 149 we assume that repressor molecules dissociate from DNA  
 150 leading to gene activation. However, when the repressor level  
 151 is high the gene may become repressed almost immediately  
 152 after the replication fork passes that gene. The mRNA, protein  
 153 monomer, and protein dimer molecules are distributed between  
 154 daughter cells in one of two ways: (1) following the binomial  
 155 distribution with parameter 0.5 so that each molecule has equal  
 156 probability to enter each of the daughter cells, or (2) almost  
 157 evenly such that the daughter cells both receive half of the  
 158 molecules of a given type, or half  $\pm 1/2$  when the half is not  
 159 an integer.

160 The transition propensities, assumed equal for both genes,  
 161 are

$$\begin{aligned}
 G_i = 0 &\rightarrow G_i = 1, & k_g(1 - G_i), \\
 G_i = 1 &\rightarrow G_i = 0, & r_g d_{3-i} G_i / V(t), \\
 M_i = m_i &\rightarrow M_i = m_i + 1, & k_m G_i, \\
 M_i = m_i &\rightarrow M_i = m_i - 1, & r_m m_i, \\
 P_i = p_i &\rightarrow P_i = p_i + 1, & k_p m_i, \\
 P_i = p_i &\rightarrow P_i = p_i - 1, & r_p p_i, \\
 D_i = d_i &\rightarrow D_i = d_i + 1, & k_d p_i (p_i - 1) / V(t), \\
 D_i = d_i &\rightarrow D_i = d_i - 1, & r_d d_i,
 \end{aligned} \tag{6}$$

162 for  $i = 1, 2$ .

The assumed reaction-rate constants are listed in Table I. 163  
 The stochastic trajectories and the central moments of protein 164  
 distributions were obtained using the Gillespie algorithm [39]. 165  
 In the deterministic approximation the state of the system is 166  
 described by eight continuous variables: gene activities  $g_1, g_2$  167  
 $\in [0, 1]$ , levels of mRNAs, proteins, and protein dimers  $m_1, m_2,$  168  
 $p_1, p_2, d_1, d_2$ . Dynamics of the system between cell divisions 169  
 follows the ODE system: 170

$$\frac{dg_i}{dt} = k_g(1 - g_i) - \frac{r_g}{V(t)} d_j g_i, \tag{7}$$

$$\frac{dm_i}{dt} = k_m g_i - r_m m_i, \tag{8}$$

$$\frac{dp_i}{dt} = k_p m_i - r_p p_i + 2r_d d_i - 2\frac{k_d}{V(t)} p_i^2, \tag{9}$$

$$\frac{dd_i}{dt} = \frac{k_d}{V(t)} p_i^2 - r_d d_i, \tag{10}$$

where  $i = 1, 2$  and  $j = 3 - i$ . 171

The deterministic approximation is accurate only when the 172  
 characteristic numbers of molecules are large enough to be 173  
 replaced by the continuous concentrations. For bacteria this 174  
 condition is never satisfied, and thus deterministic kinetics 175  
 equations may serve only as a reference for the stochastic 176  
 simulations; see Fig. 2. Here, the deterministic analysis is 177  
 applied to define the two attracting trajectories of the system. In 178  
 nondividing cells these trajectories are replaced by two stable 179  
 steady states, in which either one or the other gene dominates. 180  
 As the system is bistable, all deterministic trajectories, except 181

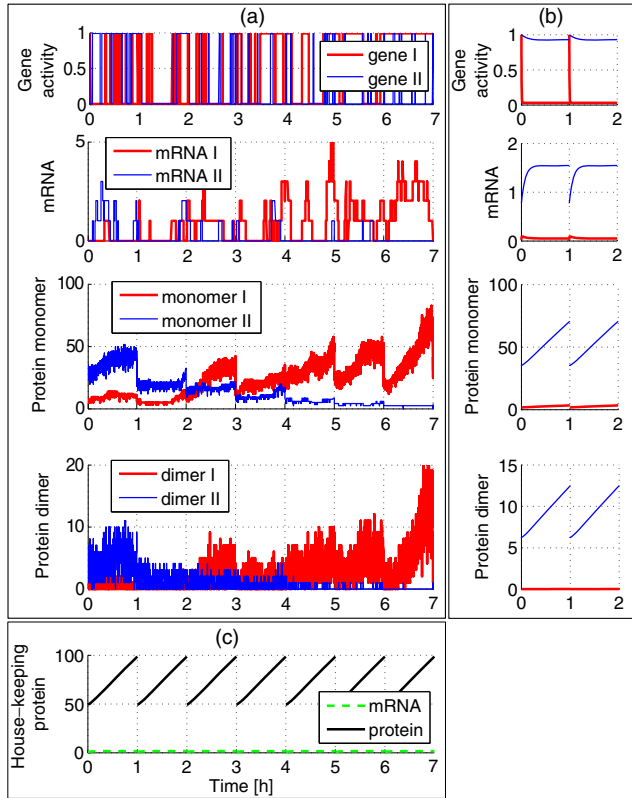


FIG. 2. (Color online) Stochastic (a) and deterministic (b) trajectories of the toggle switch components in dividing cells ( $T = 1$  h, binomial distribution of molecules between daughter cells). (c) Deterministic trajectory of the housekeeping protein level controlling cell volume  $V(t)$  and divisions.

the separatrix, converge to one of the attracting trajectories; see Fig. 2.

Let  $p_A$  and  $p_I$  denote protein levels for dominating and dominated gene at the end of the cell cycle, and let  $d_A$  and  $d_I$  denote corresponding protein dimer levels. Values  $p_A(T)$  and  $d_A(T)$  increase with  $T$ , while  $p_I(T)$  and  $d_I(T)$  decrease with  $T$  and for  $T = 1$  h are  $p_A = 70.7$ ,  $p_I = 3.4$ ,  $d_A = 12.5$ , and  $d_I = 0.0$ , while for  $T = 10$  h are  $p_A = 83.3$ ,  $p_I = 2.3$ ,  $d_A = 17.3$ , and  $d_I = 0.0$ .

### III. RESULTS

We considered two cases: (I) the transcription rate is constant and the faster protein accumulation and cell growth results from an increase of the translation rate; (II) vice versa, the transcription rate is constant and the translation rate increases. In both cases lengthening of the cell cycle leads to an increase of the mean first passage times (MFPT) between the attracting trajectories. Experimental data suggest that lengthening of the cell cycle is associated with reduced transcription and/or translation rates [28,29].

In case (I), when the transcription rate is kept constant, we found that the MFPT is a sharply increasing function of  $T$ , increasing about four orders of magnitude as  $T$  increases from 1 h to 60 h; see Fig. 3(a). Moreover, the nondividing and nongrowing cells of constant volume  $2V_0$  (the volume of

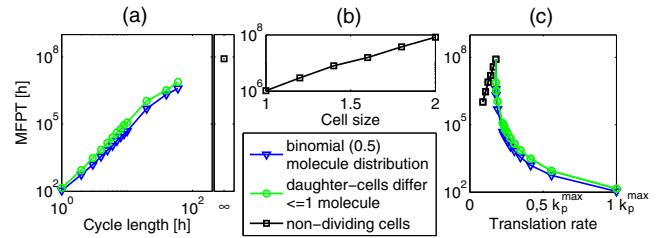


FIG. 3. (Color online) MFPT for the model with the varying protein burst size, case (I). Two types of molecule distributions between sister cells are considered: the most equal (equal in the case of even molecule number; in the uneven case, the one molecule is distributed with probability 0.5 to one of the cells), and binomial with equal probability. The MFPT as function of the cell-cycle length  $T$  (a), maximum cell volume in nondividing cells (b), and translation rate (c). For small translation rate cells do not reach volume  $2V_0$  and may not divide.

dividing cell just prior to division) have the MFPT six orders of magnitude longer than cells dividing every 1 h; see Fig. 3(a). Cells of constant volume  $V_0$  ( $V_0/3$ ) have the MFPT four (two) orders of magnitude longer than cells dividing every 1 h; see Fig. 3(b). An increase of the cell volume in nondividing cells (in which the translation rate is too small to reach the division size  $2V_0$ ) results in an increase of the MFPT by about two orders of magnitude, as  $V(t)$  increases from  $V_0$  to  $2V_0$ ; see Fig. 3(b). As a result, the dependence of the MFPT on the translation rate is a nonmonotonous function; see Fig. 3(c). It increases for small translation rates (for which cells are not able to reach the division volume  $2V_0$ ), and then for dividing cells it rapidly decreases, when an increase of the translation rate shortens  $T$ .

In case (II), when the translation rate is kept constant, the MFPT is also an increasing function of  $T$ ; however, it increases about two orders of magnitude [not four as in case (I)] as  $T$  increases from 1 h to 60 h; see Fig. 4(a). The nondividing and nongrowing cells of constant volume equal  $2V_0$  ( $V_0$ ) have the MFPT about 300 (30) times longer than cells dividing every 1 h; see Fig. 4(a). An increase of cell volume in nondividing cells results in approximately 10-fold increase of the MFPT, as  $V(t)$  increases from  $V_0$  to  $2V_0$ ; see Fig. 4(b). As a result, similar to case (I), the dependence of the MFPT on the translation rate is a nonmonotonous function; see Fig. 4(c).

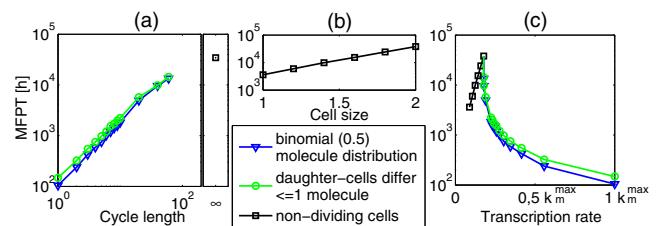


FIG. 4. (Color online) MFPT for the model with constant protein burst size, case (II). The MFPT as a function of the cell-cycle length  $T$  (a), maximum cell volume in nondividing cells (b), and transcription rate (c). For small transcription rate cells do not reach volume  $2V_0$  and may not divide.

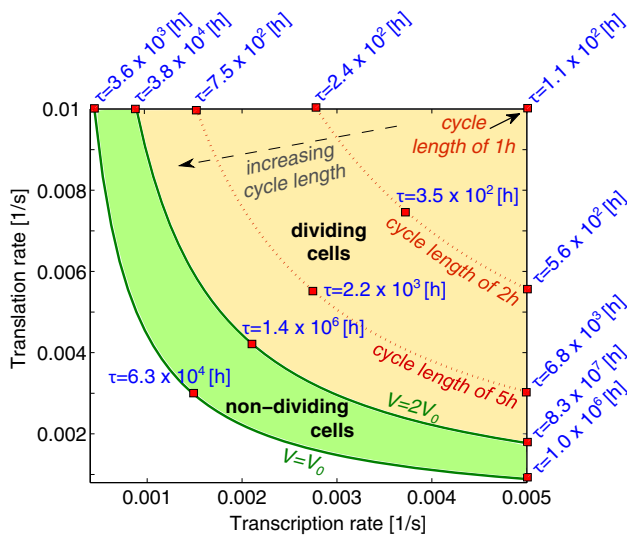


FIG. 5. (Color online) MFPT  $\tau$  for a varying transcription rate and/or varying translation rate. Cells having small product of transcription and translation rates do not divide and have size between  $V_0$  and  $2V_0$ .

231 Interestingly, although the asymmetry in the distribution  
 232 of molecules leads to shortening of the MFPT, the effect  
 233 is relatively modest. The ratio of the MFPT when molecule  
 234 distribution between daughter cells is most symmetric to the  
 235 MFPT when it is binomial with equal probabilities is less than  
 236 2; see Figs. 3 and 4. Assuming that daughter cells are unequal  
 237 in volume (following a truncated normal distribution with 10%  
 238 coefficient of variation), which implies unequal probabilities  
 239 in binomial distributions, we obtained only slightly shorter  
 240 MFPTs (result not shown).

241 Dependence of the MFPT on transcription and translation  
 242 rates for dividing and nondividing cells is summarized in  
 243 Fig. 5. The effects observed in simulations can be ex-  
 244 plained as follows. There are two main factors controlling  
 245 toggling rates [20]: the mean protein number ( $M$ ) for the  
 246 dominating gene [roughly proportional to  $V(t)$ ] and the  
 247 magnitude of noise, which can be measured by the Fano factor  
 248 ( $FF = \text{variance}/\text{mean}$ ), with contributions from the higher  
 249 moments of the protein distribution in the vicinity of the  
 250 attracting trajectories. The MFPT was reported to increase  
 251 exponentially with  $M$  [and therefore  $V(t)$ ] [20], and this  
 252 dependence is seen here for nondividing cells; see Figs. 3(b)  
 253 and 4(b). Lengthening of the cell cycle is associated with  
 254 either decrease of the protein burst size  $b = k_p/r_m$  (the  
 255 average number of proteins synthesized from a single mRNA  
 256 molecule) in case (I), or with a decrease of the mRNA burst  
 257 size (the average number of mRNA molecules synthesized  
 258 during the time when the gene is turned on) in case (II).  
 259 In the considered case a decrease of the protein burst size  
 260 has a dominant effect on noise as  $FF \approx b + 1$  [40,41], and,  
 261 as a result, on the toggling rates. As shown in Fig. 5, cells  
 262 having a small translation rate and a correspondingly larger  
 263 transcription rate (and therefore the same size or the same  $T$ )  
 264 have longer MFPTs. An increase of  $T$  [case (I)] associated  
 265 with a decrease of  $b$  leads therefore to a dramatic increase  
 266 of the MFPT. Moreover, prior to division, cells with longer

267  $T$  have a higher number of proteins associated with the  
 268 dominating gene and a lower number of proteins associated  
 269 with the dominated gene, which implies a wider separation  
 270 of the attracting trajectories. These two effects add to the  
 271 MFPT elongation with increasing  $T$ , and become dominant  
 272 in case (II), when the elongation of the MFPT (due to the  
 273 elongation of  $T$ ) is much smaller than in case (I); see Fig. 3(a)  
 274 versus Fig. 4(a). In case (II), an increase of the MFPT is also  
 275 partially attributed to the increase of the mRNA burst size; see  
 276 Appendix B, Fig. 10.

277 In Appendix B we analyze numerically the expression of a  
 278 single gene in dividing cells. We demonstrate that the standard  
 279 deviation, as well as the third and fourth central moments  
 280 of the protein distribution, decrease with  $T$ . The decrease is  
 281 substantial (at least twofold, as  $T$  changes from 1 to 10 h) in  
 282 case (I), i.e., with a varied protein burst size, Figs. 8 and 9,  
 283 or relatively modest (smaller than 25%) in case (II), when  
 284 the transcription rate varies and protein burst size remains  
 285 constant; see Figs. 10 and 11.

286 Finally, we analyze the dynamics of toggle switching  
 287 process for various  $T$ . As shown in Fig. 6, for  $T \leq 10$   
 288 h the transition between the two attracting trajectories is  
 289 accomplished in four cell cycles (on average). Only in the  
 290 case of a very long cell-cycle length ( $T = 60$  h), the transition  
 291 is accomplished within the single cell cycle. This effect can  
 292 be explained as follows. When the cell-cycle length is equal  
 293 to or shorter than about 10 h (the average protein lifetime)  
 294 the protein level decreases mostly due to dilution. In such a  
 295 case after four cell divisions (assuming zero or a very low  
 296 protein production) the dominating gene protein level may  
 297 decrease as much as  $2^4 = 16$  times and become comparable  
 298 with the repressed gene protein level enabling state transition.  
 299 Furthermore, the probability that no protein is produced  
 300 during cell cycle (or a given number of cell cycles) decreases  
 301 exponentially with  $T$ , which intuitively explains why, in the  
 302 case when the protein degradation may be neglected, the MFPT  
 303 increases exponentially with the cell-cycle length  $T$  [42]. In  
 304 nondividing (or very slowly dividing) cells, the protein level  
 305 decreases (mainly) due to degradation and therefore the above  
 306 reasoning is no longer valid, and, as demonstrated, the MFPT  
 307 is controlled by cell size.

#### IV. CONCLUSIONS

308 The genetic toggle switch was analyzed theoretically before  
 309 by several groups, who did not account for the cell cycle.  
 310 It was found that the lifetimes of toggle states can be very  
 311 long. Our analysis demonstrates, however, that the stability of  
 312 the toggle switch dramatically decreases in dividing and fast  
 313 growing bacteria. Such an effect was experimentally observed  
 314 in the  $\lambda$  phage toggle switch system in a mutant,  $\lambda prm240$ , in  
 315 which the promoter controlling expression of repressor CI is  
 316 weakened, rendering lysogens unstable [43]. Lysogens grown  
 317 in minimal medium are stable but switch at high rates when  
 318 grown in reach medium. For wild type cells, the spontaneous  
 319 switching rate was almost undetectable, estimated to be equal  
 320 to  $10^{-8}$ /generation.  
 321

322 Shortening of the cell cycle results from an increase of  
 323 the translation or transcription rates or both. In the first case  
 324 (increase of translation) the MFPT was found to be almost six

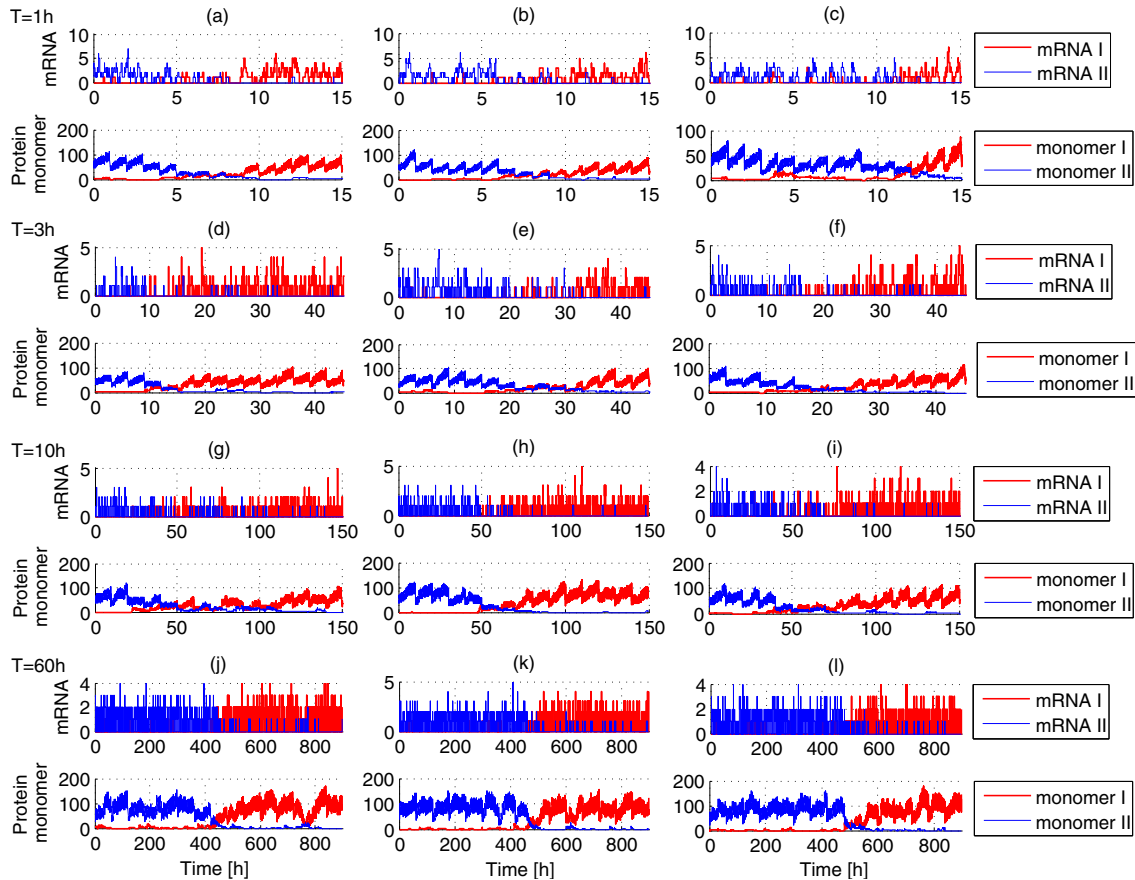


FIG. 6. (Color online) Stochastic trajectories of the toggle switch mRNA and protein monomer numbers in dividing cells with binomial distribution of molecules between daughter cells and (a)–(c) the cell-cycle length  $T = 1$  h, (d)–(f) the cell-cycle length  $T = 3$  h, (g)–(i) the cell-cycle length  $T = 10$  h, and (j)–(l) the cell-cycle length  $T = 60$  h.

orders of magnitude shorter for rapidly dividing cells ( $T = 1$  h) than for cells with suppressed growth and divisions. We should notice that in these two cases toggle state-to-state transitions are essentially different processes. Nondividing cells remain for most of the time in the tiny vicinity of one of two steady states and the toggling requires transition between these states. In rapidly dividing cells, the system is very far from the equilibrium, i.e., the protein numbers are growing throughout the whole cycle and never approach the vicinity of the steady state. In such a case toggling implies transitions between the two attracting trajectories.

When state-to-state transition is accomplished within one cell cycle (which is the case when the cell cycle is very long) the states of daughter cells remain with large probability the same. However, when cell-cycle length is shorter than the protein degradation time, state-to-state transition requires about four cycles to be accomplished, which allows cells emerging in these four generations to follow divergent trajectories, and may introduce heterogeneity to cell population.

Cell fate and fitness strongly depend on bi- and multi-stable regulatory elements controlling various aspects of cell behavior. The strong dependence of the MFPT on growth rate has important regulatory consequences. In the case when one state of the toggle is associated with a slow or inhibited growth it automatically becomes much more

stable than the opposite state (associated with faster growth). The observation that fast growth dramatically shortens the MFPT and destabilizes the corresponding toggle state suggests that rapidly growing cells vigorously explore the epigenetic landscape enabling nongenetic evolution [1], while cells with slow or inhibited growth adhere to the local optima. From a population perspective this may be an evolutionary optimal strategy. It is known that bacteria and other simple organisms have epigenetic forms, characterized by slower or inhibited growth but higher resistance to environmental stress such as antibiotics treatment, or lack of nutrients [44]. The fraction of cells in the persistent state is determined by state-to-state switching rates as well as growth rates in the persistent and normal states [45]. At favorable conditions the high transition rate from the state of fast growth to the persistent state allow for replenishing the persistent cell population (which tends to be less abundant due to slow or inhibited growth). Simultaneously, the small transition rate from the persistent to normal state enables the persistent cell subpopulation to survive long periods of unfavorable conditions.

#### ACKNOWLEDGMENTS

J.J. and T.L. were supported by the Foundation for Polish Science Grant TEAM/2009-3/6 and National Science Center

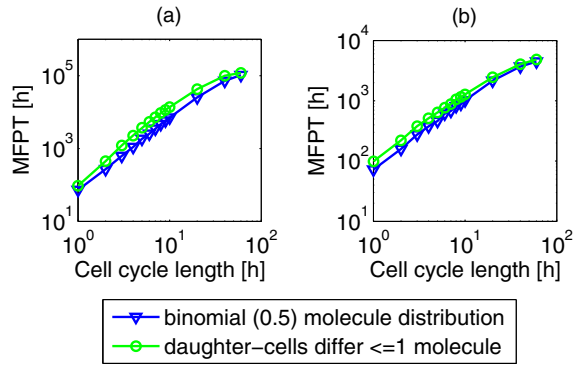


FIG. 7. (Color online) MFPT as a function of the cell-cycle length  $T$  for the model with gene replication in  $t = 0.5T$ . The MFPT for the model with varying protein burst size, case (I) (a), and constant protein burst size, case (II) (b).

373 (Poland) Grant No. 2011/03/B/NZ2/00281. M.K. was partly  
 374 supported by the National Science Center (Poland) Grant No.  
 375 2012/04/A/ST7/00353. This research was supported in part by  
 376 PL-Grid Infrastructure. Numerical simulations were carried  
 377 out at the Zeus computer cluster at the ACK Cyfronet AGH  
 378 in Cracow, Poland, and at the Grafen computer cluster at the  
 379 Institute of Fundamental Technological Research in Warsaw,  
 380 Poland.

#### APPENDIX A: GENE REPLICATION IN THE MIDDLE OF THE CYCLE

381  
 382  
 383 Here, we confirm that the MFPT increases with the cell-  
 384 cycle length  $T$  also when the toggle genes replicate not just  
 385 before division but earlier during the cell cycle. Namely, we  
 386 assume that DNA replication takes place in the middle of  
 387 the cell cycle, i.e., at  $t = 0.5T$ . To shorten the numerical  
 388 simulation time, we assume two times smaller translation rate  
 389 than in the previous case. As already discussed, the translation  
 390 rate controls the number of protein molecules and therefore  
 391 toggling rates, which become very long (hard to determine  
 392 in numerical simulations), when an increase of gene copy  
 393 number is not compensated by a decrease of translation (or  
 394 transcription rate). In this model variant in the deterministic  
 395 approximation the protein monomer and protein dimer levels  
 396 just before division are  $p_A = 53.7$ ,  $p_I = 4.4$ ,  $d_A = 7.2$ , and  
 397  $d_I = 0.0$  (for  $T = 1$  h), and  $p_A = 65.8$ ,  $p_I = 3.5$ ,  $d_A = 10.8$ ,  
 398 and  $d_I = 0.0$  (for  $T = 10$  h).

399 In case (I) (constant transcription rate), we found that the  
 400 MFPT is a sharply increasing function of  $T$ , increasing more  
 401 than three orders of magnitude as  $T$  increases from 1 h to 60 h;  
 402 see Fig. 7(a). In case (II) (constant translation rate), the MFPT  
 403 increases about 50-fold as  $T$  increases from 1 h to 60 h; see  
 404 Fig. 7(b). The obtained results confirmed that, also for gene  
 405 replication in the middle of the cell cycle, a decrease in growth  
 406 rate stabilizes the state of the system; see Fig. 7.

#### APPENDIX B: SINGLE GENE MODEL WITHOUT AUTOREGULATION IN DIVIDING CELLS

407  
 408  
 409 Toggling rates increase with an increasing width of the  
 410 protein distribution in the vicinity of each of the attracting

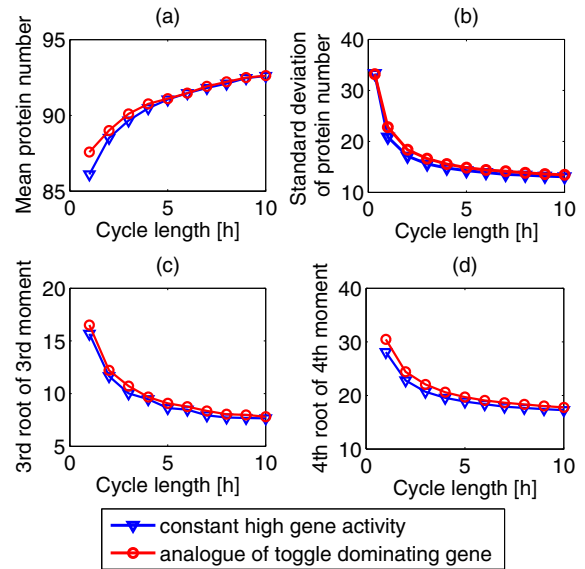


FIG. 8. (Color online) Varied protein burst size [case (I)], analog of the dominating gene. Central moments of the protein distribution just before division. Simulations were performed assuming a binomial molecule distribution, for two cases of gene expression regulation: (1) constant gene activity (blue triangles) and (2) gene switching with rates equal to switching rates of the dominating gene in the toggle (red circles).

411 trajectories. Here, we investigate how the first four central  
 412 moments of the protein distribution depend on the cell-cycle  
 413 length  $T$ . Since we are interested in the width of the protein  
 414 distribution in the basins of the attracting trajectories (not the  
 415 width of the whole protein distribution, which is controlled  
 416 mainly by the separation of the attracting trajectories), we  
 417 consider an expression of a single gene without autoregulation,  
 418 instead of the toggle switch.

419 We analyze two models (defining continuous time Markov  
 420 processes), with and without gene switching. In each model  
 421 two sets of parameters corresponding to the dominating  
 422 (Figs. 8 and 10) or dominated (Figs. 9 and 11) gene in the  
 423 toggle are considered.

424 In the model without gene switching the state of the system  
 425 is described by the two random variables: the number of mRNA  
 426 molecules  $M(t) \in \mathbb{N}$  and number of protein molecules  $P(t) \in \mathbb{N}$ .

427 The transition propensities are as follows:  
 428

$$\begin{aligned}
 M = m &\rightarrow M = m + 1, & k_m k_g / (k_g + r_g d_T), \\
 M = m &\rightarrow M = m - 1, & r_m m, \\
 P = p &\rightarrow P = p + 1, & k_p m, \\
 P = p &\rightarrow P = p - 1, & r_p p.
 \end{aligned}
 \tag{B1}$$

429 We assume  $d_T = d_A$  or  $d_T = d_I$ , where  $d_A$  and  $d_I$  are the mean  
 430 protein dimer numbers just before division, for dominating and  
 431 dominated gene, respectively, in the toggle switch model for  
 432 cells with the cycle length of  $T$ . Therefore, the gene activity  
 433  $k_g / (k_g + r_g d_T)$  is equal to the probability that the toggle gene  
 434 (dominating or dominated) is active. All other parameters are  
 435 the same as in the toggle switch model; see Table I. As a

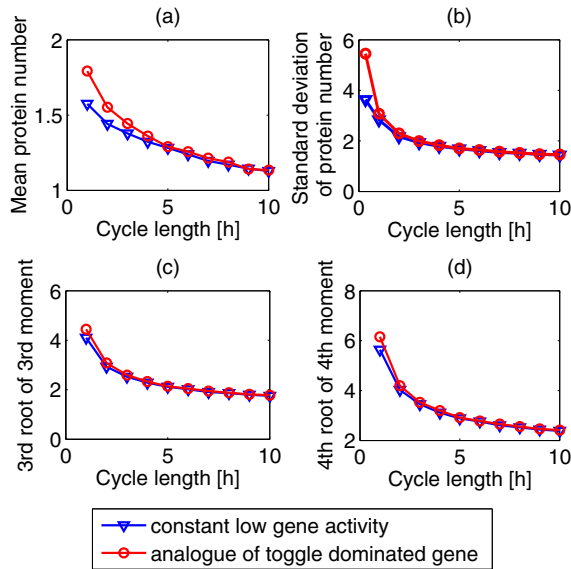


FIG. 9. (Color online) Varied protein burst size [case (I)], analog of the dominated gene. Central moments of the protein distribution just before division. Simulations were performed assuming a binomial molecule distribution, for two cases of gene expression regulation: (1) constant gene activity (blue triangles) and (2) gene switching with rates equal to switching rates of the dominated gene in the toggle (red circles).

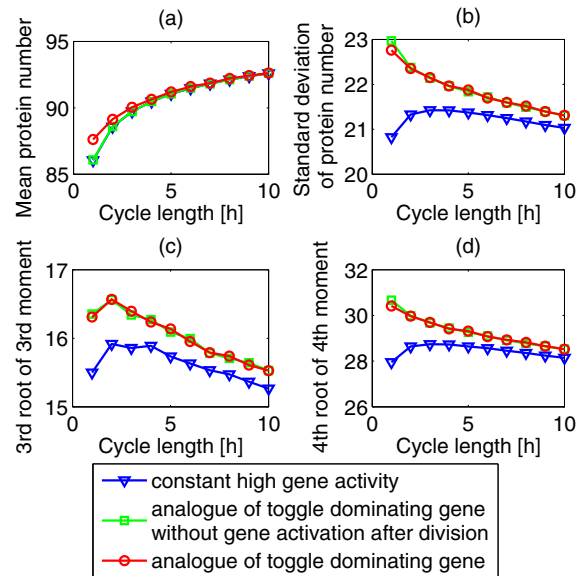


FIG. 10. (Color online) Constant protein burst size [case (II)], analog of the dominating gene. Central moments of the protein distribution just before division. Simulations were performed assuming a binomial molecule distribution, for three cases of gene expression regulation: (1) constant gene activity (blue triangles), (2) gene switching with rates equal to switching rates of the dominating gene in the toggle without gene activation after each division (green squares), and (3) gene switching with rates equal to switching rates of the dominating gene in the toggle (with gene activation after each division) (red circles).

436 result, analogous to the toggle switch system (see main text),  
 437 the mean protein number before division increases with  $T$  for  
 438 the dominating gene (Figs. 8 and 10), and decreases for the  
 439 dominated gene (Figs. 9 and 11).

440 In the model with gene switching, there is an additional  
 441 random variable, representing the gene state, either active  
 442 ( $G = 1$ ) or inactive ( $G = 0$ ). In this model the transition  
 443 propensities are

$$\begin{aligned}
 G = 0 &\rightarrow G = 1, & k_g(1 - G), \\
 G = 1 &\rightarrow G = 0, & r_g G d_T, \\
 M = m &\rightarrow M = m + 1, & G k_m, \\
 M = m &\rightarrow M = m - 1, & r_m m, \\
 P = p &\rightarrow P = p + 1, & k_p m, \\
 P = p &\rightarrow P = p - 1, & r_p p.
 \end{aligned}
 \tag{B2}$$

444 We assume  $d_T = d_A$  or  $d_T = d_I$ , where  $d_A$  or  $d_I$  are the mean  
 445 protein dimer numbers for dominating and dominated gene,  
 446 respectively, in the toggle switch model in cells with the cycle  
 447 length of  $T$ . This assumption implies that the gene is switched  
 448 on and off with the same rates as either the dominating and  
 449 dominated gene in the toggle. Analogous to the toggle switch  
 450 model we will assume that the gene is activated at the division  
 451 (due to the repressor release during the DNA replication). To  
 452 determine the influence of this assumption, we also considered  
 453 the model variant in which the assumption is released; see  
 454 Figs. 10 and 11.

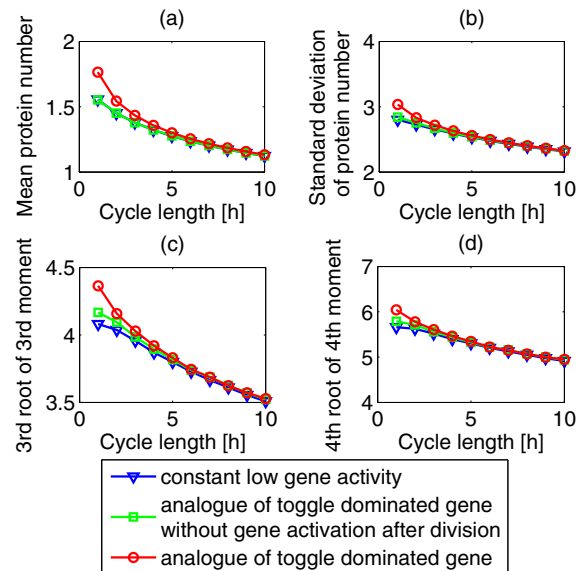


FIG. 11. (Color online) Constant protein burst size [case (II)], analog of the dominated gene. Central moments of the protein distribution just before division. Simulations were performed assuming a binomial molecule distribution, for three cases of gene expression regulation: (1) constant gene activity (blue triangles), (2) gene switching with rates equal to switching rates of the dominated gene in the toggle without gene activation after each division (green squares), and (3) gene switching with rates equal to switching rates of the dominated gene in the toggle (with gene activation after each division) (red circles).

### 1. Estimation of central moments of the protein distribution

We analyze the following two cases introduced in the main paper.

Case (I), in which an increase of  $T$  results from decreases in translation rate (decreasing protein burst size); see Figs. 8 and 9.

Case (II), in which an increase of  $T$  results from decreases in transcription rate; see Figs. 10 and 11.

In each case by means of long run multiprocessor simulations we estimate the probability distribution of the protein number at the time of division, and calculate the mean, second, third, and fourth central moments. For each set of parameters we use trajectories having at least  $10^5$  divisions for Figs. 8 and 9, or  $10^7$  for Figs. 10 and 11.

#### a. Case (I): Varied protein burst size

In case (I) the decrease of protein burst size is responsible for a significant decrease of second, third, and fourth central moments of the protein number; see Figs. 8 and 9. This effect was observed and explained previously for nondividing cells, for which the Fano factor of the protein number distribution is proportional to  $b + 1$ , where  $b$  is the protein burst size (protein translation rate divided by mRNA degradation rate) [41]. The similar dependence was obtained many years ago by Otto Berg who calculated the protein number probability distribution in dividing bacteria [40]. In the model with the constant gene activity, there is no contribution from the gene switching noise, and therefore all central moments are smaller than in the model accounting for the gene switching. However, the noise contribution from the gene switching is much smaller than that of the increasing protein burst size.

#### b. Case (II): Constant protein burst size

In case (II) the size of the protein level fluctuations for the gene corresponding to the dominating gene in the toggle changes with  $T$  mostly due to the varying average size of mRNA bursts emerging in periods of gene activity (Fig. 10).

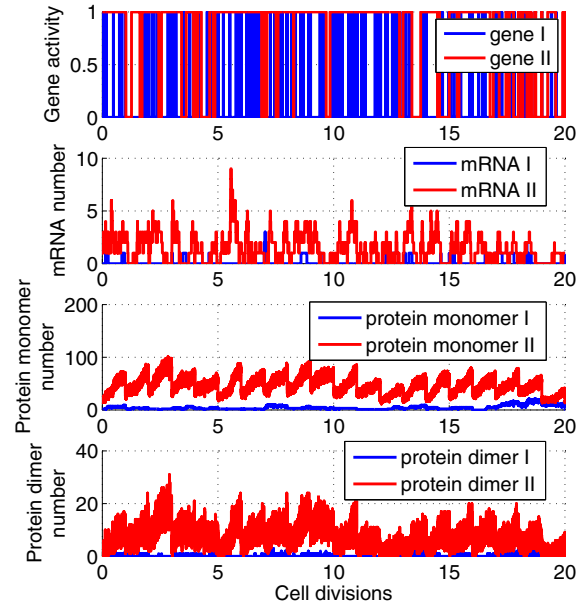


FIG. 12. (Color online) Stochastic trajectory of the toggle switch components in dividing cells. Cell-cycle length  $T = 1$  h, binomial distribution of molecules between daughter cells.

This is evident when models with and without gene switching are compared. However, in the case when the analog of the dominated gene is considered the effect of varying size of mRNA bursts is small because the transcription rate is small and the probability that more than one mRNA molecule is synthesized is relatively low. Only for a short cell cycle,  $T = 1$  h, can several mRNA molecules be synthesized in short periods of activity of the dominated gene, see Fig. 12, and correspondingly, for a short cell cycle the difference between models with and without gene switching is more pronounced. However, for the analog of the dominated gene the central moments decrease with cell-cycle lengthening simply because the mean protein level decreases.

- [1] S. Huang, *BioEssays* **34**, 149 (2012).
- [2] J. E. Ferrell, Jr., *Curr. Opin. Cell Biol.* **14**, 140 (2002).
- [3] T. Tian and K. Burrage, *Proc. Natl. Acad. Sci. U.S.A.* **103**, 8372 (2006).
- [4] A. Lipshtat, A. Loinger, N. Q. Balaban, and O. Biham, *Phys. Rev. Lett.* **96**, 188101 (2006).
- [5] A. Chatterjee, Y. N. Kaznessis, and W.-S. Hu, *Curr. Opin. Biotech.* **19**, 475 (2008).
- [6] R. B. Hoyle, D. Avitabile, and A. M. Kierzek, *PLoS Comput. Biol.* **8**, e1002396 (2012).
- [7] E. Kussell and S. Leibler, *Science* **309**, 2075 (2005).
- [8] M. Ptashne, *A Genetic Switch: Phage  $\lambda$  and Higher Organisms* (Cell Press and Blackwell Scientific Publications, Cambridge, MA, 1992).
- [9] A. Arkin, J. Ross, and H. H. McAdams, *Genetics* **149**, 1633 (1998).
- [10] T. Tian and K. Burrage, *J. Theor. Biol.* **227**, 229 (2004).
- [11] P. Laslo, C. J. Spooner, A. Warmflash, D. W. Lancki, H.-J. Lee, R. Sciammas, B. N. Gantner, A. R. Dinner, and H. Singh, *Cell* **126**, 755 (2006).
- [12] J. E. Ferrell and E. M. Machleder, *Science* **280**, 895 (1998).
- [13] U. S. Bhalla, P. T. Ram, and R. Iyengar, *Science* **297**, 1018 (2002).
- [14] C. P. Bagowski and J. E. Ferrell, Jr., *Curr. Biol.* **11**, 1176 (2001).
- [15] J. R. Pomeroy, E. D. Sontag, and J. E. Ferrell, *Nat. Cell Biol.* **5**, 346 (2003).
- [16] F. R. Cross, V. Archambault, M. Miller, and M. Klovstad, *Mol. Biol. Cell* **13**, 52 (2002).
- [17] T. S. Gardner, C. R. Cantor, and J. J. Collins, *Nature (London)* **403**, 339 (2000).
- [18] A. S. Ribeiro, *Phys. Rev. E* **78**, 061902 (2008).
- [19] P. B. Warren and P. R. ten Wolde, *Phys. Rev. Lett.* **92**, 128101 (2004).

- [20] P. B. Warren and P. R. ten Wolde, *J. Phys. Chem. B* **109**, 6812 (2005).
- [21] M. Komorowski, J. Miekisz, and A. M. Kierzek, *Biophys. J.* **96**, 372 (2009).
- [22] X. Dai, O. Yli-Harja, and A. S. Ribeiro, *Bioinformatics* **25**, 2362 (2009).
- [23] J. Jaruszewicz and T. Lipniacki, *Phys. Biol.* **10**, 035007 (2013).
- [24] J. Jaruszewicz, P. J. Zuk, and T. Lipniacki, *J. Theor. Biol.* **317**, 140 (2013).
- [25] K. P. Jayapal, S. Sui, R. J. Philp, Y.-J. Kok, M. G. Yap, T. J. Griffin, and W.-S. Hu, *J. Proteome Res.* **9**, 2087 (2010).
- [26] S. Cooper and C. E. Helmstetter, *J. Mol. Biol.* **31**, 519 (1968).
- [27] M. Scott, C. W. Gunderson, E. M. Mateescu, Z. Zhang, and T. Hwa, *Science* **330**, 1099 (2010).
- [28] S. T. Liang, Y. C. Xu, P. Dennis, and H. Bremer, *J. Bacteriol.* **182**, 3037 (2000).
- [29] H. Bremer and P. P. Dennis, *Escherichia Coli and Salmonella* (ASM Press, Washington, DC, 1996), pp. 1553–1569, chap.
- [30] J. A. Bernstein, A. B. Khodursky, P.-H. Lin, S. Lin-Chao, and S. N. Cohen, *Proc. Natl. Acad. Sci. U.S.A.* **99**, 9697 (2002).
- [31] O. Michelsen, M. J. T. de Mattos, P. R. Jensen, and F. G. Hansen, *Microbiology* **149**, 1001 (2003).
- [32] M. Bipatnath, P. P. Dennis, and H. Bremer, *J. Bacteriol.* **180**, 265 (1998).
- [33] I. Golding, J. Paulsson, S. M. Zawilski, and E. C. Cox, *Cell* **123**, 1025 (2005).
- [34] M. G. Sargent, *J. Bacteriol.* **123**, 7 (1975).
- [35] M. Osella and M. C. Lagomarsino, *Phys. Rev. E* **87**, 012726 (2013).
- [36] J. Tamames, G. Casari, C. Ouzounis, and A. Valencia, *J. Mol. Evol.* **44**, 66 (1997).
- [37] J. Tamames, *Genome Biol.* **2**, 0020 (2001).
- [38] I. M. Keseler, A. Mackie, M. Peralta-Gil, A. Santos-Zavaleta, S. Gama-Castro, C. Bonavides-Martínez, C. Fulcher, A. M. Huerta, A. Kothari, M. Krummenacker, M. Latendresse, L. Muñiz Rascado, Q. Ong, S. Paley, I. Schröder, A. G. Shearer, P. Subhraveti, M. Travers, D. Weerasinghe, V. Weiss, J. Collado-Vides, R. P. Gunsalus, I. Paulsen, and P. D. Karp, *Nucleic Acids Res.* **41**, D605 (2013).
- [39] D. T. Gillespie, *J. Phys. Chem.* **81**, 2340 (1977).
- [40] O. G. Berg, *J. Theor. Biol.* **71**, 587 (1978).
- [41] M. Thattai and A. Van Oudenaarden, *Proc. Natl. Acad. Sci. U.S.A.* **98**, 8614 (2001).
- [42] C. Zong, L.-h. So, L. A. Seplveda, S. O. Skinner, and I. Golding, *Mol. Syst. Biol.* **6**, 440 (2010).
- [43] J. W. Little and C. B. Michalowski, *J. Bacteriol.* **192**, 6064 (2010).
- [44] N. Q. Balaban, J. Merrin, R. Chait, L. Kowalik, and S. Leibler, *Science* **305**, 1622 (2004).
- [45] D. Nevozhay, R. M. Adams, E. Van Itallie, M. R. Bennett, and G. Balázsi, *PLoS Comput. Biol.* **8**, e1002480 (2012).
- [46] D. Kennell and H. Riezman, *J. Mol. Biol.* **114**, 1 (1977).
- [47] B. S. Laursen, H. P. Sørensen, K. K. Mortensen, and H. U. Sperling-Petersen, *Microbiol. Mol. Biol. Rev.* **69**, 101 (2005).
- [48] L. L. Sampson, R. W. Hendrix, W. M. Huang, and S. R. Casjens, *Proc. Natl. Acad. Sci. U.S.A.* **85**, 5439 (1988).
- [49] R. Young and H. Bremer, *Biochem. J.* **160**, 185 (1976).
- [50] H. Bremer, J. Hymes, and P. P. Dennis, *J. Theor. Biol.* **45**, 379 (1974).
- [51] H. Bai, K. Yang, D. Yu, C. Zhang, F. Chen, and L. Lai, *Proteins* **79**, 720 (2011).
- [52] B. Alberts, A. Johnson, J. Lewis, M. Raff, K. Roberts, and P. Walter, *Molecular Biology of the Cell* (Garland Science, New York, 2002).
- [53] G. Chen and M. P. Deutscher, *RNA* **16**, 667 (2010).
- [54] H. El-Samad, H. Kurata, J. C. Doyle, C. A. Gross, and M. Khammash, *Proc. Natl. Acad. Sci. U.S.A.* **102**, 2736 (2005).

IV) Zuk PJ, Kočańczyk M, Jaruszewicz J, Bednorz W, Lipniacki T, *Dynamics of a stochastic spatially extended system predicted by comparing deterministic and stochastic attractors of the corresponding birth-death process*, Physical Biology, (IOP Press, Great Britain), 9(5): 055002, 2012.

# Dynamics of a stochastic spatially extended system predicted by comparing deterministic and stochastic attractors of the corresponding birth–death process

Pawel J Zuk<sup>1,2</sup>, Marek Kočańczyk<sup>1</sup>, Joanna Jaruszewicz<sup>1</sup>, Witold Bednorz<sup>3</sup> and Tomasz Lipniacki<sup>1,4</sup>

<sup>1</sup> Institute of Fundamental Technological Research, Warsaw 02-106, Poland

<sup>2</sup> Institute of Theoretical Physics, Faculty of Physics, University of Warsaw, 00-681 Warsaw, Poland

<sup>3</sup> Faculty of Mathematics, Informatics and Mechanics, University of Warsaw, Warsaw 02-097, Poland

<sup>4</sup> Department of Statistics, Rice University, Houston, TX 77-005, USA

E-mail: [tlipnia@ippt.gov.pl](mailto:tlipnia@ippt.gov.pl)

Received 15 December 2011

Accepted for publication 25 June 2012

Published 25 September 2012

Online at [stacks.iop.org/PhysBio/9/055002](http://stacks.iop.org/PhysBio/9/055002)

## Abstract

Living cells may be considered as biochemical reactors of multiple steady states. Transitions between these states are enabled by noise, or, in spatially extended systems, may occur due to the traveling wave propagation. We analyze a one-dimensional bistable stochastic birth–death process by means of potential and temperature fields. The potential is defined by the deterministic limit of the process, while the temperature field is governed by noise. The stable steady state in which the potential has its global minimum defines the *global deterministic attractor*. For the stochastic system, in the low noise limit, the stationary probability distribution becomes unimodal, concentrated in one of two stable steady states, defined in this study as the *global stochastic attractor*. Interestingly, these two attractors may be located in different steady states. This observation suggests that the asymptotic behavior of spatially extended stochastic systems depends on the substrate diffusivity and size of the reactor. We confirmed this hypothesis within kinetic Monte Carlo simulations of a bistable reaction–diffusion model on the hexagonal lattice. In particular, we found that although the kinase–phosphatase system remains inactive in a small domain, the activatory traveling wave may propagate when a larger domain is considered.

## 1. Introduction

Bistability and stochasticity are the key concepts in molecular biology. Bistable regulatory elements are capable of introducing heterogeneity in cell population and may allow cells in a multicellular organism to specialize and specify their fates [1–5]. Decisions between cell death, survival, proliferation or senescence are associated with bistability [6–8]. Ogasawara and Kawato showed that a bistable system of brain-specific protein kinase M $\zeta$  can play role in the long-term storage of memory [9]. Transitions between stable steady states occur due to the stochastic switching [10, 11], or, in

spatially extended systems, may follow the traveling wave propagation [12].

When the magnitude of noise is relatively large, the stochastic transitions between attracting states are relatively frequent and the stationary probability distribution (SPD) associated with the stochastic process has a characteristic bimodal shape. The maxima of the SPD are approximately determined by the macroscopic steady states (although they do not necessarily exactly overlap). Song *et al* proposed a stochastic bifurcation concept describing the appearance of a new mode in the SPD, accompanying the appearance of a new stable steady state in the bifurcation diagram of

the deterministic approximation of the process [13]. As the magnitude of noise decreases, communication between the two attractors ceases. Consequently, the characteristic time in which the probability distribution (PD) converges to the SPD elongates. Kinetics near each attractor can be modeled as the Gaussian process [14], while jumping between the attractors can be modeled using the two-lumped-state Markov chain with transition propensities calculated from the full Markov process. The relative stability of two or more steady states depends on the system volume [15]. However, since the characteristic time spent in each attractor basin grows exponentially with the volume of the system, when the volume diverges to infinity, the SPD becomes (generically) unimodal, concentrated in the vicinity of the ‘most stable steady state’ or the ‘global stochastic attractor’ (GSA) [16, 17]. In this limit, bistability is manifested by a rapid transition from one unimodal SPD to the other unimodal SPD in response to the change of the bifurcation parameter.

For spatially extended bistable systems, considered in the deterministic approximation, the most stable steady state can be determined by the direction of the traveling wave propagation. Intuitively, the traveling wave propagates in such direction that the whole domain converges to the most stable steady state—which will be referred to as a global deterministic attractor (GDA). Interestingly, for a given system of reactions and parameters, the GDA and GSA may be different. This implies that the SPD of the stochastic but perfectly mixed system will concentrate in one steady state, while the corresponding spatially extended deterministic system may converge to the other steady state due to traveling wave propagation. In the case when GDA and GSA do not colocalize, one could expect that for the corresponding bistable, stochastic but spatially distributed system, the size of the compartment and substrate diffusivity control the relative stability of steady states. We verify this hypothesis simulating a stochastic kinase–phosphatase reaction–diffusion model on a hexagonal lattice.

The paper is organized as follows. In section 2, we consider a general one-dimensional birth–death (B–D) Markov process, introduce the GDA (subsection 2.1) and GSA (subsection 2.2), and show that these two attractors may not overlap.

In section 3, we propose the thermodynamic interpretation using the concepts of the potential and temperature fields associated with the B–D process (subsection 3.1). The concept of the temperature for B–D processes was introduced by Ross and colleagues [16, 18, 19]. Later, Bialek [20] and Lu *et al* [7] proposed that the temperature field is not uniform, but proportional to the sum of birth and death rates. We introduce another temperature definition, which converges to that proposed by Bialek [20] in steady states of the system.

Next, we consider two biological examples. First (subsection 3.2), we investigate analytically a simplified one-dimensional B–D process of kinase auto-activation in an open compartment. We will demonstrate that the temperature field and thus the SPD is controlled by fluxes of the active kinase to and out of the compartment, even in the case when these fluxes are equal and do not influence the deterministic mass

rate equation. In a relatively broad range of parameters the value of in- and out-flux (which can be associated with substrate diffusivity) determines the global attractor of the system. This observation suggests that for stochastic spatially distributed systems the size of the compartment and substrate diffusivity control the relative stability of steady states.

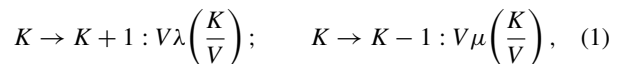
We verify this hypothesis in subsection 3.3 introducing a more realistic kinase–phosphatase model with diffusion on a hexagonal lattice. In this latter model, by performing kinetic Monte Carlo (KMC) simulations, we demonstrate that, despite the fact that the kinase molecules in a small isolated compartment remain mostly inactive, in a larger compartment the activatory traveling wave may propagate leading to persistent activation of the system.

In section 4, we review the main results in the biological context. The manuscript is supplemented by three appendices. In appendix A.1 we review and discuss Bialek’s derivation of temperature. In appendix A.2 we demonstrate that when the temperature profile is nonuniform (i.e. in the generic case), an arbitrary steady state may become the GSA, provided that the temperature in the vicinity of this state is sufficiently low. In appendix A.3 we show that the parameter range for which the bimodal SPD distribution is observed decreases to zero as the system volume diverges to the infinity.

## 2. Preliminaries

### 2.1. Global deterministic attractor

We will consider a one-dimensional B–D process:



where  $K$  is the number of substrate molecules,  $V$  is the volume of the reactor and  $\lambda\left(\frac{K}{V}\right)$  and  $\mu\left(\frac{K}{V}\right)$  denote birth and death intensities, non-negative for  $K > 0$ , with  $\mu(0) = 0$ . The assumption that birth and death intensities depend on the concentration  $x = \frac{K}{V}$ , rather than on the number of molecules  $K$ , allows for comparing reactors of different volumes. In the deterministic limit, when the volume of the reactor tends to infinity, the B–D process follows the law of mass action,

$$\frac{dx}{dt} = \lambda(x) - \mu(x) =: W(x) =: -\frac{dU(x)}{dx}. \quad (2)$$

The function  $U(x)$  can be interpreted as a potential. The stable stationary states of (2) are in the minima of  $U(x)$ . We assume that the potential has two minima in  $x_1$  and  $x_3$ , separated by a maximum in  $x_2$ . The trajectories of (2) converge to  $x_1$  or  $x_3$  depending on the initial state of the system. Equations (1) and (2) may satisfactorily describe the state of the reactor in the infinite diffusion limit, in which the concentration  $x$  is constant over the reactor. In the case of finite diffusion, (2) should be replaced by the reaction–diffusion equation for the substrate density  $x(z, t)$  (here for illustration purposes we assume that  $x$  depends on one spatial coordinate,  $z$ ),

$$\frac{\partial x}{\partial t} = D \frac{\partial^2 x}{\partial z^2} - \frac{dU(x)}{dx}, \quad (3)$$

where  $D$  is the diffusion coefficient. The above equation yields the traveling wave solutions,  $x = x(z - vt) = x(\zeta)$  connecting

steady states  $x_1$  and  $x_3$ . For this solution  $x(z) \rightarrow x_1$  for  $z \rightarrow -\infty$  and  $x(z) \rightarrow x_3$  for  $z \rightarrow \infty$ . The propagation velocity  $v$  may be given in the implicit form (see [21]) as

$$v = \frac{U(x_1) - U(x_3)}{\int_{-\infty}^{\infty} \left(\frac{dx}{d\xi}\right)^2 d\xi}. \quad (4)$$

The sign of velocity  $v$ , given by  $\text{Sgn}(U(x_1) - U(x_3))$ , ensures that the region of ‘lower energy’ expands, i.e.  $x(z, t) \rightarrow x_U$  as  $t \rightarrow \infty$ , where  $U(x_U)$  is the global minimum. Only in the non-generic case, when  $U(x_1) - U(x_3) = 0$ , the system has standing wave solutions in which states ‘ $x_1$ ’ and ‘ $x_3$ ’ coexist. Intuitively, for a ‘random’ initial condition in the sufficiently large reactor, in some areas of the reactor  $x(z)$  will be in the basin of attraction of  $x_U$ . In such a case the traveling wave or waves will be formed and in the whole reactor the substrate density  $x(z, t)$  will converge to  $x_U$ . Therefore, for the deterministic, spatially extended system (3), the state  $x_U$ , where the potential achieves the global minimum, may be considered a global attractor. We will refer to it as a GDA.

## 2.2. Global stochastic attractor

Let  $p(K, t)$  denote the probability that the number of substrate molecules equals  $K$  at time  $t$  in the process (1). The probability  $p_K(t)$  obeys the evolution (or Master) equation

$$\begin{aligned} \frac{\partial p(K, t)}{\partial t} &= p(K-1, t) V \lambda \left(\frac{K-1}{V}\right) + p(K+1, t) \\ &\times V \mu \left(\frac{K+1}{V}\right) - V \left(\lambda \left(\frac{K}{V}\right) + \mu \left(\frac{K}{V}\right)\right) p(K, t). \end{aligned} \quad (5)$$

In the steady state  $p(K, t) = p_K = \text{const}$ , the net probability flux between the neighboring states  $K$  and  $K+1$  equals zero, i.e.

$$p_K \lambda \left(\frac{K}{V}\right) - p_{K+1} \mu \left(\frac{K+1}{V}\right) = 0. \quad (6)$$

Therefore, under the assumption that  $\prod_{i=0}^{\infty} (\lambda(\frac{i}{V})/\mu(\frac{i+1}{V})) < \infty$ ,  $p_K$  satisfies

$$p_K = p_0 \prod_{i=0}^{K-1} \frac{\lambda(\frac{i}{V})}{\mu(\frac{i+1}{V})}, \quad (7)$$

where  $p_0$  is such that  $\sum p_K = 1$ . From (7) we have

$$\log p_K = \log p_0 + \sum_{i=0}^{K-1} \log \frac{\lambda(\frac{i}{V})}{\mu(\frac{i+1}{V})}. \quad (8)$$

For large  $V$  the sum can be replaced by the integral, that leads to [16, 17, 22, 23]

$$p_K \simeq p(x) = p_0 \exp(-V \Phi(x)), \quad (9)$$

where

$$\Phi(x) := - \int_0^x \log \frac{\lambda(y)}{\mu(y)} dy. \quad (10)$$

The local minima and maxima of  $\Phi(x)$  correspond to stable and unstable macroscopic steady states of (2), respectively. The Laplace method implies that for  $V \rightarrow \infty$ ,  $p(x)$  converges to the Dirac delta,  $\delta(x_\Phi)$ , where  $\Phi(x_\Phi)$  is the proper global minimum of  $\Phi(x)$ , provided that such minimum exists [24]. Only in the non-generic case, when  $\Phi(x)$  has two or more equal minima, the SPD in the zero noise limit ( $V \rightarrow \infty$ )

is distributed between these minima. In this way we showed that, generically, when  $V \rightarrow \infty$ , the SPD concentrates in the macroscopic steady state of the mass rate equation, in which  $\Phi(x)$  achieves the global minimum. The steady state  $x_\Phi$ , in which  $\Phi(x)$  achieves the global minimum, may thus be considered the GSA. The local maxima and minima of  $\Phi(x)$  correspond to the maxima and minima of  $U(x)$ . However, the global minimum of  $\Phi(x)$  may not correspond to the global minimum of  $U(x)$ ; therefore, the GSA may not be colocalized with the GDA. According to our knowledge this observation was first explicitly made in the context of the Schlögl model [25] by Nicolis [23].

Later, in the context of stochastic gene expression, it was observed that the character of noise defined by the adiabaticity parameter [26, 27] or coarse graining [28] influences the SPD. Recently, for a gene expression model with the additive or multiplicative noise, Frigola *et al* showed that the SPD is concentrated in the global minimum of the stochastic rather than the deterministic potential [29]. Frigola *et al* defined the stochastic potential based on the Fokker–Planck approximation and demonstrated that type of noise dictates in which of steady states such potential has the global minimum.

## 3. Results

### 3.1. Thermodynamic interpretation

In order to provide the thermodynamic interpretation of the above observation, we consider the problem of particles diffusing in the potential and temperature fields  $U(x)$  and  $T(x)$ . Such particles drift with flow  $J_F = -M\rho(x, t)(dU/dx)$  where  $M$  is the mobility and  $\rho(x, t)$  is the local concentration of particles. In thermal equilibrium, the drift flow is balanced by the diffusion flow  $J_D = -\frac{\partial}{\partial x}[\Gamma(x)\rho(x, t)]$ , where  $\Gamma(x) = Mk_B T(x)$  is the diffusion and  $k_B$  is the Boltzman constant. In the steady state  $J_D + J_F = 0$ , and one obtains

$$\begin{aligned} \rho \frac{dU}{dx} &= -k_B \frac{d}{dx} [\rho(x)T(x)], \\ \rho(x) &= \rho_0 \frac{T_0}{T(x)} \exp \left[ - \int \frac{dU/dx}{k_B T(x)} dx \right]. \end{aligned} \quad (11)$$

In the uniform temperature field  $T(x) = T_0$ , the last expression simplifies to  $\rho(x) = \rho_0 \exp[-U(x)/k_B T_0]$ . In such a case,  $\rho(x)$  converges to  $\delta(x_U)$  as  $T_0 \rightarrow 0$ . However, the above is not true when the temperature field  $T = \tau_0 T(x)$  is not uniform. In the case when  $\tau_0 \rightarrow 0$ ,  $\rho(x)$  converges to  $\delta(x_\Phi)$ , where  $x_\Phi$  is the point of the global minimum of  $\int \frac{dU(x)/dx}{k_B T(x)} dx$  which may be different than  $x_U$ . When temperature gradients are not very large, the prefactor  $T_0/T(x)$  can be replaced by a constant which leads to

$$\rho(x) = \rho_0 \exp \left[ - \int \frac{dU/dx}{k_B T(x)} dx \right]. \quad (12)$$

This approximation is equivalent to neglecting the component of diffusion flow  $J_D$  called spurious flow  $J_{\text{spurious}} = -\rho(x, t)d\Gamma(x)/dx = -k_B \rho(x, t)MdT(x)/dx$ , i.e. flow of particles induced by the diffusion or temperature gradient, known also as the Soret effect, see [30] and [31]. By comparing

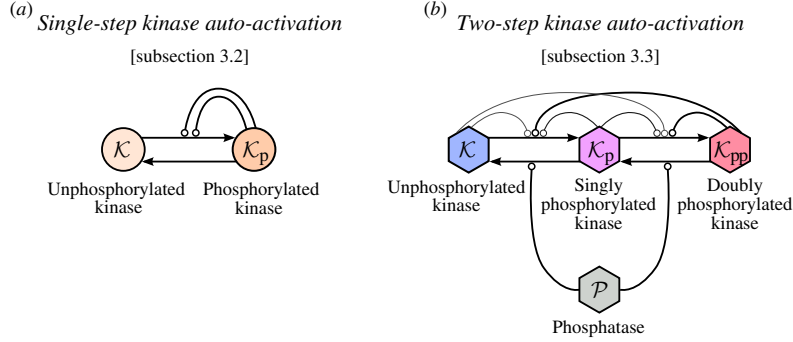


**Figure 1.** Two bistable reaction systems of kinase auto-phosphorylation. (a) A simple model with nonlinear auto-activation (circle-headed double arrow) defined by equations (14). (b) A multistate kinase model with explicit phosphatase activity described by equations (27a)–(27d). Phosphorylated kinases have higher catalytic activity (as reflected by the width of circle-headed arrows).

$p(x)$  given by (9) and (10) with the particle density  $\rho(x)$  given by (12), we obtain  $T(x)$  as

$$T(x) = \frac{1}{k_B V} \frac{\lambda(x) - \mu(x)}{\log(\lambda(x)/\mu(x))}. \quad (13)$$

That is, in the low-noise limit (large  $V$ ), the SPD of the B–D process is proportional to the density of particles diffusing in the potential  $U(x) = \int (\mu(x) - \lambda(x)) dx$  and the temperature field  $T(x)$  given by (13). Let us note that  $T(x)$  defined by (13) vanishes when either  $\lambda(x)$  or  $\mu(x)$  is zero. Points in which  $T(x) = 0$  are singular, i.e. they can be passed only in one direction. If such points exist, they bound the absorbing regions.

Another, methodologically rigorous, way of deriving temperature, based on the Fokker–Planck approximation, was proposed by Bialek [20] and then followed by Lu *et al* [7]. It led to  $\tilde{T}(x) = (\lambda(x) + \mu(x))/(2k_B V)$ . We discuss Bialek’s approach in appendix A.1; see also [32] for a recent detailed review. Finally, we mention the recent study by Feng and Wang [33] who introduced the other concept of the effective temperature for gene networks based on the correlation and the response functions. This is an entirely different approach, leading for example to negative temperatures for a self-repressing gene.

As shown in appendix A.2, any of the  $U(x)$  minima may become a global attractor depending on the temperature profile  $T(x)$ . This implies that two stochastic processes converging to the same mass rate equation in the  $V \rightarrow \infty$  limit may have two different GSAs. In the following section, we illustrate this unintuitive observation and its consequences using a simple bistable kinase auto-activation model, a version of the Schlögl model [25], classified as one of the simplest bistable systems [34]. The auto-activation is characteristic for Src, Syk, and Tec family kinases important in the immune cell signaling [35, 36].

### 3.2. Simplified kinase auto-activation model

In the model we will assume that the total concentration of kinase molecules remains constant and equals 1; thus their number is equal to the volume of the compartment  $V$ . Kinases can be in either active or inactive state, and the number of active kinases will be denoted by  $K$  (see figure 1). Inactive kinases, number of which is  $V - K$ , can be activated by

active kinases with rate proportional to the square of the active kinase concentration  $x = K/V$ , or by other kinase species with some small constant rate  $c_1$ . The second-order nonlinearity arises either when the active unit of the kinase is a dimer or when double phosphorylation is required to activate the kinase [37, 38]. In turn, active kinases are inactivated with the constant rate  $d_1$ . Under the above assumptions the number of active kinases  $K$  follows the B–D process with rates:

$$\begin{aligned} K \rightarrow K + 1 &: \left( c_1 + c_2 \left( \frac{K}{V} \right)^2 \right) \left( 1 - \left( \frac{K}{V} \right) \right) V; \\ K \rightarrow K - 1 &: d_1 \left( \frac{K}{V} \right) V. \end{aligned} \quad (14)$$

Let us note that since the total number of kinases remains constant, the number of active kinases is limited by  $V$ , which is reflected by the fact that the birth intensity is zero for  $K = V$ .

Next, we will assume that active kinases can translocate to and out of the compartment, with fluxes  $f_1$  and  $f_2$ , respectively. Such a situation arises when the considered compartment is a subvolume of a larger reactor. As a consequence, we obtain the following birth and death intensities, where concentration  $x = K/V$  is used instead of the number of molecules  $K$ ,

$$\lambda(x) = (c_1 + c_2 x^2)(1 - x) + f_1; \quad \mu(x) = d_1 x + f_2. \quad (15)$$

For the sake of simplicity and illustration purposes, we will assume that the in-flux and out-flux are equal,  $f_1 = f_2 = f$ . Such simplifying assumption ensures that the (deterministic) mass rate equation for  $x$ ,

$$\frac{dx}{dt} = \lambda(x) - \mu(x) = (c_1 + c_2 x^2)(1 - x) - d_1 x =: W(x), \quad (16)$$

does not depend on  $f$ . We will see, however, that  $f$  controls the SPD and determines the most stable stochastic attractor. We focus on the bistable case when  $W(x)$  has three real roots  $0 < x_1 < x_2 < x_3 < 1$ . In the further analysis, we will use the roots  $x_1, x_2, x_3$  as parameters describing the polynomial  $W(x)$ . The original coefficients  $c_1, c_2, d_1$  may be recovered from the roots using Vieta’s formulas by the following relations:

$$\begin{aligned} c_1 &= \frac{d_1 x_1 x_2 x_3}{(x_1 + x_2)(x_1 - 1)(x_2 - 1)}, \\ c_2 &= \frac{d_1}{(x_1 + x_2)(x_1 - 1)(x_2 - 1)}. \end{aligned} \quad (17)$$

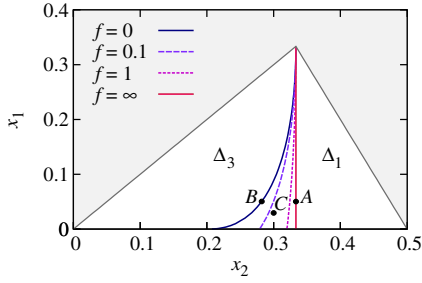


**Figure 2.** Subdomains  $\Delta_1$  and  $\Delta_3$  with their separation curves for four values of flux  $f$ .

Let us note that since  $c_1$  and  $c_2$  are proportional to  $d_1$ , the last coefficient determines only the timescale of the process,  $\tau = 1/d_1$ . Since the quotient of coefficients at the third- and

at the second-order term in  $W(x)$  equals  $-1$ , roots of  $W(x)$  satisfy  $x_1 + x_2 + x_3 = 1$ , and thus the parameter space may be reduced to the two-dimensional domain  $\Delta$ , defined as follows:

$$\Delta = \left\{ (x_1, x_2) \in \mathbb{R}^2 \mid x_1 > 0, x_2 > 0, x_1 < x_2, x_2 < \frac{1}{2} - \frac{x_1}{2} \right\} \quad (18)$$

(see figure 2). Domain  $\Delta$  splits into two subdomains,  $\Delta_1$  and  $\Delta_3$ , such that for  $(x_1, x_2) \in \Delta_1$ , the SPD of the process (14)–(15) in the  $V \rightarrow \infty$  limit converges to  $\delta(x_1)$  and for  $(x_1, x_2) \in \Delta_3$ , the SPD converges to  $\delta(x_3)$ . The curves separating  $\Delta_1$  and  $\Delta_3$  depend on  $f, x_1(x_2; f)$ . They are shown for  $f = 0, f = 0.1, f = 1$  and  $f = \infty$  in figure 2, and are given analytically based on (10) in the implicit form by

$$\Phi(x_3) - \Phi(x_1) = - \int_{x_1}^{x_3} \log \frac{\lambda(y)}{\mu(y)} dy = 0. \quad (19)$$

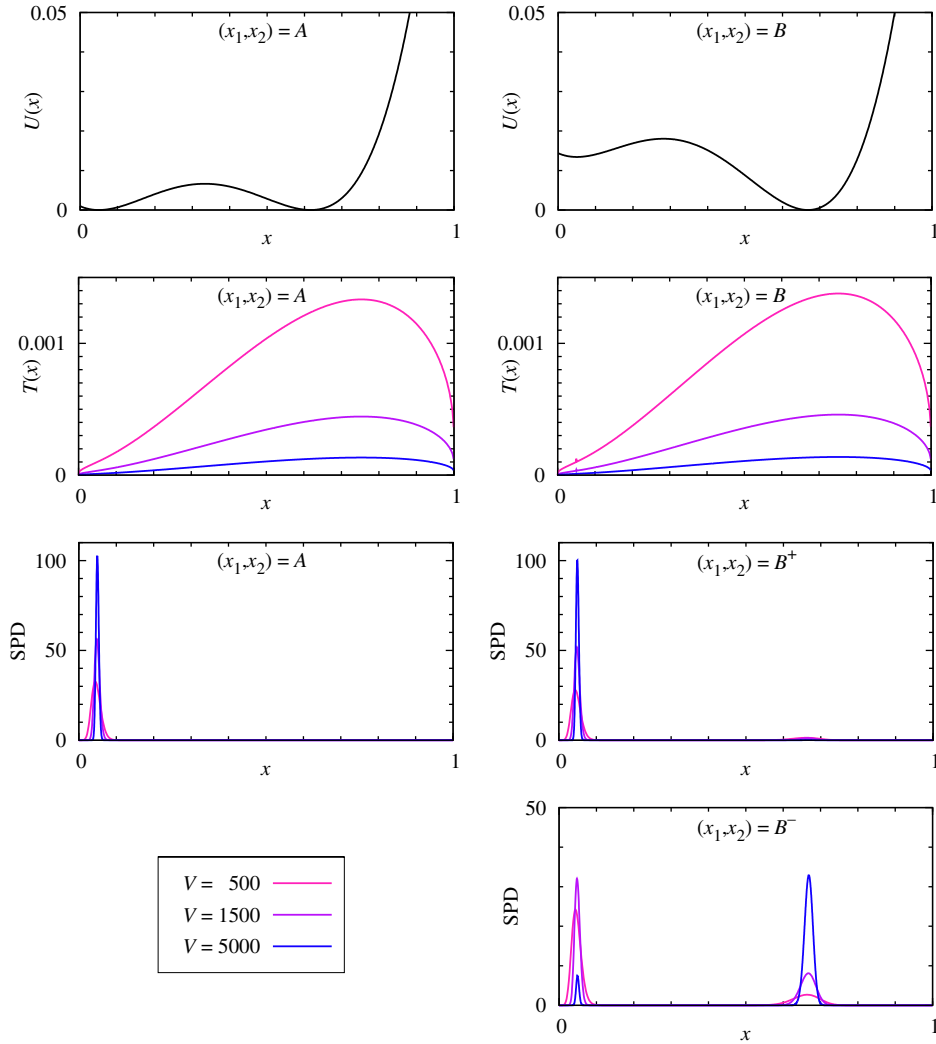


**Figure 3.** The case of zero flux,  $f = 0$ . Left column:  $(x_1, x_2) = A = (0.05, \frac{1}{3})$  (see figure 2). The potential field  $U(x)$  is symmetric with respect to the unstable steady state  $x_2$ . In this case, as the system volume  $V$  grows, the SPD concentrates on the colder attraction basin of steady state  $x_1 = 0.05$ . Right column: potential  $U(x)$  and function  $\Phi(x)$  for  $(x_1, x_2) = B \approx (0.05, 0.2818)$  on the separatrix  $f = 0$  shown in figure 2. The SPDs  $p(x)$  for  $B^- = (0.05, 0.2818 - 0.001)$  below the separatrix and  $B^+ = (0.05, 0.2818 + 0.001)$  above the separatrix are shown in two bottom panels. As  $V \rightarrow \infty$ ,  $p(x; B^-)$  converges to  $\delta(x_3)$  and  $p(x; B^+)$  converges to  $\delta(x_1)$ .

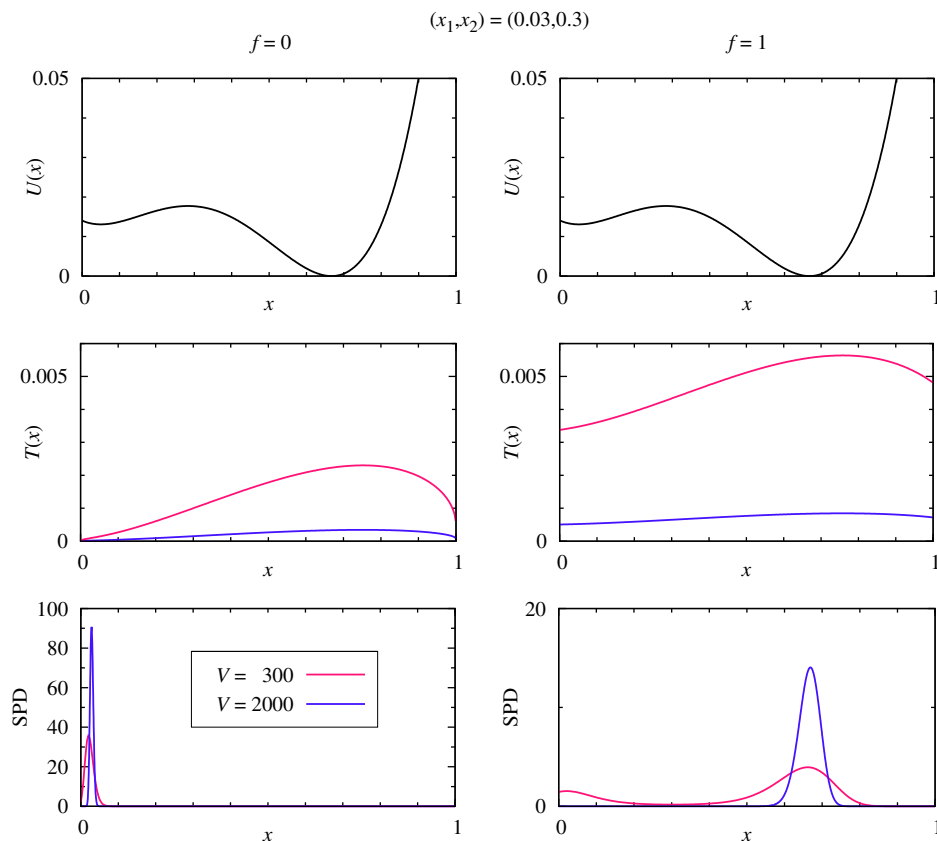


**Figure 4.** The flux controls temperature profile  $T(x)$  and the SPD. Left column:  $f = 0$ ,  $(x_1, x_2) = C = (0.03, 0.3)$ . The temperature is much lower in the left basin of attraction, and thus the SPD  $p(x)$  concentrates in  $x_1$  as  $V \rightarrow \infty$ . Right column:  $f = 1$ ,  $(x_1, x_2) = C$ ; the temperature profile is flatter than for  $f = 0$  and the SPD  $p(x)$  concentrates in the global potential minima at  $x_3 = 0.67$ . The potential  $U(x)$  is the same for both columns.

In the case with zero flux,  $f = 0$ , the temperature profile is not uniform and for the symmetric potential  $U(x)$ , the SPD is not symmetric, but is concentrated in the colder attraction basin of point  $x_1$  (figure 3, left column). The temperature effect may be balanced by the asymmetry of the potential (figure 3, right column). For the point  $B = (x_1, x_2(x_1))$  on the separatrix  $f = 0$ , in the  $V \rightarrow \infty$  limit the SPD  $p(x)$  converges to  $\alpha\delta(x_1) + \beta\delta(x_3)$ . However, this cannot be explicitly numerically demonstrated, because even a tiny deviation from the separatrix causes the SPD to be redistributed either to  $x_1$  or  $x_3$  as  $V \rightarrow \infty$  (figure 3, right column, two bottom panels). As shown in appendix A.3, in figure 9, the bimodal SPD expected for bistable systems may be observed only if the magnitude of noise is sufficiently large. Interestingly, as shown in the lowest panel of figure 3, the SPD for large temperatures concentrates mostly in the  $x_1$  basin, and then in the  $T \rightarrow 0$  limit it converges to  $\delta(x_3)$ . This confirms the observation made by Vellela and Qian that the relative stability of steady states depends on the system volume [15].

When the system communicates with environment, i.e. when  $f > 0$ , the temperature profile  $T(x)$  is modified, figure 4. For  $f = 0$  (figure 4, left column) the temperature is much lower in the left attraction basin and thus the SPD concentrates in this basin. For  $f = 1$  (figure 4, right column), the temperature profile is flatter and the SPD concentrates in

the global potential minimum  $x_3$  as  $V \rightarrow \infty$ . For  $f \rightarrow \infty$ , the temperature profile  $T(x)$  becomes uniform, and SPD converges to  $\delta(x_U)$  as  $V \rightarrow \infty$ , where  $x_U$  is the steady state in which potential  $U(x)$  has the global minimum. It should be noted that for larger  $f$ , larger  $V$  is required to reach the unimodal SPD, figure 4. In the  $f \rightarrow \infty$  limit,  $\Phi(x)$  becomes proportional to  $U(x)$  and SPD  $f(x)$  becomes symmetric for the symmetric potential  $U(x)$ , i.e. when  $U(x_1) = U(x_3)$ , which implies  $x_2 = (x_1 + x_3)/2 = 1/3$ .

At this point, let us recall the reaction–diffusion system (3). As follows from (4), for  $U(x_1) = U(x_3)$  the traveling wave velocity is  $v = 0$ . In our specific example, (3) takes the form of the Nagumo equation [21],

$$\frac{\partial x}{\partial t} = D \frac{\partial^2 x}{\partial z^2} + (x_1 - x)(x_2 - x)(x_3 - x), \quad (20)$$

which yields the traveling wave solutions

$$x(z - vt) = x(\xi) = \frac{x_3 + x_1 \exp[(2D)^{-1/2}(x_3 - x_1)\xi]}{1 + \exp[(2D)^{-1/2}(x_3 - x_1)\xi]} \quad (21)$$

with

$$v = (x_1 - 2x_2 + x_3) \sqrt{\frac{D}{2}}. \quad (22)$$

The last result implies that in the  $f \rightarrow \infty$  limit the stochastic process is diffusion driven and the associated temperature field

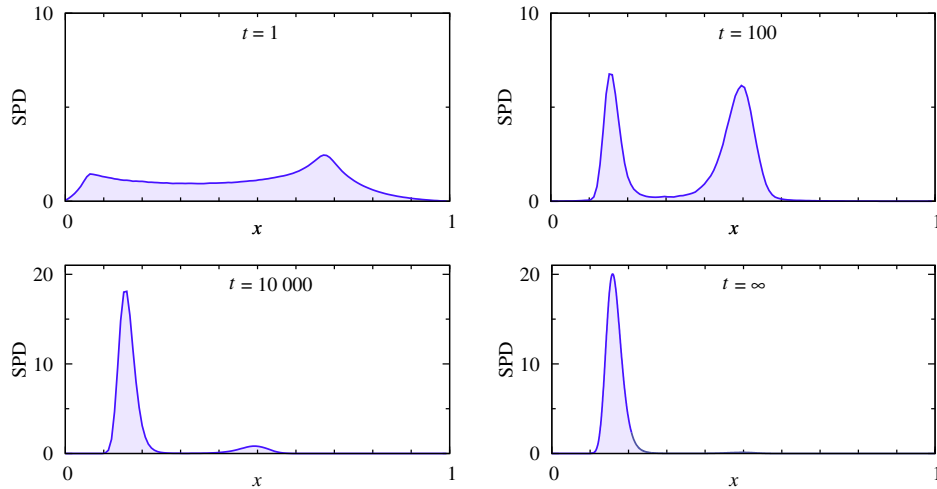


**Figure 5.** Evolution of the PD based on Monte Carlo simulations for  $(x_1, x_2) = (\frac{1}{6} - 0.005, \frac{1}{3} + 0.005)$  with  $V = 2000$ . For  $(x_1, x_2) = (\frac{1}{6}, \frac{1}{3})$  and  $x_3 = 1 - x_1 - x_2 = \frac{1}{2}$  the potential  $U(x)$  is symmetric with respect to  $x_2$ . At  $t = 0$ , the PD is uniform; at intermediate times it becomes bimodal, determined by the size of attraction basins; then at  $t \rightarrow \infty$  it becomes unimodal, determined by the global attractor.

becomes uniform. As  $f$  increases, the parameter range for which GSA and GDA are localized in different steady states decreases and only for the  $f \rightarrow \infty$  limit the two attractors must colocalize.

In summary, we found that there is a broad range of parameters (figure 2, between separatrices for  $f = 0$  and  $f = \infty$ ) in which GDA corresponds to the active state  $x_3$ , while GSA corresponds to the inactive state  $x_1$ . That is, there exists a broad parameter range in which

- the discrete, perfectly mixed stochastic system, considered in the isolated reactor, will converge to the inactive state,
- while in its spatially extended deterministic counterpart the activatory traveling waves will propagate, leading to the activation of the system.

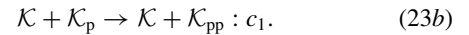
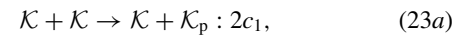
This suggests that in stochastic spatially distributed systems the global attractor is determined by the diffusion and size of the reactor. In the following section, we will confirm this hypothesis considering a more realistic reaction–diffusion model on a hexagonal lattice.

*Remark.* The SPD may inadequately represent the behavior of bistable systems in the low noise limit. As noise decreases, the communication between steady states ceases, and the characteristic state-to-state transition time lengthens, and thus time in which the PD approaches the SPD may become longer than time in which external conditions defining potential may be considered constant. In the low noise limit the bistable system has two distinct timescales: the intermediate (in which the initially uniform PD becomes bimodal) and the asymptotic timescale in which the PD converges to the unimodal SPD (figure 5). At intermediate timescale the system behavior is close to deterministic. Depending on the nature of the biochemical process, each of the two timescales and associated ‘limiting’ PDs can be important.

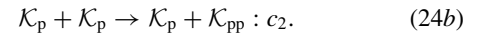
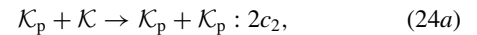
### 3.3. Kinase auto-activation reaction–diffusion model on a 2D hexagonal lattice

In the model, we consider two molecular species, kinase  $\mathcal{K}$  and phosphatase  $\mathcal{P}$ . We assume that the kinase molecules can be in one of three states, unphosphorylated  $\mathcal{K}$ , singly phosphorylated  $\mathcal{K}_p$  and doubly phosphorylated  $\mathcal{K}_{pp}$ . Kinases may activate one another, and in turn are dephosphorylated by phosphatases with intensity  $d$ . The phosphorylation intensities  $c_1$ ,  $c_2$  and  $c_3$ , of, respectively,  $\mathcal{K}$ ,  $\mathcal{K}_p$ , and  $\mathcal{K}_{pp}$ , increase with the kinase phosphorylation level. The following reactions are considered.

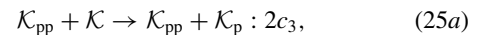
*Phosphorylation by an unphosphorylated kinase:*



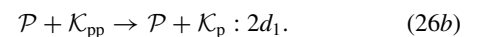
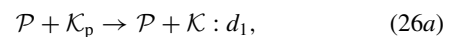
*Phosphorylation by a singly phosphorylated kinase:*



*Phosphorylation by a doubly phosphorylated kinase:*



*Dephosphorylations:*



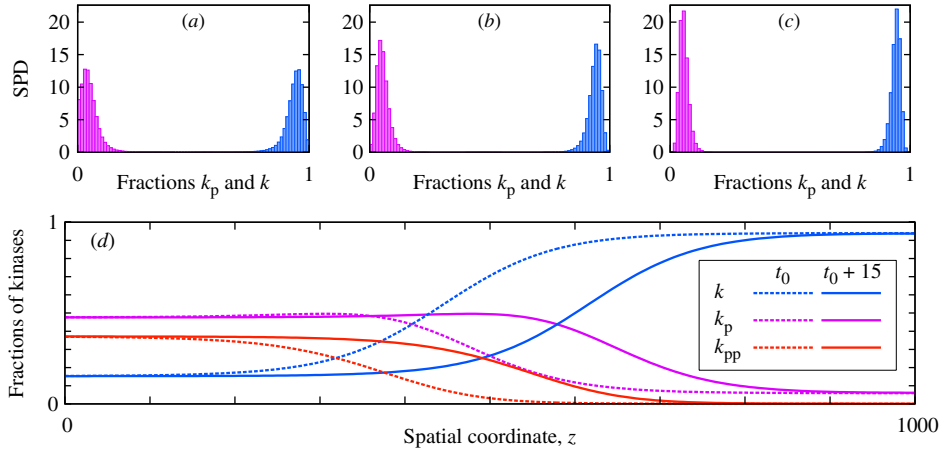


**Figure 6.** Comparison of behavior of stochastic perfectly mixed systems with their deterministic spatially extended counterpart. (a), (b) and (c) SPDs estimated in the Gillespie algorithm (assuming spatial homogeneity of the system) simulations of the stochastic system (23a)–(26b), containing 80, 160 or 320 interacting kinases, respectively. SPDs concentrate in the decreasing vicinity of the inactive state ( $k = 0.94$ ,  $k_p = 0.06$ ,  $k_{pp} = 0.00$ ) as the number of kinases grows. (d) Profile of the activatory traveling wave, that propagates from the active to inactive state (the assumed diffusion coefficient  $D = 625$  corresponds to the motility  $M = 5000$ ). The SPD in Gillespie algorithm simulations was estimated from long trajectories containing more than ten switches between the active and inactive states in the case of 320 molecules, and much more switches for 160 and 80 molecules.

By convention, the first molecule on both reaction sides is considered the enzyme, while the second represents the substrate. The factor 2 multiplying rates of reactions involving  $\mathcal{K}$  and  $\mathcal{K}_{pp}$  as a substrate reflects the fact that an unphosphorylated kinase can be phosphorylated at any of its two residues, and similarly the doubly phosphorylated kinase can be dephosphorylated at any of its two residues.

The deterministic approximation of the system leads to three partial differential equations for concentrations of  $\mathcal{K}$ ,  $\mathcal{K}_p$  and  $\mathcal{K}_{pp}$ . We confine to the case in which the diffusion coefficient  $D$  is equal for all kinase forms regardless of their phosphorylation level. In such a case we may assume that the total surface concentration of kinase  $C_{\mathcal{K}}$  remains constant and uniform over the surface. The phosphatase surface concentration will be denoted by  $C_{\mathcal{P}}$ . The fractional concentrations of  $\mathcal{K}$ ,  $\mathcal{K}_p$  and  $\mathcal{K}_{pp}$  will be denoted by  $k$ ,  $k_p$  and  $k_{pp}$ ; thus by definition  $k + k_p + k_{pp} = 1$ .

$$\frac{\partial k}{\partial t} = D \frac{\partial^2 k}{\partial z^2} + d_1 C_{\mathcal{P}} k_p - 2(c_1 k + c_2 k_p + c_3 k_{pp}) k C_{\mathcal{K}}, \quad (27a)$$

$$\frac{\partial k_p}{\partial t} = D \frac{\partial^2 k_p}{\partial z^2} + 2(c_1 k + c_2 k_p + c_3 k_{pp}) k C_{\mathcal{K}} + 2d_1 C_{\mathcal{P}} k_{pp} - (c_1 k + c_2 k_p + c_3 k_{pp}) k_p C_{\mathcal{K}} - d_1 C_{\mathcal{P}} k_p, \quad (27b)$$

$$- (c_1 k + c_2 k_p + c_3 k_{pp}) k_p C_{\mathcal{K}} - d_1 C_{\mathcal{P}} k_p, \quad (27c)$$

$$\frac{\partial k_{pp}}{\partial t} = D \frac{\partial^2 k_{pp}}{\partial z^2} + (c_1 k + c_2 k_p + c_3 k_{pp}) k_p C_{\mathcal{K}} - 2d_1 C_{\mathcal{P}} k_{pp}. \quad (27d)$$

Here for the sake of simplicity we assume the dependence on only one spatial coordinate  $z$ . The above system exhibits bistability in a broad range of parameters. Let us note that in the deterministic approximation the system dynamics depends

on only four parameters, values of which will be set constant for the rest of these considerations:

$$C_1 = c_1 C_{\mathcal{K}} = 0.02; \quad C_2 = c_2 C_{\mathcal{K}} = 0.15; \\ C_3 = c_3 C_{\mathcal{K}} = 4; \quad D_1 = d_1 C_{\mathcal{P}} = 1. \quad (28)$$

The values of parameters are chosen so that the system (27a)–(27d) has three steady state solutions, two stable (active with low level of unphosphorylated kinase,  $k = 0.15$ , and inactive with high level of unphosphorylated kinase,  $k = 0.94$ ) and one unstable:

- inactive: ( $k = 0.94$ ,  $k_p = 0.06$ ,  $k_{pp} = 0.00$ ),
- unstable: ( $k = 0.50$ ,  $k_p = 0.41$ ,  $k_{pp} = 0.08$ ),
- active: ( $k = 0.15$ ,  $k_p = 0.48$ ,  $k_{pp} = 0.37$ ).

For these parameters we found the following.

- (1) The SPD obtained in Gillespie algorithm simulations for the stochastic perfectly mixed system defined by reactions (23a)–(26b) concentrates in the decreasing vicinity of the inactive state as the number of kinases grows, figures 6(a)–(c). Values of parameters employed for Gillespie algorithm simulations are  $c_1 = C_1/N_{\mathcal{K}}$ ,  $c_2 = C_2/N_{\mathcal{K}}$ ,  $c_3 = C_3/N_{\mathcal{K}}$ ,  $d_1 = D_1/N_{\mathcal{P}}$ , where  $N_{\mathcal{K}}$  and  $N_{\mathcal{P}}$  are the numbers of kinase and phosphatase molecules. That is, the reaction rates are scaled by the number of molecules, which is equivalent to the assumption that the concentrations are independent of the number of substrate molecules. In spatially homogeneous systems the kinases dephosphorylation rate  $D_1$  is a product of phosphatase activity and the number of phosphatases  $D_1 = C_{\mathcal{P}} d_1 = 1$ . In reactions (23a)–(26b) the number of phosphatases remains unchanged, and is unimportant for the system dynamics.
- (2) The system (27a)–(27d) with parameters  $C_1$ ,  $C_2$ ,  $C_3$ ,  $D_1$  (28) describes an activatory traveling wave solution, i.e. waves that propagate from the active to inactive state, figure 6(d).

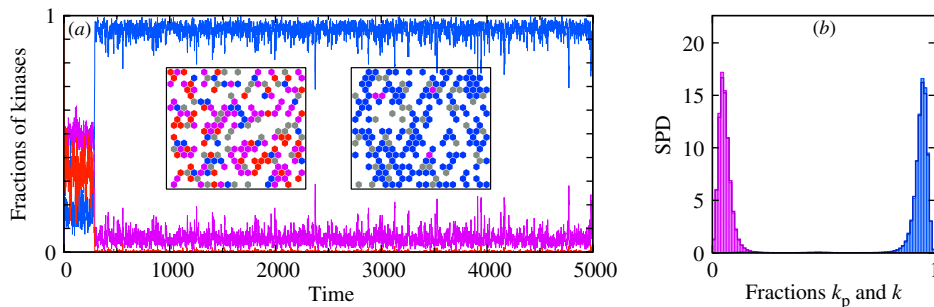


**Figure 7.** KMC simulations of the system (23a)–(26b) on the hexagonal lattice of size  $20 \times 20$ , for motility equal  $M = 5000$ . A fraction of lattice sites  $\chi_K = 0.4$  is occupied by kinase molecules, while phosphatase molecules occupy  $\chi_P = 0.1$  of the lattice. (a) Fraction of unphosphorylated, singly phosphorylated and doubly phosphorylated kinases in time. Insets: snapshots of the system in its active (left) and inactive (right) states. (b) SPDs obtained in Gillespie simulations (boxes) and KMC (thick lines). In the case of KMC simulations, the distribution was estimated from multiple runs starting from the active and inactive state, and the mean first-passage time analysis.

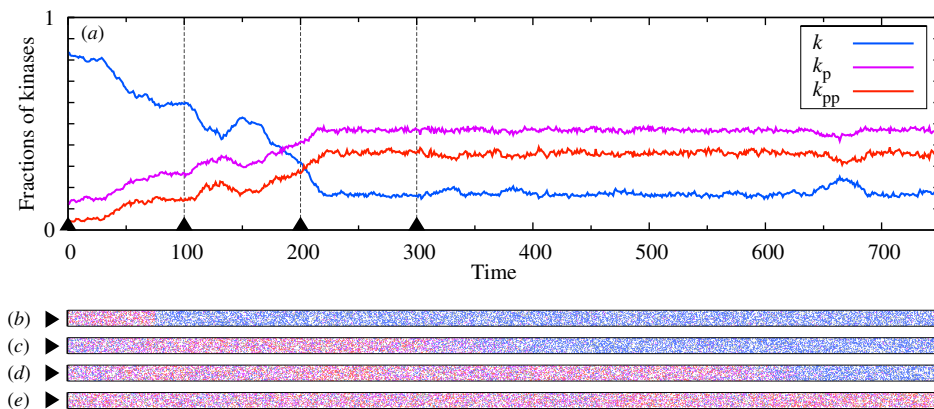


**Figure 8.** KMC simulations of the system (23a)–(26b) on the hexagonal lattice of size,  $20 \times 1000$ , showing the activatory traveling wave propagation. The same kinetic parameters, substrate fractions and motility  $M$  are assumed as in figure 7. (a) Fraction of unphosphorylated, singly phosphorylated and doubly phosphorylated kinases in time. (b), (c), (d), (e) Four snapshots of the system in time points as marked in (a).

The above finding implies that for the system defined by reactions (23a)–(26b) and parameters (28), the stochastic and deterministic global attractors diverge, and are defined, respectively, by the inactive and active states. Therefore, although a potential may not be defined for the system (27a)–(27d), the system exhibits an analogous behavior as the simpler system (16) analyzed in the previous section.

Finally, to confirm the hypothesis stated in the previous section, we performed KMC simulations on hexagonal lattices,  $20 \times 20$  (with periodic boundary conditions, i.e. toroidal topology) and  $20 \times 1000$  (with periodic-reflecting boundary conditions, i.e. cylindrical topology). In these two simulations we assumed that fraction of lattice sites  $\chi_K = 0.4$  is occupied by kinases, while fraction of lattice sites  $\chi_P = 0.1$  is occupied by phosphatases. In KMC simulations, molecules can interact only when in contact. All molecules move with the same motility  $M = 5000$ , that is, the propensity that a given molecule jumps to a neighboring empty site is  $M/6$ . The relation between diffusion and motility on 2D lattice is  $D = (1 - \chi_K - \chi_P)s^2M/4$ , where  $(1 - \chi_K - \chi_P)$  is the fraction of empty sites on the lattice, and  $s$  is the distance between the centers of adjacent hexagonal cells. Thus, in units in which  $s = 1$ , we obtain for  $\chi_K = 0.4$  and  $\chi_P = 0.1$ ,  $D = M/8$ . For KMC simulations, we set  $\hat{c}_1 = C_1/n_K$ ,  $\hat{c}_2 = C_2/n_K$ ,

$\hat{c}_3 = C_3/n_K$ ,  $\hat{d}_1 = D_1/n_P$ , where  $n_K = 6\chi_K$  (and  $n_P = 6\chi_P$ ) are expected values of the number of kinase (and phosphatase) molecules that are in the immediate vicinity of any molecule. The use of coefficients  $c_1 = C_1/N_K$ ,  $c_2 = C_2/N_K$ ,  $c_3 = C_3/N_K$ ,  $d_1 = D_1/N_P$  in Gillespie simulations, and coefficients  $\hat{c}_1 = C_1/n_K$ ,  $\hat{c}_2 = C_2/n_K$ ,  $\hat{c}_3 = C_3/n_K$ ,  $\hat{d}_1 = D_1/n_P$  in KMC simulations, provides that these two approaches converge in the infinite diffusion limit [39].

In simulations performed on a small toroidal lattice,  $20 \times 20$ , we found, as already expected from Gillespie algorithm simulations shown in figure 6(b), that the system remains in the inactive state for most of the time (figure 7). In these two simulations (shown in figure 6(b) and figure 7) the number of kinase molecules was the same (equal 160). The assumed large motility  $M = 5000$  implies that the relatively small reactor  $20 \times 20$  can be considered to be almost perfectly mixed, and thus the obtained SPD is nearly identical to the one obtained in Gillespie algorithm simulations for 160 kinases, figure 7(b). In both approaches more than 0.99 of mass is concentrated in the vicinity of the inactive state.

In contrast to simulations on the small toroidal lattice,  $20 \times 20$ , in simulations performed on the  $20 \times 1000$  lattice, we observed propagation of an activatory traveling wave, followed

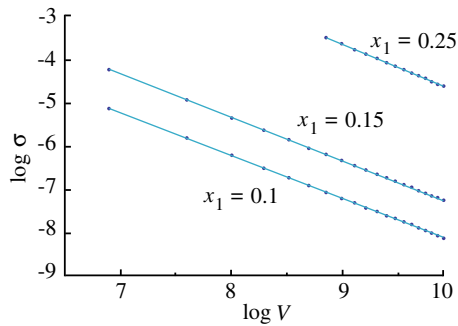


**Figure 9.** Width of the bistability zone  $\sigma$  in the  $(x_1, x_2)$  plane as a function of  $V$  for three values of  $x_1$ . The width  $\sigma$  decreases as  $1/V$ . For a given system volume  $V$ ,  $\sigma$  decreases as the distance between the two stable steady states  $x_1$  and  $x_3$  grows (i.e. when the value of  $x_1$  decreases).

by persistent activity of the system (figure 8). The system remains persistently active because, even when any region is inactivated due to stochastic fluctuations, it is quickly sealed by the activatory traveling wave. On the other hand, the motility  $M = 5000$  is about three orders of magnitude too small to render the  $20 \times 1000$  reactor mixed.

The behavior observed in KMC simulations remains in agreement with the expectations coming from the deterministic approximation of the system (figure 6). Activation of the systems on the  $20 \times 1000$  lattice can be interpreted on the basis of the analysis we made in the previous section. The  $20 \times 1000$  lattice can be viewed as an array of small  $20 \times 20$  compartments. When these compartments are isolated, as in simulations shown in figure 7, the in-flux and out-flux of active kinase  $f$  equals zero, and the system remains in the vicinity of GSA—in this case the inactive state (figure 4). However, when compartments are connected, the flux  $f$  makes the temperature profile flatter and the system converges to GDA, which corresponds to the active state (figure 4 and figure 8). In summary, we demonstrated that the spatially extended system converges to GSA when diffusion is fast enough to make the reactor perfectly mixed, but when the same system is considered in a larger reactor, the traveling waves may form and can drive the system to GDA.

#### 4. Conclusions

Bi- and multistable systems play a prominent role in signal processing. The attractors of molecular dynamical systems control the cell evolution and fate. Transitions between attractors can be due to stochastic switching, or may result from the traveling wave propagation. The first mode is characteristic for perfectly mixed systems for which noise provides the unique possibility of selecting the most stable steady state—termed here the global stochastic attractor (GSA). The second transition mode dominates in spatially extended systems characterized by relatively slow diffusion. These systems may achieve the global deterministic attractor (GDA) due to the traveling wave propagation in which the more stable steady state expands. Interestingly, as we discussed in this study, in bistable systems these two attractors (i.e. GSA and GDA) can be different.

We studied analytically the one-dimensional birth–death process for which potential and temperature fields may be constructed. In such a case, the GDA is defined by the global minimum of the potential, while the GSA can be in any of the potential minima for a particular temperature profile. As an example, we consider the bistable kinase auto-activation model in the open compartment, such that the active kinase can flow in and out of the compartment. Even in the case when the in-flux and out-flux are equal and do not influence the deterministic mass rate equation and the related potential, they control the temperature profile, and as a consequence, the GSA. When the in-flux and out-flux increase (which can be interpreted as the increase of kinase diffusivity), the temperature grows and its profile becomes uniform, and in the infinite flux limit the GSA is determined by the global minimum of the potential, i.e. it collocates with the GDA. This finding allows us to put forward the hypothesis that in stochastic spatially extended biochemical reactors the relative stability of attractors is governed by the substrate diffusivity and size of the compartment. When for a given diffusion, the reactor is small enough to be considered as perfectly mixed, the system of interacting molecules converges to the GSA. In a much larger reactor, in which traveling waves can be formed, the same system converges to GDA.

We confirmed this hypothesis by performing KMC simulations for the kinase–phosphatase system, in the parameter range in which the GSA is located in the inactive steady state, while the GDA is located in the active steady state (figure 6). Accordingly, we found that the kinase–phosphatase system simulated in a small toroidal compartment remains in a mostly inactive state (figure 7), while the same system simulated in a long cylindrical compartment is activated due to the traveling wave propagation and remains active (figure 8).

In summary, we found that the relative stability of attractors in bi- (or multi-)stable systems is controlled by the diffusivity of substrates and the size of the compartment. These two parameters can be controlled and modified in cell evolution. Buffers, extracellular ligands, can control diffusivity of cytoplasmic or membrane proteins. The effective size of the reactor can be modified by plasma membrane deformation, formation of lipid rafts and other barriers. It is thus tempting to speculate that cells may employ these mechanisms for their activation or inactivation. Such modes of activation may be relevant in immune cell signaling, which requires the aggregation of membrane receptors.

#### Appendix

##### A.1. Temperature derivation based on the Fokker–Planck approximation.

To derive temperature Bialek [20] used the Fokker–Planck (or diffusion) approximation of the Master equation (5), see e.g. [30],

$$\frac{\partial p(x, t)}{\partial t} = \frac{\partial}{\partial x} \left( \frac{dU(x)}{dx} p(x, t) \right) + \frac{\partial^2}{\partial x^2} \left( \frac{\lambda(x) + \mu(x)}{2V} p(x, t) \right). \quad (\text{A.1})$$

In the stationary case the above equation can be solved explicitly:

$$p(x) = p_0 \frac{2V}{\lambda(x) + \mu(x)} \times \exp \left[ - \int_0^x \frac{dU(x')}{dx'} \frac{2V}{\lambda(x') + \mu(x')} dx' \right]. \quad (\text{A.2})$$

It is known, however, that the Fokker–Planck approximation obtained by truncating the Kramers–Moyal expansion after the second term is not a satisfactory approximation for bistable systems [40]. As a result, the SPD  $p(x)$  given by (A.2) differs from the ‘exact’  $p(x)$  obtained directly from the stationary Master equation in the  $V \rightarrow \infty$  limit, (9) and (10). In particular, equation (A.2) may lead to the incorrect determination of the GSA. In equation (A.1)  $\Gamma(x) = k_B T(x) = \frac{\lambda(x) + \mu(x)}{2V}$  is the diffusion coefficient. Thus the effective temperature is (Bialek writes it simply as  $T_{\text{eff}} = (\lambda(x) + \mu(x))/2$ )

$$\tilde{T}(x) = \frac{\lambda(x) + \mu(x)}{2k_B V}. \quad (\text{A.3})$$

Our and Bialek’s expressions for temperature converge in the limit  $|\lambda(x) - \mu(x)|/(\lambda(x) + \mu(x)) \rightarrow 0$ , i.e. in the steady states of (2). The main difference between Bialek’s and our expression is that  $T(x)$  defined by (13) vanishes when either  $\lambda(x)$  or  $\mu(x)$  is zero, that is when the direction of motion is deterministic, while  $\tilde{T}(x)$  vanishes when both birth and death rates are zero, i.e. there is no motion at all. Points in which  $T(x) = 0$  bound absorbing regions for the original Markov process; however, these points state no barrier when the process is considered in the diffusion approximation. This intuitively explains the observation by Hänggi *et al* [40] that the Fokker–Planck approximation overestimates transition rates between steady states. For that reason we prefer our definition. Finally, let us recall that Ross *et al* and Chu *et al* [16, 19] considered  $\Phi(x)$  given in (10) as a ‘stochastic potential’, which leads to a constant temperature equal to  $1/(k_B V)$ . In a sense our approach is equivalent to that of Ross *et al*, i.e. our temperature (13) combined with deterministic potential  $U(x)$  gives the same SPD as Ross’ temperature and stochastic potential  $\Phi(x)$ .

#### A.2. Each of the minima of the potential $U(x)$ may become a global attractor for a particular noise characteristic.

Two stochastic processes, characterized by B–D rates  $\lambda(x)$ ,  $\mu(x)$  and  $\lambda^*(x) = \lambda(x) + f(x)$ ,  $\mu^*(x) = \mu(x) + f(x)$  have the same deterministic mass rate equation, but are associated with different temperature fields and thus have different SPDs. In particular, let us consider the case in which (2) has three steady states  $x_1 < x_2 < x_3$ , such that  $x_1$  and  $x_3$  are stable and  $x_2$  is unstable. This implies that  $W(x) = \lambda(x) - \mu(x) < 0$  on  $(x_1, x_2)$  and  $W(x) > 0$  on  $(x_2, x_3)$ . Without loss of generality we may assume that for the process characterized by transitions  $\lambda(x)$  and  $\mu(x)$ , the function  $\Phi(x)$  has the global minimum in  $x_1$ , and thus the SPD of this process converges to  $\delta(x_1)$ . We will demonstrate that there exists a function  $f(x)$  such that the SPD of the B–D process with transitions  $\lambda(x) + f(x)$  and  $\mu(x) + f(x)$  converges to  $\delta(x_3)$ . The function  $f(x)$  must thus

satisfy

$$\Phi^*(x_3) - \Phi^*(x_1) = - \int_{x_1}^{x_3} \log \frac{\lambda(x) + f(x)}{\mu(x) + f(x)} dx < 0, \quad (\text{A.4})$$

which holds when

$$\left| \int_{x_1}^{x_2} \log \frac{\lambda(x) + f(x)}{\mu(x) + f(x)} dx \right| < \int_{x_2}^{x_3} \log \frac{\lambda(x) + f(x)}{\mu(x) + f(x)} dx. \quad (\text{A.5})$$

The last inequality holds when

- (i)  $f(x)$  is sufficiently large on  $(x_1, x_2)$  and equals zero elsewhere, that is equivalent to the increase of  $T(x)$  in the attraction basin of  $x_1$ , or
- (ii)  $f(x)$  is negative on  $(x_2, x_3)$  and equals zero elsewhere, and the new death rate  $\mu^*(x) < \lambda^*(x)$  is sufficiently small on  $(x_2, x_3)$ . Such a choice of  $f(x)$  is equivalent to the decrease of  $T(x)$  in the basin of  $x_3$ . In particular, we can take  $f(x)$  such that  $\min \mu^*(x) = 0$  on  $(x_2, x_3)$ . In such a case the system is no longer ergodic, and the domain  $x > x_{\min}$  (where  $\mu^*(x_{\min}) = 0$ ) is absorbing.

We thus demonstrated that in the bistable B–D process, the SPD in the zero noise limit (generically) converges to the Dirac delta in one of the two minima of the corresponding potential  $U(x)$ , but the choice of a particular minimum depends on the temperature field  $T(x)$  of the process. The proof for a multistable system is analogous. In the field of evolutionary games it has been shown similarly that the long-run behavior of a population depends on its size and the mutation intensity [41].

#### A.3. The parameter range in which the bimodal SPD is observed decreases to zero as the system volume diverges to infinity.

The bimodal probability distributions are typically associated with bistability. This is true when the magnitude of noise is sufficiently large, i.e. when the volume of the system is sufficiently small. However, when the system volume grows, the bimodal distribution is replaced by the unimodal distribution concentrated around the most stable steady state or the GSA. As shown in figure 9, the parameter range in which the bimodal SPD  $p(x)$  associated with the process (14) is observed decreases to zero as  $1/V$ . By the bimodal SPD in this context we understand  $p(x)$  that satisfies

$$0.1 < \int_0^{x_2} p(x) < 0.9. \quad (\text{A.6})$$

#### Acknowledgments

We would like to thank an anonymous referee for constructive comments which helped us to improve the paper. This research was funded by the following grants: Foundation for Polish Science grant TEAM/2009-3/6, Polish Ministry of Science and Higher Education grant no. N501 132 936 and NSF/NIH grant no. R01-GM086 885.

## References

- [1] Becskei A, S eraphin B and Serrano L 2001 Positive feedback in eukaryotic gene networks: cell differentiation by graded to binary response conversion *EMBO J.* **20** 2528–35
- [2] Ferrell J E Jr 2002 Self-perpetuating states in signal transduction: positive feedback, double-negative feedback and bistability *Curr. Opin. Cell. Biol.* **14** 140–8
- [3] Ptashne M 2004 *A Genetic Switch: Phage Lambda Revisited* (Cold Spring Harbor, NY: Cold Spring Harbor Laboratory Press)
- [4] Chatterjee A, Kaznessis Y N and Hu W S 2008 Tweaking biological switches through a better understanding of bistability behavior *Curr. Opin. Biotechnol.* **19** 475–81
- [5] Sprinzak D, Lakhnpal A, LeBon L, Santat L A, Fontes M E, Anderson G A, Garcia-Ojalvo J and Elowitz M B 2010 Cis-interactions between Notch and Delta generate mutually exclusive signalling states *Nature* **465** 86–90
- [6] Acar M, Becskei A and van Oudenaarden A 2005 Enhancement of cellular memory by reducing stochastic transitions *Nature* **435** 228–32
- [7] Lu T, Hasty J and Wolynes P G 2006 Effective temperature in stochastic kinetics and gene networks *Biophys. J.* **91** 84–94
- [8] Zhang Q, Bhattacharya S, Kline D E, Crawford R B, Conolly R B, Thomas R S, Kaminski N E and Andersen M E 2010 Stochastic modeling of B lymphocyte terminal differentiation and its suppression by dioxin *BMC Syst. Biol.* **4** 40
- [9] Ogasawara H and Kawato M 2010 The protein kinase M $\zeta$  network as a bistable switch to store neuronal memory *BMC Syst. Biol.* **4** 181
- [10] Lipniacki T, Hat B, Faeder J R and Hlavacek W S 2008 Stochastic effects and bistability in T cell receptor signaling *J. Theor. Biol.* **254** 110–22
- [11] Puszynski K, Hat B and Lipniacki T 2008 Oscillations and bistability in the stochastic model of p53 regulation *J. Theor. Biol.* **254** 452–65
- [12] Hat B, Kazmierczak B and Lipniacki T 2011 B cell activation triggered by the formation of the small receptor cluster: a computational study *PLoS Comput. Biol.* **7** e1002197
- [13] Song C, Phenix H, Abedi V, Scott M, Ingalls B P, K ern M and Perkins T J 2010 Estimating the stochastic bifurcation structure of cellular networks *PLoS Comput. Biol.* **6** e1000699
- [14] Keizer J 1978 Maxwell-type constructions for multiple nonequilibrium steady states *Proc. Natl Acad. Sci. USA* **75** 3023–6
- [15] Vellela M and Qian H 2009 Stochastic dynamics and non-equilibrium thermodynamics of a bistable chemical system: the Schl ogl model revisited *J. R. Soc. Interface* **6** 925–40 PMID: 19095615
- [16] Ross J, Hunt K L C and Hunt P M 1988 Thermodynamics far from equilibrium: reactions with multiple stationary states *J. Chem. Phys.* **88** 2719–29
- [17] Ge H and Qian H 2009 Thermodynamic limit of a nonequilibrium steady state: Maxwell-type construction for a bistable biochemical system *Phys. Rev. Lett.* **103** 148103
- [18] Ross J, Hunt K L C and Hunt P M 1992 Thermodynamic and stochastic theory for nonequilibrium systems with multiple reactive intermediates: the concept and role of excess work *J. Chem. Phys.* **96** 618–29
- [19] Chu X, Ross J, Hunt P M and Hunt K L C 1993 Thermodynamic and stochastic theory of reaction-diffusion systems with multiple stationary states *J. Chem. Phys.* **99** 3444–54
- [20] Bialek W 2000 Stability and noise in biochemical switches arXiv:cond-mat/0005235
- [21] Murray J D 2003 *Mathematical Biology* (New York: Springer)
- [22] Matheson I, Walls D F and Gardiner C W 1975 Stochastic models of first-order nonequilibrium phase transitions in chemical reactions *J. Stat. Phys.* **12** 21–34
- [23] Nicolis G and Lefever R 1977 Comment on the kinetic potential and the Maxwell construction in non-equilibrium chemical phase transitions *Phys. Lett. A* **62** 469–71
- [24] Barndorff-Nielsen O E and Cox D R 1989 *Asymptotic Techniques for Use in Statistics* (London: Chapman and Hall)
- [25] Schl ogl F 1971 On thermodynamics near a steady state *Z. Phys. A* **248** 446–58
- [26] Hornos E M, Schultz D, Innocentini G C P, Wang J, Walczak A M, Onuchic J N and Wolynes P G 2005 Self-regulating gene: an exact solution *Phys. Rev. E* **72** 051907
- [27] Feng H, Han B and Wang J 2011 Adiabatic and non-adiabatic non-equilibrium stochastic dynamics of single regulating genes *J. Phys. Chem. B* **115** 1254–61
- [28] Morelli M J, Allen R J, Tanase-Nicola S and ten Wolde P R 2008 Eliminating fast reactions in stochastic simulations of biochemical networks: a bistable genetic switch *J. Chem. Phys.* **128** 045105
- [29] Frigola D, Casanellas L, Sancho J M and Iba es M 2012 Asymmetric stochastic switching driven by intrinsic molecular noise *PLoS ONE* **7** E31407
- [30] Van Kampen N G 2007 *Stochastic Processes in Physics and Chemistry* (Amsterdam: Elsevier)
- [31] Groot S R and Mazur P 1962 *Non-Equilibrium Thermodynamics* (Amsterdam: North-Holland)
- [32] Walczak A M, Mugler A and Wiggins C H 2012 Analytic methods for modeling stochastic regulatory networks *Computational Modeling of Signaling Networks (Methods in Molecular Biology vol 880)* ed M Betterton and X Liu (New York: Humana)
- [33] Feng H D and Wang J 2011 Correlation function, response function and effective temperature of gene networks *Chem. Phys. Lett.* **510** 267–72
- [34] Wilhelm T 2009 The smallest chemical reaction system with bistability *BMC Syst. Biol.* **3** 90
- [35] Roskoski R Jr 2005 Src kinase regulation by phosphorylation and dephosphorylation *Biochem. Biophys. Res. Commun.* **331** 1–14
- [36] Bradshaw J M 2010 The Src, Syk, and Tec family kinases: distinct types of molecular switches *Cell. Signal.* **22** 1175–84
- [37] Markevich N I, Hoek J B and Kholodenko B N 2004 Signaling switches and bistability arising from multisite phosphorylation in protein kinase cascades *J. Cell. Biol.* **164** 353–9
- [38] Gilfillan A M and Rivera J 2009 The tyrosine kinase network regulating mast cell activation *Immunol. Rev.* **228** 149–69
- [39] Stamatakis M and Vlachos D G 2011 Equivalence of on-lattice stochastic chemical kinetics with the well-mixed chemical master equation in the limit of fast diffusion *Comput. Chem. Eng.* **35** 2602–10
- [40] H anggi P, Grabert H, Talker P and Thomas H 1984 Bistable systems: master equation versus Fokker–Planck modeling *Phys. Rev. A* **29** 371–378
- [41] Miekisz J 2005 Equilibrium selection in evolutionary games with random matching of players *J. Theor. Biol.* **232** 47–53

V) Kočańczyk M, Jaruszewicz J, Lipniacki T, *Stochastic transitions in a bistable reaction system on the membrane*, Journal of the Royal Society Interface, (Royal Society Publishing), 10(84): 20130151, 2013.

## Research



**Cite this article:** Kočańczyk M, Jaruszewicz J, Lipniacki T. 2013 Stochastic transitions in a bistable reaction system on the membrane. *J R Soc Interface* 10: 20130151.  
<http://dx.doi.org/10.1098/rsif.2013.0151>

Received: 15 February 2013

Accepted: 11 April 2013

### Subject Areas:

biophysics, systems biology,  
computational biology

### Keywords:

multi-stability, Markov process, spatially extended system, kinetic Monte Carlo on the lattice, kinase autophosphorylation, cell signalling

### Author for correspondence:

Tomasz Lipniacki  
e-mail: [tlipnia@ippt.gov.pl](mailto:tlipnia@ippt.gov.pl)

Electronic supplementary material is available at <http://dx.doi.org/10.1098/rsif.2013.0151> or via <http://rsif.royalsocietypublishing.org>.

# Stochastic transitions in a bistable reaction system on the membrane

Marek Kočańczyk<sup>1</sup>, Joanna Jaruszewicz<sup>1</sup> and Tomasz Lipniacki<sup>1,2</sup>

<sup>1</sup>Institute of Fundamental Technological Research, Polish Academy of Sciences, Warsaw 02106, Poland

<sup>2</sup>Department of Statistics, Rice University, Houston, 77005 TX, USA

Transitions between steady states of a multi-stable stochastic system in the perfectly mixed chemical reactor are possible only because of stochastic switching. In realistic cellular conditions, where diffusion is limited, transitions between steady states can also follow from the propagation of travelling waves. Here, we study the interplay between the two modes of transition for a prototype bistable system of kinase–phosphatase interactions on the plasma membrane. Within microscopic kinetic Monte Carlo simulations on the hexagonal lattice, we observed that for finite diffusion the behaviour of the spatially extended system differs qualitatively from the behaviour of the same system in the well-mixed regime. Even when a small isolated sub-compartment remains mostly inactive, the chemical travelling wave may propagate, leading to the activation of a larger compartment. The activating wave can be induced after a small subdomain is activated as a result of a stochastic fluctuation. Such a spontaneous onset of activity is radically more probable in subdomains characterized by slower diffusion. Our results show that a local immobilization of substrates can lead to the global activation of membrane proteins by the mechanism that involves stochastic fluctuations followed by the propagation of a semi-deterministic travelling wave.

## 1. Introduction

Living cells receive stimuli and process information with a circuitry of interacting genes and proteins. From the mathematical perspective, cell fates can be identified with attractors of the dynamical system defined by the interaction network [1]. Accordingly, cellular decisions correspond to transitions between multiple steady states of this dynamical system [2], allowing for phenotypical differentiation of genetically uniform cells [3]. Remarkably, many key biological regulatory and signalling modules are controlled by bistable switches, often leading to binary cellular responses of crucial importance, such as death or survival, senescence or proliferation [4,5]. In this work, we consider state-to-state transitions leading to the activation of proteins diffusing on the plasma membrane.

### 1.1. State-to-state transitions in homogeneous and heterogeneous reactors

Transitions between steady states in the perfectly mixed chemical reactor are possible only because of stochastic switching. (The classic monographs on stochastic processes covering material used in this study are those by van Kampen [6], Gardiner [7] and Nicolis & Prigogine [8].) In well-mixed reactors, however, the expected time to switch  $\tau$  depends exponentially on the system size,  $\tau \propto \exp(\alpha V)$ ,  $\alpha > 0$ , assuming a constant concentration of molecules  $N/V$  [9]. The number of reacting molecules in the plasma membrane is of order  $N = 10^3$  to  $10^5$  [10,11], implying an infinitesimal rate of switching between macroscopic states of activity and inactivity in the well-mixed approximation. In spatially extended reactors, the characteristic size of the well-mixed subcompartment is effectively controlled by diffusion. Relatively small diffusion coefficients of membrane proteins,  $D \approx 10^{-2}$  to  $10^{-1} \mu\text{m}^2 \text{s}^{-1}$  [12,13], coinciding with fast reaction rate constants of order  $c \approx 1/\text{s}$  [14] imply a correlation length  $\lambda \propto \sqrt{D/c}$  shorter than  $1 \mu\text{m}$ . The membrane can be therefore heterogeneous without any molecular

structure imposed by cytoskeletal corrals, protein scaffolds or lipid rafts. In stochastic spatially extended bistable systems, the diffusion-limited number of interacting molecules controls the transition rates between macroscopic states. Interestingly, even when in the deterministic approximation a system is monostable, the volume of the well-mixed stochastic reactor can serve as a ‘bifurcation parameter’ controlling the emergence of noise-induced bimodality [15].

In deterministic spatially extended reactors, transitions between steady states of bistable systems can result from the propagation of heteroclinic travelling waves. (See the book by Murray [16] for an extensive introduction.) A local state-to-state transition can initiate the propagation of a travelling front driving the whole system towards the ‘more stable’ steady state, in which the system would eventually persist. Crucially, for a bistable birth–death process, the deterministically preferred steady state (global deterministic attractor) can be different from the steady state in which the stationary probability distribution (SPD) concentrates (global stochastic attractor) [17,18]. For gradient systems, the macroscopic (deterministic) state-coexistence line in the parameter space is obtained for the potential which exhibits minima of equal depth. In spatially extended systems, this coexistence line corresponds to standing heteroclinic wave solutions. The stochastic state-coexistence line results from the solution of the (stochastic) chemical master equation, and in particular cases can be found analytically in the limit of zero noise by the Maxwell-type construction [19]. This implies that the spatially extended reactor may remain in a stochastically preferred steady state until a local but sufficiently large fluctuation initiates a semi-deterministic transition of the whole reactor to the state preferred in the deterministic approximation [20].

Simulations of Newtonian hard sphere dynamics provided evidence [21] that in the bistable perfectly stirred system the global attractor is correctly defined by the (stochastic) master equation, while using the Fokker–Planck equation with either linear (additive) or nonlinear (multiplicative) noise may lead to incorrect predictions [9]. Baras *et al.* [21] used the Bird’s direct simulation Monte Carlo method [22] to study the chemical kinetics in a homogeneous Boltzmann gas by associating the entire system volume with a single collisional cell. The method was proposed to perform simulations of rarified gas for which the Knudsen number is greater than 1, which is equivalent to the assumption of perfect homogeneity. By employing on-lattice kinetic Monte Carlo (KMC) simulations, we recapitulate here this result in the infinite diffusion limit (see [23]). We will demonstrate, however, that in reactors characterized by finite diffusion the global attractor can be prescribed either through the deterministic or through the stochastic approach, depending on the diffusion coefficient. Interestingly, the deterministic description in which the system is modelled by means of reaction–diffusion equations predicts the same global attractor as that obtained in the Langevin approach based on the macroscopic (deterministic) law of evolution into which an external additive noise term is incorporated. This places the discrepancy between the master equation and the diffusion approximation in the new context.

## 1.2. State-to-state transitions in biological membrane systems

The highly organized structure of cells, comprising zones of confinement [24,25] or altered motility [26–28], should

allow signalling systems to employ intricately both transition modes, i.e. stochastic switching and semi-deterministic travelling wave propagation. Thus far, selected aspects of these phenomena have been investigated in the context of membrane-proximal signalling and spontaneous cell polarization. It has been shown that the self-recruitment of cytoplasmic proteins to the cell membrane leads to the generation of a single cluster of active molecules and thus may define a unique axis of cell polarity [29]. A local increase in the density of molecules in the presence of positive feedback is able to work as an activating switch [30]. In the context of Ras nanoswitches, it has been demonstrated that at uniform slow motility the sole positive feedback in the interaction network of membrane-anchored proteins generates expanding activity patches [31]. In excitable networks, transient clans of activated molecules emerge and vanish spontaneously, even without directional spatial cues [32,33]. Spatio-temporal oscillations of membrane-recruited Min proteins in *Escherichia coli* were demonstrated to be enabled by the inherent noise [34]; on the other hand, macroscopically stable homogeneous oscillations can be abolished by local fluctuations, depending critically on the size and dimensionality of the reactor [35]. In stimulated thin neuronal protrusions, it has been observed that slowly diffusing autocatalytic CaMKII kinases exhibit pulsatile compartmentalized activity [36]; a spatially extended bistable system can spontaneously generate subregions, where different steady states dominate [37]. Self-organized foci of activity can generate activating travelling waves [38]. Propagation of waves can give rise to long-lasting cell polarity when the fast-diffusing inhibitor accumulates proportionally to the amount of slow-diffusing activated molecules so that the wavefront can be stalled. This mechanism, known as wave pinning, has been investigated for bistable systems [39,40]. When the diffusion coefficient of the inhibitor is very large (in principle, infinite), the mechanism of polarization is known as the local excitation, global inhibition [41,42].

## 1.3. Overview of results

In order to provide a comprehensive view and to be able to recognize new mechanisms of macroscopic state-to-state transitions available in spatially extended systems, we study a generic bistable system of membrane-bound autophosphorylating kinases and phosphatases by means of KMC simulations on the hexagonal lattice. These simulations are compared with the simulations of the Markov process in the perfectly mixed reactor and with the deterministic approximation, i.e. reaction–diffusion partial differential equations (PDEs).

In the limit of infinite diffusion, unsurprisingly, the SPD in the spatial on-lattice KMC simulations converges to the SPD obtained from Gillespie algorithm simulations of the well-mixed system. For slower diffusion, however, we observe that the SPD is qualitatively different from the case of the perfectly mixed system; specifically, the bimodality can emerge or vanish. We demonstrate that the probability mass fraction concentrated in the stochastically and deterministically preferred steady states depends on the speed of diffusion and properties of the reactor, such as volume and shape. We show that the state-to-state transitions in large reactors can follow from the propagation of semi-deterministic travelling waves. These waves can be induced deterministically by the externally triggered state transition in a sub-volume of the spatially extended reactor; they can

also arise spontaneously as a result of local stochastic fluctuations. We found that the expected time to transition on the membrane grows exponentially with diffusivity. For a given diffusion coefficient, the expected time to transition increases exponentially with the volume of the reactor  $V$  as long as the reactor is perfectly mixed, and then it decreases as  $1/V$ . At slow diffusion, for some parameters, the reactor may exhibit a dynamical structure of perpetual local activations and inactivations, and refrain from assuming uniformly a single steady state. Finally, we identify a novel mechanism in which the coexistence of stochastic and deterministic effects can give rise to the global activation of membrane proteins in response to a localized cue.

## 2. Material and methods

### 2.1. Model

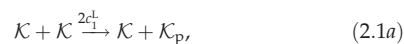
The analysed system of reactions involves two molecular species: kinases and phosphatases. Each kinase molecule contains two indistinguishable phosphorylation sites, hence it can assume three states: dephosphorylated, monophosphorylated or bisphosphorylated. The (auto)phosphorylation activity of a kinase increases with its phosphorylation level. Phosphatases are explicitly present in the system although they are not modified in any process.

The interaction network comprises the variant of the two-step phosphorylation–dephosphorylation motif, where kinases autophosphorylate one another and are dephosphorylated by phosphatases, which act non-specifically with respect to the level of phosphorylation of a substrate kinase [15,43]. The system encompasses the simplest case of the ubiquitous multi-site phosphorylation and exhibits bistability [44,45]. Since it consists of eight reactions, it may be viewed as far from minimal [46]; however, in contrast to other small bistable systems [47,48], all its reactions are bimolecular and elementary (i.e. only one of two reacting molecules changes its state), rendering the system appropriate for microscopic lattice-based simulations of diffusion-influenced reaction kinetics.

### 2.2. Reaction–diffusion system: kinetic Monte Carlo on the lattice

The spatial and stochastic simulations of the system are performed using the on-lattice KMC at the single molecule resolution. Molecules are allowed to hop between adjacent sites of a hexagonal lattice with propensity proportional to the diffusion coefficient. It is assumed that two molecules cannot occupy the same lattice site. Kinases  $\mathcal{K}$  and phosphatases  $\mathcal{P}$  can react only when in adjacent sites according to the following rules:

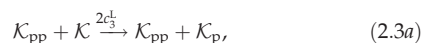
Phosphorylation by a dephosphorylated kinase:



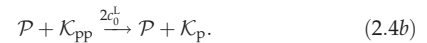
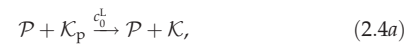
Phosphorylation by a monophosphorylated kinase:



Phosphorylation by a bisphosphorylated kinase:



Dephosphorylation (by a phosphatase):



The relative activity of a kinase increases strongly with its phosphorylation level:  $c_1 < c_2 < c_3$  (parameter values are given in the electronic supplementary material, table S1). Two molecules can diffuse away without reacting; on the other hand, a series of reactions involving two molecules is allowed, and such consecutive events are more probable at small diffusion coefficients when contacts last longer. The total numbers of kinases  $N_{\mathcal{K}}$  and phosphatases  $N_{\mathcal{P}}$  are constant in a simulation and their fractional surface concentrations (i.e. the fraction of lattice sites occupied by a species) are assumed to be  $\rho_{\mathcal{K}} = 0.4$  and  $\rho_{\mathcal{P}} = 0.1$ , respectively. For the sake of simplicity, we assume the same motility  $M$  of kinases and phosphatases; the propensity of hopping to a neighbouring empty site of a hexagonal lattice is  $M/6$ . We will consider both spatially uniform and non-uniform motility to account for subdomains of slower diffusion, e.g. large lipid rafts [27]. In a two-dimensional reactor, the macroscopic diffusion coefficient  $D$  depends on the total fractional concentration of membrane molecules  $\rho = \rho_{\mathcal{K}} + \rho_{\mathcal{P}}$  and the lattice constant  $\ell$ ,

$$D = \frac{(1-\rho)\ell^2 M}{4}. \quad (2.5)$$

The lattice constant is equal to the characteristic mean centre-to-centre spacing between neighbouring membrane proteins, which is of order  $\ell = 10$  nm [49].

### 2.3. Spatially homogeneous Markov process:

#### Gillespie algorithm

The Gillespie algorithm for KMC was employed for stochastic simulations in the limit of the perfectly mixed chemical reactor [50]. To provide a basis for the comparison of well-mixed Gillespie (superscript G) with on-lattice (superscript L) KMC simulations, kinetic rate constants  $c_1^G, c_2^G, c_3^G, c_0^G$  have to be rescaled according to the general rule

$$c_i^G = \frac{n_c}{V} c_i^L, \quad (2.6)$$

which reflects the fact that the propensity of each reaction in the perfectly mixed reactor is inversely proportional to the volume (or, here, surface) of the reactor  $V$  and is proportional to the number of possible contacts ( $n_c = 6$  for the hexagonal lattice). The scaling ensures that in the limit of  $M \rightarrow \infty$  the SPD obtained in on-lattice KMC simulations converges to that obtained with Gillespie KMC simulations (see the electronic supplementary material, figure S1c) [23].

### 2.4. Spatially extended deterministic approximation:

#### partial differential equations

We will also consider the deterministic limit of the on-lattice KMC described by a system of PDEs. For this approximation, kinetic rate constants  $c_1^L, c_2^L, c_3^L, c_0^L$  are scaled according to the following rules:

$$c_i = 6\rho_{\mathcal{K}} c_i^L =: \Omega_{\mathcal{K}} c_i^L \text{ for } i \in \{1, 2, 3\}, \quad (2.7a)$$

$$c_0 = 6\rho_{\mathcal{P}} c_0^L =: \Omega_{\mathcal{P}} c_0^L. \quad (2.7b)$$

These coefficients are used to parametrize dimensionless reaction–diffusion PDEs. Since we assume that the diffusion coefficient of kinase molecules is independent of their phosphorylation level, we may introduce fractional concentrations of dephosphorylated, monophosphorylated and bisphosphorylated kinases denoted by

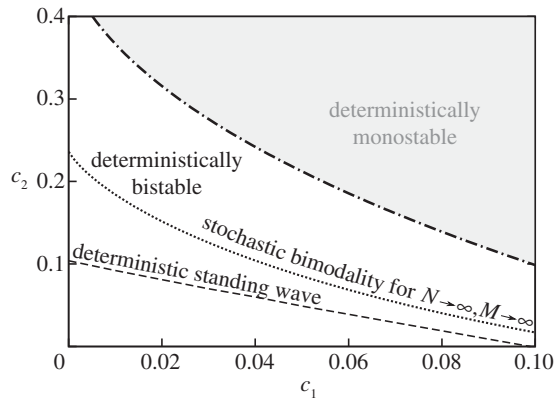


**Figure 1.** Bistability region of equations (2.8a–c) in the parameter space of  $(c_1, c_2)$ ; remaining parameters are fixed:  $c_3 = 4$  and  $c_0 = 1$ . The region is divided into two lines: the deterministic coexistence line (dashed), obtained numerically in COMSOL, and the stochastic coexistence line (dotted), obtained numerically as an approximate limit of curves determined for increasing numbers of molecules in the perfectly mixed regime. Above and below these lines global deterministic and stochastic attractors converge in the active and inactive steady state, respectively. Between these lines, the well-mixed stochastic system is preferentially inactive, while activating travelling waves may propagate.

$k$ ,  $k_p$  and  $k_{pp}$  ( $k + k_p + k_{pp} = 1$ ). The fraction of phosphorylated kinases,  $k_p + k_{pp}$ , will be considered as a measure of activity of the system. The resulting PDEs read as follows:

$$\frac{\partial k}{\partial t} = D\nabla^2 k + c_0 k_p - 2(c_1 k + c_2 k_p + c_3 k_{pp})k, \quad (2.8a)$$

$$\frac{\partial k_p}{\partial t} = D\nabla^2 k_p + 2(c_1 k + c_2 k_p + c_3 k_{pp})k + 2c_0 k_{pp} - (c_1 k + c_2 k_p + c_3 k_{pp})k_p - c_0 k_p, \quad (2.8b)$$

$$\frac{\partial k_{pp}}{\partial t} = D\nabla^2 k_{pp} + (c_1 k + c_2 k_p + c_3 k_{pp})k_p - 2c_0 k_{pp}. \quad (2.8c)$$

Evolution of the above system was simulated using the finite-element method implemented in COMSOL MULTIPHYSICS (Comsol Inc., Sweden).

For a certain range of parameters, equations (2.8a–c) exhibit bistability (figure 1). The stable steady state corresponding to a high and a low value of  $k_p + k_{pp}$  will be referred to as the active and the inactive state, respectively. For default parameters:  $c_0 = 1$ ,  $c_1 = 0.02$ ,  $c_3 = 4$  (see the electronic supplementary material, table S1) and  $c_2 = 0.2$ , in the active state  $k_p + k_{pp} = 0.86$  and in the inactive state  $k_p + k_{pp} = 0.07$  (see the electronic supplementary material, figure S1b).

## 2.5. Estimation of the stationary probability distribution for rarely switching systems

An important characteristic of (homogeneous or heterogeneous) stochastic bistable systems is the expected time to switch from one to the other steady state, or the mean first-passage time (MFPT). Numerical estimates of the MFPT for activation  $\tau_{on}$  and deactivation  $\tau_{off}$  can be obtained from running multiple (parallel) simulations with initial conditions in both basins of attraction. When switches are too rare to provide a reliable estimation of the SPD from a single trajectory, MFPTs allow one to quantify relative probabilities of finding a system in the basin of attraction of the active steady state  $p_{on} = \tau_{off}/(\tau_{on} + \tau_{off})$  and inactive steady state  $p_{off} = 1 - p_{on}$ .

If  $n$  independent simulations of the initially inactive system were running until finite times  $T_{1 \leq i \leq n}$ , it could happen that spontaneous activations were observed only in a fraction of

trajectories at times  $\tau_i \leq T_i$ . Then one can use the maximum-likelihood estimate for  $\tau_{on}$ ,

$$\tau_{on} = \sum_{i=1}^n \frac{\min(\tau_i, T_i)}{n_{on}}, \quad (2.9)$$

where  $n_{on}$  is the number of observed *on* switches [51];  $\tau_{off}$  can be estimated analogously.

## 3. Results

### 3.1. General considerations

We are interested primarily in macroscopic state-to-state transitions of a bistable reaction–diffusion Markov process on the membrane. Depending on the chemical reaction rate parameters, diffusion coefficients of molecules and the size of the domain, the process can be approximated by means of the perfectly mixed stochastic system, perfectly mixed deterministic system or the spatially extended deterministic system:

- The reactor can be considered as perfectly mixed when its diameter  $L$  is smaller than the characteristic distance  $\lambda$  travelled by a molecule in the characteristic time  $\tau_r$  between two subsequent reactions. In estimations of  $\lambda$  and  $\tau_r$ , we employ the rate constant  $c_0$ , because the dephosphorylation reaction is both relatively fast and density-independent ( $\rho_p$  is constant, while densities of kinases at a particular phosphorylation level evolve in time). We assign  $\tau_r = 1/c_0$  and obtain  $\lambda = 2\sqrt{D}\tau_r = 2\sqrt{D}/c_0$  [6,52]. When  $\lambda > L$ , the positions of a molecule subjected to subsequent reaction events can be regarded as uncorrelated.
- The process in the well-mixed reactor can be considered in the deterministic approximation when MFPTs of macroscopic state-to-state transitions are longer than the duration of other processes modifying the system; for instance, the duration of the cell cycle  $T$ . The characteristic MFPT  $\tau$  grows exponentially with the size of the well-mixed reactor [9],

$$\tau = \left(\frac{1}{c_0}\right) \exp(\rho_p V). \quad (3.1)$$

When  $\tau \gg T$ , the process can be considered as deterministic, in the sense that the chance for a stochastic transition in the considered time interval  $T$  is negligible.

- In the non-mixed reactor, the volume of the mixed subcompartment in two dimensions can be defined as  $V_0 = D/c_0$ . The characteristic transition time for such a sub-volume is

$$\tau_0 = \left(\frac{1}{c_0}\right) \exp(\rho_p V_0). \quad (3.2)$$

As we will see, a stochastic transition in any subcompartment, depending on parameters, may trigger travelling waves leading to the macroscopic state-to-state transition of the whole reactor. In large reactors for which  $V_0 < V$ , the MFPT for such locally induced transition  $\tau^*$  is given as the waiting time of  $V/V_0$  concurrent processes,

$$\tau^* = \left(\frac{V_0}{V}\right) \left(\frac{1}{c_0}\right) \exp(\rho_p V_0) = \left(\frac{V_0}{V}\right) \tau_0. \quad (3.3)$$

It is assumed here that the expected time to switch is much longer than the time of the wavefront propagation over the whole reactor, and that every local ignition can effectively give rise to a propagating front. When  $\tau^* \gg T$ , the process can be considered deterministic: the

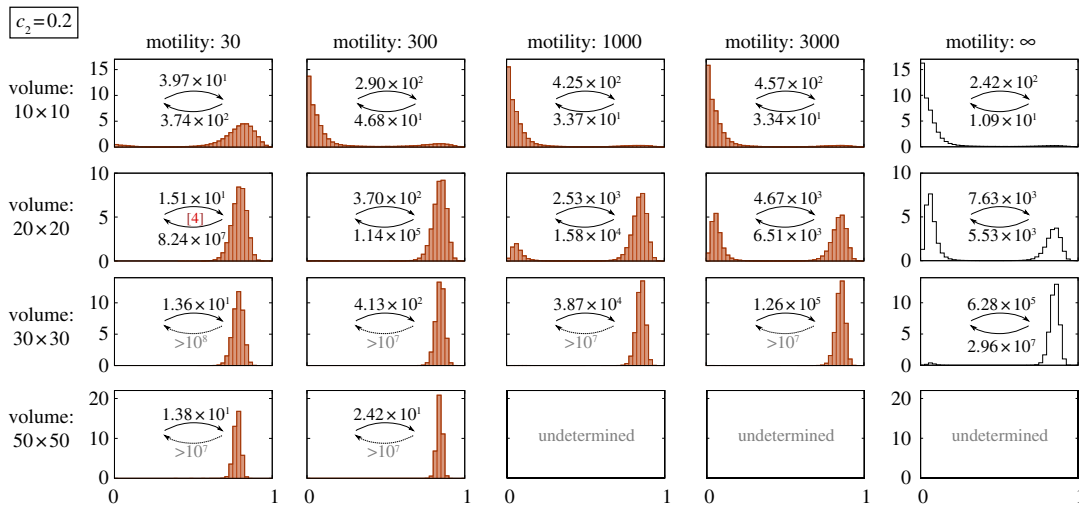


**Figure 2.** SPDs for different motility coefficients and square domains of different sizes. The lattice-based KMC simulations were performed on toroidal domains (i.e. square domains with periodic boundary conditions) for  $(c_1 = 0.02, c_2 = 0.2)$  and the remaining parameters with their default values:  $c_3 = 4, c_0 = 1$ . In the last column, SPDs were obtained using (spatially homogeneous) Gillespie algorithm simulations. The MFPTs  $\tau_{\text{on}}$  and  $\tau_{\text{off}}$  are shown in each panel. A small number in square brackets reports the number of observed switches  $n_{\text{on}}$  or  $n_{\text{off}}$  if smaller than 20. The SPD is marked as ‘undetermined’ when no switches were observed during simulations. (Online version in colour.)

chance for a stochastic state-to-state transition is negligible at the considered time scale.

Although in the above considerations we used  $D$ , in the further analysis of the on-lattice system the speed of diffusion will be expressed in terms of the motility  $M$ . According to equation (2.5), for default parameters in non-dimensionalized units  $M = 8D$ .

### 3.2. Different preferred steady states of the stochastic system and its deterministic approximation

The bistability domain of equations (2.8a–c) in the  $(c_1, c_2)$  parameter space for fixed  $c_3 = 4$  and  $c_0 = 1$  is shown in figure 1. The domain is divided by the  $c_2(c_1)$  line (dashed) on which the standing wave solutions exist. These heteroclinic solutions connect the active and inactive stable steady states. For parameters from above the dashed line, travelling waves propagate from the active to the inactive state. This can be interpreted as the domination of the active steady state. For parameters below the line, the travelling waves propagate in the opposite direction, i.e. the inactive state is dominant. This deterministic separatrix (dashed line) can be compared with the separatrix for the stochastic perfectly mixed system (dotted line). For parameters from the latter line the SPD of the perfectly mixed process described by reactions (2.1a–2.4b) remains bimodal in the limit of the infinite reactor volume. In the same limit, for parameters above (below) the line, the SPD converges to the Dirac delta in the active (inactive) steady state [17]. Interestingly, these two separatrices do not overlap and they delineate a region where the system of PDEs prefers the active state, while the stochastic perfectly mixed system in the limit of the infinite reactor volume is inactive. The divergence of these separatrices suggests that for realistic reactors characterized by a finite diffusion the choice between the active and the inactive state depends on the speed of diffusion and the size or even shape of the reactor [20].

### 3.3. Diffusion and size of the reactor control system activity

Here, we analyse the expected activity of the kinase–phosphatase system by means of the SPD obtained in on-lattice KMC simulations, as a function of the compartment volume (surface)  $V$  and reactants motility coefficient  $M$ . First, let us remember that when  $M \rightarrow \infty$  the SPD from on-lattice KMC simulations converges to that obtained from Gillespie KMC simulations ( $M = \infty$ ). For  $M = 3000$ , the difference is still discernible (last two columns in figure 2) but the agreement becomes nearly perfect for  $M = 10\,000$  (see the electronic supplementary material, figure S1c). In figure 2, we consider the case of  $(c_1 = 0.02, c_2 = 0.2)$ , for which the stochastic system and its deterministic approximation are preferentially in the active state. As shown, the probability of the active state increases with  $V$  for finite  $M$  as well as in the limit of the perfectly mixed reactor ( $M = \infty$ , last column in figure 2). For large motility ( $M \geq 300$ ), the active state probability increases from nearly 0 to almost 1 as the compartment volume increases from  $V = 10 \times 10$  to  $V = 30 \times 30$ . It demonstrates that the relative stability of steady states is controlled by the volume of the reactor. For perfectly mixed systems, this effect has been reported previously by Zheng *et al.* [53].

In figure 3, we consider a more interesting case of  $(c_1 = 0.02, c_2 = 0.15)$ , for which the stochastic perfectly mixed system is preferentially in the inactive state, but its deterministic approximation is preferentially active. In this case, in addition to the compartment volume, the activity of the system is controlled by the substrate motility  $M$ . For chosen parameters, the system is preferentially in the active state for small motility ( $M = 30$ ) and in the inactive state for large motility ( $M \geq 1000$ ). For intermediate values ( $100 \leq M \leq 300$ ), the choice of the dominant state is controlled by the volume of the reactor. The tendency of the system to inactivate as  $M \rightarrow \infty$  is visible also in figure 2, although it is pronounced only for small system volumes, for which the perfectly mixed system remains prevalently in the inactive state.

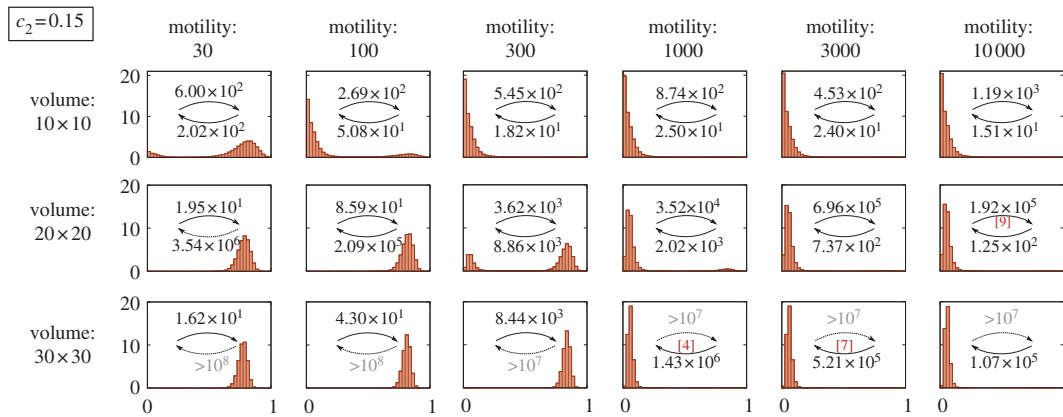


**Figure 3.** SPDs for different motility coefficients and square domains of different sizes. The simulations are in the same set-up as for figure 2 but with kinase activity coefficient  $c_2 = 0.15$  (instead of  $c_2 = 0.2$ ). (Online version in colour.)

In the subsequent analysis, we employ the mean first-passage time of the transition from the inactive to active steady state  $\tau_{\text{on}}$  and the time for the reverse transition  $\tau_{\text{off}}$ . At large substrate motility ( $M \geq 1000$ ), MFPTs (given in each panel of figures 2 and 3) increase dramatically with the volume of the compartment. It is known that in a perfectly mixed reactor MFPTs increase exponentially with its volume [9]. In the case of finite motility, the situation is more complicated. Let us consider the case of a fixed motility for which one can determine a characteristic distance  $\lambda$  and the well-mixed sub-volume  $V_0$ . When the reactor diameter exceeds  $\lambda$ , it should be considered as a composition of multiple ( $\approx V/V_0$ ) well-mixed sub-reactors. In such a structured reactor, the transition to the active steady state can result from a stochastic switch occurring in any of these sub-reactors, followed by the propagation of the activating wave, as discussed in §3.4. In this regime,  $\tau_{\text{on}}$  decreases with the number of well-mixed sub-compartments ( $\approx V/V_0$ ), and thus it is inversely proportional to the volume of the reactor,  $\tau_{\text{on}} \propto 1/V$ . These diverging limiting behaviours jointly result in the non-monotonic dependence of  $\tau_{\text{on}}$  on the volume of the reactor (figure 4a):  $\tau_{\text{on}}$  increases exponentially until the volume of the reactor  $V$  exceeds the volume of the well-mixed compartment  $V_0$ , and then decreases with the reactor volume as  $\tau_{\text{on}} \propto 1/V$ . Since larger motility implies larger perfectly mixed sub-volumes, the volume of the reactor for which the MFPT reaches its maximum increases with motility. The activation and inactivation processes are not symmetric, because for given parameters either activating or inactivating travelling waves may propagate. For the parameters considered in figure 4a, the activating travelling waves propagate. As a result, after a local inactivation, the activity is promptly recovered by waves from surrounding subcompartments, and thus the only possible mode of transition towards inactivity requires simultaneous inactivation of the whole reactor. Consequently, while  $\tau_{\text{on}}$  decreases for small motility ( $V > V_0$  regime) and increases for large motility ( $V < V_0$  regime),  $\tau_{\text{off}}$  grows exponentially with  $V$  in both regimes (figures 2 and 3).

Irrespective of the volume of the reactor and for both considered values of  $c_2$ , one can observe that for sufficiently low motility the active state is preferred. There are two properties of the system that give rise to such behaviour at decreased motility: (i) in addition to the less effective distributive mechanism, the more effective processive phosphorylation reactions are more likely to happen (when two kinase molecules stay in

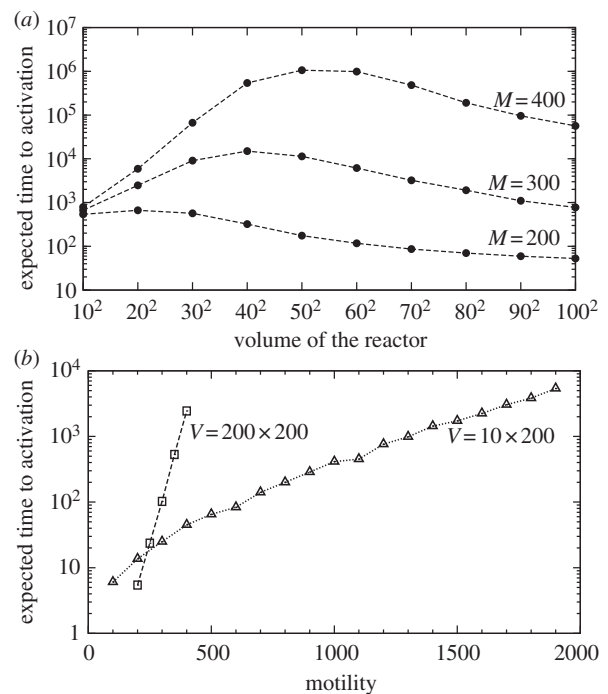


**Figure 4.** (a) Mean first-passage time for activation  $\tau_{\text{on}}$  as a function of the volume  $V$  of the square-shaped reactor with periodic boundary conditions, obtained in on-lattice KMC simulations for three values of motility and ( $c_1 = 0.02$ ,  $c_2 = 0.15$ ), and other parameters with default values. For small  $V$ ,  $\tau_{\text{on}}$  grows exponentially with  $V$  (well-mixed regime), while for large  $V$ ,  $\tau_{\text{on}}$  decreases as  $1/V$ . Every  $\tau_{\text{on}}$  is a maximum-likelihood estimate from a time series with fixed censoring time, calculated based on thousands of trajectories and at least  $n_{\text{on}} = 10$  observed switches. (b) Dependence of  $\tau_{\text{on}}$  on the motility  $M$  for reactors of two different geometries, for the same parameters as in (a). For the square-shaped reactor, the expected  $\tau_{\text{on}}$  grows exponentially with increasing motility  $M$ ; for the long rectangular reactor with periodic boundary conditions,  $\tau_{\text{on}}$  grows faster than  $\sim \exp(\sqrt{M})$  but slower than  $\sim \exp(M)$ .

contact longer, it is more probable that the substrate kinase will be phosphorylated twice by the same catalytic kinase; also, once the substrate kinase is phosphorylated it becomes more amenable to ‘fire back’ and to activate the first kinase) and (ii) the catalytic capacity of less abundant phosphatase molecules becomes dampened after they saturate their

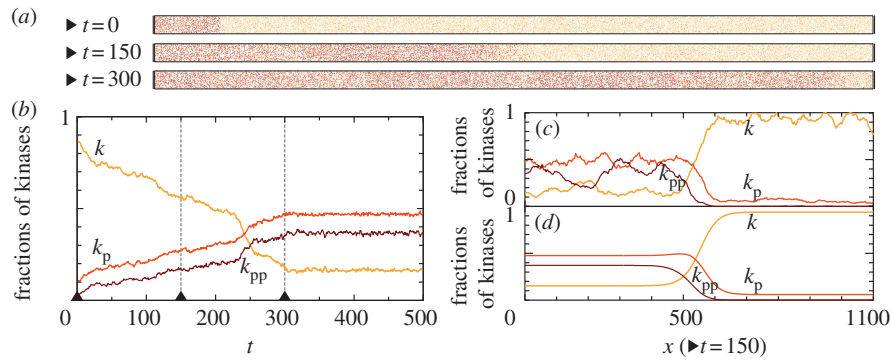


**Figure 5.** Kinase activity wave propagation on the cylindrical domain  $30 \times 1100$  for parameters ( $c_1 = 0.02$ ,  $c_2 = 0.15$ ) and  $M = 3000$ . At  $t = 0$ , a fragment of the cylinder ( $30 \times 100$ ) is in the active state. (a) Three snapshots from an on-lattice KMC simulation. (b) Time profile of the kinase activity profile integrated over the whole domain. (c) Kinase activity profile across the domain at time  $t = 150$ , averaged using the sliding window of width  $w = 11$ . (d) Kinase activity profile obtained from corresponding PDEs in COMSOL. (Online version in colour.)

neighbourhoods (a phosphatase molecule can dephosphorylate all kinases in its vicinity, rendering itself idle).

### 3.4. Propagation of waves of kinase activity on cylindrical domains

In this section, we consider travelling wave propagation on long cylindrical domains. Elongated thin membrane protrusions constitute, for example, pseudopodia of motile cells and dendritic spines of neurons. First, we focus on parameters ( $c_1 = 0.02$ ,  $c_2 = 0.15$ ) lying in the range in which the preferred steady states for well-mixed and spatially extended reactors diverge (figure 1). For these parameters and large motility,  $M = 3000$ , the  $30 \times 30$  reactor is principally inactive (figure 3). However, in a semi-one-dimensional array of a large number of such reactors the activating travelling waves can propagate as predicted by the deterministic approximation, equations (2.8a–c). In figure 5a, we show snapshots from on-lattice KMC simulations of the stochastic travelling wave in the cylindrical domain  $30 \times 1100$  (top–bottom boundary conditions are periodic, left–right reflecting). At  $t = 0$ , the left  $30 \times 100$  area (‘seed’) is assigned to be in the active steady state and the rest of the cylinder,  $30 \times 1000$ , is set to the inactive state. At the very beginning of the simulation, the transition between the active and the inactive region becomes smooth and a wave profile is formed, which then propagates so that eventually the whole reactor adopts the active steady state (figure 5a,b). This surprising divergence of system behaviours in a small  $30 \times 30$  and in a long  $30 \times 1100$  reactor is due to the fact that motility  $M = 3000$  renders the small reactor mixed, but it is by far too small to mix the longer reactor:  $30/2 < \lambda \ll 1100$ , where  $30/2$  is the effective diameter of the  $30 \times 30$  reactor in periodic boundary conditions, and  $\lambda = \sqrt{M/(2c_0)}$ . Therefore, in the long reactor, the system converges to the attractor preferred by the deterministic approximation. Moreover, since the number of molecules on the wavefront (the width of which grows  $\propto \sqrt{M/c_0}$ ) is quite large, the stochastic wave profile resembles the deterministic profile obtained from PDEs (figure 5c,d).

For parameters ( $c_1, c_2$ ) below the deterministic standing wave line (figure 1), the travelling wave can propagate in the opposite direction such that the whole system becomes inactive, provided that the diffusion is sufficiently fast, as discussed in §3.5 (see the electronic supplementary material, figure S6).

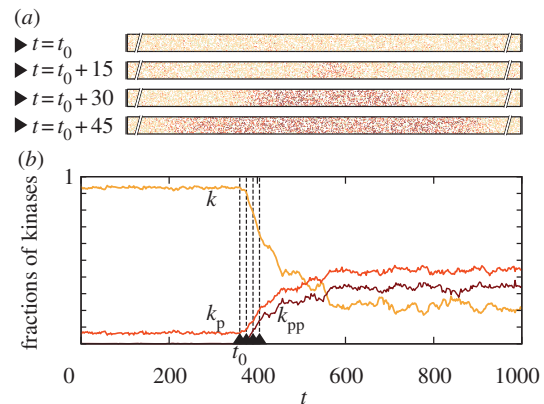


**Figure 6.** Spontaneous initiation of the activity wave in a subdomain of the cylindrical domain  $20 \times 1000$  for parameters ( $c_1 = 0.02$ ,  $c_2 = 0.15$ ) and  $M = 1000$ . The expected waiting time for the activation is  $\tau_{\text{on}} = 596$  s. (a) Four snapshots from an on-lattice KMC simulation (inessential parts of the reactor are truncated) and (b) time profile. (Online version in colour.)

With increasing motility, the velocity of the wave in on-lattice KMC simulations approaches the velocity in PDEs, which is  $\propto \sqrt{Mc_0}$  (see the electronic supplementary material, figure S3). The number of molecules on the length of the wavefront increases with motility and, as a consequence of the reduced noise, at higher motilities the activating front propagates more steadily. The size of the activating seed also increases with motility and at higher motilities seeds are more likely to be swept away (see the electronic supplementary material, figure S2). Consequently, as we will see in §3.5, at large motility the stochastic wave initiations are much less frequent: they need the creation of a larger seed, and thus the initiating stochastic fluctuation must involve a larger number of molecules.

### 3.5. Spontaneous wave activation

The two already discussed transition modes, the stochastic switching in a well-mixed system and semi-deterministic travelling wave propagation in a spatially extended system, can work in conjunction. The initially inactive system can be excited owing to a local fluctuation, which could in turn initiate an activating travelling wave. We investigate this mechanism in the system with ( $c_1 = 0.02$ ,  $c_2 = 0.15$ ) and  $M = 1000$  in the semi-one-dimensional reactor of  $V = 20 \times 1000$  (figure 6). A spontaneous local activation, occurring in

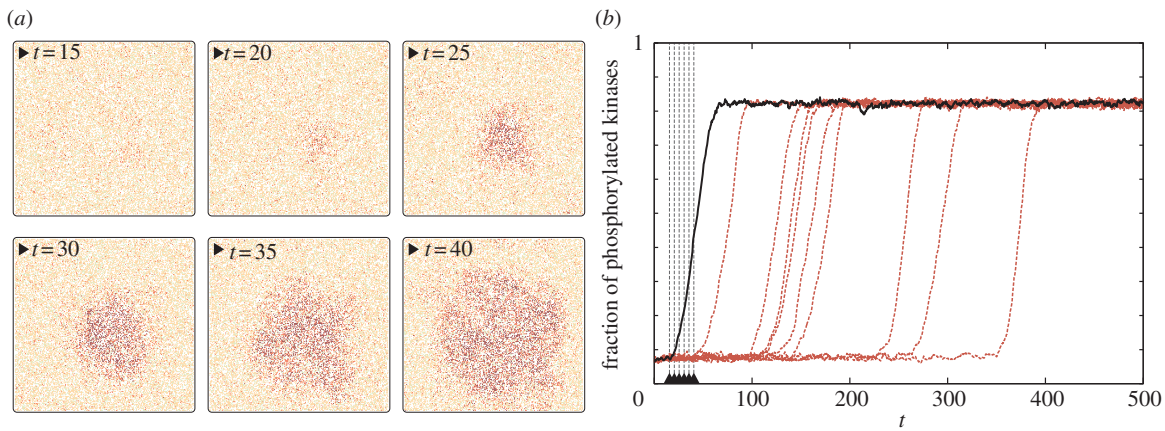


**Figure 7.** Spontaneous initiation of the activity wave on the square domain  $200 \times 200$  for parameters ( $c_1 = 0.02$ ,  $c_2 = 0.15$ ) and  $M = 300$ . For larger motility  $M = 1000$ , activity waves were not self-initiated. Snapshots in (a) correspond to the trajectory represented by the solid black line in (b). (Online version in colour.)

a random place of the reactor, gives rise to two fronts, which propagate in opposite directions, driving the whole reactor to the active state. The average time to switch on was estimated as  $\tau_{\text{on}}^{20 \times 1000} = 596$  (from  $n_{\text{on}} = 16$  switches). Based on the analysis in §§3.3 and 3.4, the activation mechanism can be understood as follows: the  $20 \times 1000$  reactor can be considered as an array of 50 smaller  $20 \times 20$  sub-reactors. These small sub-reactors switch on and off with switching times  $\tau_{\text{on}}^{20 \times 20} = 3.52 \times 10^4$ ,  $\tau_{\text{off}}^{20 \times 20} = 2.02 \times 10^3$  (figure 3). Thus, the expected time to switch on in the whole reactor can be estimated as  $\tau_{\text{on}} = \tau_{\text{on}}^{20 \times 20} / 50 = 700$ , which agrees (unexpectedly well) with the measured  $\tau_{\text{on}}^{20 \times 1000} = 596$ .

The same reasoning fails for a two-dimensional reactor of  $V = 200 \times 200$ . For the same parameters, a spontaneous activation was not observed in long simulations (with total simulation time  $\approx 2 \times 10^4$ ). In the two-dimensional case, the spontaneously appearing seeds of activity are extinguished by the inactive neighbourhood more easily than in the reactor of cylindrical geometry. The spontaneous activation was observed only after reducing motility to  $M = 300$  (figure 7).

Increasing motility increases the number of communicated molecules and thus reduces the switch rate:  $\tau_{\text{on}}$  grows exponentially with the motility in the case of the two-dimensional reactor (figure 4b). One could expect that  $\tau_{\text{on}}(M)$  for the one-dimensional reactor grows  $\propto \exp(\sqrt{M})$ . However, such dependence does not fit well to obtained data points, although it yields a better fit than  $\tau_{\text{on}} \propto \exp(M)$ . The divergence from the ' $\propto \exp(\sqrt{M})$ ' prediction can be due to the fact that in the cylindrical reactor  $\tau_{\text{on}}(M)$  spans the large range of motilities involving the change of the stochastically preferred steady state (figure 3).

The observation that the reduced motility increases the probability of system activation suggests that regions of reduced diffusivity can serve as ignition points for the activation of the whole reactor. We verified this hypothesis by performing simulations of the  $200 \times 200$  domain with a spatially varying diffusion coefficient. The overall motility was set to  $M = 1000$ , while in a circular region of  $r = 14$  motility was reduced 10 times to  $M_{\text{patch}} = 100$ . In order to minimize possible peculiarities caused by the sharp jump on the brink of the patch, the motility in its vicinity was increasing linearly, concentrically until reaching the outer circle of radius  $r' = r + 10$ , beyond which  $M = 1000$ . Within this set-up, we observed that

the patch of lowered diffusivity acts as an ignition centre: stochastic activation switches are much more probable in this region, and the local activation, with some probability, again, can start the semi-deterministic travelling wave (figure 8). As one can expect,  $\tau_{\text{on}}$  decreases sharply with the radius of the patch (see the electronic supplementary material, figure S7).

For completeness, it should be noted that, when the stochastic and deterministic global attractors coincide in the active state (which happens for parameters  $c_1$  and  $c_2$  above the stochastic bimodality curve in figure 1), the initially inactive system is more likely to be activated by local stochastic fluctuations: for small diffusion, the activating seeds plausibly appear in several places simultaneously, giving rise to several travelling fronts (see the electronic supplementary material, figure S4).

In the already considered case of ( $c_1 = 0.02$ ,  $c_2 = 0.06$ ) depicted in the electronic supplementary material, figure S6, the stochastic and deterministic global attractors coincide in the inactive state. In this case, simultaneous local inactivations can occur probably in various places of the compartment. To avoid spontaneous switching and illustrate the possibility of the propagation of the inactivating wave, we considered  $M = 10000$  in the wider  $50 \times 1100$  reactor, where stochastic switches are rare.

Interestingly, in the  $30 \times 1000$  toroidal domain at  $M = 300$ , the reactor is able to maintain a fractional activity (see the electronic supplementary material, figure S5). Since in the parameter space the point ( $c_1 = 0.02$ ,  $c_2 = 0.06$ ) is closer to the curve of the deterministic standing wave than point ( $c_1 = 0.02$ ,  $c_2 = 0.2$ ), it can be expected that for ( $c_1 = 0.02$ ,  $c_2 = 0.06$ ) inactivating travelling waves are not formed as easily as activating waves for ( $c_1 = 0.02$ ,  $c_2 = 0.2$ ). Hence, scattered local *on* or *off* switches do not propagate; they render the reactor dynamically yet persistently spatially structured. As a consequence, most of the probability mass is contained between stable steady states of the deterministic system, in contrast to all previously analysed cases.

## 4. Discussion

In this study, in order to understand the principal mechanisms of biochemical information processing and cellular

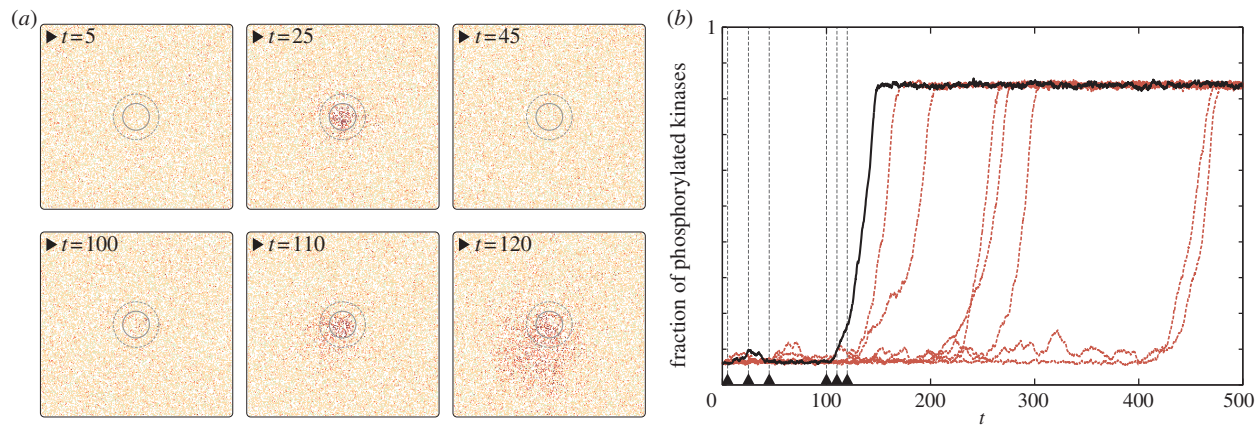


**Figure 8.** Activity wave initiation in the domain  $200 \times 200$  owing to the locally reduced motility coefficient ( $M = 100$  in the inner circle,  $M = 1000$  outside the outer circle, and gradually increasing  $M$  in between circles) for parameters ( $c_1 = 0.02$ ,  $c_2 = 0.15$ ). Snapshots in (a) correspond to the trajectory represented by the solid black line in (b). (Online version in colour.)

decision-making, we systematically investigated transition modes available to a generic bistable reaction system in the spatially extended reactor. We used primarily microscopic simulations on the two-dimensional lattice complemented by the analysis of approximations neglecting either stochasticity or spatial resolution. In the well-mixed compartment (the size of which is determined by the diffusion coefficient), the transition rates between macroscopic steady states of the system decrease exponentially with the number of reacting molecules or the size of the compartment. In larger, non-mixed compartments, transition rates are controlled by the number of diffusively communicated molecules, which is typically much smaller than the total number of molecules. We demonstrated that the local stochastic state-to-state transitions occasionally initiate travelling waves, which expand in the semi-deterministic manner leading to the (in)activation of the whole reactor: either a local activation or inactivation can be amplified spatially, depending on the reaction rate constants. At increasing diffusivity, more molecules become communicated and local transitions become less probable. On the other hand, travelling waves can propagate only when the diffusion is sufficiently fast. At large diffusion coefficients, the wavefronts are thicker, contain more molecules and thus are less affected by fluctuations. As a result, in the limit of large diffusion, the velocity of a wavefront in the discrete stochastic system converges to that of its deterministic approximation modelled by PDEs.

Importantly, there exists a range of parameters for which the macroscopic, stochastically preferred steady state (or global stochastic attractor, i.e. the state which is prevalently occupied in a perfectly mixed regime) is different from the steady state preferred deterministically (or global deterministic attractor, i.e. the state which expands as a result of the propagation of travelling waves) [17,20]. We demonstrated that in this range of parameters, even when a small compartment is predominantly inactive, a travelling wave may spread the active state over the larger reactor. If parameters are such that global stochastic and deterministic attractors converge (in either the active or inactive state), the system is effectively monostable, i.e. the escapes from the ‘less stable’ macroscopic steady state can arise spontaneously with a high probability. Consequently, the reactor settles in the more stable steady state or remains

spatially heterogeneous with its regions flipping between steady states, giving rise to transient clans of activated molecules [37]. Our macroscopic analysis thus implies that the well-known mechanism of state-to-state transitions arising in bistable reaction–diffusion systems is restricted only to the sub-domain of the bistability domain in the parameter space. Only these bistable systems which exploit in the parameter space the region of diverging stochastic and deterministic attractors are expected to be both resistant to spontaneous autoactivation (caused by stochastic switching) and sensitive to external stimuli (allowing for deterministic activation by means of the propagation of travelling waves). This physiologically relevant region in the parameter space (delineated by two separatrices in figure 1) grows with the increasing differences between reaction rate constants,  $c_1 < c_2 < c_3$ . We note that the catalytic activity of a kinase can grow with its phosphorylation level even stronger than is assumed in the analysed system, i.e. kinetic rate constants can span several orders of magnitude:  $c_1 \ll c_2 \ll c_3$  [54].

In living cells, travelling waves may be induced by an external stimulus; for example, upon binding of a specific extracellular ligand (antigen and chemoattractant) by membrane receptors. We demonstrated that partial immobilization of a tiny fraction of kinases on the membrane may lead to the global activation of the system. Since the locally constrained motility does not lead to a locally increased surface concentration of molecules, this activation mechanism is different from the recently proposed density-dependent switch [30]. In the mechanism introduced here, there is an inherent threshold number of activated clustered molecules required for triggering a travelling wave with a sufficiently high probability. It has been proposed theoretically and recently investigated numerically that a tiny fraction of membrane receptors clustered upon binding of antigens are capable of initiating immunogenic responses in B cells (see [55] and references therein). In other cases, proteins can become co-sequestered in lipid microdomains after the activation. Such confinement reduces their lateral diffusion and presumably facilitates subsequent signalling events [56].

We analysed exhaustively the SPD with respect to the diffusion coefficient and size of the reactor. In the context of the recruitment of cytoplasmic proteins to the membrane milieu,

Abel *et al.* [57] showed that decreasing motility or altering the depth of a submembrane layer promotes or suppresses SPD bimodality, depending on the topology of the interaction network. In their case, the unimodal distribution arises from averaging over the reactor and peaks between two steady states. In the system analysed in this study, the unimodality results from the preference of one of two steady states of the deterministic approximation. We showed that the SPD is controlled by both the motility of molecules and the volume of the reaction chamber. In our case, a single reaction rate parameter dictates the state to which the system converges at the increasing diffusivity. We found that, despite the system being bistable, the SPDs may be bimodal only in small well-mixed compartments. Large compartments have, generically, unimodal SPDs analogously to the perfectly mixed systems of large numbers of molecules [20,58].

In a spatially extended system, which in the case of slow diffusion can be considered as a composition of multiple well-mixed reactors, the expected time to activation has been shown to shorten with increasing volume, which is in stark contrast to a perfectly mixed reactor, for which the time increases exponentially with the volume. Furthermore, spatially extended reactors of similar volumes but different geometries can have vastly different expected times to activation. In a two-dimensional reactor, the minimal size of the 'nucleation centre' required for the initiation of a wave is larger than in a semi-one-dimensional reactor, and thus the expected time to the stochastic activation is longer. Propagation of waves is also dependent on the reactor geometry. In a semi-one-dimensional reactor, the front curvature is negligible, while in a two-dimensional reactor the curvature reduces the velocity of the travelling front, and may prohibit spreading of the wave when the initial cluster is too small [55].

Our work provides further evidence that biochemical reactions on the membrane can be reproduced only with spatial stochastic simulations. In addition to the discussed phenomena, in which local stochastic fluctuations lead to global state-to-state transitions not captured by deterministic reaction–diffusion equations, we found that in the discrete system the effective reaction rates are controlled by the diffusion. It can be observed that, in the case of slow

diffusion, the more effective processive phosphorylation mode prevails over the less efficient distributive mechanism, boosting the system's activity [59,60]. Additionally, molecular crowding (and self-crowding), which is reflected explicitly in our lattice-based simulations and is expected to be significant at assumed surface densities of reacting molecules, facilitates consecutive phosphorylation events [61,62]. In the well-mixed approximation, kinases are dephosphorylated at the rate proportional to the product of phosphatase activity and the number of phosphatases. Phosphatases, which are modelled explicitly in spatial simulations, can become unemployed after dephosphorylating all their neighbouring kinases, resulting in the reduction of their effective enzymatic activity [63].

The applied method of on-lattice KMC simulates the master equation in continuous time and discretized space at the single event and single molecule resolution. For large systems, such simulations are inevitably computationally demanding, but provide accurate estimations of MFPTs, which are crucial for the performed analysis. Spatially or temporally coarse-grained algorithms have lower computational cost but also lower, in fact unknown, accuracy. The results presented in this paper consumed years of aggregate CPU time of a computer cluster, but in the hope that they could be used to calibrate faster approximate algorithms.

In summary, transitions in a bistable system on the membrane employ both stochastic and deterministic effects. Transitions between macroscopic steady states of spatially extended systems are qualitatively different from transitions available in well-mixed compartments. These transitions employ travelling waves that can be initiated spontaneously as a result of stochastic fluctuations. We demonstrated that the SPD and MFPTs depend strongly on the diffusion coefficient, size and shape of the reactor. These factors (in addition to reaction rates) decide the activity (or inactivity) of a spatially extended bistable system.

This study was supported by the Foundation for Polish Science grant TEAM/2009-3/6 and Polish Ministry of Science and Higher Education grant no. N N501 13 29 36. Numerical simulations of on-lattice KMC were carried out at the Zeus computer cluster at the ACK Cyfronet AGH in Kraków and at the Grafen computer cluster of the Ochota Biocentre in Warsaw.

## References

- Huang S, Eichler G, Bar-Yam Y, Ingber DE. 2005 Cell fates as high-dimensional attractor states of a complex gene regulatory network. *Phys. Rev. Lett.* **94**, 128701. (doi:10.1103/PhysRevLett.94.128701)
- Ozbudak EM, Thattai M, Lim HN, Shraiman BI, Oudenaarden AV. 2004 Multistability in the lactose utilization network of *Escherichia coli*. *Nature* **427**, 737–740. (doi:10.1038/nature02298)
- Smits WK, Kuipers OP, Veening J-W. 2006 Phenotypic variation in bacteria: the role of feedback regulation. *Nat. Rev. Microbiol.* **4**, 259–271. (doi:10.1038/nrmicro1381)
- Ferrell JE. 2002 Self-perpetuating states in signal transduction: positive feedback, double-negative feedback and bistability. *Curr. Opin. Cell Biol.* **14**, 140–148. (doi:10.1016/S0955-0674(02)300314-9)
- Das J, Ho M, Zikherman J, Govern C, Yang M, Weiss A, Chakraborty AK, Roose JP. 2009 Digital signaling and hysteresis characterize Ras activation in lymphoid cells. *Cell* **136**, 337–351. (doi:10.1016/j.cell.2008.11.051)
- van Kampen N. 2007 *Stochastic processes in physics and chemistry*. Amsterdam, The Netherlands: Elsevier.
- Gardiner CW. 1985 *Handbook of stochastic methods for physics, chemistry and the natural sciences*, 2nd edn. Berlin, Germany: Springer.
- Nicolis G, Prigogine I. 1977 *Self-organization in non-equilibrium systems*. Hoboken, NJ: Wiley.
- Vellela M, Qian H. 2009 Stochastic dynamics and non-equilibrium thermodynamics of a bistable chemical system: the Schlögl model revisited. *J. R. Soc. Interface* **6**, 925–940. (doi:10.1098/rsif.2008.0476)
- Kasai RS, Suzuki KGN, Prossnitz ER, Koyama-Honda I, Nakada C, Fujiwara TK, Kusumi A. 2011 Full characterization of GPCR monomer–dimer dynamic equilibrium by single molecule imaging. *J. Cell. Biol.* **192**, 463–480. (doi:10.1083/jcb.201009128)
- Kalay Z, Fujiwara TK, Kusumi A. 2012 Confining domains lead to reaction bursts: reaction kinetics in the plasma membrane. *PLoS ONE* **7**, e32948. (doi:10.1371/journal.pone.0032948)

12. Elowitz MB, Surette MG, Wolf PE, Stock JB, Leibler S. 1999 Protein mobility in the cytoplasm of *Escherichia coli*. *J. Bacteriol.* **181**, 197–203.
13. Ramadurai S, Holt A, Krasnikov V, van den Bogaart G, Killian JA, Poolman B. 2009 Lateral diffusion of membrane proteins. *J. Am. Chem. Soc.* **131**, 12 650–12 656. (doi:10.1021/ja902853g)
14. Faeder JR, Hlavacek WS, Reischl I, Blinov ML, Metzger H, Redondo A, Wofsy C, Goldstein B. 2003 Investigation of early events in FcεRI-mediated signaling using a detailed mathematical model. *J. Immunol.* **170**, 3769–3781.
15. Bishop LM, Qian H. 2010 Stochastic bistability and bifurcation in a mesoscopic signaling system with autocatalytic kinase. *Biophys. J.* **98**, 1–11. (doi:10.1016/j.bpj.2009.09.055)
16. Murray JD. 2007 *Mathematical biology*. New York, NY: Springer.
17. Nicolis G, Lefever R. 1977 Comment on the kinetic potential and the Maxwell construction in non-equilibrium chemical phase transitions. *Phys. Lett. A* **62**, 469–471. (doi:10.1016/0375-9601(77)90069-X)
18. Baras F, Malek Mansour M. 1997 Microscopic simulations of chemical instabilities. *Adv. Chem. Phys.* **100**, 393–474. (doi:10.1002/9780470141595.ch5)
19. Ge H, Qian H. 2009 Thermodynamic limit of a nonequilibrium steady state: Maxwell-type construction for a bistable biochemical system. *Phys. Rev. Lett.* **103**, 148103. (doi:10.1103/PhysRevLett.103.148103)
20. Zuk PJ, Kocharczyk M, Jaruszewicz J, Bednorz W, Lipniacki T. 2012 Dynamics of a stochastic spatially extended system predicted by comparing deterministic and stochastic attractors of the corresponding birth–death process. *Phys. Biol.* **9**, 055002. (doi:10.1088/1478-3975/9/5/055002)
21. Baras F, Malek Mansour M, Pearson JE. 1996 Microscopic simulation of chemical bistability in homogeneous systems. *J. Chem. Phys.* **105**, 8257–8261. (doi:10.1063/1.472679)
22. Bird GA. 1994 *Molecular gas dynamics and the direct simulation of gas flows*. Oxford, UK: Clarendon.
23. Stamatakis M, Vlachos DG. 2011 Equivalence of on-lattice stochastic chemical kinetics with the well-mixed chemical master equation in the limit of fast diffusion. *Comput. Chem. Eng.* **35**, 2602–2610. (doi:10.1016/j.compchemeng.2011.05.008)
24. Potma EO, de Boeij WP, Bosgraaf L, Roelofs J, van Haastert PJ, Wiersma DA. 2001 Reduced protein diffusion rate by cytoskeleton in vegetative and polarized dictyostelium cells. *Biophys. J.* **81**, 2010–2019. (doi:10.1016/S0006-3495(01)75851-1)
25. Sbalzarini IF, Mezzacasa A, Helenius A, Koumoutsakos P. 2005 Effects of organelle shape on fluorescence recovery after photobleaching. *Biophys. J.* **89**, 1482–1492. (doi:10.1529/biophysj.104.057885)
26. Luby-Phelps K. 2000 Cytoarchitecture and physical properties of cytoplasm: volume, viscosity, diffusion, intracellular surface area. *Int. Rev. Cytol.* **192**, 189–221. (doi:10.1016/S0074-7696(08)60527-6)
27. Lu S, Ouyang M, Seong J, Zhang J, Chien S, Wang Y. 2008 The spatiotemporal pattern of Src activation at lipid rafts revealed by diffusion-corrected FRET imaging. *PLoS Comput. Biol.* **4**, e1000127. (doi:10.1371/journal.pcbi.1000127)
28. Kalwarczyk T *et al.* 2011 Comparative analysis of viscosity of complex liquids and cytoplasm of mammalian cells at the nanoscale. *Nano Lett.* **11**, 2157–2163. (doi:10.1021/nl2008218)
29. Altschuler SJ, Angenent SB, Wang Y, Wu LF. 2008 On the spontaneous emergence of cell polarity. *Nature* **454**, 886–889. (doi:10.1038/nature07119)
30. Jilkine A, Angenent SB, Wu LF, Altschuler SJ. 2011 A density-dependent switch drives stochastic clustering and polarization of signaling molecules. *PLoS Comput. Biol.* **7**, e1002271. (doi:10.1371/journal.pcbi.1002271)
31. Das J, Kardar M, Chakraborty AK. 2009 Positive feedback regulation results in spatial clustering and fast spreading of active signaling molecules on a cell membrane. *J. Chem. Phys.* **130**, 245102. (doi:10.1063/1.3149861)
32. Postma M, Roelofs J, Goedhart J, Gadella TWJ, Visser AJWJ, Haastert PJMV. 2003 Uniform cAMP stimulation of Dictyostelium cells induces localized patches of signal transduction and pseudopodia. *Mol. Biol. Cell.* **14**, 5019–5027. (doi:10.1091/mbc.E03-08-0566)
33. Hecht I, Kessler DA, Levine H. 2010 Transient localized patterns in noise-driven reaction–diffusion systems. *Phys. Rev. Lett.* **104**, 158301. (doi:10.1103/PhysRevLett.104.158301)
34. Fange D, Elf J. 2006 Noise-induced Min phenotypes in *E. coli*. *PLoS Comput. Biol.* **2**, e80. (doi:10.1371/journal.pcbi.0020080)
35. Malek Mansour M, Dethier J, Baras F. 2001 Onset of homogeneous oscillations in reactive systems. *J. Chem. Phys.* **114**, 9265–9275. (doi:10.1063/1.1367389)
36. Lee S-JR, Escobedo-Lozoya Y, Szatmari EM, Yasuda R. 2009 Activation of CaMKII in single dendritic spines during long-term potentiation. *Nature* **458**, 299–304. (doi:10.1038/nature07842)
37. Elf J, Ehrenberg M. 2004 Spontaneous separation of bi-stable biochemical systems into spatial domains of opposite phases. *Syst. Biol.* **1**, 230–236. (doi:10.1049/sb:20045021)
38. Arai Y, Shibata T, Matsuoka S, Sato JM, Yanagida T, Ueda M. 2010 Self-organization of the phosphatidylinositol lipids signaling system for random cell migration. *Proc. Natl Acad. Sci. USA* **107**, 12 399–12 404. (doi:10.1073/pnas.0908278107)
39. Mori Y, Jilkine A, Edelstein-Keshet L. 2008 Wave-pinning and cell polarity from a bistable reaction–diffusion system. *Biophys. J.* **94**, 3684–3697. (doi:10.1529/biophysj.107.120824)
40. Walther GR, Marée AFM, Edelstein-Keshet L, Grieneisen VA. 2012 Deterministic versus stochastic cell polarisation through wave-pinning. *Bull. Math. Biol.* **74**, 2570–2599. (doi:10.1007/s11538-012-9766-5)
41. Xiong Y, Huang C-H, Iglesias PA, Devreotes PN. 2010 Cells navigate with a local-excitation, global-inhibition-biased excitable network. *Proc. Natl Acad. Sci. USA* **107**, 17 079–17 086. (doi:10.1073/pnas.1011271107)
42. Jilkine A, Edelstein-Keshet L. 2011 A comparison of mathematical models for polarization of single eukaryotic cells in response to guided cues. *PLoS Comput. Biol.* **7**, e1001121. (doi:10.1371/journal.pcbi.1001121)
43. Huang Q, Qian H. 2009 Ultrasensitive dual phosphorylation dephosphorylation cycle kinetics exhibits canonical competition behavior. *Chaos* **19**, 033109. (doi:10.1063/1.3187790)
44. Lisman JE. 1985 A mechanism for memory storage insensitive to molecular turnover: a bistable autophosphorylating kinase. *Proc. Natl Acad. Sci. USA* **82**, 3055–3057. (doi:10.1073/pnas.82.9.3055)
45. Markevich NI, Hoek JB, Kholodenko BN. 2004 Signaling switches and bistability arising from multisite phosphorylation in protein kinase cascades. *J. Cell. Biol.* **164**, 353–359. (doi:10.1083/jcb.200308060)
46. Wilhelm T. 2009 The smallest chemical reaction system with bistability. *BMC Syst. Biol.* **3**, 90. (doi:10.1186/1752-0509-3-90)
47. Schlögl F. 1971 On thermodynamics near a steady state. *Z. Physik.* **248**, 446–458. (doi:10.1007/BF01395694)
48. Ferrell JE, Xiong W. 2001 Bistability in cell signaling: how to make continuous processes discontinuous, and reversible processes irreversible. *Chaos* **11**, 227–236. (doi:10.1063/1.1349894)
49. Phillips R, Ursell T, Wiggins P, Sens P. 2009 Emerging roles for lipids in shaping membrane-protein function. *Nature* **459**, 379–385. (doi:10.1038/nature08147)
50. Gillespie DT. 1977 Exact stochastic simulation of coupled chemical reactions. *J. Phys. Chem.* **81**, 2340–2361. (doi:10.1021/j100540a008)
51. Lawless JF. 2003 *Statistical models and methods for lifetime data*. Hoboken, NJ: Wiley-Interscience.
52. Kuramoto Y. 1974 Effects of diffusion on the fluctuations in open chemical systems. *Prog. Theor. Phys.* **52**, 711–713. (doi:10.1143/PTP.52.711)
53. Zheng Q, Ross J, Hunt KLC, Hunt PM. 1992 Stationary solutions of the master equation for single and multi-intermediate autocatalytic chemical systems. *J. Chem. Phys.* **96**, 630–640. (doi:10.1063/1.462446)
54. Alessi DR, Saito Y, Campbell DG, Cohen P, Sithanandam G, Rapp U, Ashworth A, Marshall CJ, Cowley S. 1994 Identification of the sites in MAP kinase kinase-1 phosphorylated by p74raf-1. *EMBO J.* **13**, 1610–1619.
55. Hat B, Kazmierczak B, Lipniacki T. 2011 B cell activation triggered by the formation of the small receptor cluster: a computational study. *PLoS Comput. Biol.* **7**, e1002197. (doi:10.1371/journal.pcbi.1002197)
56. Wang Q, Zhang X, Zhang L, He F, Zhang G, Jamrich M, Wensel TG. 2008 Activation-dependent

- hindrance of photoreceptor G protein diffusion by lipid microdomains. *J. Biol. Chem.* **283**, 30 015–30 024. (doi:10.1074/jbc.M803953200)
57. Abel SM, Roose JP, Groves JT, Weiss A, Chakraborty AK. 2012 The membrane environment can promote or suppress bistability in cell signaling networks. *J. Phys. Chem. B* **116**, 3630–3640. (doi:10.1021/jp2102385)
  58. Jaruszewicz J, Zuk PJ, Lipniacki T. 2013 Type of noise defines global attractors in bistable molecular regulatory systems. *J. Theor. Biol.* **317**, 140–151. (doi:10.1016/j.jtbi.2012.10.004)
  59. Takahashi K, Tanase-Nicola S, ten Wolde PR. 2010 Spatio-temporal correlations can drastically change the response of a MAPK pathway. *Proc. Natl Acad. Sci. USA* **107**, 2473–2478. (doi:10.1073/pnas.0906885107)
  60. Mugler A, Bailey AG, Takahashi K, ten Wolde PR. 2012 Membrane clustering and the role of rebinding in biochemical signaling. *Biophys. J.* **102**, 1069–1078. (doi:10.1016/j.bpj.2012.02.005)
  61. Zhou H-X. 2009 Crowding effects of membrane proteins. *J. Phys. Chem. B* **113**, 7995–8005. (doi:10.1021/jp8107446)
  62. Aoki K, Yamada M, Kunida K, Yasuda S, Matsuda M. 2011 Processive phosphorylation of ERK MAP kinase in mammalian cells. *Proc. Natl Acad. Sci. USA* **108**, 12 675–12 680. (doi:10.1073/pnas.1104030108)
  63. Dushek O, van der Merwe PA, Shahrezaei V. 2011 Ultrasensitivity in multisite phosphorylation of membrane-anchored proteins. *Biophys. J.* **100**, 1189–1197. (doi:10.1016/j.bpj.2011.01.060)

ELECTRONIC SUPPLEMENTARY MATERIAL

**Stochastic transitions in a bistable reaction system  
on the membrane**

Marek Kočańczyk, Joanna Jaruszewicz, and Tomasz Lipniacki

This material features the article published in the *Journal of the Royal Society Interface*, 2013.

**Supplementary table**

**Parameters of the analysed system used in simulations**

Parameter	Dimensionless values			Dimensional values for $c_0 = 10/\text{s}$ , $\ell = 0.01 \mu\text{m}$
	On-lattice KMC	Gillespie KMC	PDEs	On-lattice KMC
$c_0$	1.667	$10/V$	1	10/s
$c_1$	0.008333	$0.05/V$	0.02	0.05/s
$c_2$	{0.025, 0.0625, 0.08333}	{0.15/ $V$ , 0.375/ $V$ , 0.5/ $V$ }	{0.06, 0.15, 0.2}	{0.15/s, 0.375/s, 0.5/s}
$c_3$	1.667	$10/V$	4	10/s
$M$	18 to 6000	$\infty$	18 to 6000	300 to 10 000/s
$D$	2.25 to 750	$\infty$	2.25 to 750	$3.75 \times 10^{-3}$ to 1.25 $\mu\text{m}^2/\text{s}$
$l$	1	—	1	0.01 $\mu\text{m}$
$\rho\kappa$	0.4	—	—	4619/ $\mu\text{m}^2$
$\rho\mathcal{P}$	0.1	—	—	1155/ $\mu\text{m}^2$

TABLE S1: *Parameters of the analysed system.* Parameters are described in the main text. Only  $c_2$  and  $M$  (and  $D$ ) vary between simulations; other parameters, referred to as default parameters in the main text, are the same in all simulations.

*Physiological relevance of parameter values used in simulations:*

- Rate constants of reactions on the membrane can be as fast as 100/s [S1]; the relation  $c_1 < c_2 < c_3$  reflects the strong boost to the catalytic activity of a kinase resulting from the increase in the number of its phosphorylated sites [S2].
- Diffusion coefficients of membrane proteins lie in the range of  $10^{-2}$  to  $10^{-1}$   $\mu\text{m}^2/\text{s}$  (which is at least an order of magnitude lower than in the cytoplasm) [S3, S4].
- The lattice constant  $\ell$  is assumed to correspond exactly to the average centre-to-centre spacing of neighbouring membrane proteins [S5]. At  $\ell = 10$  nm compartment volumes analysed in simulations correspond well to sizes of plasma membrane confinement zones, which e.g. in NRK cells have the mean diameter of about 230 nm as revealed by single-particle tracking experiments [S6]; on the other hand, as we consider isolated chambers, transient trapping of proteins in zones of confinement is not reflected in simulations.
- A significant fraction of the membrane surface can be covered by proteins [S7]. The surface density of membrane proteins is of order of  $100/\mu\text{m}^2$ , but in some cases can be even as high as  $10\,000/\mu\text{m}^2$  [S8]. (The calculation of dimensional densities of molecules involves the formula for the surface of a hexagon:  $A = \frac{\sqrt{3}}{2}\ell^2$ .)

*Supplementary references:*

- S1 Faeder, J. R., Hlavacek, W. S., Reischl, I., Blinov, M. L., Metzger, H., Redondo, A., Wofsy, C. & Goldstein, B. 2003 Investigation of early events in Fc $\epsilon$ RI-mediated signaling using a detailed mathematical model. *J. Immunol.* **170**, 3769–3781.
- S2 Alessi, D. R., Saito, Y., Campbell, D. G., Cohen, P., Sithanandam, G., Rapp, U., Ashworth, A., Marshall, C. J. & Cowley, S. 1994 Identification of the sites in MAP kinase kinase-1 phosphorylated by p74raf-1. *EMBO J.* **13**, 1610–1619.
- S3 Elowitz, M. B., Surette, M. G., Wolf, P. E., Stock, J. B. & Leibler, S. 1999 Protein mobility in the cytoplasm of *Escherichia coli*. *J. Bacteriol.* **181**, 197–203.
- S4 Ramadurai, S., Holt, A., Krasnikov, V., van den Bogaart, G., Killian, J. A. & Poolman, B. 2009 Lateral diffusion of membrane proteins. *J. Am. Chem. Soc.* **131**, 12650–12656. (doi:10.1021/ja902853g)
- S5 Phillips, R., Ursell, T., Wiggins, P. & Sens, P. 2009 Emerging roles for lipids in shaping membrane-protein function. *Nature* **459**, 379–385. (doi:10.1038/nature08147)
- S6 Kusumi, A., Nakada, C., Ritchie, K., Murase, K., Suzuki, K., Murakoshi, H., Kasai, R. S., Kondo, J. & Fujiwara, T. 2005 Paradigm shift of the plasma membrane concept from the two-dimensional continuum fluid to the partitioned fluid: high-speed single-molecule tracking of membrane molecules. *Annu. Rev. Biophys. Biomol. Struct.* **34**, 351–378. (doi:10.1146/annurev.biophys.34.040204.144637)
- S7 Zhou, H.-X. 2009 Crowding effects of membrane proteins. *J. Phys. Chem. B* **113**, 7995–8005. (doi:10.1021/jp8107446)
- S8 Kalay, Z., Fujiwara, T. K. & Kusumi, A. 2012 Confining domains lead to reaction bursts: reaction kinetics in the plasma membrane. *PLoS One* **7**, e32948. (doi:10.1371/journal.pone.0032948)

# Supplementary figures

## Gillespie algorithm versus on-lattice KMC for large motility

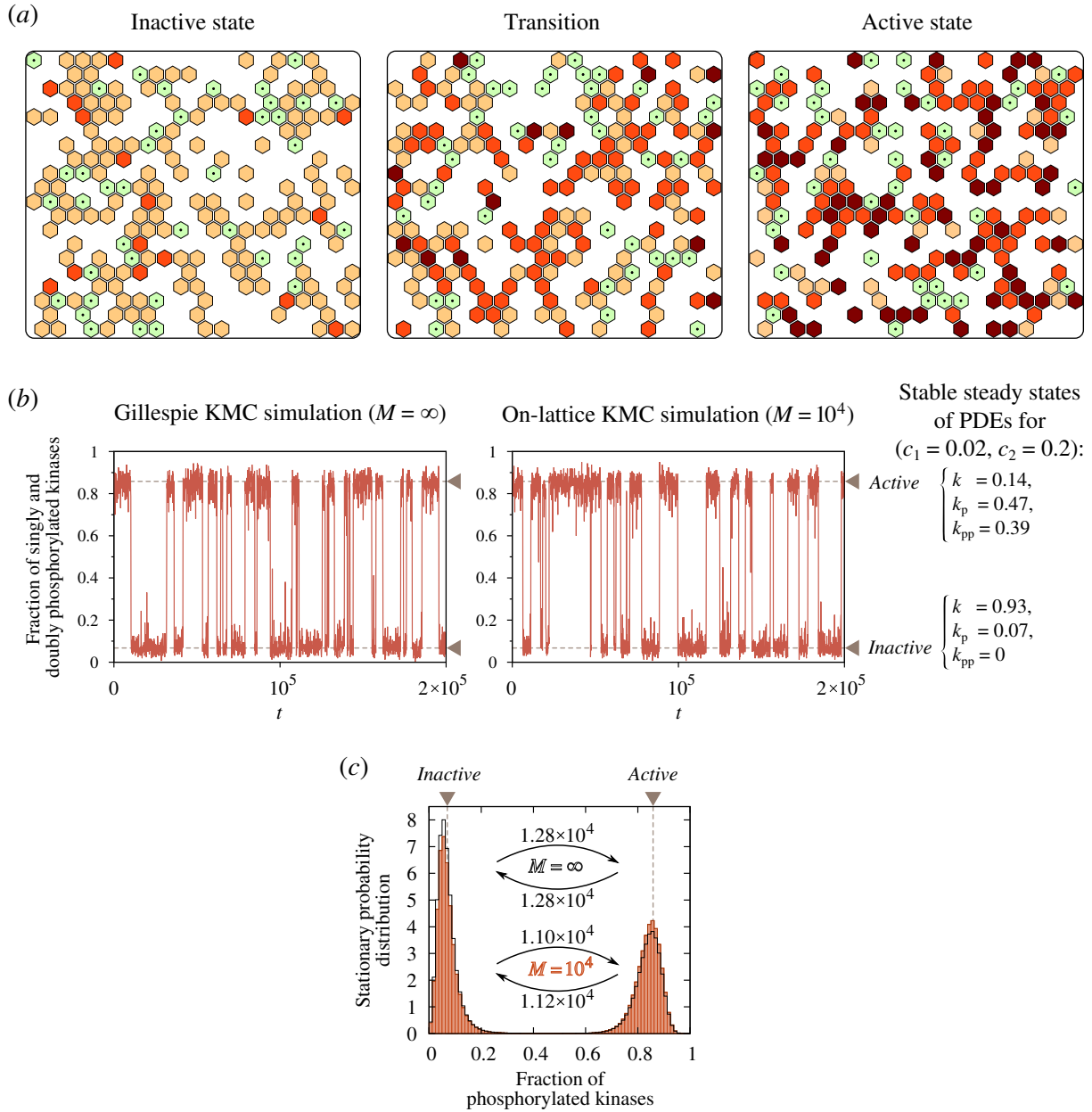


FIGURE S1: Comparison of KMC on the lattice simulations for large motility coefficient  $M = 10^4$  and the corresponding spatially homogeneous Markov process simulated with Gillespie algorithm. Domain size:  $20 \times 20$ , periodic boundary conditions; parameters: ( $c_1 = 0.02, c_2 = 0.2$ ). (a) Three snapshots from on-lattice KMC simulations (dephosphorylated kinases – orange, monophosphorylated – red, bisphosphorylated – brown; phosphatases – pale green, marked with a dot). (b) Trajectories of the fraction of phosphorylated kinases  $k_p + k_{pp}$  from the Gillespie algorithm and on-lattice KMC simulations. (c) Bimodal stationary probability distribution of  $k_p + k_{pp}$  calculated from long on-lattice (boxes) and Gillespie algorithm (thick black overlay) KMC simulations. MFPTs  $\tau_{\text{on}}$  and  $\tau_{\text{off}}$  are shown for both methods.

## Propagation of induced travelling waves in the semi-1-D reactor

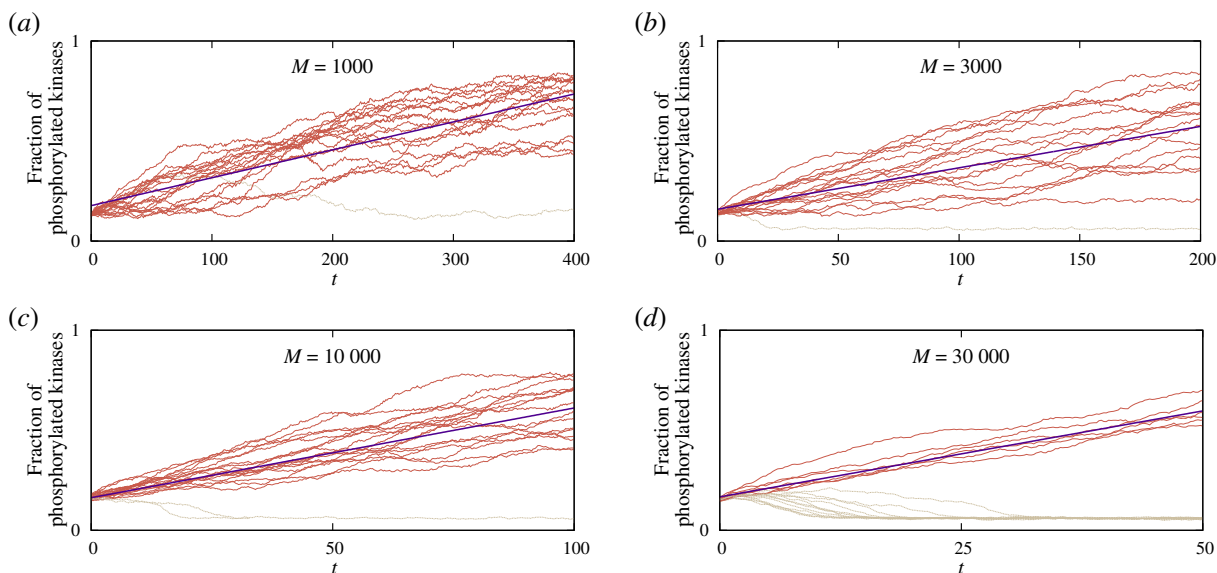


FIGURE S2: *Fraction of phosphorylated kinases  $k_p + k_{pp}$  averaged over the whole reactor  $30 \times 1100$  during the induced wave propagation.* Travelling wave velocities shown in figure S3 were estimated from linear fits to these trajectories. When the “seed” had become deactivated, so that the travelling wave did not form, the corresponding trajectory was not taken into account in fitting (dashed pale lines). At higher diffusivities the probability that the initially active area (“seed”) is swept away and cannot induce the wave is larger.

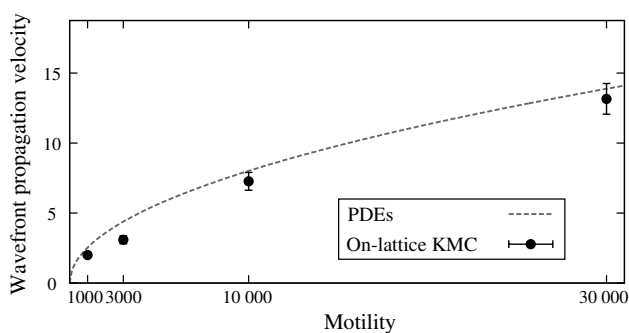


FIGURE S3: *Travelling wave velocity as a function of motility.* Velocities were calculated from simulations of PDEs and estimated in on-lattice KMC simulations for  $(c_1 = 0.02, c_2 = 0.15)$  (figure S2). Error bars – SD.

## Coinciding stochastically and deterministically preferred steady states

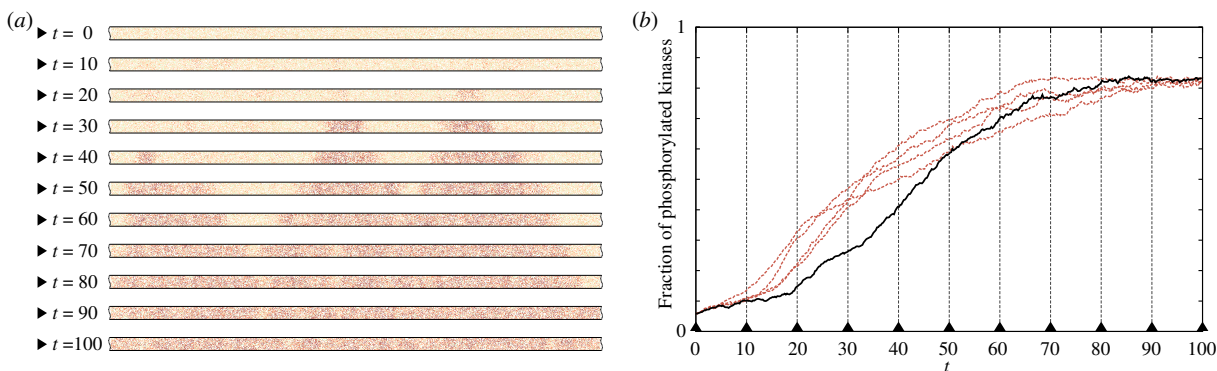


FIGURE S4: *Simultaneous spontaneous activation on the long toroidal domain  $30 \times 1000$ . Parameters: ( $c_1 = 0.02$ ,  $c_2 = 0.2$ ) and  $M = 300$ . (a) Snapshots from the on-lattice KMC simulation, (b) five example time profiles of phosphorylated kinases  $k_p + k_{pp}$ . Snapshots in (a) correspond to the trajectory represented by the solid black line in (b).*

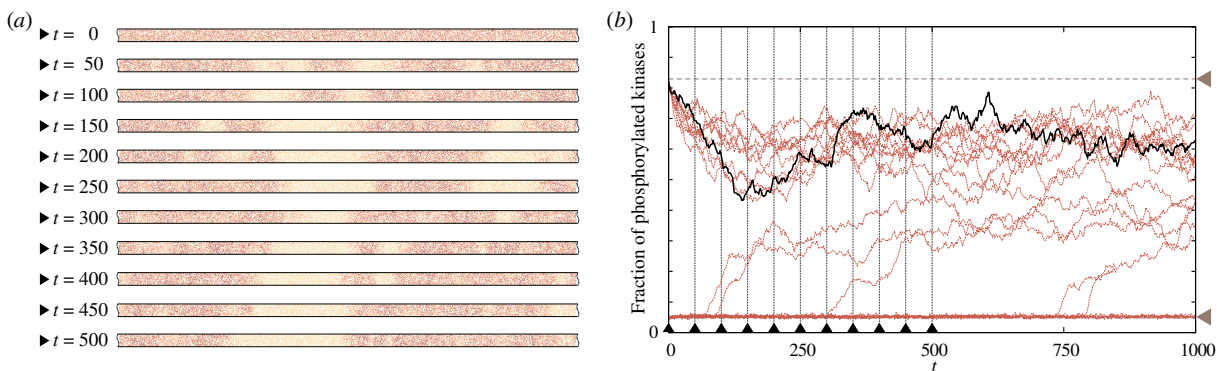


FIGURE S5: *Self-sustaining transient patches of activity in a toroidal domain  $30 \times 1000$ . Parameters: ( $c_1 = 0.02$ ,  $c_2 = 0.06$ ) and  $M = 300$ . (a) Snapshots from the on-lattice KMC simulation, (b) time profiles of 10 + 10 trajectories starting from the spatially homogeneous active and inactive steady states (horizontal dashed lines). Snapshots in (a) correspond to the trajectory represented by the solid black line in (b).*



FIGURE S6: *Kinase inactivity wave propagation on the cylindrical domain  $50 \times 1000$  for very large motility  $M = 10\,000$ . Three snapshots from an on-lattice KMC simulation. Parameters: ( $c_1 = 0.02$ ,  $c_2 = 0.06$ ).*

## Activation due to a locally reduced motility

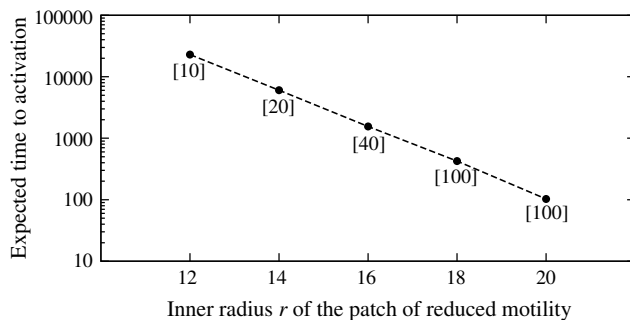


FIGURE S7: *Dependence of the expected time to activation  $\tau_{\text{on}}$  on the radius of the patch of lowered motility  $M_{\text{patch}} = 100$  with the overall motility  $M = 1000$  obtained from on-lattice KMC simulations. Parameters: ( $c_1 = 0.02$ ,  $c_2 = 0.06$ ) as in figure 8 in the main text. The expected  $\tau_{\text{on}}$  is estimated based on  $n_{\text{on}}$  observed switches given in square brackets.*

## Supplementary movies

*Movies are available on-line at:*

[http://pmbm.ippt.gov.pl/publications/supplementary/  
Kochanczyk-2013-JRSocInterface-Movies.zip](http://pmbm.ippt.gov.pl/publications/supplementary/Kochanczyk-2013-JRSocInterface-Movies.zip)

MOVIE S1: *Activity wave initiation on the square domain due to the locally reduced motility coefficient. System parameters as in figure 8 in the main text.*

MOVIE S2: *Self-sustaining transient patches of activity in a toroidal domain. All parameters as in figure S5.*